Electrochemical detection of bromate in food at MWCNT/Ni/Pc and MWCNT/Co/Pc modified electrode

SA Balogun

orcid.org/0000-0002-6618-2711

Thesis accepted in fulfilment of the requirements for the degree

Doctor of Philosophy in Chemistry

at the North-West University

Promoter: Prof. OE Fayemi

Graduation ceremony: May 2023

Student number: 33757968

DECLARATION

I, the undersigned, hereby declare that the thesis which I hereby submit to the Department of Chemistry, Faculty of Natural and Agricultural Sciences, North-West University, is entirely original to me with the exception of the citations and that I have not previously submitted it for a degree at any other University.

Name: Sheriff Aweda Balogun

Signature: ……...

Date: 28 November, 2022.

Supervisor: Prof. O.E. Fayemi

Signature: ……...

Date:

DEDICATION

I dedicate this thesis to Allah, the Almighty, the creator of the heaven and the earth, the ever living, the omnipotent, the omniscience and the everlasting for His guidance, mercy, protection and gift of life.

ACKNOWLEDGEMENTS

I sincerely give thanks to the Almighty Allah, the lord of the universe for His immeasurable favours on me throughout my study and my entire life. I praise and glorify Him in amount equivalent to the number of His creatures, the mightiness of His throne and the number of His words.

My profound gratitude goes to my supervisor, Professor O.E Fayemi for her moral and financial support, encouragement, and mentorship throughout the program. I equally appreciate her prompt response to requests and counsel on academic issues.

Special thanks goes to my parents, Alhaji Abubakr Balogun and Alhaja Memunat Balogun for their love and support. May Almighty Allah enrich them abundantly in goodness and make them reap the fruits of their labour. Similarly, I appreciate the care, encouragement, support, sacrifice and endurance of my wife (my best friend), Alhaja Bilqees Morayo Balogun and my children (Muhammad, Muadh, Asmaa, Abdullah, AbdurRahman and Al-Hassan) throughout the programme.

I am grateful to the Chemistry Department of the Faculty of Natural and Agricultural Sciences at North-West University, for the opportunity to study and the resources provided for the completion of this project. I equally thank the staff member of the Department of Chemistry, Faculty of Natural and Agricultural Sciences, North-West University. Specifically, I appreciate the efforts of Mr. Sizwe, Mr. Michael, Miss Maria, Mr. Peter, and Miss Murendeni for their technical assistance.

My undiluted thanks goes to my friends and colleagues at the North-West University: Dr. S.E. Elugoke, Dr. T.W. Quadri, Dr. Gloria Uwaya, Dr. E. Chima, Mrs. Funmilola Adesanya, Mr. Monsuru Shobande, Mr. Teslim Bolarinwa, Mr. N. Baakene, Mr. A. Afeez, Mr. Seleke Mokole, Mr. Poloso Calvin, Mr. Wole Dina, Mr. Onkarabile Pooe, Miss Judith, Mr. Tsholofelo Mosalashuping and Miss Ncomeka Mgxadeni for their support and encouragement.

Finally, this acknowledgement will not be completed without recognizing the assistance and support rendered to me by my Dawah brothers in South Africa and Nigeria, most especially Dr. S.O. Muse, Dr. F.O. Balogun, Dr. Rasheed Adebayo, Dr. (Engr.) Osein Amoo, Dr. N.A. Adebare, Ustadh Amin Mutiu, Dr. M. Ogunlola, Dr. H.O. Ojugbele, Dr. K.A. Adegoke, Alhaji AbdulHakeem Abioye and others, who had contributed to the successful completion of the programme.

ABSTRACT

Bromate in food and water has been linked to cancer risks for lifetime exposures, and the present techniques for its detection have significant limitations that necessitate the development of new and more efficient approaches. The study describes the synthesis and characterization of CoPcMWCNTs and NiPcMWCNTs nanocomposites prior to the modification of a glassy carbon electrode for bromate detection. The two nanocomposites were prepared from cobalt or nickel nanoparticles, phthalocyanine and functionalized multiwalled carbon nanotubes fMWCNTs. The successful synthesis of the nanoparticles and the nanocomposites were confirmed by the microscopic and spectroscopic techniques such as the X-ray diffraction spectroscopy (XRD), UV-visible spectroscopy, transmission electron microscopy (TEM), and scanning electron microscopy (SEM). The synthesized nanoparticles and nanocomposites were used to modify the glassy carbon electrode (GCE). The electrochemical characterization of the bare GCE and the modified electrodes (GCE-Co, GCE-Ni, GCE-MWCNTs, GCE-CoPcMWCNTs, and GCE-NiPcMWCNTs) was performed using cyclic voltammetry (CV) and electrochemical impedance spectroscopy (EIS) techniques in 5 mM ferricyanide/ferricyanide ($[Fe(CN)_6]^{4-/3-}$) prepared in 0.1 M phosphate-buffered solution PBS (pH 7). The CV results showed that the GCE-CoPcMWCNTs, and GCE-NiPcMWCNTs nanocomposites exhibited the highest current response (259.1 & 457.0 μA) and specific capacitance (7.47 & 6.80 F/g), respectively, than the other nanomaterials. A similar trend was obtained in the EIS experiment with the GCE-CoPcMWCNTs, and GCE-NiPcMWCNTs nanocomposites having lower charge transfer resistance (R_{ct}) than the individual nanomaterials. The nanocomposites' higher electronic properties as compared to those of the individual nanomaterials demonstrated that the synergy created by combining the nanomaterials during composite production resulted in improved electron transport capabilities.

The electroanalysis of the analyte (bromate) at the CoPcMWCNTs, and GCE-NiPcMWCNTs using cyclic voltammetry (CV) and EIS revealed that both CoPcMWCNTs, and GCE-NiPcMWCNTs exhibited higher reduction peak currents (I_{pc}) and faster electron transport, thus having better electrocatalytic behaviour. According to scan rate studies, scan rate (v) is directly proportional to the bromate cathodic current responses (I_{pc}) at GCE-CoPcMWCNTs and GCE-NiPcMWCNTs. Based on the linear relationship between reduction peak currents (Ipc) and the square root of the scan rate ($v^{1/2}$), the bromate reduction mechanism at GCE-CoPcMWCNTs and GCE-NiPcMWCNTs was diffusion controlled.

Using EIS technique, a LoD of 11.54 and 21.81 μM was obtained for the GCE-CoPcMWCNTs and GCE-NiPcMWCNTs over linear dynamic ranges (LDRs) of 48-167 and 48-200 μM, respectively. The sensitivities of the sensors were 125.5 and 485.6 μA μM^{-1}, respectively. Whereas, with square wave voltammetry (SWV) technique, an LoD of 8.87 and 3.09 μM was obtained for the GCE-CoPcMWCNTs and GCE-NiPcMWCNTs over linear dynamic ranges (LDRs) of 24-149 and 24-111 μM, respectively. The sensitivities offered by the two sensors were 485.6 and 1290 μA μM^{-1}, respectively. The two sensors demonstrated a good selectivity towards the bromate detection in the presence of interfering species (K^+, Na^+, NH_4^+, SO_4^{2-}, Cl^-, ClO_3^-, and CO_3^{2-}), except for IO_3^{2-} and Mg^{2+}. Both sensors offered the same performance regarding stability, reproducibility, selectivity and real sample analysis. Importantly, the two sensors were effectively used for bromate determination in bread samples with a good recovery, demonstrating the practical application of the sensors to detect bromate in food.

Table of Contents

LIST OF FIGURES

LIST OF TABLES

LIST OF SCHEMES

LIST OF ABBREVIATION

CoNPs:	Cobalt nanoparticles
NiNPs:	Nickel nanoparticles
EIS:	Electrochemical impedance spectroscopy
Pc:	Phthalocyanine
MPc:	Metal phthalocyanine
BrO_3^-:	Bromate
MWCNTs:	Multi-walled carbon nanotubes
SWCNTs:	Single-walled carbon nanotubes
NPs:	Nanoparticles
CV:	Cyclic voltammetry
SWV:	Square wave voltammetry
DPV:	Differential pulse voltammetry
PBS:	Phosphate buffer solution
SEM:	Scanning electron microscopy
XRD:	X-ray diffraction spectroscopy
TEM:	Transmission electron spectroscopy
Rct:	Charge transfer resistance
Rs:	Solution resistance
ΔEP:	Peak separation
E_{pa}:	Anodic peak potential
Epc:	Cathodic peak potential
I_{pa}:	Anodic peak current
I_{pc}:	Cathodic peak current
GCE:	Glassy carbon electrode
LoD:	Limit of detection
LDR	Linear dynamic range
LoQ:	Limit of quantitation
AP:	Amperometry
CNTs:	Carbon nanotubes
ECL:	Electrochemiluminescence
SPCE:	Screen-printed carbon electrode

LIST OF SYMBOLS

δ	Standard deviation of the intercept of the linear calibration curve
ks	Charge transfer rate constant
v	Scan rate
I	Current
A	Surface area
R	Molar gas constant
T	Temperature
μ	Micro
b	Tafel slope
b1	Slope of a plot of E_{ap} against log v
b2	Slope of a plot of E_{cp} against log v
n	Number of electrons transferred
F	Faraday's constant
D_o	Diffusion coefficient

CHAPTER ONE

1.1 Introduction

This chapter emphasizes the importance and health implications of Potassium bromate ($KBrO_3$), as well as the need to develop a fast, sensitive, selective, and economical electrochemical sensor for bromate detection. The chapter also enumerates the classification, characteristics, and applications of sensors. Lastly, the aim and objectives of the study are detailed in the chapter.

Potassium bromate is a white granule or crystal with a molecular weight of 167 g/mol, melting point of about 350 °C, density of 3.27 g/cm^3, and decomposes with the evolution of oxygen at a temperature of 370 °C. It is highly water-soluble but slightly soluble in toluene, dimethyl sulfoxide, methanol, acetone, and ethanol [1]. It is mainly used as a flour maturing agent and a dough conditioner. It also serves as a food additive, oxidizing agent, laboratory reagent, and is used in explosives and permanent-wave compounds. Potassium bromate, a well-known oxidizing agent, is widely regarded as one of the best and most affordable dough improvers in the baking industry. Due to this, its value in the baking sector cannot be overstated. As a result of the $KBrO_3$ addition to dough, macromolecules such as starch and protein in the dough are influenced physically and chemically, leading to the desired baking outcome. Notably, the swelling characteristics of the dough, the extent of gelatinization, the viscosity, and the disulfide linkage formation (in gluten proteins) are affected by the use of $KBrO_3$ as an additive in bread baking [2]. In most drinking-water samples, bromate (BrO_3^-) is often present as a by-product of ozone disinfection and is widely used as a food additive in baking to prepare flour for maturation due to its oxidizing nature. Its usage also extends to the manufacture of fermented beverages, making of fish paste and cold-wave hair treatments as a neutralizer [3].

1.2 Health Implications of Bromate

Despite bromate's usefulness in water treatment and food production, there are several instances of its negative impact on human health. It has been explicitly reported to be connected to peripheral neuropathy, renal diseases, and anemia [2, 3] if ingested beyond the World Health Organization's authorized threshold of 25 µg L^{-1} (WHO, 1996). It has been linked to malignant growth in laboratory animals. Additionally, the increased incidences of kidney tumors, thyroid cells, and peritoneal mesotheliomas have been associated with bromate in mice and rats' drinking water.

Human and animal auditory functions are also affected due to high bromate intake, according to scientific evidence [4]. The World Health Organization, together with the United States Environmental Protection Agency (USEPA), have recommended 10 µg L^{-1} (0.078 µM) as the maximum acceptable level (MAL) owing to its carcinogenicity [5]. Bromate-related cancer cases have increased at an alarming rate worldwide owing to bromate consumption in foods and water. This necessitates controlling and determining bromate concentrations in foods and water using a fast, sensitive, selective, and economical technique to guarantee the safety of the consumers. The toxicological investigations by WHO (1996) categorized bromate as a class B2 carcinogen in foods and water [6].

1.3 Problem Statement

The detection of BrO_3^- at trace levels entails using fast, economical, reliable, highly selective, and sensitive analytical techniques. Gas chromatography, spectrophotometry liquid chromatography, and ion chromatography [7-10] are previously employed analytical techniques to detect bromate. However, tedious and time-demanding, special sample preparation, multiple extraction and hydrolysis, low sensitivity and high-temperature requirement, and costly and sophisticated instrumentation limit the usage of these techniques for bromate detection [11].

Most of these setbacks can be addressed to a greater extent by employing electrochemical methods with electrochemical sensors fabricated with nanocatalysts (multi-walled carbon nanotubes and ferromagnetic nanoparticles). The study, therefore, explored the advantages of the sizable surface area of the phthalocyanine and fMWCNTs, and the high electrical conductivity of the fMWCNTs and nickel to fabricate fast, sensitive, selective, and economical electrochemical sensors for bromate detection.

Furthermore, a fast, reliable, versatile, and modern technique for the detection of bromate would have to fulfill these requirements:

(i) Ability to detect BrO_3^- as low as 25 % of the MAL,
(ii) Low cost and quick analysis period,
(iii) No sample pre-treatment and,
(iv) Accessibility of the technique.

Electrochemical methods offer all of these characteristics, making them ideal techniques for detecting bromate [12].

1.4 Sensor

Sensors are devices that detect the changes in electrical, physical, or other quantities, producing an output as an acknowledgment of change in the quantity. Usually, the signal from a sensor can be optical or electrical [13].

1.4.1 Classification of Sensor

Sensors are either classified based on the principle of signal transduction or application fields/ receptor applications. Considering the signal transduction principle, these classes occur:

- Optical sensor – This uses absorbance, fluorescence, reflectance, optothermal effect, luminescence, light scattering, and refractive index.
- Electrochemical sensors – These include potentiometric and voltammetric devices, potentiometric solid electrolyte gas sensors and chemically field effect transistors (CHEMFET).
- Mass sensitive sensors – These include sensors based on surface acoustic waves and piezoelectric devices.
- Thermometric sensors – These sensors work by measuring the heat produced by a particular chemical process or by adsorption involving the analyte.
- Electrical sensors – These include sensors constructed with organic semiconductors, metal oxide, and electrolytic conductivity sensors.
- Magnetic sensors – These are majorly for oxygen sensors that are based on paramagnetic gas properties.

Biosensors are also considered as a class of sensors based on application fields or receptor applications. Biosensors are chemical sensors that use a biochemical mechanism for the recognition system.

1.4.2 Electrochemical Sensor

An electrochemical sensor is a small device that transmutes chemical or biochemical information (either quantitatively or qualitatively), ranging from concentration of a specific component to total composition analysis, into an analytically useful signal due to the chemical interaction between

the sensor device and the analyte molecule. Typically, a sensor's signal is electronic in nature, which is in the form of changes in voltage, current, or conductance/impedance due to changes in analyte quality or composition [13, 14]. Electrochemical sensors are small-sized devices containing a chemically sensitive layer (recognition layer), a physical transducer, and a signal processor capable of continuously and reversibly reporting a chemical concentration or a spectrometer that sends out an energy signal in the form of optical, electrical, or thermal, and reads the change in this same property caused by the intervening chemical. In electrochemical sensors, the target is a chemical compound or molecule, whereas in biosensors, the target is a biomolecule of interest [13, 14]. A biosensor is often viewed as a subset of chemical sensors because the sensor platforms, otherwise known as the transduction methods, are the same as those of chemical sensors. Electrochemical sensors are fabricated from various electrochemical sensing materials such as metal/metal oxides nanoparticles, metal phthalocyanines MPcs, carbon-based components (MWCNTs, graphene, SWCNTs, sheets, quantum dots), and other conducting polymers.

1.4.3 Characteristics of Electrochemical Sensors

A good electrochemical sensor must possess the following characteristics:

- Ability to transform chemical quantities into electrical signals,
- Fast rapid response,
- Good repeatability, reproducibility, and stability,
- Small and economical
- High selectivity and sensitivity,
- Low detection limit

1.4.4 Applications of Electrochemical Sensors

Electrochemical sensors have received a broader applications such as in product quality controls, critical care, safety, home safety alarms, industrial hygiene, process controls, automotive, human comfort controls, clinical diagnostics, homeland security, and emissions monitoring. In these applications, there are both financial and social advantages to using electrochemical sensors. Electrochemical sensors are often used for detecting liquid and gaseous analytes but sometimes solid analytes. Solid electrolytes can withstand high temperatures because the sensor devices are made with high-temperature materials [13, 14] . Electrochemical sensors have been successfully used to detect numerous analytes such as acetaminophen, glucose, paracetamol, dopamine, lactic

acid, uric acid, ascorbic acid, nevirapine, glutathione, procalcitonin, carbaryl, hydrazine, pyridoxine, nitrite, cysteine, epinephrine, hydrogen peroxide, diethylstilbestrol, kanamycin, and other, resulting in an outstanding performance such as high sensitivity, good selectivity, low limit of detection, and a broader concentration range [15].

The present study focused on developing a new method based on the electrochemical impedance spectroscopy (EIS) technique and fabricating electrochemical sensors for bromate detection in foods.

1.5 Aim of the Study

Detection of bromate in food samples using electrochemical impedance spectroscopy at metal phthalocyanine functionalized MWCNTs modified electrodes.

1.5.1 Objectives of the Study

i. To synthesize cobalt nanoparticles (CoNPs) and nickel nanoparticles (NiNPs) using a chemical synthesis.
ii. To functionalized the raw MWCNTs and fabricate nanocomposites of CoPcMWCNTs and NiPcMWCNTs.
iii. To characterize the synthesized nanoparticles and their nanocomposites using morphological and spectroscopic techniques such as scanning electron microscope (SEM), transmission electron microscopy (TEM), EDX, UV-vis spectroscopy, X-ray diffraction spectroscopy (XRD), cyclic voltammetry, and electrochemical impedance spectroscopy (EIS).
iv. To fabricate electrochemical sensor by modifying the working electrode GCE with NiNPs, CoNPs, fMWCNTs, CoPcMWCNTs, and NiPcMWCNTs nanocomposites.
v. To investigate the effect of scan rate, electrolytes and pH on the fabricated sensors.
vi. To investigate the stability, sensitivity, selectivity, and reproducibility of the fabricated sensors toward bromate detection.
vii. To evaluate the sensor performance towards the detection of bromate using electrochemical impedance spectroscopy and square wave voltammetry.
viii. To determine bromate content in selected food samples using electrochemical impedance spectroscopy.

CHAPTER TWO

Literature Review

2.1 Nanotechnology

Nanotechnology is defined as materials and processes involving at least one dimension in the range of 0.1–100 nanometres. Nanotechnology can also be defined as research, manipulation, development, control, and use of materials at the nanoscale level. This definition encompasses naturally occurring and engineered particles such as metal-based, carbon-based, composites, dendrimers, and DNA. Nanotechnology also finds wide applications in many fields, such as detection, waste reduction, filtration, remediation, and energy production [16].

The following terminologies emanate from the word nanotechnology:

i. Nanoscale: material with one or more dimensions of 100 nm or less.
ii. Nanoparticle: particle having one or more dimensions at the nanoscale.
iii. Nanocomposite: composites having a nanoscale dimension in at least one of its phases.
iv. Nanomaterial: a material having one or more internal structures or external dimensions with novel characteristics that differ from the same material without nanoscale features. A material is considered a nanomaterial only if its properties at the nanoscale differ from those at bulk or higher scales.
v. Nanoscience: the study of phenomena and manipulation of materials at atomic, molecular, and macromolecular scales with entirely different properties from the bulk material.
vi. Nanostructured: a material having a structure at the nanoscale,

Nanotechnology manifests in various forms such as nanoparticles, nanosensors, and nanodectectors, nanochips (used as nanosized components in computers), nanowires, nano transistors, nanoclays, nanocoatings, and nanofilms (used to strengthen joint replacement parts, pacemakers, and medical devices, etc.) [16, 17].

2.1.1 Nanoparticles (NPs)

Nanoparticles (NPs) are small particles with sizes ranging from 1 to 100 nanometres. Nanoparticles have significantly distinct physical and chemical characteristics compared to their

larger material counterparts. Due to their small size and high surface area to volume ratio, nanoparticles are suitable electrochemical sensing materials and can be used as filters, bio-labels, catalysis, and microelectronics [17].

2.1.2 Synthesis of Nanoparticles

Nanoparticles are generally synthesized via two approaches, namely bottom-up and top-down. The bottom-up approach includes chemical and biological (green) methods, while the top-down approach is majorly a physical method. The physical method involves mechanical grinding, sputtering, thermal decomposition, electrolysis, and laser irradiation to reduce the size of bulk materials in which high temperatures, energy-intensive, and high-cost vacuum systems with supporting equipment are usually required [18]. The chemical method of NPs synthesis often involves the use of chemicals. In contrast, biological (Green) synthesis involves the use of plant extracts (leaves, peels, seeds, fruits, peels of the plant), and microorganisms such as bacteria, fungi and algae, which serve as the reducing agent together with a precursor [19, 20]. Recent research is tending toward green synthesis because they are low cost, nontoxicity, and environmentally friendly [21]. A summary flow diagram for nanoparticle synthesis is shown in Figure 2.1.

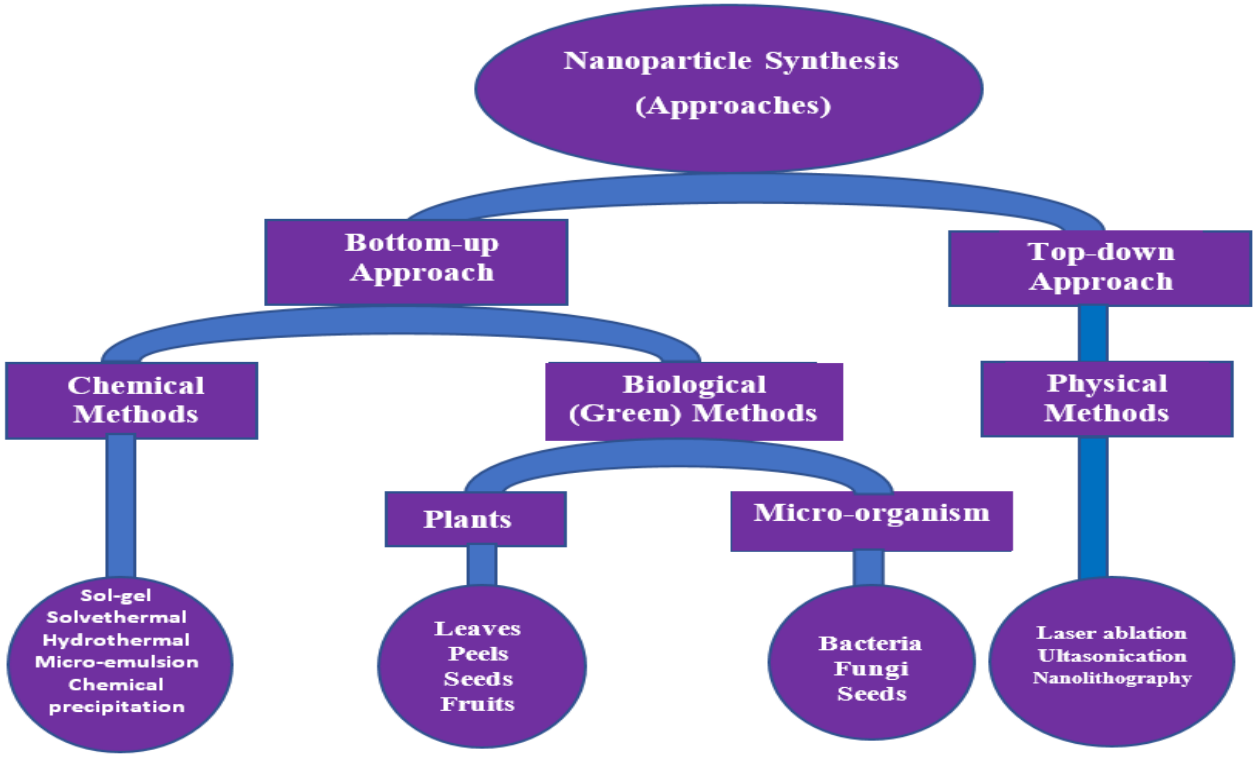

Figure 2.1. Nanoparticles synthetic approaches.

2.1.3 Application of Nanoparticles

Nanoparticles have been widely employed as electrochemical sensing materials for detecting various analytes such as dopamine, serotonin, acetylcholine, histamine, glutamate, norepinephrine, epinephrine, glycine, and heavy metals. They also found application in many other fields, including wastewater treatment, corrosion inhibition, investigation of forensic drugs, and heavy oil due to their small size, biocompatibility, and non-toxicity properties [22, 23].

2.1.4 Cobalt and Nickel Nanoparticles

Metal nanoparticles have drawn much interest owing to their exciting size-dependent optical, thermal, electronic, catalytic, and magnetic properties compared with their corresponding bulk metals. Magnetic nanomaterials exhibit very high Curie temperatures, high magnetoresistance, low saturation magnetization, and large coercivities. Consequently, magnetic nanoparticles have received a lot of attention in ferrofluids, magnetic storage, imaging, and sensors applications [24]. In the last decade, the synthesis of magnetic NPs of Co, Ni, and Fe has attracted increasing attention due to their exceptional magnetic properties and prospective applications in various sectors, such as sensors, memory storage devices, and catalysis [25]. In medicine, they are used for hyperthermic cancer cell therapy, magnetic resonance imaging, and magnetically controlled drug delivery [25]. Nickel nanoparticles have been gaining considerable attention for their applications in sensing, catalysts, and magnetic materials [26]. Besides its magnetic properties, size-dependent melting properties of NiNPs have also been employed to diffusion braze stainless steel at lower temperatures and pressures [24]. Cobalt nanoparticles have recently proven to be promising materials due to their wide applications in data storage, electrochromic devices, gas-sensing, catalysis, and lithium-ion batteries [27].

2.2 Characterization Techniques

Characterization of nanomaterials focuses majorly on investigating the size and shape of the nanomaterials. Information such as physical properties, optical properties, crystal structure, and elemental composition of the nanomaterials can also be obtained from the characterization of nanomaterials. Additionally, size distribution, surface area, surface charge, degree of aggregation, and surface chemistry are examined. There are different techniques available for characterizing nanomaterials. These methods are occasionally exclusive for examining a particular property,

while in other cases, they are merged. The technique's choice is often affected by factors such as availability, simplicity, cost, non-destructive nature, precision, selectivity, and affinity for specific compositions or materials. Specifically, nanomaterials have been largely characterized using microscopic, spectroscopic, and electrochemical techniques [28].

2.2.1 Spectroscopic Techniques

2.2.1.1 Fourier Transform Infrared Spectroscopy (FTIR)

FTIR spectroscopy is a valuable technique for identifying organic, inorganic, and polymeric materials by passing infrared light through a given sample or scanning a sample with infrared light. A change in the material composition is clearly shown with the alterations in the typical pattern of absorption bands. FTIR helps identify and characterize unknown materials, detect contaminants in a material, find additives, and identify decomposition and oxidation. A standard FTIR spectrometer comprises a light source, detector, sample cell, A/D convertor, amplifier, and computer. After passing through the interferometer, the radiation from the sources enters the detector. The amplifier and A/D convertor magnifies the signal, converts it to a digital signal, and then transfer it to the computer to perform the Fourier transform [28, 29]

The principle of FTIR spectroscopy involves passing IR radiation through a sample, with some of the radiations absorbed while others pass through. The sample converts the absorbed radiation to vibrational or rotational energy. The resultant signal obtained at the detector is generally from 1500 to 500 cm^{-1}, representing the samples' molecular fingerprint. Every molecule has a unique fingerprint, making FTIR an invaluable chemical identification tool [30]. A typical FTIR has a resolution of 4 cm^{-1}. In FTIR, simultaneous measurement of light or radiation of several frequencies is achieved; this accords the technique with an advantage of a higher signal-to-noise ratio for a given scanning time. FTIR spectroscopy helps obtain information regarding the wavelength and intensity of adsorption and identify the functional group present in a particular compound [30]. FTIR as a primary and essential tool for characterizing nanomaterials has been discussed in several reports [31-33].

2.2.1.2 UV-Visible Spectroscopy

UV-Vis spectroscopy is another relatively simple, fast, and affordable characterization technique that is frequently employed to investigate nanoscale materials. It measures the light reflection intensity from a sample and contrasts it with the light reflection intensity from a reference material

[28, 34]. UV-Vis spectroscopy is a crucial tool for identifying, characterizing, and investigating these materials and assessing nanoparticle colloidal solutions' stability due to the optical properties of nanoparticles being sensitive to concentration, size, agglomeration state, shape, and refractive index close to the NP surface. In UV-visible spectroscopy, a form of absorption spectroscopy, the molecule absorbs UV-visible light. The excitation of electrons from lower to higher energy levels happens because of the UV-visible radiations being absorbed. Only specific functional groups (chromophores) in organic compounds with valence electrons and low excitation energy can absorb ultraviolet and visible light. In contrast to IR spectroscopy, which uses vibrational transitions to study molecules, UV-Vis spectroscopy uses electronic transitions occurring in the ultraviolet or visible region to study molecules [34, 35].

Using the Beer-Lambert law (Eqn. 2.1), the elemental concentrations of a sample can be quantitatively determined with UV–vis spectroscopy.

$$A = Log_{10}\frac{I_0}{I} = \varepsilon cL \qquad (2.1)$$

where:

A represents the measured absorbance,

I_0 represents the intensity of the incident light at a specific wavelength,

I stands for the transmitted intensity,

L stands for the path length through the sample,

c denotes the concentration of the absorbing species, and

ε denotes the extinction coefficient or molar absorptivity of individual wavelength and species.

According to the equation, the analyte concentration can be determined when other parameters are known. The analyte concentration can be calculated more accurately from a plotted calibration curve using ε at the wavelength of maximum absorption (λ_{max}).

2.2.1.3 X-ray Diffraction (XRD)

XRD is one of the most effective and widely utilized techniques for characterizing nanomaterials. Typically, XRD offers details about the crystal structure, crystalline grain size, lattice parameters, and the nature of the phase. The crystalline size (particle size D) of a given nanomaterial is estimated from the broadening of the most prominent peak of an XRD spectrum using the Scherrer

equation (Eqn. 2.2). The advantage of using XRD techniques is that its offers statistically representative, volume-averaged values with the used of powdery form samples, typically obtained after drying their respective colloidal solutions. The particle composition can also be estimated by comparing the peak locations and intensities with the reference patterns provided by the International Centre for Diffraction Data (ICDD) [28]. Additionally, XRD is a non-destructive technique and can as well used to characterize crystalline materials such as metals, semiconductors, pharmaceuticals, polymers, and plastics [36, 37]. The synthesized nanomaterials used in the study were characterized using a Bruker X-ray diffractometer (Bruker-AXS, Madison, Wisconsin) coupled with a graphite crystal monochrometer and a copper target tube. X-ray patterns for each nanomaterial were obtained using the Ni-filtered CuKα radiation (λ = 1.5418 Å) at a scan range of 2θ from 20-90^{o}.

$$D = \frac{0.89\lambda}{\mathrm{B}\cos\theta} \qquad (2.2)$$

Where λ represents the wavelength (0.15418 nm), B stands for the full width at half-maximum peak, and θ denotes the XRD peak's Bragg angle.

2.2.1.4 Energy Dispersive X-ray Spectroscopy (EDS)

Energy dispersive X-ray spectroscopy is a surface characterization technique used to obtain a sample's elemental composition through X-ray mapping. EDS offers qualitative and quantitative information about a specific sample by identifying the lines in the spectrum and determining the amount of element present. EDS, in theory, uses the X-ray spectrum produced when a solid specimen is struck by a focused electron beam to produce a localized chemical analysis. The ED spectrophotometer detects the generated X-rays and divides them into different energy levels. Instrumentally, it involves the emission of X-rays by bombarding an electron beam on the sample. When the emitted X-rays hit the detector, a charge pulse that reflects the energy of the X-ray detected is transformed into a voltage pulse. The voltage pulse is then transformed into a signal with an additional count representing the energy channel. An element's characteristic X-rays are distinctive and can be used to distinguish it from other elements [38, 39].

2.2.1.5 X-ray Photoelectron Spectroscopy (XPS)

X-ray photoelectron spectroscopy XPS is an effective quantitative method for determining the oxidation states, elemental composition, and electronic structure of elements in a material. It is the most used analytical method for surface chemical analysis, which is also used to characterize materials at the nanoscale [28, 40]. The fundamental principle behind XPS lies in the photoelectric effect, which functions under extremely high vacuum conditions. Analysis of core/shell structures, surface functionalization of a nanomaterial, and ligand exchange interactions are also accomplished with XPS. Research revealed that XPS has been successfully employed to study the internal heterostructures of nanoparticles, investigating the environment-dependent crystal structure tuning of metal chalcogenide nanoparticles of different sizes, distinguishing homogeneous alloy structures from core/shell, and identifying the mode of ligand attachment to the surface of metal chalcogenide nanoparticles [28].

2.2.1.6 Thermal Gravimetric Analysis (TGA)

Thermal gravimetric analysis is a vital characterization technique that offers information on the composition and mass of synthesized nanomaterials. This method involves heating a nanomaterial sample, decomposing and vaporizing components with different degradation temperatures, and measuring the change in mass. The TGA equipment measures the mass loss with the respective temperatures, and while considering the starting mass of the sample, the TGA can identify the type and quantity of the nanoparticle organic ligands. The efficiency of TGA is enhanced with the development of a microthermogravimetric analysis (μ-TGA) in which the sample mass is in the order of 1 μg and can detect mass changes lower than 1 nanogram, thereby significantly improving the detection limits of conventional TGA [28, 41].

2.2.2 Microscopic Techniques

2.2.2.1 Scanning Electron Microscopy (SEM)

Scanning electron microscopy is one of the most popular characterization techniques that produces images of a specimen by employing raster scanning and a focused electron beam to scan the specimen's surface. SEM provides information on the morphology and microstructure of the surface of a material [42]. SEM images are produced by detecting and collecting secondary electrons emitted by sample atoms excited by the incident electron beam. A typical SEM comprises

an electron gun that emits the electron, a hairpin tungsten gun that generates high-diameter electron beam which produces high-resolution images, an electromagnetic lenses that helps the electron beam to be focused and shaped to create a tiny concentrated electron spot on the material and a high-vacuum environment that permits electron movement without risk of air scattering or absorption. In SEM, a low-energy electron beam is transmitted to the material and scans the sample's surface. As the beam enters the material, several interactions take place that causes photons and electrons to be emitted from or close to the sample surface. Depending on the SEM mode being utilized, several types of detectors are used to detect the receiving signals produced by the electron-sample interactions to create an image. SEM depends on the secondary emission of electrons from the specimen's surface for a visible magnified image. With suitable detectors, information on composition, optical, phase, thermal, electrical, and other properties can be drawn with exceptional resolution. SEM is often considered for particle size analysis owing to 2.5 nm resolution. SEM also offers other specific information when coupled with other techniques, such as energy-dispersive X-ray EDX to determine the orientation of individual crystals or the elemental composition of a material [42].

2.2.2.2 Transmission Electron Microscopy (TEM)

TEM, a microscopy technique, helps determine the internal structure of a material and is thereby valuable for estimating the average particle size of a material. TEM exhibits a high spatial resolution owing to the short de Broglie wavelengths, which aids in determining the crystal structure, shape, and size of materials [43]. The basic idea behind TEM operation is passing electron streams through a sample at a high voltage of 100 - 300 kV, created by thermionic emission in the electron gun. While some of the electron beams transmit, others interact with the material. The objective lens focuses the transmitted electrons onto an imaging device, producing an image. While traveling through the projector and intermediate lenses, the image is enlarged. The images are captured after being projected onto a fluorescent screen. The high effectiveness of TEM is mainly achieved when combined with other techniques, such as XRD, in determining the shape and size of nanomaterials. TEM is given more consideration than SEM in determining nanomaterials particle sizes owing to its spatial resolution of higher quality and accurate particle size [44].

2.3 Electrochemical Sensor Analysis

Electrochemical sensor analyses are usually carried out in an electrochemical cell (containing the electrodes and electrolyte) using electrochemical techniques. Electrolytes are chosen based on the type of analytes of interest. The electrolyte aids the promotion of reaction within the cell and transports efficient ionic charge across the electrodes. Good electrolytes must be compatible with materials within the cells, they should not be volatile as that could lead to a decline in the sensor signal, and they should form a stable reference potential with the reference electrodes. The effective performance of an electrochemical sensor also lies in the usage of the three kinds of electrodes. These include the working, counter, and reference electrodes as shown in Figure 2.2.

i. Working electrode (WE): The working electrode, which is sensitive to analyte concentrations, is the sensing electrode on which the reaction of interest takes place in an electrochemical system. In the standard three-electrode system, the working electrode is frequently used along with a reference electrode and a counter electrode. The working electrode is sometimes called anodic or cathodic based on either oxidation or reduction reaction at the surface of the electrode, either oxidation or reduction. The working electrodes are usually made up of inert materials such as inert carbon and metals like pyrolytic graphite or boron-doped diamond, glassy carbon, platinum, gold, and film electrodes. At times, it could be paraffin composite electrodes, carbon paste electrodes, or screen-printed electrodes [45-47]. These electrodes are then modified with various sensing materials such as metal/metal oxide nanoparticles, carbon-based components (graphene, SWCNTs, MWCNTs, quantum dots), metal phthalocyanine, polyaniline, and other conducting materials to obtain sensors with improved conductivity, selectivity, and sensitivity, An excellent working electrode has high electrical stability, good signal-to-noise ratio, is affordable, readily available, and is less hazardous [48-50].

ii. Reference electrode (RE): The reference electrode enhances the sensor's performance by providing a constant potential that regulates the working electrode. In other words, it controls or measures the potential of the WE without allowing current to flow through it. The RE is positioned close to the WE in order to reduce the drop in cell resistance. Saturated calomel electrode (SCE) and Ag/AgCl electrode are the commonly known reference electrodes. The Ag/AgCl electrode is the most frequently used in a high concentration of KCl due to steady voltage at the interfaces of

Ag-AgCl and AgCl-KCl via rapid charge transfer steps, irrespective of current density magnitude. The high concentration of KCl supports the stable voltage [45, 51, 52].

iii. Counter electrode (CE): The counter electrode, also referred to as the auxiliary electrode, controls the current that is applied to the working electrode. Typically, it is made of an inert substance (such as Au, Pt, glassy carbon, or graphite) and does not participate in an electrochemical reaction. The overall CE's surface area must be greater than the WE because the current flows between both, preventing the WE from acting as a limiting factor in the kinetics of the investigated electrochemical reaction [45, 53].

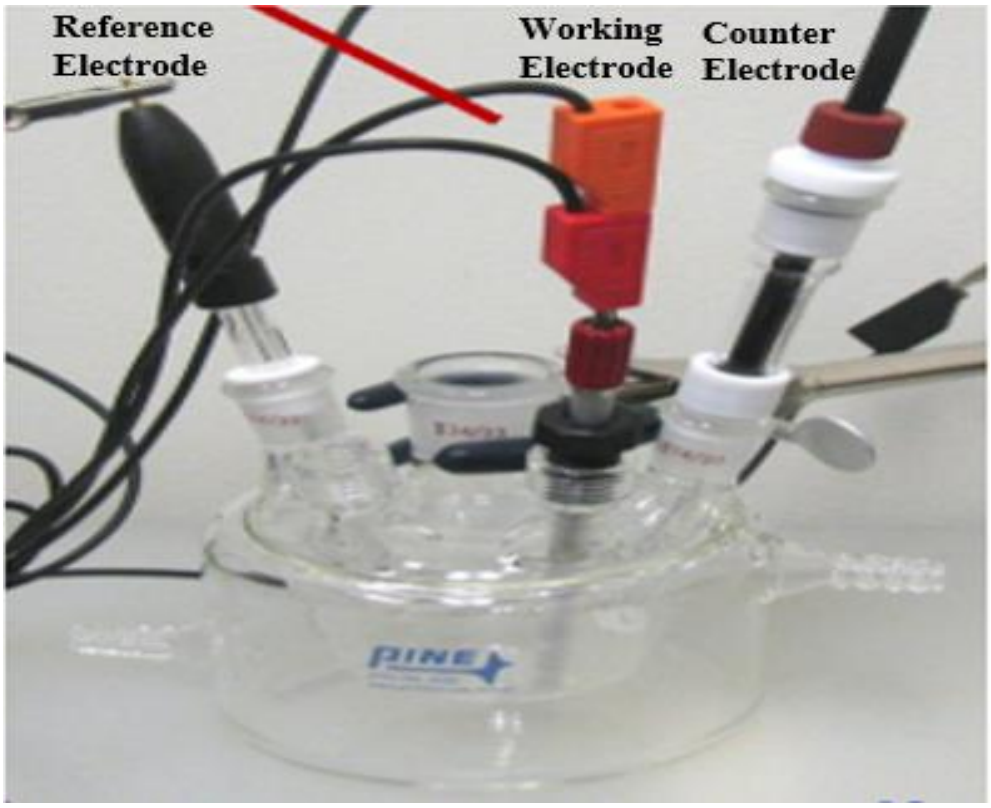

Figure 2.2. A typical three electrodes system showing the electrochemical cell and the three electrodes.

Electrolytes: The electrolyte, sometimes called the supporting electrolyte, is the medium in which an electrochemical analysis takes place. An analyte requires a dissolving medium prior to its analysis. Salts highly concentrated than the analyte of interest are often used as electrolytes. In addition, they must be highly conducting to ensure a quick electron transfer from the analyte to

the working electrode [54, 55]. The supporting electrolyte contributes to the completion of the circuit by providing ions to balance the electrons produced by the working electrode. Aqueous KCl is mainly used as supporting electrolytes in most current electrochemical setups [56, 57].

In some cases, other electrolytes like ammonium salts dissolved in dichloromethane or acetonitrile are used. A buffer solution can be employed as the electrolyte when the pH of the medium is crucial for the analyte's solubility or the replication of a biological media. Common examples of buffer solutions include phosphate buffer saline PBS, and acetate buffer, among others. It should be noted that while choosing a supporting electrolyte for an electrochemical reaction, high consideration must be given to the purity and chemical inertness of the electrolytes concerning the analyte.

2.4 Electroanalytical Methods

Electroanalytical methods are techniques used to determine the quantity of an analyte in chemical reactions based on the relationship between an analyte’s concentration and potential (or current). It is a quantitative analysis method based on electrochemical processes within a medium or at the interface between a sensor and a medium. These electrochemical processes are influenced by the analyte concentration, structural changes during analysis, or chemical composition. Electroanalytical methods involve the use of electrochemical techniques incorporated with electrochemical sensors in detecting analytes of interest. Electroanalytical methods have tremendous advantages over other methods. In addition to aiding in determining the elemental concentration in solutions, they can also determine an element's oxidation states. Beyond these, electroanalytical methods offer simplicity, low detection limits, rapid analyte detection, good characterization, cost-effectiveness, and valuable information on chemical reaction kinetics [58-60]. These methods have been employed successfully for detecting various analytes such as ascorbic acid, dopamine, nitrite, citric acid, iodate, hydrazine, glucose, oxalic acid, glutathione, epinephrine, phthalates, hydroquinone, peroxide, to mention few [61]. The electrochemical techniques include cyclic voltammetry CV, amperometry AP, differential pulse voltammetry DPV, square wave voltammetry SWV, electrochemiluminescence ECL, and electrochemical impedance spectroscopy EIS, among others.

2.4.1 Cyclic Voltammetry CV

CV is a widely used voltammetric electroanalytical method that provides qualitative and quantitative information about electrochemical processes, such as the reversibility of reactions, electrocatalytic processes, reaction mechanisms, electrochemical kinetics, and other features. It provides rapid qualitative information on catalysts and electrochemical reactions, including the electrochemical response of catalysts, their interactions with the electrolyte, and their catalytic activity [62]. CV offers fast information about the kinetics of heterogeneous electron-transfer reactions, thermodynamic redox processes, and adsorption processes or coupled chemical reactions [63].

A potentiostat is an instrument used in the technique. The experiment is usually conducted in a three-electrode system or electrochemical cell containing a reference electrode, counter electrode, and working electrode with a suitable supporting electrolyte [63, 64]. The working electrode potential in the understudied system is measured in relation to the reference electrode during a CV measurement, and the potential is then alternately scanned between predetermined upper and lower limits. At the same time, the current flowing between the working electrode and the counter electrode is measured. This is plotted against the potential to obtain the analyte's cyclic voltammogram CV. Typically, the potential is linear over time, with a slope corresponding to the potential's scan rate. The potential scan rate, the working electrode's condition, and the electrolyte's composition all significantly impact the current flowing through them [64, 65].

The analyte oxidation and reduction potentials and the diffusion coefficients of species involved in the electrochemical reaction are also found by thoroughly examining the cyclic voltammogram.

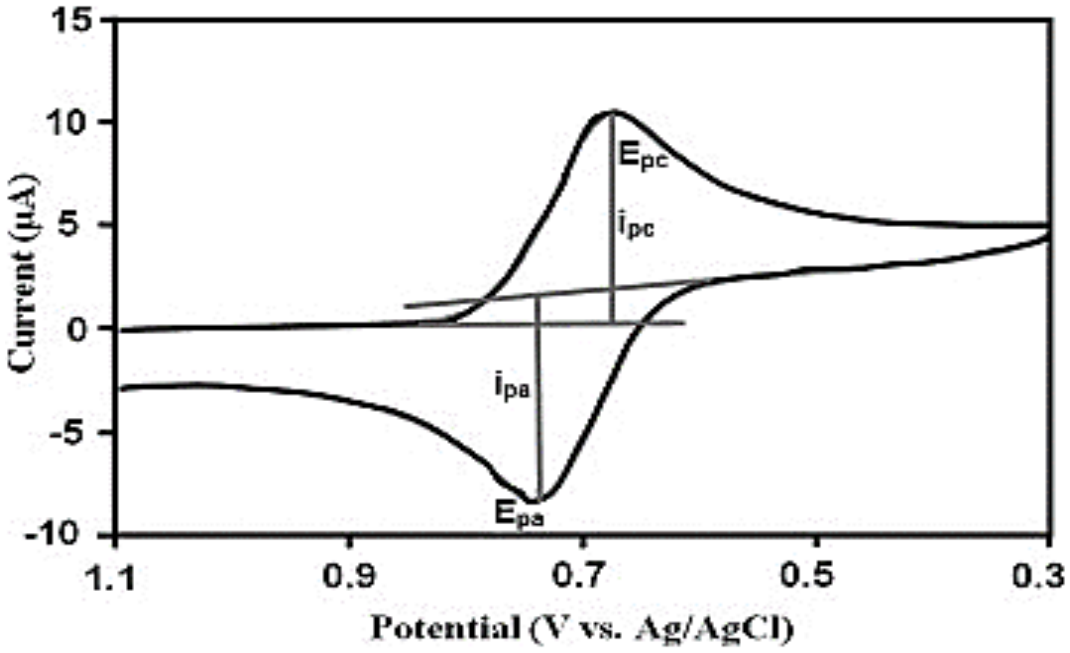

Figure 2.3. A typical cyclic voltammogram.

Figure 2.3 depicts a typical cyclic voltammogram of a diffusion-controlled and electrochemically reversible redox process. In a CV, the anodic peak currents (i_{pc}), the cathodic peak currents (i_{pa}), the anodic peak potentials (E_{pa}), and the cathodic peak potentials (E_{pc}) are the most important parameters. By the International Union of Pure and Applied Chemistry (IUPAC) convention, both anodic and cathodic currents assume to be positive and negative.

A plot of √v against I_p gives a curve from which the surface area of the electrode can be obtained using the Randle Sevcik equation given in equation 2.3.

$$I_p = 0.4463nFAC_o\left(\frac{\mathrm{nFvD}_o}{\mathrm{RT}}\right)^{\frac{1}{2}} \qquad (2.3)$$

Where,

i_p presents the peak current in *A*;

n presents the number of electrons involved in the redox reaction;

F stands for Faraday's constant in C mol^{-1});

A stands for the electrode's surface area in cm^2;

R stands for the molar gas constant in $J.mol.K^{-1}$;

D stands for the diffusion coefficient in $cm^2\ s^{-1}$;

C denotes the bulk concentration of the electroactive species in mol cm^{-3};
K denotes the absolute temperature in K; and
v denotes the scan rate in V s^{-1}.

By taking the temperature as 298.15 °K (25 °C), all the constant terms can be evaluated as one, and the equation becomes (Eqn. 2.4)

$$I_p = (2.69 \times 10^5) n^{\frac{3}{2}} A C_o (D_o v)^{\frac{1}{2}} \quad (2.4)$$

The unit of the single constant term (2.687 x 10^5) becomes $C.mol^{-1}.V^{-1/2}$
The electroactive surface coverage of the electrode can be obtained from Equation 2.5.

$$I_p = \left(\frac{n^2F^2}{4RT}\right) vAr \quad (2.5)$$

The number of transferred electrons can as well be calculated from equation 2.6 if the quantity of charge Q is known.

$$I_p = \frac{nFQv}{4RT} \quad (2.6)$$

The equilibrium potential of the redox process is related to the peak positions on the potential axes (E_p). A reversible couple's equilibrium potential is obtained from the difference between E_{pa} and E_{pc} as expressed in equation 2.7.

$$E_o = \frac{E_{pa} - E_{pa}}{2} \quad (2.7)$$

The peak potentials difference of a reversible couple can be employed for determining the number of electrons transferred, which also validates the Nerstian behavior, as shown in equation 2.8.

$$\Delta E_p = E_{pa} - E_{pc} = \frac{0.059}{n} \quad (2.8)$$

A reversible process is also expected to have the value of I_{ap}/I_{cp} as 1; the nearer this value is to 1, the more reversible the process.

The kinetics of redox processes at an electrode can be investigated using the Laviron equation [64]. The charge transfer coefficient (α) can be calculated from the slope of a plot of ln v versus peak potentials in either equation 2.9 or 2.10. The rate constant, k_s can be calculated from Equation 2.11.

$$E_{pa} = a + \left(\frac{RT}{(1-\propto)nF}\right) \ln v \quad (2.9)$$

$$E_{pc} = b + \left(\frac{RT}{\propto Nf}\right) \ln v \quad (2.10)$$

$$Logk = \propto \log(1-\propto) - \log\left(\frac{RT}{nFv}\right) - \propto (1-\propto)\left(\frac{Nf\delta e}{RT}\right) \quad (2.11)$$

CV has received wide applications in the electrochemical characterization of nanomaterials for analyzing food stuff additives, herbicides, pollutants, drugs, and insecticides.

2.4.2 Square Wave Voltammetry (SWV)

SWV is a potent electrochemical method ideal for electroanalytical applications, electrokinetic measurements, and mechanistic studies of electrode processes. Square wave voltammetry combines the advantages of different pulse voltammetric techniques, such as the diagnostic value of normal pulse voltammetry (NPV), the sensitivity and background suppression of differential pulse voltammetry (DPV), and the capability to directly interrogate products in the manner of reverse NPV [66, 67]. In a SWV experiment, the working electrode's potential is stepped from an initial potential to a final potential using a series of forward and reverse pulses. The square amplitude determines the forward step, and the square increment is subtracted from the square amplitude to calculate the reverse step. A typical square wave voltammogram with an increase in analyte concentration. A typical square wave voltammogram showing an increase in peak current with an increase in analyte concentration is depicted in figure 2.4. The measurement of current at each pulse helps in background (charging) current reduction. SWV offers excellent sensitivity and high rejection to capacitive currents and is thus widely employed in developing sensors and biosensors owing to its high selectivity and sensitivity [66, 68].

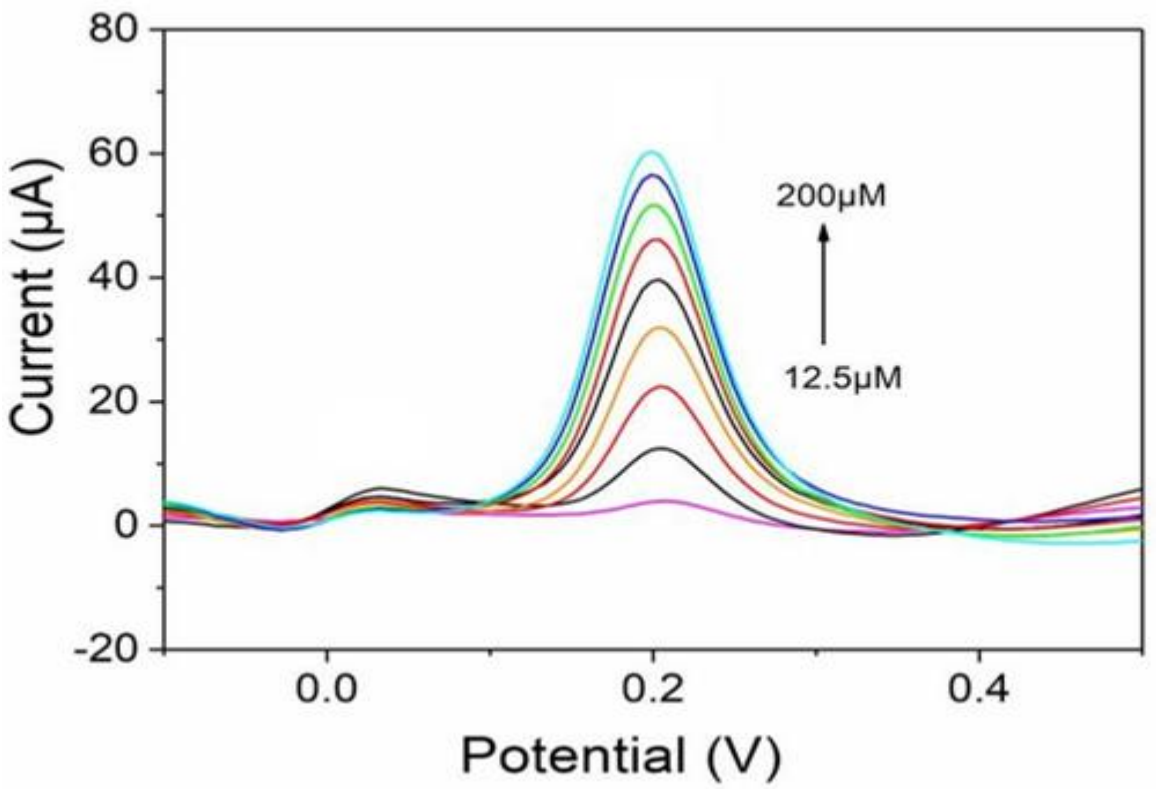

Figure 2.4. A typical square wave voltammogram with an increase in analyte concentration.

2.4.3 Electrochemical Impedance Spectroscopy (EIS)

EIS is a powerful technique for characterizing several electrical properties of materials and their interactions with electronically conducting electrodes [69]. Impedance spectroscopy has remained a valuable technique due to its ability to differentiate between the electric and dielectric properties of various contributions of the components under study. EIS is a non-destructive technique that offers time-dependent quantitative data regarding electrode processes, intricate interfaces, and some material properties, including high-resistance materials [70]. EIS has been widely employed as a standard technique for analyzing several material systems and applications such as fuel cells, corrosion, batteries, and plating) [71].

The electrochemical impedance technique determines the electrode's response to a sinusoidal potential modulation at various frequencies. EIS evaluates the impedance based on the applied alternating current ac potential frequency. Impedance is determined by passing a small, known-frequency, low-amplitude alternating current through a system to calculate the phase difference and amplitude of the resulting electrical potential [72]. The imaginary and real impedances are estimated using this data and plotted against one another for various perturbation frequencies. Due

to the inherent properties of many materials, impedance changes with changes in the frequency of the applied voltage. This could result from its physical makeup, internal chemical activities, or a combination [72]. Similar to Ohm's law, electrochemical impedance is defined as the quotient of the voltage-time function v(t) and the corresponding current-time function i(t):

$$Z = \frac{E(t)}{I(t)} \tag{2.12}$$

The Nyquist plot or Cole-Cole plot is a common format for analyzing EIS data which involves plotting the imaginary impedance component (Z'') against the real impedance component (Z') at each excitation frequency. The Nyquist plot highlights circuit elements within a series and makes it simple to visualize the effects of the ohmic resistance. However, this plot does not give a precise frequency, while the electrode capacitance can only be calculated until the frequency information is known, even though the charge transfer resistance and ohmic resistance can be easily read directly from the Nyquist plot [70].

The Bode plot is a plot of the impedance modulus versus the logarithm of the frequency. Given that one of the axes in this figure is frequency, it is simple to grasp how impedance varies with frequency. A very wide frequency range can be shown on one graph using the logarithm of frequency, but each decade is given equal weight. The Bode plot also lessens the longer measurement periods related to low-frequency measurements of charge transfer resistance since the plot of log |Z| versus log ω plot occasionally enables a more successful extrapolation of data from higher frequencies. However, the plot's curves can alter in shape if the circuit values change, such as uncompensated resistance [70].

Nevertheless, both plots are usually used to analyze EIS data. The EIS data are commonly interpreted with equivalent circuit element models. The EIS data are generally interpreted with the aid of equivalent circuit element models. These models are constructed using distributed elements like Warburg impedance and constant phase elements in addition to commonly used passive elements like resistors, capacitors, and inductors. When these elements are combined in parallel or series, they generate a complex equivalent circuit. The individual equivalent circuit elements are then given specific physical meanings. The equivalent circuit element model offers a fast visualization tool for comprehending the system behavior. Using these model equations, the electrochemical impedance can be calculated as a frequency function and verify the theoretical model's conformity with experimental data, employing commercial software, Autolab® with frequency response analyzer (FRA) [73]. A standard electrochemical impedance experimental

setup is made up of an electrochemical cell, a potentiostat/galvanostat with a frequency response analyzer (FRA). The FRA applies the sine wave and measures the system's response to generate the system's impedance.

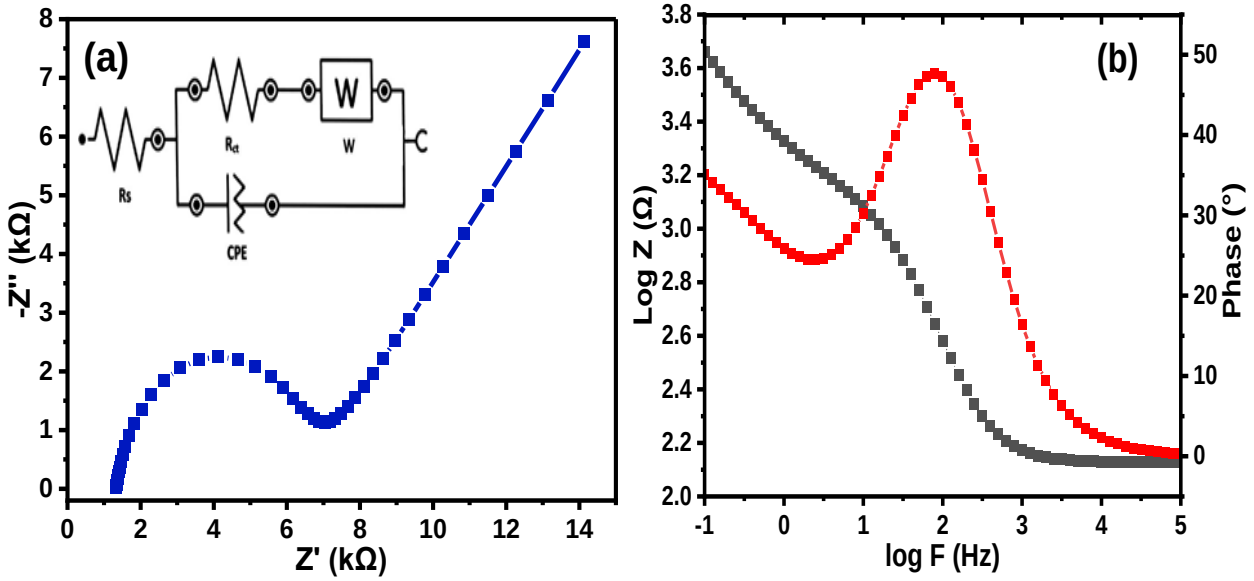

Figure 2.5. Typical (a) Nyquist plot with equivalent circuit used for EIS data fitting and (b) Bode plot and phase angle diagram.

From these plots (Figure 2.5), information regarding the capacitive behaviors of the electrode under investigation can be obtained. The “knee” frequency (f°), a measure of a supercapacitor’s power capability, is defined as the transition point between the low-frequency and high-frequency components. The larger the f°, the faster the supercapacitor charge and discharge capability, or the greater the power density of the supercapacitors [74].

A phase angle is a linear approach for assessing the relationship between reactance and resistance in either parallel or series circuits. The phase angle value is obtained from the Bode plots of phase angle (°) vs. log f°, and it determines whether the material possesses an ideal capacitive property or not. If the phase angle value is 0°, the circuit is only resistive; at 90° circuit is an ideal capacitive, while at 45°, the circuit is a non-ideal capacitor i.e, an equal amount of capacitive resistance and reactance [74].

Similarly, the slope value from the graph of log |Z| against log f° is also a useful parameter for investigating the capacitive behaviors of a material. A slope value of 1 indicates pure capacitive behaviors, while values less than 1 suggest that the studied material is a high-specific-capacitance,

high-energy-density hybrid supercapacitor that combines the faradaic pseudocapacitive and electric double-layer system [75, 76].

2.5 Application of CoPcMWCNTs and NiPcMWCNTs Nanocomposites as Electrochemical Sensing Materials

One of the most important and quickly expanding fields in materials science is the construction of novel electrochemical sensing materials with improved electrocatalytic characteristics, good reproducibility and repeatability, high stability, high selectivity and sensitivity [77]. Carbon nanotubes (CNTs) have been a material to be reckoned with for fabricating sensors of diversified applications owing to their outstanding mechanical strength, chemical inertness, exceptional one-dimensional structure that enables quick electron transfer, sizable surface area and good electrical conductivity [78]. The usefulness of CNTs has manifested in many areas such as energy storage materials, electronics, catalysis, sensors, polymer composites and gas storage materials [79]. Multiwalled carbon nanotubes (MWCNTs) have a large specific surface area, strong mechanical strength, and improved surface activity. They are commonly used in structural materials, thermally stable materials, water filtration, sensor fabrication, and biological applications [80, 81]. Moreover, the MWCNTs functionalized with acid (fMWCNTs) are also attractive as catalyst supports because they can be connected to organic molecules in multiple ways [32]. It has been established by research that MWCNTs can transfer electrons rapidly in both acidic and basic medium, resulting to a reduced redox potential and a huge current density. In this way, MWCNTs outperform single-walled carbon nanotubes in terms of redox activity (SWCNTs) [82]. Notably, both MWCNTs and SWCNTs have been widely exploited as a sensing material to produce several nanocomposites that have been effectively used to determine a variety of analytes. such as styrene, epinephrine [82, 83], thiols, carbaryl, bisphenols [84-86], ascorbic acid, uric acid, dopamine [87, 88], paracetamol hydrogen peroxide [89, 90], cysteine, glutathione, acetaminophen [91, 92], hydrazine, lactic acid, glucose [93-95], nitrite, bromate, [96], and others.

A phthalocyanine (Pc) is a macrocyclic compound with a central planar molecule and a delocalized 18- π electron system on carbon-nitrogen double bonds [74]. Phthalocyanine is one of the important chemicals with numerous applications including electrochemical sensors, photovoltaic cells, electrocatalysis, liquid crystal materials, photodynamic therapy, catalyst, and photosensitizer because of their good spectral performance and high stability [33, 97, 98]**.** The presence of

hydrogen bonds, coordination interactions, and van der Waal forces allow Pc to bind a variety of analytes in an indifferent way [99]. The chemical and thermal stability of these materials makes them an essential component of electrochemical sensor. In addition, the ability to accommodate up to 70 different metal atoms into the rings and to vary the side chain substituents result in unique and efficient thin films with varying degrees of selectivity, stability, and sensitivity [74].

The metal phthalocyanines (MPcs) have recently attracted much attention for their catalytic properties. In metal phthalocyanine, the central metal ions play a major role in its high catalytic activity [32, 100]. The high activity and selectivity for oxidation processes makes cobalt phthalocyanines (CoPc) stand out among the MPcs for a wide range of organic reactions [32, 101-103]. Due to its electrical, semi-conductor, and catalytic properties, CoPc has been utilized extensively as a mediator in electrochemical sensors fabrication and in electronic devices. In addition, it may be attached to cationic substrates using straightforward adsorption procedures [104, 105]. Besides, the exceptional electrocatalytic activity of CoPc for a variety of compounds, quick electron transfer capability and its rich redox chemistry have made it more widely used in sensor development [93].

The core metal of the CoPc can easily alter its coordination environment, thus significantly boosting its selectivity and catalytic activity. The ease with which organic groups can be substituted in the axial and equatorial positions of the complex, resulting in a variety of functionalities for anchoring complexes in solid substrates, is one of CoPc's outstanding properties that makes it a superior material in fabricating electrochemical sensors [106-109]. The six coordination sites of the core metal ions in MPc (as shown in Figure 2.6) include two additional coordination sites in addition to the four N coordination sites. By adding an axial ligand, the MPc can be fastened to the carrier in an axial coordination way, enhancing the catalyst's stability, selectivity, and activity [110-113].

A series of approaches have been developed to synthesize CoPcMWCNTs, including ultrasonic impregnation, solid phase synthesis, chemical deposition, amide bridge synthesis, electropolymerization, and drop coating. CoPcMWCNTs nanocomposites are formed by the π-π interactions between the -COOH of acidified functionalized MWCNT and the -NH_2 terminal of CoPc composites. Through these π-π interactions, CoPc molecules can be anchored on the wall of MWCNTs by axial coordination to achieve molecular dispersion of CoPc on MWCNTs. The axial

coordination of metal phthalocyanine also provides another driving force for immobilization, which invariably increase the electrocatalytic activity, selectivity, and stability of the nanocomposites. Additionally, the high solubility of CoPc offers a huge advantage in fabricating several sensors due to its film-forming capacity with a polyelectrolyte positively charged, which are widely used in layer-by-layer (LbL) method and LB method of film forming [114-116].

Researchers have found that phthalocyanine–CNT complexes exhibit excellent catalytic properties of Pc while retaining all the electronic properties of carbon nanotubes [117]. Moreover, PCs have been widely studied for functionalizing CNTs because they demonstrate rich electronic and photoelectronic properties, which make CNTs-based devices more efficient. Recent reports show that MPc-CNTs hybrids exhibit enhanced electrochemical responses compared to CNTs or MPc alone [118]. According to reports in the literature, redox overpotentials are decreased, and electrode faradaic currents are increased when thin films of MPcs are immobilized on working electrodes together with other highly conductive materials [119, 120]. Noteworthy, incorporating metallic nanoparticles and carbon-based components (grapheme, sheets, MWCNTs, quantum dots, SWCNTs) into the MPc-based films increases its conductivity [121]. With these conductivity-enhancing materials, electron transfer is faster between the surface of the electrode and the analytes adsorbed on the thin film. In addition, electrochemical sensors produced from MPcs and other nanomaterials exhibit large electroactive surface areas for an improved immobilization of analytes compared to bare electrodes [119].

CoPcMWCNTs and NiPcMWCNTs nanocomposites have recently been studied and exhibit improved capacitive behavior due to the enlarged surface area of the phthalocyanine and MWCNTs, as well as the excellent conductivity and stability of cobalt/Nickel and the MWCNTs [122]**.** The top qualities of MWCNTs, Cobalt (Co)/nickel (Ni), and Pc, are combined to construct electrochemical sensors with high current response, huge capacitance, remarkable cycling stability, good repeatability and reproducibility, high sensitivity, and selectivity. Electrochemical sensors fabricated with CoPcMWCNTs and NiPcMWCNTs nanocomposites have been employed to determine numerous types of analytes with outstanding performances ranging from the low limit of detection and high sensitivity to a wider concentration range. Hence, the main reason for the wide usage of these nanocomposites in fabricating electrochemical sensors, either alone or in combination with other conducting materials. A detailed discussion on the detection of various

analytes using CoPcMWCNTs and NiPcMWCNTs nanocomposites is presented in the subsequent sections.

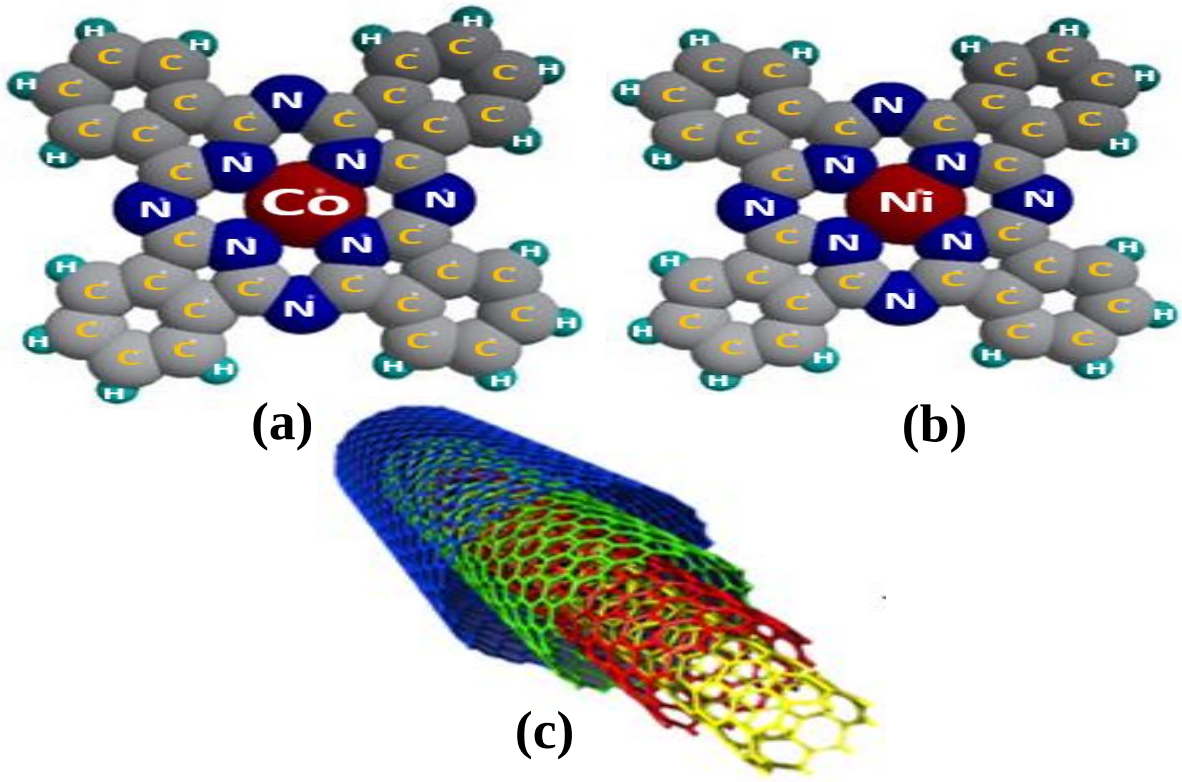

Figure 2.6. Diagram of (a) CoPc, (b) NiPc, and (c) MWCNTs.

2.5.1 Application of CoPc-MWCNTs Nanocomposites

2.5.1.1 Detection of Ascorbic Acid, Dopamine, Paracetamol

Kutluay and Aslanoglu [123] developed an electrochemical sensor to simultaneously detect dopamine (DA) and paracetamol (PAR) via chemical deposition. The SEM image of the prepared CoNPs/MWCNT/GCE clearly shows the surface of the MWCNTs having spherical and evenly dispersed CoNPs. The CoNPs/MWCNT/GCE could simultaneously detect DA and PAR in 0.1 M phosphate buffer solution PBS (pH 7) using square wave voltammetry (SWV). The electrode exhibited a good linear concentrations range of 0.05 – 3.0 μM and 0.0052 – 0.45 μM for DA and PAR, respectively. A limit of detection (LoD) of 0.015 and 0.001 μM were obtained for DA and PAR, respectively. The developed electrode exhibited good stability, reproducibility, repeatability, and high recovery. An interference study showed that UA and AA did not affect the detection of

PAR and DA. This technique accomplished the determination of PAR and DA in pharmaceutical drugs.

Xia Zuo and his research group [124] fabricated CoPc-MWCNTs/GCE electrode via a drop coating method to determine ascorbic acid (AA). The fabrication of CoPc-MWCNTs nanocomposites was actualized by exploiting the advantage of strong non-covalent interactions between the highly delocalized π-bonding network of MWCNTs and the metal phthalocyanines conjugated ring. This consequently influenced the electrode performance having strong electrocatalytic activity toward AA with the oxidation potential of the AA simultaneously decreased. The study revealed that the fabricated electrode exhibited enhanced electrocatalytic behavior towards the oxidation of ascorbic acid in 0.1 M PBS at a pH of 7. The biosensor offered a LoD of 1 μM and a wider concentration range of 1.0 X 10^{-5} M to 2.6 × 10^{-3} M. The CoPc-MWCNTs/GCE electrode is characterized by high stability, high reproducibility, and fast response time. A complex interaction occurs between the central metal ion and the activated AA as it diffuses from the bulk solution to the sensor surface and is adsorbed on the macrocyclic 18-electron conjugated system of phthalocyanine that is bonded to the MWCNTs surface. The Co^{III}/Co^{II} absorb the electrons lost from AA and transfer them to MWCNTs on the hydrophobic surface of the GCE. The authors also established that the CoPc-MWCNTs/GCE modified electrode exhibited good selectivity for AA determination in the presence of glucose, potassium chloride, l-phenylalanine, citric acid, and uric acid.

Jilani et al. [125] have fabricated a GCE/MWCNT-CoTMBANAPc electrode to simultaneously detect ascorbic acid and dopamine in PBS at a pH of 7.0 via AP and differential pulse voltammetry (DPV). The tetra8[(*E*)(4methoxybenzylidene)amino] naphthalene1amine cobalt (II) phthalocyanine (CoTMBANAPc) was synthesized from cobalt (II) tetracarboxylic acid phthalocyanine (CoTCAPc) via amide bridge. The fabricated sensor determined both AA and DA with a low LoD of 0.33 and 6.6 μM for DA and AA, respectively, and a limit of quantification from 1 to 15 μM. The authors reported that the fabricated sensor exhibited high selectivity for AA and DA amidst interferents like glycine, glucose, hydrogen peroxide, tyrosine, and L-cysteine. The stability, reproducibility, and sensitivity of the fabricated electrode were good.

Another CoPc-MWCNTs-based sensor for dopamine and paracetamol detection from Mounesh and Reddy [126] was produced by drop-casting tetra 1-benzyl-1H-pyrazol-3-carboxamide

cobalt(II) phthalocyanine (CoTBPCAPc) with MWCNTs on a GCE's surface. In 0.1 M PBS (pH 7), the CoTBPCAPc/MWCNTs/GCE electrode's electrocatalytic activity towards DA and PAR was performed using cyclic voltammetry (CV), DPV, and chronoamperometry (CA). The developed sensor displayed excellent DA and PAR detection performance in linear ranges of 50 to 750 nM, with a LoD of 17 and 19 nM, respectively. The authors described the sensor with high stability, excellent reproducibility, and repeatability. The sensor gave satisfactory results when applied to detect DA and PAR in both commercial and urine samples.

Again, Moraes and his research team [127] used CoPcMWCNTs/GCE modified electrodes to fabricate an electrochemical sensor to detect dopamine in ascorbic acid. Under optimum conditions, in 0.2 M PBS (pH 4.0), dopamine was successfully detected by the CoPcMWCNTs/GCE modified electrode via DPV with a low LoD of 0.256 μM and a wide LDR of 3.11 to 93.2 μM. The authors described the sensor as reliable for determining DA due to its exceptional qualities, including good stability, repeatability and reproducibility, high sensitivity, and selectivity.

A summary of the analytes detected with CoPc-MWCNTs modified electrodes with the techniques employed, LoD, and LDR is given in Table 1.

Table 1. Detection of ascorbic acid, dopamine, and paracetamol with CoPc-MWCNTs modified electrodes.

Electrode	**Analyte**	**Technique**	**LoD** (μM)	**LDR** (μM)	**Ref**
CoNPs/MWCNT/GCE	Dopamine	SWV	0.015	0.015-3	[123]
	Paracetamol	SWV	0.001	0.005-0.45	[123]
CoPc-MWCNTs/GCE	Ascorbic acid	CV	1	10-2600	[124]
MWCNT-CoTMBANAPc/GCE	Ascorbic acid	AP	6.6	$7.5x10^{-3}$-0.07	[125]
	Dopamine	DPV	0.33	$7.5x10^{-3}$-0.07	[125]
CoTBPCAPc/MWCNTs/GCE	Dopamine	CA	0.017	0.05-0.75	[126]
	Paracetamol	CA	0.019	0.05-0.75	[126]
CoPcMWCNTs/GCE	Dopamine	DPV	0.256	3.11-93.2	[127]
Pt-CoPc-MWCNTs/GCE	Dopamine	SWV	2.6	5-170	[128]

2.5.1.2 Detection of Hydrogen Peroxide, Nitrite and Heavy Metals

Mounesh and Reddy [129] accomplished the fabrication of the CoPcMWCNTs/GCE for the detection of heavy metals (Pb^{2+} and Cd^{2+}) in water. Electro-spraying was explicitly used to modify the CoTEIndCAPc/MWCNTs on the GCE since it forms particles with a sizable surface area that can potentially provide a fast electron transfer and ultra-high sensitivity for Cd^{2+} and Pb^{2+} detection. The modified CoPc-MWCNTs/GCE detected both Pb^{2+} and Cd^{2+} with a very low LoD of 9 and 10 nM in PBS at a pH of 7.0 via DPV and CA techniques. The electrocatalytic property of the CoPc-MWCNTs/GCE electrode was characterized by high reproducibility and repeatability. This sensor displayed an excellent selectivity for both Cd^{2+} and Pb^{2+} in the presence of other similar ions (Al^{3+}, Ca^{2+}, Cu^{2+}, Mg^{2+}, Mn^{2+}, Zn^{2+}, As^{3+}, $Cr^{3+,}$ and Fe^{3+}). The sensor's excellent selectivity for Cd^{2+} and Pb^{2+} ions is attributed to the selective movement of the analyte ions from the buffer solution to the electrode surface, owing to the stronger affinity of CoTEIndCAPc/MWCNTs/GCE electrode for Cd^{2+} and Pb^{2+} ions. The electrode was also applied to determine Pb^{2+} and Cd^{2+} in river water.

Mounesh and Reddy [99] fabricated another CoPc-MWCNTs/GCE to simultaneously detect hydrogen peroxide (H_2O_2) and nitrite using CV, CA, and DPV techniques. The best electrocatalytic oxidation of CoPc-MWCNTs/GCE was achieved in PBS solution (pH 7.0) with high stability, repeatability, reproducibility, and sensitivity. The authors found that the electrocatalytic oxidation of CoPc-MWCNTs/GCE towards nitrite and hydrogen peroxide was diffusion controlled with specific adsorption of electro-redos process and intermediates products. The electrode offered a good linear concentration between 0.1 and 0.8 μM and a low LOD of 10nM and 30 nM for H_2O_2 and nitrite via CV. The developed sensor utilized the advantage of simple preparation, low cost, high selectivity, and real sample application (in beetroot vegetables).

Lu et al. [130] presented a nitrite sensor using CoPcMWCNTs nanocomposite GCE modified electrode. Using the DPV technique, the developed CoPcMWCNTs/GCE electrode detected nitrite in 0.1 M PBS at a pH of 7.4 in a linear dynamic range (LDR) from 0.01 to 1050 mM and a detection limit of 2.11 μM. Thus, the electrode is said to be a facile, sensitive, and rapid electrochemical technique for detecting nitrite. Aside from this, it also offers good stability, sensitivity, and reproducibility. The outstanding performance of the fabricated sensor is attributed to the synergistic interaction of MWCNT and CoPc, thereby demonstrating the potential applications of

CoPcMWCNTs/GCE in real-life biosensing analysis. The sensor's selectivity investigation showed that nitrite detection was unaffected by the presence of these interferents (CH_3COONa, NaCl, $NaNO_3$, Na_2SO_4, KCl, ascorbic acid, and glucose).

Table 2 below summarises the analytes detected with CoPc-MWCNTs modified electrodes with the techniques employed, LoD and LDR.

Table 2. Detection of hydrogen peroxide, nitrite, and heavy metals with CoPcMWCNTs modified electrodes.

Electrode	Analyte	Technique	LoD µM	LDR µM	Ref
CoPc-MWCNTs/GCE	H_2O_2	CV	0.01	0.1-0.8	[99]
	Nitrite	CV	0.03	0.05-0.75	[99]
CoPc-MWCNTs/GCE	Cd^{2+}	CV	0.01	0.1-1	[129]
		DPV	0.006	0.1-1	[129]
		CA	0.005	0.1-1	[129]
	Pb^{2+}	CV	0.009	0.1-1	[129]
		DPV	0.005	0.1-1	[129]
		CA	0.01	0.1-1	[129]
CoPcMWCNTs/GCE	Nitrite	DPV	2.11	$10\text{-}1.1x10^6$	[130]
$CoTPEG_2BAPc$-MWCNTs/GCE	H_2O_2	CV	1.5	5–25	[131]
		DPV	5	2–22	[131]
		CA	10	5–50	[131]

2.5.1.3 Detection of Carbaryl, Acetaminophen, Epinephrine, and Procalcitonin

Moraes and his research group [132] fabricated a sensor by modifying GCE with MWCNTs/CoPc nanocomposites prepared through ultrasonic impregnation of CoPc onto the MWCNTs. The fabrication and modification process of CoPcMWCNTs nanocomposite with GCE are shown in Figure 2. The fabricated MWCNTs/CoPc/GCE film electrode was employed to detect carbaryl in acetate buffer solution (pH 4.0) via SWV. The sensor gave an LDR and LoD of 0.33–6.61 µM and 5.46±0.02 nM, respectively. The sensor was proven suitable in carbaryl spiked water samples.

Aragao and his research group [133] developed an electrochemical sensor for diethylstilbestrol (DES) detection by modifying GCE with gold (Au) nanoparticles and CoPcMWCNTs

nanocomposites via electrodeposition. Prior to this, the synthesis of the nanocomposites was achieved through an ultrasonication method. The mechanism of the oxidation of DES on the CoPcMWCNTs/AuNPTs/GCE (which was mainly an adsorption-controlled process) involves two-step processes with one electron each. The first step is oxidizing neutral DES molecule to phenoxy ion, while the second step is the formation of phenoxonium anion. The developed CoPc-fMWCNTs/Au/GCE catalyzed diethylstilbestrol's electrochemical oxidation and enhanced its sensitivity compared with the unmodified electrode. Using the SWV technique, DES was determined in Britton-Robinson (BR) buffer solution (pH 10) with a LoD of 0.199 μM and quantification limits of 0.664 μM. An interference study showed that most ions and molecules (K^+, Na^+, Ca^{2+}, Mg^{2+}, Zn^{2+}, Pb^{2+}, Al^{3+}, Cl^-, NO_3^-, SO_4^-, $H_2PO_4^-$, ascorbic acid, citric acid, glucose, uric acid, dopamine, and urea) did not interfere the detection of DES, indicating the good anti-interference ability of the electrode. The excellent reproducibility and repeatability exhibited by the developed electrode indicate the suitability of the electrode modification for DES detection. The proposed sensor was successfully employed to determine DES in meat, and water with satisfying outcomes, indicating that the developed sensor is reliable for DES detection in complex samples.

To present a sensing platform for acetaminophen detection, Kantize et al. [119] ultrasonically fabricated CoPc/MWCNTs nanocomposite, which was then modified on a GCE using a drop-dry method. The CoPcMWCNTs/GCE electrode exhibited good stability and sensitivity in CV experiments. The best electrocatalytic behavior of the electrode for acetaminophen detection was achieved in 0.1 M PBS at a pH of 7.4, giving a LoD of 1 μM and LDR of 0.975–1000 μM. The fabricated electrodes also showed excellent selectivity when tested in various pharmaceutical interferent species.

Furthermore, Holanda and his research group [134] have used functionalized multiwalled carbon nanotubes, gold nanoparticles, cobalt (II) phthalocyanine, and GCE for fabricating a sensor for acetaminophen detection. The preparation involves ultrasonic mixing of fMWCNT and CoPc in dimethylformamide (DMF) followed by drop-drying the fMWCNT-CoPc suspension on the AuNPs/GCE to obtain the fMWCNT-CoPc/AuNPs/GCE. A very low charge transfer resistance (Rct) value obtained for the fMWCNT-CoPc/AuNPs/GCE modified electrode via an EIS experiment confirms that the modification of fMWCNT-CoPc and AuNPs onto the GCE

significantly enhanced the electron transfer, predominantly due to the high conductivity of AuNPs and the improved catalytic activity from the synergy effect between CoPc and fMWCNTs since the CoPc acts as a charge transfer mediator. The fabricated sensor reached a detection limit of 0.135 μM within the linear range of 1.49 to 47.6 μM. The fabricated sensor was used to detect acetaminophen in four sample matrices of commercial pharmaceuticals with good recovery to prove the real sample application.

Moraes and his research team [135] produced another electrochemical sensor for the detection of epinephrine (EP) in urine using a paraffin composite electrode PCE modified with cobalt phthalocyanine and multiwalled carbon nanotubes. In 0.1 M PBS at a pH of 6.0, the CoPcMWCNT/PCE electrode successfully detected epinephrine via differential pulse voltammetry with a limit of detection (LoD) of 15.6 nM and a wide linear range LDR of 1.33 - 5.50 μM. The authors established that the sensor is reliable for determining epinephrine due to its good stability, repeatability and reproducibility, sensitivity, and selectivity.

Agboola and his research team [136] constructed another sensing platform for epinephrine detection by modifying edge-plane pyrolytic graphite (PG) electrode with CoPc and acid-functionalized SWCNTs. The modification process involves the drop-dry method and electrodeposition. SWCNTs was first modified on the PG electrode by the drop-dry method, followed by the electrodeposition of the CoPc complex on the PG containing SWCNT. The edge-plane PG/SWCNTs-CoPc electrode displayed suitable electrocatalytic properties towards epinephrine oxidation with enhanced peak currents. At a pH of 7.4 in 0.1 M PBS, the fabricated sensor detected epinephrine with high sensitivity, low LoD, and good limit of quantification of 8.71 ± 0.31 A.M^{-1}, 0.04 μM, and 1.31 μM, respectively. Good reproducibility, high stability, high selectivity, and sensitivity are the attributes of the electrode. It was also found that ascorbic acid did not interfere with epinephrine analysis. The sensor was employed to determine epinephrine in epinephrine tartaric acid injection solution with good recovery.

Yang and his research group [137] constructed an immunosensor using nanoCoPc-fMWCNTs/GCE to detect procalcitonin (PCT). Figure 2.7 illustrates the stepwise preparation of the nanoCoPc-fMWCNTs. The electrochemical study was done via CV, while the PCT detection was performed in 0.1 M PBS at a pH of 7.4 using DPV. CoPc-MWCNTs/GCE produced electrochemical signals without needing additional redox mediators or labeling. Additionally, a

pseudobienzyme system based on the catalytic properties of choline oxidase (ChOx) and CoPc was made to improve the sensor's sensitivity. The authors found that the fabricated immunosensor demonstrated good performance for PCT with a low LoD of 1.23 pg mL^{-1} and a wide LDR of 0.01 to 100 ng mL^{-1}. The fabricated immunosensor is a promising sensor for electrochemical detection of PCT in real biological samples (human serum).

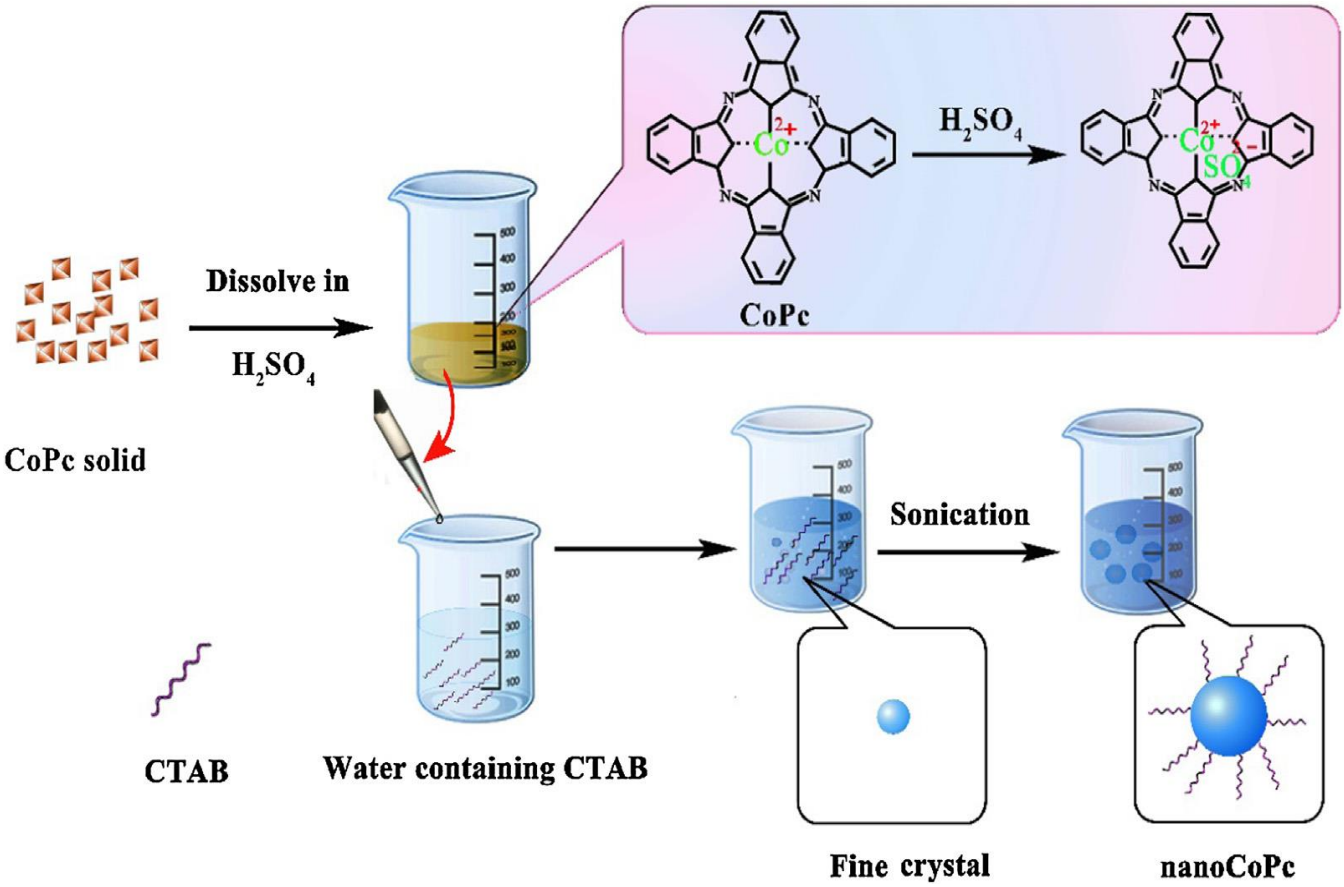

Figure 2.7. Stepwise preparation of the nanoCoPc-fMWCNTs (adapted from [64] with permission).

The determination of the Nevirapine in the drug sample was done by Kantize et al. [138] using a polymeric CoPc-nafion-CNTs composite modified on a platinum electrode. CoPc-nafion-CNTs composite synthesis was accomplished by consecutive drop-casting of a nanocomposite consisting a fMWCNTs and tetra-substituted coumarin CoPc (CoPc-cou), followed by immobilizing 5% Nafion perfluorinated resin solution (Naf-5). The CoPc-cou-f-MWCNTs/Naf-5/Pt electrode was used to determine antiretroviral drug nevirapine (NVP) in PBS (pH 12) via linear sweep voltammetry (LSV) and chronoamperometry. The LSV gave a LoD and LDR of 0.2 nM and 0.6

nM to 30 µM, whereas the CA offered a LoD and LDR of 0.21 nM and 2.5 to 30 µM. This sensor demonstrated a better selectivity for NVP in the presence of interferents (uric acid, ascorbic acid, cysteine, dopamine, metronidazole) with very good recovery in spiked river water sample analysis.

Table 3 summarizes the analytes detected with CoPc-MWCNTs modified electrodes with the techniques employed, LoD, and LDR.

Table 3. Detection of acetaminophen, carbaryl, DES, and epinephrine with CoPc-MWCNTs modified electrodes.

Electrode	Analyte	Technique	LoD µM	LDR µM	Ref
CoPc-fMWCNTs/Au/GCE	DES	SWV	0.199	0.7-5.66	[133]
CoPcMWCNTs/GCE	Acetaminophen	CV	1	1–1000	[119]
MWCNTs/CoPc/GCE	Carbaryl	SWV	0.006	0.33–6.61	[132]
fMWCNT-CoPc/AuNPs/GCE	Acetaminophen	SWV	0.135	1.49 - 47.6	[134]
CoPcMWCNT/PCE	Epinephrine	DPV	0.016	1.33 - 5.50	[135]
SWCNTs-CoPc/PG	Epinephrine	CA	0.04		[136]
CoPc-MWCNTs/GCE	Procalcitonin	DPV			[137]
CoPc-cou-fMWCNTs/Naf-5/Pt	Nevirapine	LSV	0.0002	0.0006-30	[138]
		CA	0.00021	2.5-30	[138]

2.5.1.4 Detection of Uric Acid, Glutathione, and Cysteine

Pari and Reddy [139] developed a simple and sensitive method for uric acid (UA) determination by modifying GCE with 2,4-dibromo-6-aniline-tetra (DBCMAT) substituted on CoPcMWCNTs via drop casting. Under optimum conditions, UA was determined in 0.1 M PBS at a pH of 7 via three techniques- CV, CA, and DPV. The DBCMAT-CoPc/MWCNTs/GCE modified electrode demonstrated enhanced electrocatalytic activity and a lower potential for UA oxidation. The electrode gave a LoD of 0.03(CV), 0.066 (DPV) and 0.016 µM(CA) and a LDR of 0.1–1.8(CV), 0.2–2.8 (DPV), 0.05–0.8 µM(CA) with a sensitivity of 131.85(CV), 22.634(DPV), and 2.509 $\mu A \mu M^{-1} cm^{-2}$(CA). The developed sensor demonstrated unique benefits, including low operating

potential, good stability, high sensitivity, and remarkable repeatability and reproducibility for uric acid detection. In the presence of these molecules; cysteine, glucose, glycine, H_2O_2, and L-tyrosine, it was discovered that the sensor was highly selective for UA. The fabricated electrode was expediently applied for UA and DA determination in urine samples with good results. This electrode offers a lower LoD than the obtained result in [140].

Giarola and Pereira [140] further developed a voltammetric sensor to detect uric acid using CoPc-MWCNTs/GCE. Before this, the CoPc-MWCNTs composites was prepared by ultrasonic agitation of CoPc and MWCNTs in DMSO. The electrochemical behavior of UA at the CoPc-MWCNTs/GCE was investigated in 0.1 M PBS at a pH of 7 via CV. Under optimal conditions, the sensor gave a wide LDR of 125 to 4000 μM with LoD and a Limit of quantitation (LoQ) of 260 and 860 μM, respectively, via the SWV technique. The electrode is characterized by good stability, sensitivity, and reproducibility. The presence of DA and AA do not interfere with UA detection, portraying good selectivity of the sensor. The fabricated sensor was successfully employed to determine UA in human urine samples.

Wang and his research group [128] investigated the fabrication of Pt-CoPc-MWCNTs/GCE to detect UA and DA simultaneously. The modified electrode was made by immobilizing GCE with MWCNTs covered with CoPc composite and platinum nanoparticles via *in situ* synthesis. The electrocatalyst displayed good electrochemical activity for uric acid (UA) and dopamine (DA). The LoD obtained for UA and DA were 1.4 and 2.6 μM, while the linear responses ranged from 5 to 100 μM and 5 to 170 μM, respectively. Notably, AA has no interference while simultaneously detecting UA and DA.

Gutierrez et al. [141] presented a GCE modified with pyrrole (Ppy), CoPc, and MWCNTs via electropolymerization to determine glutathione and cysteine. The best electrocatalytic activity of the CoPc-MWCNTs-PPy/GCE electrode towards the analytes was obtained in 5 mM ferrocyanide solution in 0.5 M NaOH. The sensor gave a sensitivity, LoD, and limit of quantification of 2.930 μA/mM, 0.03 mM, and 0.10 mM, respectively, for cysteine. For glutathione, the sensor offered 1.15 μA/mM, 0.02 mM, and 0.66 mM for sensitivity, LoD, and limit of quantification, respectively. Despite the low sensitivity of the electrode, it offered a low LoD and limit of quantification. Hence, they are good candidates as voltammetric sensors for biological samples.

A similar electrochemical sensor for glutathione and l-cysteine detection was also fabricated by Argote et al. [142] by immobilizing CoPc and MWCNTs on GCE via electropolymerization of the pyrrole surfactant. The hybrid sensor displayed a good electrocatalytic behavior towards the oxidation of glutathione and l-cysteine in 0.1 M NaOH. The hybrid $PyC_{10}MIM^{+}Br^{-}$-CoPc-MWCNT/GCE electrode offered a sensitivity of 5.240 and 6.733 μA/mM for glutathione and l-cysteine, respectively. The LoD and LoQ obtained for glutathione were 0.013 and 0.040 mM, respectively, while 0.014 and 0.043 mM were obtained for l-cysteine. The authors established that the pyrrole surfactant-derived hybrid electrodes have substantially smaller values, making them better suited for fabricating thiols electrochemical sensors in aqueous solutions. A low LoD obtained by this sensor is proof of its reliability for detecting thiols in biological samples. This hybrid sensor gave a higher sensitivity with a better LoD than the results obtained in [141].

Sun and his research team [143] have utilized the synergistic effect between CoPc and fMWCNTs to develop an aptasensor for kanamycin detection. The aptasensor was made by modifying a gold electrode (GE) surface with CoPc-MWCNTs nanocomposites. Under optimal conditions, in 0.1 M PBS at a pH of 7.4 via DPV, the CoPc-fMWCNTs/GE electrode displayed excellent stability, good reproducibility and repeatability, high sensitivity, high specificity, an LDR of 0.15 to 10 μM and a low detection limit (0.0058 μM). The fabricated sensor demonstrated an excellent selectivity for kanamycin amidst interferents like chlortetracycline, chloromycetin, neomycin sulfate, and oxytetracycline. The aptasensor was successfully employed to detect kanamycin in the spiked milk sample.

A summary of the analytes detected with CoPc-MWCNTs modified electrodes with the techniques employed, LoD, and LDR is given in Table 4.

Table 4. Detection of cysteine, glutathione, uric acid, and kanamycin with CoPc-MWCNTs modified electrodes.

Electrode	Analyte	Technique	LoD μM	LDR μM	Ref
Pt-CoPc-MWCNTs/GCE	Uric acid	SWV	1.4	5-100	[128]
DBCMAT-CoPc/MWCNTs/GCE	Uric acid	CV	0.03	0.1–1.8	[139]
		DPV	0.066	0.2–2.8	[139]
		CA	0.016	0.05–0.8	[139]
CoPc-MWCNTs/GCE	Uric acid	SWV	260	125-4000	[140]
CoPc-MWCNTs-PPy/GCE	Glutathione	CV	20	$1\text{-}5x10^{3}$	[141]
	Cysteine	CV	30	$1\text{-}5x10^{3}$	[141]
$PyC_{10}MIM^{+}Br^{-}$-CoPc-MWCNT/GCE	Glutathione	CV	13		[142]
	Cysteine	CV	14		[142]
CoPc-fMWCNTs/GE	Kanamycin	DPV	0.0058	0.01-0.15	[143]
TPLLCA-CoPc/MWCNTs/GCE	Cysteine	CV	$1.3x10^{-3}$	$2\text{-}10x10^{-3}$	[144]
		DPV	$1x10^{-3}$	$1\text{-}10x10^{-3}$	[144]
		CA	$3.3x10^{-3}$	$5\text{-}50x10^{-3}$	[144]

2.5.1.5 Detection of Lactic Acid, Glucose, and Hydrazine

In an attempt to detect lactic acid, Shao and group [93] fabricated a novel sensor by modifying GCE with cobalt polyphthalocyanine (CoPPc) nanocomposite and MWCNTs-COOH. The reduction mechanism of lactic acid on the CoPPc/MWCNTs-COOH/GCE surface is illustrated in Scheme 1. The electrocatalytic activities of the CoPPc/*f*MWCNTs/GCE towards lactic acid detection was assessed via CV in 0.1 M PBS at a pH of 4. The fabricated electrode exhibited outstanding electrochemical performance for lactic acid reduction over a wide LDR of 10-240 μM and a low LoD of 2 μM. It also displayed a high selectivity against common interfering molecules (glucose, ascorbic acid, sodium chloride, dopamine, hydrogen peroxide, and uric acid). Notably, the sensor was effectively used for lactic acid determination in rice wine samples, demonstrating the excellent potential for quick monitoring applications.

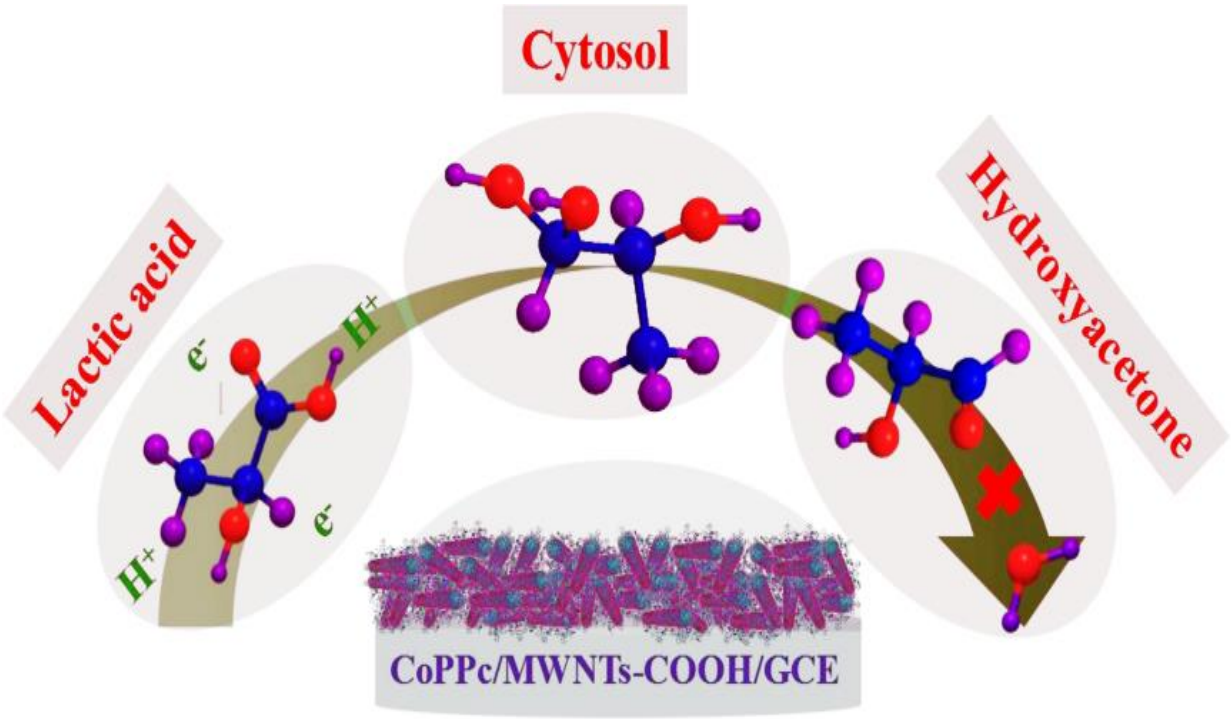

Scheme 1. The reduction mechanism of lactic acid reduction on the CoPPc/MWCNTs-COOH/GCE surface, with permission from [93].

Porto and his group [145] developed a sensor to determine pyridoxine by modifying a pyrolytic graphite electrode (PGE) with CoPcMWCNTs Composite. Under optimum conditions of 0.3 M PBS at a pH of 5.5, the CoPcMWCNT/PGE was employed to detect pyridoxine (vitamin B6) via the DPV technique. The LoD, LoQ, and LDR obtained were 0.50 µM, 1.67 µM, and 10 to 400 µM, respectively. It also offers the benefits of a quick response, low cost, and a sensitivity of 0.037 µAL µmol^{-1}, testifying to the technique's excellent sensitivity. The sensor was conveniently applied for pyridoxine determination in real samples of pharmaceutical formulations (RSD < 5%), indicating the suitability of the developed electrode for pyridoxine detection in pharmaceutical formulations containing pyridoxine accurately.

Mounesh and his research team [146] developed an amperometric sensor for glucose by modifying tetracinnamide Cobalt phthalocyanine (TCIDCoPc) and MWCNTs on GCE. The modified TCIDCoPc-MWCNTs/GCE exhibited excellent electrocatalytic properties and reduced potential for glucose oxidation. Under optimized conditions, at a pH of 7 in 0.1 M PBS, the developed sensor gave a wide LDR from 2 - 20(CV); 2 – 12(DPV); 5 – 50(CA) mM/L, detection limit of 0.9(CV); 5.33(DPV); 6(CA) mM) and sensitivity of 1.905(CV); 3.483(DPV); 1.035(CA) mA mM^{-1} cm^{-2}).

The fabricated sensor was characterized by a quick response time, good sensitivity, reduced working potential, and good reproducibility and repeatability. The developed sensor also demonstrated a better selectivity for glucose amidst interfering biological species such as UA, DA, and AA.

In another study conducted by Devasenathipathy and his team [147], an amperometric biosensor based on MWCNT cobalt tetrasulfonated phthalocyanine (CoTsPc-MWCNT) nanocomposite-modified GCE was fabricated for glucose detection. The fabricated electrode tagged MWCNT–CoTsPc/GCE displayed an excellent electrocatalytic activity towards detecting glucose in 0.1 M NaOH using an amperometry technique. A reasonable sensitivity (122.5 µA mM^{-1} cm^{-2}), a wide LDR (10 µM - 6.34 mM), along with a LoD of 0.14 µM were reported for this sensor. The proposed sensor is characterized by high stability, good sensitivity, low working potential, repeatability, reproducibility, and quick response time (2s). Amperometry study established that the fabricated sensor has high selectivity for detecting glucose amidst interfering molecules like AA, DA, UA, galactose, fructose, lactose, and sucrose. The sensor was practically employed to detect glucose in serum samples from human blood.

Mounesh and Reddy [131] developed another amperometric sensor for hydrogen peroxide (H_2O_2) and glucose by modifying GCE with the synthesized tetra-cobalt(II) carboxamide-PEG_2-biotin phthalocyanine composite (CoTPEG_2BAPc) and MWCNTs via drop-casting. Under optimized conditions of pH 7 in 0.1 M PBS, the developed biosensor gave a wide LDR of (CA: 5–50, DPV: 2–22; CV: 5–25 µmol) and (CA: 5–50, DPV: 2–22; CV: 2–16 µmol) for H_2O_2 and glucose, respectively, LoD of (CA: 12.5; DPV: 2; CV: 0.33 µM) and (CV: 1.5; DPV: 5; CA: 10 µM) for glucose and H_2O_2 and a good sensitivity of (CA: 0.101; DPV: 1.978; CV: 0.947 µA μM^{-1} cm^{-2}) and (CA: 0.162; DPV: 1.888; CV: 1.250 µA μM^{-1} cm^{-2}) for glucose and H_2O_2. The biosensor is characterized by a rapid response time, good sensitivity, repeatability, and reproducibility. It also demonstrated a high selectivity for glucose and H_2O_2 amidst interfering molecules like L-cysteine, glycine, DA, UA, and AA. The remarkable selectivity of the fabricated sensor is attributed to the comparatively low potential for detection, which greatly minimizes the responses of typical electroactive interference. Likewise, adding MWCNTs to the modified electrode also helped reduce interference since their neutral charge prevented interfering molecules from penetrating the

electrode's surface. The practicability of the electrode was demonstrated by the successful detection of H_2O_2 and glucose in human blood samples and contact lens care solution, respectively.

Again, Mounesh et al. [144] fabricated a sensor to detect hydrazine and L-cysteine by modification of GCE with a poly (L-lactide)-carboxamide-Cobalt Phthalocyanine composite (TPLLCA-CoPc) and MWCNTs. Under optimized conditions of pH 7 in 0.1 M PBS, the modified TPLLCA-CoPc/MWCNTs/GCE detected L-Cysteine and hydrazine in the nanomolar. The modified electrode offered a linear range of (CA: 5-50, DPV: 1-10, CV: 2-10 nmol L^{-1}) for L-cysteine and Hydrazine, a low LoD of (CA: 3.33, DPV: 1, CV: 1.33 nmol) and (CA: 6, DPV: 0.033, CV: 0.33 nmol) for L-cysteine and hydrazine, respectively, and high sensitivity of (CA: 0.945, DPV: 4.325, CV: 1.299 μA nM^{-1} cm^{-2}) and (CA: 0.770, DPV: 4.193, CV: 1.719 μA nM^{-1} cm^{-2}) for hydrazine and L-Cysteine, respectively. The TPLLCA-CoPc/MWCNTs/GCE exhibits high stability and sensitivity, good reproducibility, and repeatability. The authors reported that these molecules (dopamine, glucose, ascorbic acid, glycine, uric acid, and hydrogen peroxide) do not interfere with the detection of L-cysteine and hydrazine.

Table 5 summarises the analytes detected with CoPc-MWCNTs modified electrodes with the techniques employed, LoD and LDR.

Table 5. Detection of glucose, hydrazine, lactic acid, and pyridoxine with CoPc-MWCNTs modified electrodes.

Electrode	**Analyte**	**Technique**	**LoD** (μM)	**LDR** (μM)	**Ref**
CoPPc/*f*MWCNTs/GCE	Lactic acid	CV	2	10-240	[93]
CoPcMWCNT/PGE	Pyridoxine	DPV	0.50	10 to 400	[145]
TCIDCoPc-MWCNTs/GCE	Glucose	CV	900	$2\text{-}20\text{x}10^{3}$	[146]
		DPV	5330	$2\text{-}12\text{x}10^{3}$	[146]
		CA	6000	$5\text{-}50\text{x}10^{3}$	[146]
MWCNT–CoTsPc/GCE	Glucose	AP	0.14	10-6340	[147]
$CoTPEG_2BAPc$-MWCNTs/GCE	Glucose	CV	0.33	2–16	[131]
		DPV	2	2–22	[131]
		CA	12.5	5–50	[131]
TPLLCA-CoPc/MWCNTs/GCE	Hydrazine	CV	$3.3\text{x}10^{-4}$	$2\text{-}10\text{x}10^{-3}$	[144]
		DPV	$3.3\text{x}10^{-5}$	$1\text{-}10\text{x}10^{-3}$	[144]
		CA	$6\text{x}10^{-3}$	$5\text{-}50\text{x}10^{-3}$	[144]

Aside from these, CoPcMWCNTs nanocomposite has been utilized in various other processes such as oxidation of styrene to benzaldehyde [82, 148, 149], catalytic oxidation of benzyl alcohol to benzaldehyde [32, 33], electrochemical reduction of oxygen [150-154], electrochemical conversion of CO_2 to CO [155], removal of mercaptan from natural gas [156], photocatalytic oxidation of butan-2-ol [157], a catalyst for microbial fuel cell [158], catalyst in glucose/O_2 fuel cells [159], electrochemical reduction of carbon dioxide and carbon monoxide to methanol [160]. The conversion rate and selectivity recorded in these processes were satisfactory.

The use of Cobalt Phthalocyanine (CoPc) has been favored over other MPcs owing to its greater advantages such as high charge transfer capabilities [161], stability, high catalytic current density [162], reduced overpotential, diversified preparation methods, and high water-solubility [114-116]. It is also important to note the challenges researchers [148, 163] encountered while using CoPc-MWCNTs nanocomposite as a sensing material. CoPc suffers from aggregation and hydrophobicity due to huge π-π-conjugated systems. An aggregation of MPc forms inside the reaction medium as either a polymer or an inactive dimer due to the structural characteristics of the metal Pc itself. The dimers' formation reduces the axial ligand's active point; meanwhile, most of the catalytic process occurs at the axial position, thereby leading to a significant reduction in catalytic activity [82]. A single dispersed molecule in the reaction medium was employed to overcome this setback and improve the catalytic activity of the MPc. The MPc aggregation between molecules can be effectively prevented by immobilizing it on a solid carrier [163]. Silica, carbon nanotubes, activated carbon, zeolites, and graphene are the most used carriers. The addition of the carrier enables the Pc molecules to be evenly distributed on its surface, exposing more active sites that can increase the contact possibility of the catalyst with the target substrate and speed up the reaction [82]. Alternatively, the Pc aggregation can be prevented by uniform loading Pc onto MWCNTs using an ultrasonic approach. As a result, the agglomeration impact of Pcs is significantly diminished, allowing for an increase in the catalytic surface area and an improvement in catalytic efficiency [148].

Going by Table 1 - 5, the CoPc-MWCNTs nanocomposite modified electrodes have been successfully employed to detect a large variety of analytes such as ascorbic acid, acetaminophen, carbaryl, cysteine, epinephrine, diethylstilbestrol, dopamine, glucose, glutathione, hydrazine, hydrogen peroxide, kanamycin, nevirapine, nitrite, lactic acid, paracetamol, procalcitonin,

pyridoxine, uric acid, Cd^{2+}, and Pb^{2+}. These CoPc-MWCNTs nanocomposite modified electrodes have achieved a very low LoD, wide LDR, high sensitivity, and selectivity required for analyzing trace amounts of these analytes. The lowest LoD (0.033 nM) detected by this modified electrode was obtained from the detection of hydrazine using the DPV technique, followed by Nevirapine (0.2 nM) using the CA technique.

2.5.2 Application of NiPc-MWCNTs Nanocomposites

Karuppiah et al. [164] presented a similar NiTsPc-*f*MWCNTs/GCE electrode for dopamine detection. The electrode was made by modifying GCE with nickel tetrasulfonated phthalocyanine (NiTsPc) and *f*MWCNTs using a simple sonochemical method. Here, the NiTsPc was used as the dispersing medium for the *f*MWCNTs. The constructed sensor demonstrated a good electrocatalytic ability for dopamine in 0.05 M PBS (pH 7) via DPV. This electrode achieved a good LDR of 20 nM – 1.384 mM, a sensitivity of 0.17 $\mu A\ \mu M^{-1}\ cm^{-2}$, and a low LoD of 1 nM. The electrode was suitable for selectively detecting dopamine in the presence of AA and UA. The authors, thus, described the sensor with high stability, selectivity, and reproducibility. Lastly, the sensor was applied to detect DA in human serum samples with good results. This has proven to be better than the previous sensors for DA in terms of LoD.

Another dopamine sensor was fabricated by Kang and his research team [165] via electropolymerization of GCE with tetraaminophthalo-cyanatonickel(II) (p-NiTAPc) and Nafion solution. The fabricated electrode tagged as p-NiTAPc/Nafion-GCE exhibited a good electrocatalytic behavior for DA detection in 0.1 M PBS of pH 7.4 using LSV. The sensor offered a LoD of 9 X 10^{-8} M within an LDR of 2 X 10^{-7} - 2 X 10^{-5} M. The sensor's selectivity for DA detection was improved by covering the (p-NiTAPc/GCE surface with Nafion. Thus, the detection of DA with the sensor was unaffected by these ions and molecules: Br^-, Cl^-, Ca^{2+}, Mg^{2+}, AA, UA, arginine, cysteine, glutamic acid, histidine, lysine, tryptophan, tyrosine, and valine. The sensor was also characterized by good reproducibility, stability, and sensitivity. The sensor offered a better LOD than the one obtained by Karuppiah et al. [164].

A simple electrode constructed by the immobilizing NiPc nanoparticles and functionalized MWCNTs on basal plane pyrolytic graphite electrode was fabricated by Msimelelo Siswana [166]. The fabricated electrode tagged NiPc/MWCNT-BPPGE was used as the working electrode. The modified electrode exhibited excellent electrocatalytic behavior for detecting asulam in 0.1 M PBS (pH 7) via the chronoamperometry CA. Within an LDR of 91- 412 X 10^{-6} M, a LoD of 0.29 μM

and 0.045 μA/μM were obtained by the NiPc/MWCNT-BPPGE modified electrode. The electrode was reported to be stable haven retained 86 % of its initial current upon rinsing in 0.1 M PBS (pH 7) after the measurement.

O'Donoghue et al. [166] employed a slightly different GCE modification procedure to produce CoPc2-clicked-GCE and NiPc3-clicked-GCE using the click chemistry approach. This was made by modifying the GCE with a diazonium salt (via in situ diazotization) to cover the GCE surface with azide group layers, followed by clicking the CoPc or the NiPc to the surface of the grafted GCE through 1, 3-dipolar cycloaddition reaction. Employing the CA technique, the electrografted electrodes (CoP2-clicked-GCE and NiP3-clicked-GCE) showed an excellent electrocatalytic behavior towards hydrazine detection in 0.2 M NaOH solution. These electrodes gave LoD of 6.09 μM and 8.69 μM for the CoPc2-clicked-GCE and NiPc3-clicked-GCE electrodes, respectively, with a sensitivity of 51.32 μA mM^{-1} and 111.2 μA mM^{-1}. The sensors were also found to displayed good stability

De Oliveira et al. [167] synthesized copper nanoparticles/nickel phthalocyanine in indium-doped tin-oxide electrodes through a layer-by-layer (LbL) approach. The developed sensor was employed for the electrochemical detection of serotonin in 0.04 M Britton–Robinson (BR) buffer (pH 2.2) via CV. The sensor exhibited high sensitivity and selectivity and could detect 5- HT in the presence of interferents such as aspartic acid, ascorbic acid, cysteine, hydrogen peroxide, and sulfamethoxazole. The electrochemical signal of 5-HT was unaffected even in the presence of ascorbic acid at the same concentration, while there was a 400% increase in the current densities of the film in the presence of 20 μmol L^{-1} of 5-HT. The PAH/NiTsPc/PAH/CuNPs-ITO electrode exhibited a low detection limit of 0.13 μmol L^{-1} and a wider concentration range of 0.35–135 μmol L^{-1}. The developed sensor is a promising 5-HT sensor for biological samples. The schematic illustration of the PAH/NiTsPc/PAH/CuNPs-ITO nanocomposite is given in Figure 2.8.

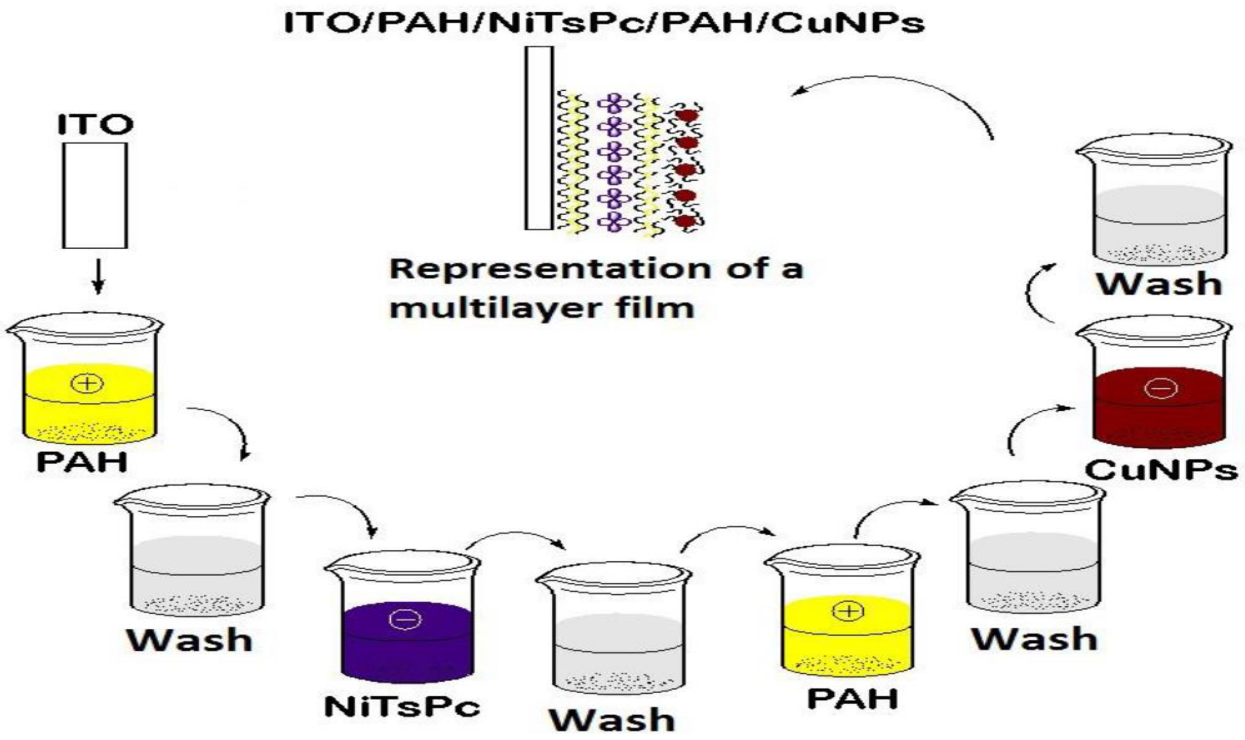

Figure 2.8. Illustrative scheme for preparing an ITO/(PAH/NiTsPc/PAH/ CuNPs) film, with permission from [167].

A two-step covalent modification method was employed by Wu and his research group [168] to design a nitrite sensor by modifying GCE with polyethylene oxide PEO and nickel-tetrahydroxy-phthalocyanine $NiPc(OH)_4$. Under optimized conditions, the $NiPc(OH)_4$/PEO-GCE modified electrode detected nitrite in 0.2 M PBS (pH 7) with a low LoD of 0.0522 μM, a sensitivity of 59.36 μA/mM, and an LDR of 0.1–5,300 μM using DPV technique. The excellent performance of the fabricated electrode towards oxidation was credited to the synergistic effect of PEO and $NiPc(OH)_4$ as well as the high electrochemical effective surface area after drying. Various interferent ions and molecules such as Na^+, K^+, Ba^{2+}, Ca^{2+}, Mn^{2+}, Zn^{2+}, Cl^-, NO_3^-, SO_4^{2-}, HPO_4^{2-}, $H_2PO_4^-$, H_2O_2 and glucose do not interfere with nitrite detection. The sensor exhibited good reproducibility, repeatability, stability, selectivity, and sensitivity and was successfully used to detect nitrite in water samples.

Wen and Kang [169] developed another nitrite sensor by coating GCE with a polymeric nickel tetraaminothphalocyanine (p-NiTAPc) film. Using DPV, the developed sensor exhibited a fast response towards nitrite detection in 0.1 M H_2SO_4–Na_2SO_4 solution (pH 2) with a LOD of 1×10^{-7} M within an LDR of 5×10^{-7} to 8×10^{-3} M obtained. The p-NiTAPc/GCE electrode is

characterized by high stability, excellent reproducibility, high sensitivity, and selectivity. The sensor experienced no interference from these ions Na+, Ba^{2+}, Ca^{2+}, Mg^{2+}, Zn^{2+}, Br^{-}, Cl^{-}, NO_3^{-}, SO_4^{2-}, and $H_2PO_4^{-}$, likewise from some oxidable species like Co^{2+}, Fe^{2+}, and Mn^{2+}. The proposed sensor was successfully applied to detect nitrite in real samples. The electrode reported by Wu and his research group [9b] has a better LoD compared to this, going by the LoD values for nitrite detection.

A working electrode fabricated by modifying carbon paste electrode (CPE) using Nickel (II) phthalocyanine was used by Eradya et al. [170] to detect morin in *Psidium guajava* leaf extract. The fabricated CPE-NiPc electrode exhibited excellent electrocatalytic activity for morin detection in 0.1 M PBS of pH 7. Using the fabricated electrode in a solution of various concentrations of morin in a DPV experiment, a LoD of 2.0 nM, a LOQ OF 6.9 Nm, with an LDR of 1.0×10^{-7} to 2.5×10^{-3} M were obtained. The sensor can quickly and concurrently resolve the peaks of morin and quercetin. The proposed sensor is quick, easy to produce, has low detection limits, and has outstanding antifouling qualities. The sensor's selectivity test indicated that ascorbic acid, caffeic acid, gallic acid, glucose, L-tyrosine, and uric acid have negligible effects in the detection of morin, except for quercetin. With satisfactory recoveries, the sensor was employed to validate tea decoction, human urine, commercially available guava leaf capsules, and spiked red wine.

Table 6. Summary of the analytes detected with CoPc-MWCNTs modified electrodes.

Electrode	**Analyte**	**Technique**	**LoD** (μM)	**LDR** (μM)	**Ref**
NiTsPc-*f*MWCNTs/GCE	Dopamine	DPV	0.001	0.02–1384	[164]
p-NiTAPc/Nafion-GCE	Dopamine	LSV	0.09	0.2–20	[165]
NiPc/MWCNT-BPPGE	Asulam	CA	0.29	91- 412	[166]
NiPc3-clicked-GCE	Hydrazine	CA	8.69		[171]
PAH/NiTsPc/PAH/CuNPs-ITO	Serotonin	CV	0.13	0.35–135	[167]
$NiPc(OH)_4$/PEO-GCE	Nitrite	DPV	0.05	$0.1–5.3\times10^3$	[168]
p-NiTAPc/GCE	Nitrite	DPV	0.1	$0.5–8\times10^3$	[169]
CPE-NiPc	Morin	DPV	0.002	$0.1\text{-}2.5x10^3$	[170]

Table 6 reveals all the analytes detected using NiPc-MWCNTs nanocomposite as the sensing material. It also shows that the nanocomposite has never been employed for detecting bromate, therefore emphasizing the significance of this study.

In this section, an effort was made to summarize various analytes detected using electrochemical sensors fabricated with CoPcMWCNTs or NiPcMWCNTs nanocomposite. Importantly, emphasis was made on the detection techniques, supporting electrolytes/pH, LoD, and LDR. It also pointed out those analytes yet to be detected by these sensing materials, such as bromate. Hence, this present study explored the use of an electrochemical method (i.e EIS) and CoPc-MWCNTs and NiPc-MWCNTs nanocomposites to fabricate electrochemical sensors for bromate detection in foods.

2.6 Electrochemical Techniques and Sensors for Bromate Determination

The detection of bromate at micro and nano level has been achieved using different electrochemical techniques and sensing materials. These techniques and the sensors employed for bromate determination are herein discussed.

2.6.1 Determination of Bromate at Conducting Polymer-Based Modified Electrodes

Conducting polymers are electroactive polymeric materials that have recorded tremendous success as an essential component of technological innovations, such as electrochemical sensors, batteries, and anti-corrosion coatings. Conducting polymer-based sensors have shown to be particularly promising for the electroanalysis of analytes in solution, owing to the exciting properties of the conducting polymers, such as their high chemical stability and electrical conductivity [172].

Balamurugan and Shen-Ming used the common conducting polymer poly(3,4-ethylene dioxythiophene) (PEDOT) synthesized by electropolymerized its monomeric unit (PEDOT) and silicomolybdate ($SiMo_{12}O_{40}^{4-}$) to modify an electrode for BrO_3^- detection [4]. The resulting electrode could propagate charges quickly in an acidic media and had a quick response time (less than 10 seconds). This quick response was attributed to BrO_3^-'s short penetration depth through a highly active polymeric layer. The authors established that the electrode could reliably measure BrO_3^- concentration in 0.2 M H_2SO_4 solution (pH 7) over an LDR range of 30-8000 µM and can also be used to detect ascorbic acid (AA).

Li et al. [173] fabricated an ECL sensor using poly[3-(1,1'-dimethyl-4-piperidinemethylene)thiophene-2,5- diyl chloride] (PTh-D) and nafion for the modification of the Au electrode. It was quite impressive that the Au-S linkage between PTh-D and the Au electrode aided the successful attachment of PTh-D on the Au electrode in the presence of nafion. The resultant ECL sensor was used to detect bromate in Mcllvaine buffered saline MBS (pH 5.0) containing 0.1 M KCl, giving a low detection limit of 1 µM and a linear concentration range of 1 µM - 0.1 M. The sensor was also applied to detect BrO_3^- in drinking and river water with a good recovery.

Salimi and his team [174] developed a sensor for iodate, chlorate and BrO_3^- detection by modifying glassy carbon electrode (GCE) with MWCNTs and 5,10,15,20-tetraphenyl-21H,23H-porphyrine iron (III) chloride (FeP) composite. Using this electrode, cyclic voltammetry (CV) yielded a pair of well-defined redox couples. The rate constant (ks) and surface coverage obtained for the electrode led to the quick electron transport between MWCNTs and FeP. The fast response time, high stability, good reproducibility, technical simplicity, low limit of detection (LoD), and wide linear dynamic range (LDR) of this electrode defined its good electrocatalytic activity towards BrO_3^- reduction in an acidic medium. In PBS (containing H_3PO_4, K_2HPO_4, and KH_2PO_4) at a pH of 2, the BrO_3^- detection by this electrode yielded a LOD, LDR, and sensitivity of 0.6 µM, 2-150 µM, and 11 nA/µM, respectively, using AP.

Using a layer-by-layer (LBL) approach, Yong-Gu and his group [175] fabricated a sensor by assembling a metalloporphyrin (FeP), polyelectrolyte (polystyrene sulfonate, PSS), and CNTs on screen-printed carbon electrode (SPCE) as illustrated in figure 2.9. In 0.2 M sodium acetate buffer (SAB) at a pH of 7, a LoD of 43 nM and an LDR of 100 nM - 2.5 µM were obtained using AP. The authors established that the LBL sensor could detect BrO_3^- in water samples quickly and selectively. In the presence of interferents (Na^+, Ca^{2+}, Mg^{2+}, SO_4^{2-}, Cl^-, and ClO_4^-), the electrode exhibited good selectivity for BrO_3^-, except HCO_3^-, which displayed a substantial interference effect. In comparison, utilizing the same sensor material, this result has a better LOD than [174].

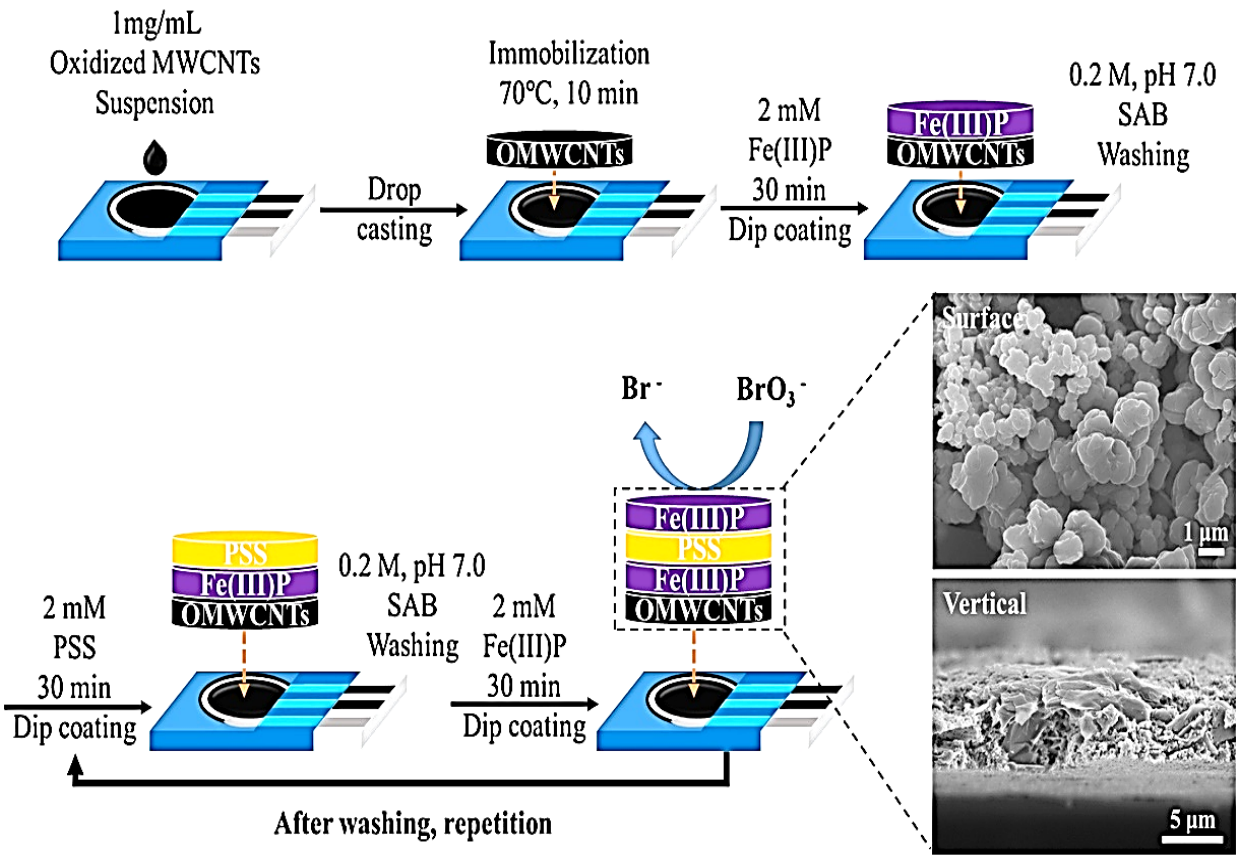

Figure 2.9. Flowchart showing the fabrication process for LBL electrodes and FESEM images of the fabricated (Fe(III)P-PSS)n-Fe(III)P-OMWCNTs/SPCE (adapted from [175] with permission).

Wang et al. [176] presented a simple method for BrO_3^- detection in water and food samples. This sensor was made using a monolith column consisting of poly(glycidyl methacrylate-co-ethylene dimethacrylate) produced via in-situ polymerization followed by modification of quaternary amine. The sensor detected BrO_3^- after a post-column reaction with KI at a wavelength of 352 nm. Within an analytical period of only 8.5 minutes, LoD and LDR of 1.5 g/L and 5-30 g/L, respectively, were obtained with a low standard deviation (n = 6, 0.043 percent).

Ali and her research team [177] developed an electrode via electropolymerization of pyrrole and Ni substituted polyoxometalate (POM) for the electrocatalytic reduction of BrO_3^- in a water sample. The polymer films were produced in various film thicknesses and characterized prior to the analyte detection. Importantly, this POM-doped polypyrrole (Ppy) co-polymer film's conductivity was validated by EIS. The best of the polymer films concerning its electrocatalytic activity and stability was used for BrO_3^- detection in a water sample. The electrode provided a

good sensing platform in 0.1M Na_2SO_4 solution (pH 2), giving an LDR and LoD of 0.1 - 2 mM and 0.2 µM, respectively. The electrode has also been proven selective for BrO_3^- in the presence of interferents (NO_3^-, NO_2^-, PO_4^{3-}, ClO_3^-).

A reproducible electrochemical sensor was produced by Shaojun and his research team [178] for the detection of BrO_3^- using an electrode modified with Ppy film and lanthanide-molybdate (LM) complex. The pH studies showed the influence of various forms of Ppy on the relationship between pH and the formal potential of LM-Ppy during the redox process. In 0.1 M Na_2SO_4 (pH 1.23), the CV studies established the modified electrode as a reliable sensor for determining BrO_3^- owing to its good stability and a wide LDR (1-32 nM). The result obtained here shows a better LDR than [177].

TiO_2 sol containing Poly(4-vinylpyridine) and $Na_2H_6CoW_{11}Co(H_2O)O_{39}.14H_2O$ complex were combined by Li et al. [179] to make an amperometric sensor for detecting bromate. The produced sensor gave 5.0×10^{-6} M as its detection limit, and an LDR between 2.0×10^{-5} and 4.4×10^{-3} M. Casella and Contursi [180] also used a tungsten oxide sheet to fabricate an amperometric sensor for the electrochemical detection of BrO_3^-. This has 45 mM as its LoD. Unfortunately, these sensors could not offer a low LoD for BrO_3^- detection.

Another Ppy-based sensor for BrO_3^- detection from Zou et al. [181] was produced by immobilizing Ppy and polyaniline (PANI) on an electrode's surface using a dopant (POM). The study revealed that the presence of the polymers affected the electrocatalytic properties of the POM. Other similar POM-based sensors have also been reported in various studies [182, 183].

Rasheed et al. [184] investigated the detection of bromate via differential pulse voltammetry DPV using a GCE modified with MXene (lamellar $Ti_3C_2T_x$). The good electrocatalytic properties of this sensor in 0.5 M Na_2SO_4 contributed to the wide LDR and a low LoD of 50 nM - 5 µM and 41 nM, respectively. The formation of TiO_2 on the $Ti_3C_2T_x$ surface during BrO_3^- reduction corroborated the redox reaction between MXene and BrO_3^-. The electrode exhibited excellent selectivity in the presence of interferents (Br^-, Cl^-. ClO^-, $H_2PO_4^-$, HPO_4^{2-}, SO_4^{2-}, $PO_4^{3-,}$ and NO_3^-) during BrO_3^- detection. This electrode remains one of the viable sensors for water contaminants with the simplicity of preparation. In comparison to [173], this technique yielded a higher LOD.

Through a layer-by-layer (LBL) approach, Pang and his group [185] fabricated another AP sensor by assembling a polydiallyldimethylammonium chloride (PDDA), PM, and MWCNTs on glassy carbon electrode GCE. The authors produced the working electrode by electropolymerization of PM on PDDA/MWCNTs modified GCE. An extremely low LoD (20 nM), a wide LDR (50-400 nM), and high sensitivity (13.81 mA cm^{-2} mM^{-1}) with a rapid response time (1.53 s) obtained were attributed to the excellent electrocatalytic activity of the sensor.

Sheen et al. [186] invented a sensor for BrO_3^- detection by modifying gold electrode (GE) with Manganese (III) chloride (Mn(III)Cl) and 5, 10, 15, 20-tetrakis (4-methoxyphenylporphyrinato] (TMOPP). The resultant sensor TMOPP-Mn(III)Cl)/GE was used for BrO_3^- determination in bread sample. Using SWV techniques, the sensor demonstrated a better electrocatalytic activity towards BrO_3^- in 0.1 M Na_2SO_4 solution (pH 7), giving a LoD of 3.56 nM and an LDR of 0.1 – 1 X 10^4 µM. In the presence of interferents (Ca^{2+}, K^+, glucose, sodium chloride, and sodium carbonate), the electrode also showed to be selective for BrO_3^-.

2.6.2 Determination of Bromate with Carbon Nanotubes CNTs-based Electrodes

Carbon nanotubes have received wide attention in nanotechnology due to their extraordinary optoelectronic properties. Their good conductivity, high reactivity, modifiable sidewall, and biocompatibility have made their application in sensor fabrication highly accepted in electroanalytical chemistry [187, 188]. The success of those sensors has manifested in improved current response of some biological cells, biomolecules, and inorganic compounds when CNTs are used as part of a composite for electrode modification. Furthermore, CNTs are unique as a sensing material because of their rapid electron transfer kinetics, chemical stability, and electrocatalytic activity toward various analytes in aqueous and non-aqueous conditions [188, 189].

In line with the trend, Li et al. [190] produced an amperometric BrO_3^- sensor based on MWCNTs and phosphomolybdic (PM) acid composite. This composite was used to modify the pyrolytic graphite electrode (PGE) for improved sensitivity of PGE towards BrO_3^-. The supporting electrolyte used in this study involved 0.5 M H_2SO_4 (PH≤2). The relatively low LoD (0.5 µM), the wide LDR (5-15000 µM), and the fast response time (< 2s) offered by this sensor are credited to the synergy between the composite's components. A study of interference found that most ions

(K^+, Na^+, NH_4^+, Zn^{2+}, Ca^{2+}, Mg^{2+}, Br^-, Cl^-, I^-, $H_2PO_4^-$, HPO_4^{2-}, SO_4^{2-}, PO_4^{3-}) do not interfere with the detection of BrO_3^-, except for a few ions (ClO_3^-, CO_3^{2-}, Fe^{3+}, IO_3^-, and NO_2^-) that displayed interference to varying degrees.

Similarly, Salami and his group of researchers fabricated a GCE modified with single-walled CNTs and Os (III) complex [191] for BrO_3^- detection. This electrode gave LoD and LDR of 36 nM and 1-2000 µM, respectively, in 0.1 M Na_2SO_4 at a pH 7. The aptness of the electrode for BrO_3^- detection was also characterized by its technical simplicity, good reproducibility, reversibility of the redox couple, and quick response time.

Vilian and his colleagues [192] fabricated a biosensor for the simultaneous detection of H_2O_2 and BrO_3^-. The biosensor was fabricated (as illustrated in figure 2.10) by immobilizing hemoglobin (Hb) on a composite produced by combining ZnO nanoparticles, poly-L-histidine (P-his), and functionalized MWCNTs. The sensor *ks* value was 5.16 s^{-1} while the response time and the surface coverage of Hb were < 3s, and 1.88 X 10^{-9} mol cm^{-2}, respectively. In 0.05 M PBS (pH 7), the LDR and LoD reported for this electrode via AP were 2-15000 µM, and 0.3 µM, respectively. The sensor was applied for BrO_3^- and H_2O_2 detection in milk and urine samples with good recovery.

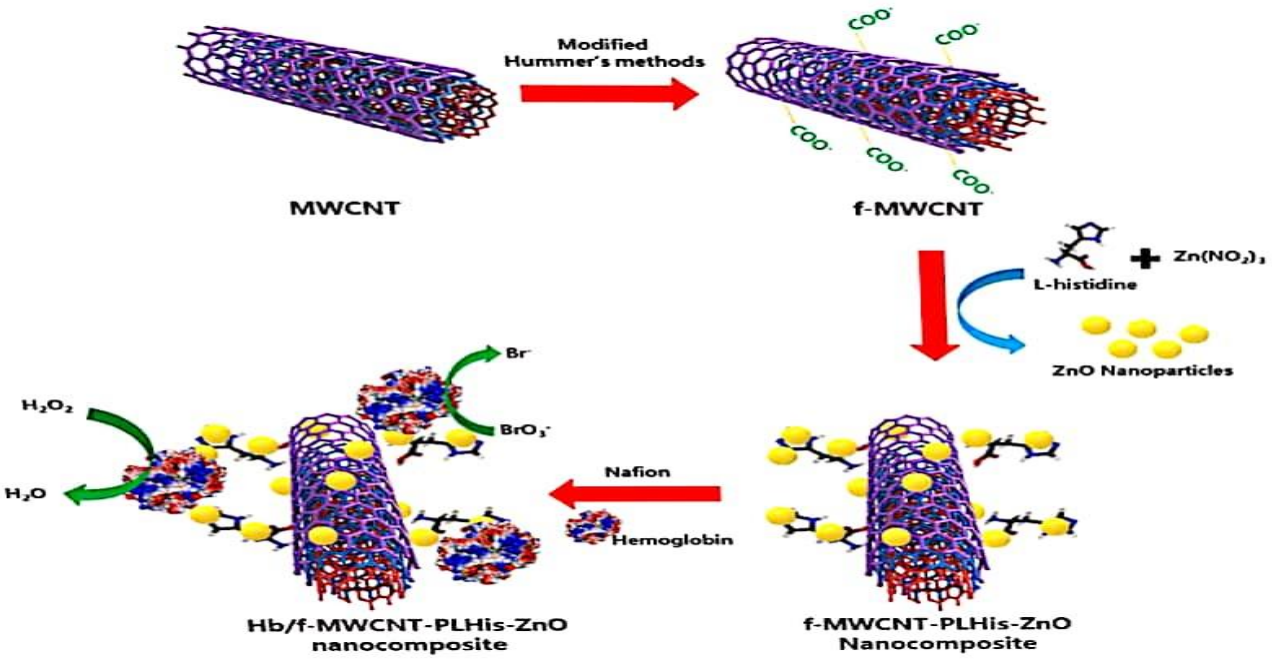

Figure 2.10. Schematic representation of the preparation of Hb/f-MWCNT–P-l-His–ZnO modified electrode for developing a biosensor for H_2O_2 and bromate (adapted from [192] with permission).

Salimi et al. [193] produced another copper complex $[Cu(bpy)_2]Br_2$ and silicomolybdate and SWCNT immobilized onto GCE for electrochemical detection of BrO_3^-. The fabrication of the $SiMo_{12}O_{40}^{4-}/[Cu(bpy)_2]^{2+}$/CNT/GCE was aided by the electrostatic interaction between the SWCNTs and $[Cu(bpy)_2]Br_2/\alpha$-$SiMo_{12}O_{40}^{4-}$. The presence of SWCNTs improved the fabricated electrode's porosity and conductivity. CV was employed to investigate the electron transfer kinetics of the adsorbed redox couples and the electrode's stability and electrochemical behavior. The supporting electrolyte for this study was 0.1M PBS (containing H_3PO_4), NaH_2PO_4, and Na_2HPO_4) at a pH of 7. Thus, this electrode gave a high sensitivity, LoD, and LDR of 6.7 nA nM^{-1}, 1.1 nM, and 0.01–20 μM, respectively, via AP.

Dan-dan et al. [194] constructed a selective BrO_3^- sensor using a nanocomposite produced from MWCNTs and Pd nanoparticles. The reduction peak potentials were observed between 0.15 and -0.25 V for BrO_3^-. Using a chronoamperometry (CA) technique, a high sensitivity (768.08 $\mu AmM^{-1}cm^{-2}$), a short response time (5s), and a very wide LDR (0.1-40 mM) were obtained by this electrode in 0.5 M H_2SO_4 at a pH 1. The authors confirmed that Pd/MWCNTs nanocomposite is an apt sensing material for BrO_3^- detection.

Another hemoglobin (Hb) based electrode for BrO_3^- determination was prepared by Li et al. [195] by modifying the GCE with Hb and MWCNTs dispersed in PLL. The prepared Hb/MWCNT/PLL/GCE electrode displayed excellent electrocatalytic activity towards BrO_3^- detection in 0.1 M acetate buffer solution (pH 5.6). This electrode offered a LoD (0.96 μM) and LDR (15-6000 μM) via amperometry. The authors concluded that the electrode is a simple and accurate means of BrO_3^- detection. A similar study was carried out by Vilian and his group [192], having a very low LoD.

2.6.3 Determination of Bromate at Graphene/Graphene Oxide-based Electrodes

Graphene has received significant attention as a carbon nanomaterial for electrode production since studies on its electrochemistry first surfaced in 2008 because of its two-dimensional structure [196]. Over the years, many publications have been on the modification of GCE with graphene prepared by the chemical reduction of graphitic oxide [196-199]. These electrodes have been utilized since then as electrochemical sensors (electro-catalyst) in an oxygen reduction reaction [199].

Recently, many polymers and nanomaterials have been coupled with graphene to generate highly sensitive sensors for diverse analytes. This was possible because of graphene's distinctive physical and mechanical qualities and optical and electrocatalytic properties, such as high transparency, high mechanical strength, superior electrical conductivity, potent ambipolar electric field effect, and large surface area. The improved electron transport properties of graphene-modified sensors due to the electrical conductivity of graphene resulted from the sp^2 hybridization and the availability of various oxygen-containing functions in graphene or its oxidized state. These features cause the rising popularity of graphene and its derivatives in electrochemistry and global nanotechnology. The use of these materials in transparent conductive films, sensors, capacitors, fuel cells, and batteries is evidence of its growing popularity [172, 200].

Majid and his research team [12] developed a sensor from graphene oxide (GO) modified GCE for BrO_3^- determination. Afterward, the working electrode (Pd-GO/GCE) was fabricated by deposing GO and Pd nanocomposite on the GCE. The developed sensor gave a LoD of 0.10 µM over an LDR of 1-1000 µM via Amperometry studies. The LoD Sheen et al. [185] reported is lower than the one obtained in this study. Real sample analysis of BrO_3^- was carried out with flour and bread samples with good recovery.

GCE modification with graphene (Gr) and *β*-cycLoDextrin (*β*-CD) for BrO_3^- detection was achieved by Palanisamy et al. [201]. This was actualized by further immobilizing Hemoglobin Hb on the modified electrode (*β*-CD-Gr/GCE) to produce a sensor with fast charge transport capability. In an electrolyte solution of 0.05 M PBS (PH 7) and at a voltage of -0.33 V, this electrode displayed high ks (3.18 0.7 s^{-1}), a low LoD (33 nM), and a reasonably wide LDR (0.1-176.6 M). According to the authors, the electrode shows good repeatability and selectivity for bromate in the presence of competing ions (Ca^{2+}, Mg^{2+}, Fe^{2+}, Fe^{3+}, Ni^{2+}, Br^-, Cl^-, I^-, IO_3^-, NO_2^-, and NO_3^-).

Ding et al. [202] produced a BrO_3^- sensor by further modifying rGO modified GCE with poly(diallyldimethylammonium chloride) PDDA and Phosphomolybdate PM. Figure 2.11 illustrates the three steps in fabricating the rGO-PDDA/PMo_{12}/GCE modified electrode. The stability of the electrode largely depends on the electrostatic attraction between the negatively charged PM and the cationic PDDA. The stability and electrocatalytic reduction of BrO_3^- were established using CV in 0.1 M H_2SO_4 solution. This electrode was characterized by a high

sensitivity (454 $\mu Acm^{-2}mM^{-1}$) and a wide LDR (0.02-10 µM). Pang and his group [185] worked on similar PDDA/PMo_{12} but with a better result, LoD (20 nM).

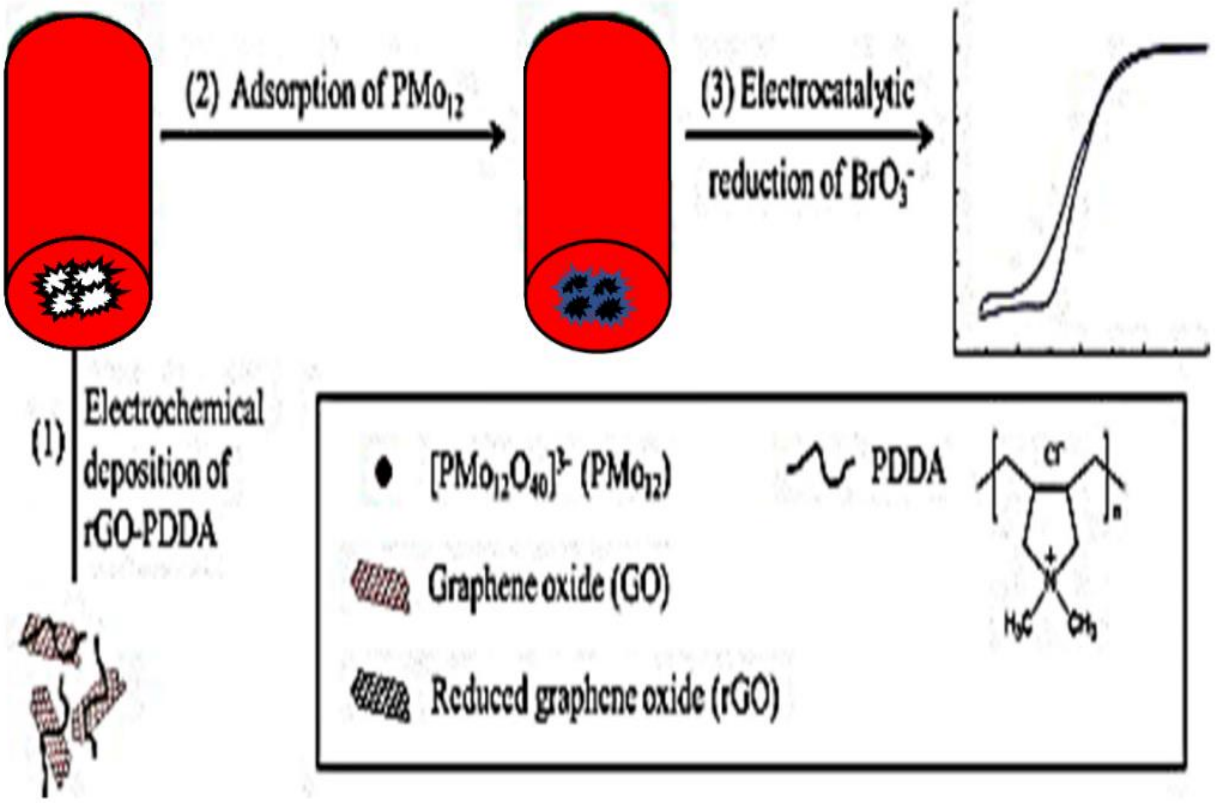

Figure 2.11. Schematic illustration of the fabrication process of a PMo_{12}@rGO-PDDA/GCE fabrication and the catalytic reduction of bromate.

Recently, Zhang et al. accomplished a photocatalytic sensor for simultaneous detection of ibuprofen (IBP) and BrO_3^- using TiO_2 doped with fluorine particles and GO (FGT). At optimum conditions, the photocatalytic degradation of IBP and BrO_3^- agreed with Langmuir-Hinshelwood first-order kinetics. The fast electron transfer process led to the reduction of BrO_3^- to bromine, while the simultaneous consumption of IBP and BrO_3 inhibited electrons and hole recombination, thus extensively utilizing the FGT redox potentials. This study provides evidence that the FGT assemblage is reliable for measuring specific water contaminants [203].

2.6.4 Determination of Bromate at Metal/Metal Oxide-based Modified Electrodes

The necessity to quickly fill the void left by the exclusive use of polymers and carbon nanomaterials (Gr, GO, CNTs, and carbon quantum dots, CQDs) led to the development of metal

and metal oxide nanoparticles in constructing electrochemical sensors. These materials have been combined with metal and metal oxide nanoparticles to overcome setbacks, such as the adhesion of CNTs, stacking of Gr lamellae, and agglomeration of CQDs [204, 205]. Subsequently, metal and metal oxide nanoparticles have thrived in functionalizing other materials. The nanocomposites produced here have been employed in a wide range of applications since a composite combines the attributes of its components [206]. This combination often leads to the formation of materials with large surface area, enhanced electrocatalytic activity, improved biocompatibility, and good conductivity, resulting in better electron transfer kinetics than individual materials [207]. As they have better chemical and electrical properties than bulk materials, nanoparticles have been employed to make sensors [22].

Ourari et al. [208] modified a carbon paste electrode with a Cu II-[N,N′-bis(2,5-dihydroxybenzylidene)-1,2-diaminoethane] (Cu II-DHB) that was used for the simultaneous detection of BrO_3^- and NO_2^- via AP and DPV. CV revealed that the rate-determining step involved one electron, thus indicating that the process was purely diffusion-controlled. Using DPV, LoD and LDR of 1.5 nM and 2–14 nM were obtained for NO_2^- while LoD and LDR of 10 nM and 2–14 nM, respectively, were obtained for BrO_3^- via AP. The proposed sensor offered a high selectivity for both bromate and nitrite in the presence of interferents (Cl^-, SO_4^-, and NO_3^-), except for lO_3^- (owing to its equal potential range with copper (II) Schiff base complex). This result implied that the modified [CuII-DHB]-CPE electrode is a suitable electrochemical sensor for detecting bromate, especially in 0.1M Phosphate buffer solution PBS (pH 2).

A novel cadmium-ionic liquid-carbon paste electrode (Cd-IL/CPE) was fabricated by Zhuang and his research team [209] for the simultaneous detection of bromate and trichloroacetic acid (TCA). CV studies showed that the developed electrode exhibits good electrocatalytic activity towards BrO_3^- and TCA reduction in 0.1 M BR buffer solution at pH 6.1. The electrochemical detection of BrO_3^- with this electrode offered a LoD, LDR, and sensitivity of 3 nM, 0.005–0.020 μM, and 496.15 $\mu A \mu M^{-1,}$ respectively. The authors also ascribed to the electrode a much lower detection limit than earlier reports [174] and [189] involving the use of other modified electrodes.

In an attempt to design a platform for simultaneous chlorate, iodate, and bromate detection, Arumugam et al. [210] fabricated a sensor by modifying GCE with silver-phosphomolybdate-polybenzidine nanocomposite ($Ag/PMo_{12}/PBz$). Amperometric studies showed that the fabricated

Ag/PMo_{12}/PBz/GCE electrode gave a higher sensitivity and a much lower LoD for BrO_3^- than IO_3^- and ClO_3^-. The best electrocatalytic activity of the Ag/PMo_{12}/PBz/GCE electrode towards BrO_3^- was attained in 1 M H_2SO_4 solutions at a pH of 2. Under optimal conditions, this electrode gave LOD and LDR of 86.3 nM and 2.34 nA μM^{-1}, respectively. The main advantages of this electrode are its simplicity in production, rapid response, and mechanical and electrochemical stability. Surprisingly, this LoD is significantly lower than the previously reported for another amperometric sensor created by Li et al. [190].

Akinremi and his group [211] investigated the cross-linkage of chitosan (CHT) with a zero-valent cobalt 2,6-pyridine dicarboxylic acid (ZVCo-PDCA-CHT) to produce a nanocomposite for detecting bromate in water. The performance of this technique for complete BrO_3^- reduction majorly depends on the reduction of Co (II) with $NaBH_4$. This composite achieved 99 % BrO_3^- reduction in water for 1 hour, in contrast with 65 % obtained for PDCA crosslinked CHT.

Sun et al. [212] fabricated a BrO_3^- detection sensor by depositing Pd nanoparticles (PdNPs) on PANI on mesoporous SBA-15 support via an in-situ method. Figure 2.12 depicts a stepwise description of the electrocatalytic reduction process of BrO_3^- at the Pd-NPs/PANI/SBA-15 interface, while Figure 2.13 shows the cyclic voltammograms of the modified electrode in 0.5 M H_2SO_4 containing different BrO_3 concentrations. The electrode demonstrated high electrocatalytic activity for the reduction of BrO_3^- over a potential range of 0.12 to -0.22 V. A low LoD and a very wide LDR of 5 µM and 8-40000 µM, respectively, were achieved by this electrode. The electrode was proven to be stable over 200 cycles of CV scans. The electrode also exhibited great potential for practical BrO_3^- detection in real samples. Noteworthy, the electrode's sensitivity was credited to the improved surface area of the electrode due to the presence of SBA-15, the availability of large nitrogen sites on the composite for PdNPs anchorage, and the availability of enough H^+ for BrO_3^- reduction.

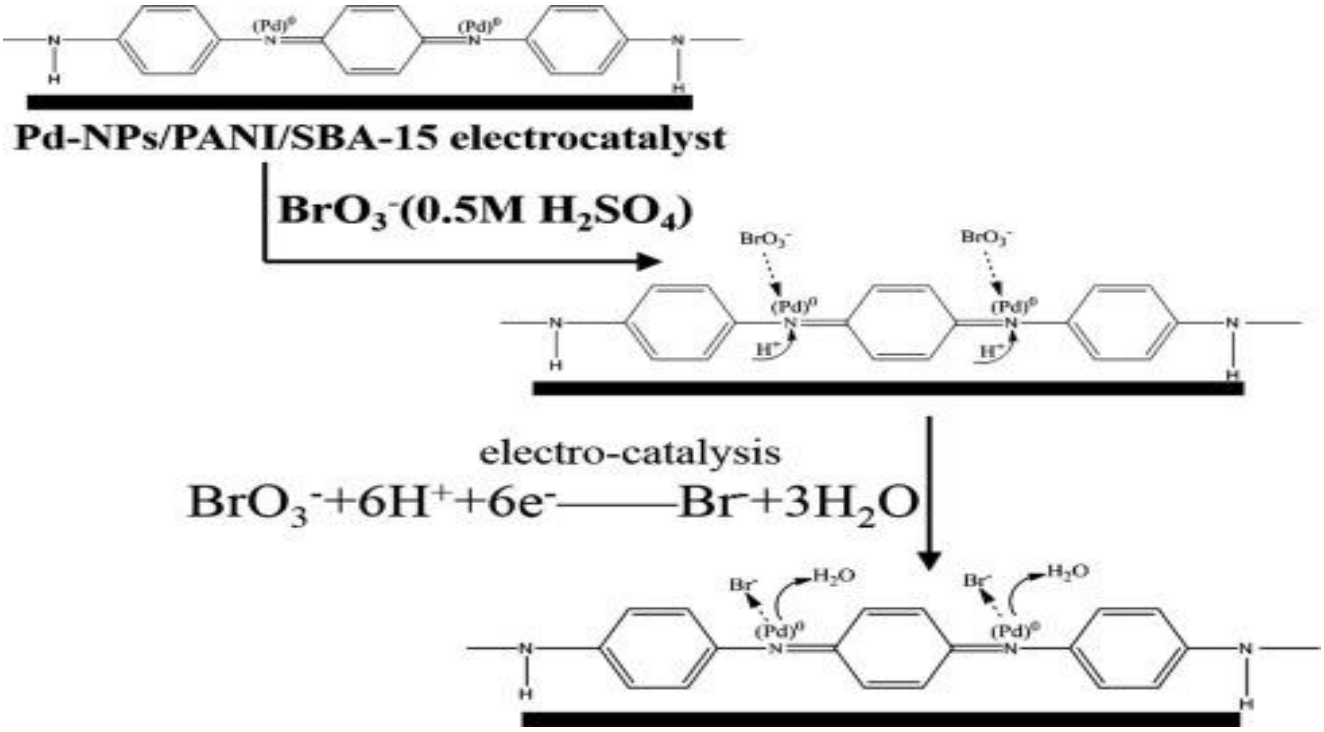

Figure 2.12. Schematic diagram of the electrocatalytic reduction of BrO_3 by the proposed Pd-NPs/PANI/SBA-15 interface electrode.

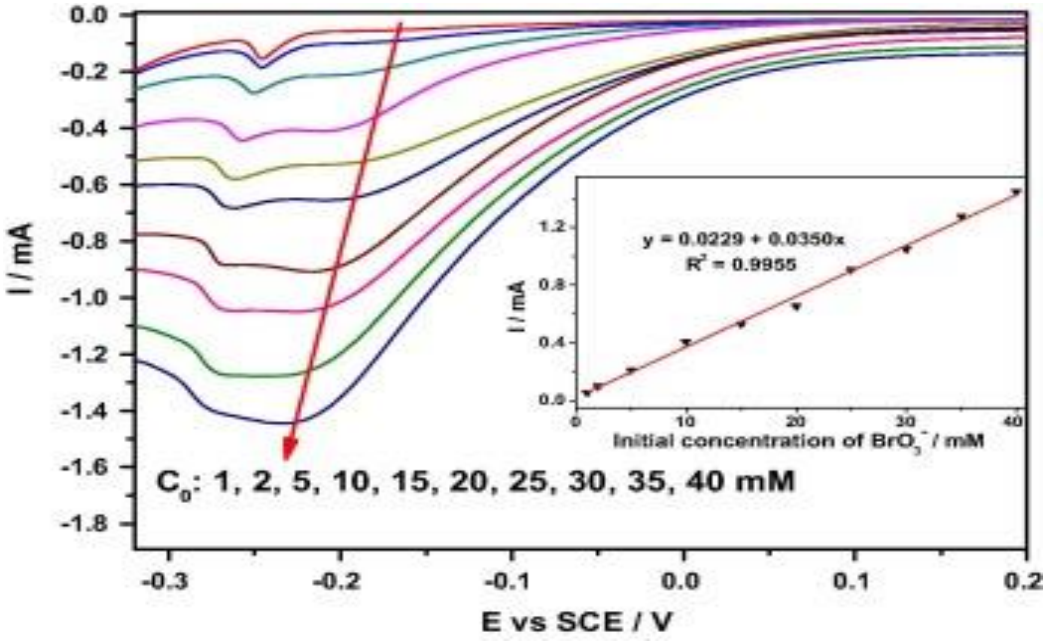

Figure 2.13. CV of Pd-NPs/PANI/SBA-15 in 0.5 mol L^{-1} H_2SO_4 with different BrO_3^- concentrations ranging from 1 to 40 mmol L^{-1} (scan rate: 20 mV s^1). The inset plot is the corresponding reduction peak current vs. the BrO_3 concentration.

Sun et al. [5] disclosed the three factors that led to the high sensitivity of Pd-NPs/PANI/SBA-15 for BrO_3^- reduction. These include

1. The large number of PANI/SBA-15 nitrogen sites available for the anchorage of Pd-NPs that ensure a large quantity of uniformly dispersed small Pd-NPs.
2. The successful incorporation of mesoporous SBA-15 significantly increases the effective electrode surface and electrolyte diffusion velocity.
3. The strong acidity of the medium provides abundant H^+ for the BrO_3^- reduction.

Cheng et al. [213] fabricated a sensor for BrO_3^- detection based on gold-rhodium AuRh nanoparticles modified GCE. The decrease in the overpotential and the appearance of a well-defined peak for BrO_3^- detection in 0.05 M PBS (pH 7.0) in a CV experiment were partially caused by the AuRh nanoparticles' tiny particle size. This nanoparticles-based-sensor gave LDR of 1-26 µM and LoD of 1.0 mM.

Chen and his group [214] developed a sensor to determine the BrO_3^-'s content of hair care products using SPCE modified with CuO nanoparticles (CuO NPs). This was accomplished by depositing CuO NPs on SPCE, which improved BrO_3^- reduction in weakly acidic media. The CuO/SPCE was integrated into a flow injection analysis system to construct a sensitive platform for BrO_3^- detection. The reported sensor offered a LoD and LDR of 3.5 µg L^{-1} and 0.01-300 mg $L^{-1,}$ respectively, in 0.1 M Phosphate buffer solution PBS. Additionally, this method demonstrated excellent BrO_3^- selectivity in the presence of interferents ($Br^{-,}$ Cl^-, F^-, ClO_4^-, NO_3^-, and SO_4^{2-}, neither the sensitivity nor the response time of the electrode was affected by the addition of these anions) and good recovery while analyzing real samples. Ourari et al. also reported a similar nanoparticle [208] but with an impressively low LoD.

Tamiji and Nezamzadeh-Ejhieh [215] constructed a carbon paste electrode (CPE) modified with a Tin (II) exchanged clinoptilolite NPs for BrO_3^- detection. The electrode's optimum electrocatalytic performance towards the bromate was achieved in an acidic medium at a pH of 2. This sensor offered LoD and LDR of 0.06 µM and 5-100 µM, respectively. A further investigation on the effect of other oxidants on Br determination was performed; however, the result indicated that the presence of these oxidizing agents increased the maximum error involved in BrO_3^- detection.

2.6.5 Bromate Determination by Modified Electrode with Quantum Dots

The biocompatibility and minimal cytotoxicity of carbon quantum dots or carbon dots (CQDs) afforded them a suitable substitute for metal-based quantum dots [216]. CQDs are fluorescent zero-dimensional materials with a diameter < 10 nm. They have wide applications in bioimaging probes design, drug delivery, gene transmission, and biosensor fabrication. Their fluorescent characteristics have been extensively utilized in analytical chemistry [217]. Noteworthy, CQDs are chemically stable, easy to synthesize, water-soluble, and can be made from cheap precursors and thus have a considerable potential of being used as an electrochemical sensor component.

CQDs have been utilized to fabricate sensors with high sensitivity and low LOD towards analytes such as acids, vitamins, drugs, DNA, metal ions, hematin, water pollutants, and polypeptides, among others [218]. These sensors could detect analytes as low as the femtomolar [219, 220].

Xiang et al. [221] developed an effective fluorescent probe for BrO_3^- detection by doping silica nanoparticles with CQDs made from the pyrolysis of citric acid (CA). BrO_3^- in an acidic medium quenched the resultant probe's fluorescence. After optimizing the electrolyte concentration, temperature, reaction time, and pH, the sensor could detect BrO_3^- at a low LoD (1.1 ng mL^{-1}) with a relatively wide LDR (8–400 ng mL^{-1}) was obtained. Real sample analysis of BrO_3^- was performed in drinking water samples yielding good recoveries.

Li et al. [222] also functionalized the ionic polymer polyethyleneimine (PEI) with CQDs made from the pyrolysis of CA in order to create a photoluminescence (PL) sensor for BrO_3^- detection. The experimental parameters were optimized in order to produce a very sensitive sensor. The interference analysis showed that the electrode displayed good selectivity for BrO_3^- detection even in the presence of interfering ions (Cu^{2+}, Fe^{3+}, AC^-, Cl^-, CO_3^{2-}, ClO_3^-, SO_4^{2-}, HPO_4^{2-}), except for I^-, ClO^-, IO_3^-, $Cr_2O_7^{2-}$ that showed a noticeable interference effect. The resultant PL sensor offered a LoD of 0.17 nM over a linear range of 0.04-0.35 μM. The sensor was applied on real samples like pastry, bottled water, lake water, and drinking water with good recovery.

Chemiluminescence (CL) sensor was developed for BrO_3^- detection by Liping and his research team [223] using sulfite and CQDs. The amount of BrO_3^- in the solution was measured using the CL peak that resulted from the injection of BrO_3^-. With a LoD of 0.1 μM, the CL signal rose linearly between 0.3 and 10 μM. The mechanism of BrO_3^- detection depends mainly on the reaction between BrO_3^-, sulfite, and CQDs in an acidic medium, which leads to the creation of holes and

electron-injected CQDs. The CL was formed as a result of the duo's recombination. This mechanism contrasts with the assumption that energy transfer occurs between SO_2^* and CQDs.

Table 7. Summary of different electrochemical methods and sensors for bromate detection.

Sensor Category	Modified Electrode	Technique	Sample	Linear range (µM)	LoD (µM)	Ref.
Conducting	PEDOT/$SiMo_{12}$/GCE	AP	-	30 - 8 x 10^3	-	[4]
Polymer	PTh-D/nafion/AuE	ECL	-	1 - 1 x10^5	1	[173]
	Fe(III)P/MWCNT/GCE	AP	-	2 - 150	0.6	[174]
	Fe(III)P/MWCNT/SPCE	AP	Water	0.1 - 2.5	0.043	[175]
	Ni/POM/Ppy/GCE	EIS	Water	100 - 2 x 10^3	0.2	[177]
	$Nd(SiMo_7W_4)_2$/PPy/GCE	CV	-	0.001 ~ 0.032	-	[178]
	Nafion/$Ti_3C_2T_x$/GCE	DPV	Water	0.05 - 5	0.041	[184]
	$MWCNT_5$/PDDA/PMo_{12}/PGE	AP	Water	0.05 – 0.4	0.020	[185]
	TMOPP-Mn(III)Cl)/GE	SWV	Bread	0.1 – 1 x 10^4	0.004	[186]
Carbon	PMo_{12}/MWCNTs/PGE	AP	-	5 – 15 x 10^3	0.50	[190]
nanotubes	SWCNT/Os(III)/GCE	AP	-	1 - 2 x 10^3	0.036	[191]
	f-MWCNT–P-L-His–ZnO/GCE	AP	Water	2 – 15 x 10^3	0.30	[192]
	$SiMo_{12}O_{40}^{4-}$/$[Cu(bpy)_2]^{2+}$/CNT/GCE	AP	-	0.01 – 20	0.001	[193]
	MWCNT/Pd/GCE	AP	-	100 – 40 x 10^3	-	[194]
	MWCNT/PLL/Hb/GCE	AP	Water	15 - 6 x 10^3	0.96	[195]
Graphene	GO-PdNPs/GCE	AP	Bread	1 - 1 x10^3	0.105	[12]
	Graphene-β-CD/GCE	AP	Water	0.1 - 177	0.033	[203]
	rGO-PDDA/PMo_{12}/GCE	CV	-	20 - 10 x 10^3	-	[202]

Metal (oxide)	CuII-DHB/CPE	AP	-	2 - 14 x 10^3	0.010	[208]
	Cd-IL/CPE	CV	-	0.005 – 0.020	0.003	[209]
	Ag/PMo_{12}/PBz/GCE	AP	-	-	0.086	[210]
	Pd-NPs/PANI/SBA-15/GCE	CV	-	8 – 40 x 10^3	5	[212]
	AuRh/GCE	CV	-	1 - 26	1	[213]
	CuO/FIA/SPCE	CV	-	0.066 – 1990	0.027	[214]
	CNP-Sn(II)/CPE	SWV	Water	5 - 100	0.060	[215]
Carbon dots	CDs-PEI	ECL	Water	0.04 - 0.35	0.0002	[222]

Table 7 shows that several electroanalytical methods, such as AP, CV, ECL, EIS, and SWV, have been used to detect BrO_3^- with AP and CV leading the group. These methods have successfully achieved the degree of sensitivity and detection limit necessary for analyzing trace amounts of BrO_3^-, but the fact that EIS has not been employed as frequently as these other methods demand attention. Remarkably, only one instance of EIS was utilized for BrO_3^- detection in the literature (as far as we know). A summary of the electrochemical techniques and sensors that have been previously employed for bromate detection is given in Figure 2.14.

EIS has become one of the most widely used electroanalytical techniques due to its applicability for the precise determination of surface electrochemical processes through the measurement of the interaction of an analyte with a sensor's surface [12]. Besides, EIS is a relatively straightforward technique [224] that delivers data in a simple way to understand. It also aids in separating the charge transport associated with the bulk membrane and the interfacial processes.

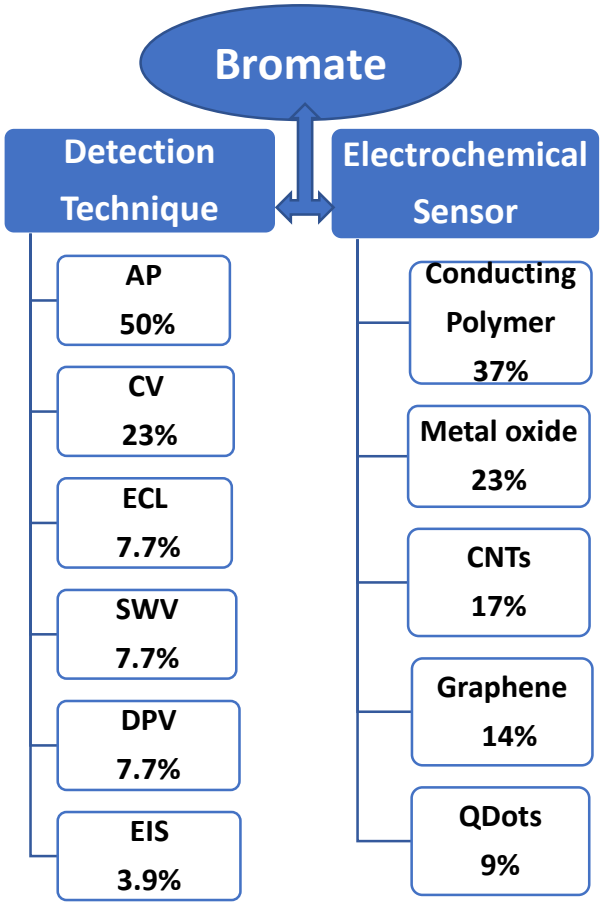

Figure 2.14. Summary of the electrochemical techniques and sensors for bromate detection.

Meanwhile, EIS has been successfully used for the determination of many analytes such as ascorbic acid AA [225], amitrole, glyphosate [226], aldehyde [227], iodate, chlorate, phthalates, perchlorate [8], etc. Here, only a few of them are discussed.

An EIS sensor was developed by Qiu et al. [225] for the detection of AA using a Cu (I) catalyst. This sensor offered LoD and LDR of 2.6 pM and 5-1000 pM, respectively as well as high sensitivity, selectivity, and stability. This sensor has a good recovery when applied to a real sample such as urine.

Another EIS sensor was fabricated by Fares et al. [226] for glyphosate determination in water using a molecularly imprinted chitosan. The sensor showed good sensitivity and selectivity for glyphosate detection giving a wide LDR of 0.31-50000 pg mL^{-1} with a very low LoD of 0.001 pg mL^{-1} over. The detection of different pesticides confirmed the selectivity of this technique. Very high selectivity factors were obtained for glyfosinate (7.9), phosmet (14.5), and chlorpyrifos (43.5).

Boumya and his group [227] researched on aldehyde detection via the EIS technique. This study showed that the electrode has a LoD of around 0.0109 µM and can detect over an LDR of 0.05-1000 µM. Real sample analysis of BrO_3^- in drinking water, apple, and orange juice was performed with good recovery and standard deviation.

Several materials have been used to fabricate sensors for BrO_3^- detection, but despite their unique features, neither phthalocyanines nor metal phthalocyanines were used to create any such sensor. Only a few with carbon quantum dots. Meanwhile, numerous publications detailing the uses of metal phthalocyanines with good sensitivity and low LoD are available, few examples include the determination of paracetamol [228], carbohydrates [229], metronidazole [230], phenols, chlorophenols, cresols [231], thiols [232], hydroxyquinoline [233], glutathione [234], NADH [235], glucose and hydrogen peroxide [236], hydrogen sulphide [237], hydrazine [238], toluene [239] and citrate [240].

This section has summarized the efforts made in the electrochemical detection of bromate with high selectivity and sensitivity by modifying the electrode surface with different modifiers. It has also pointed out techniques and sensors that still need to be explored for sensitive and selective

determination of bromate. In brief, CoPcMWCNTs-GCE and NiPcMWCNTs-GCE have never been used for bromate detection, while EIS only appeared once.

Hence, this present study explores the use of an electrochemical method (EIS) and cobalt/nickel, phthalocyanine, and fMWCNTs to fabricate electrochemical sensors for bromate detection in foods.

CHAPTER THREE

Materials and Methods

A general overview of the chemicals, equipment, and methods of synthesizing the nanoparticles and nanocomposites are explained in this chapter. The methodology involved in MWCNTs functionalization, electrode modification, analyte preparation, bread samples preparation, electrochemical and Impedance studies, concentration studies, and Interference studies are also discussed herein.

3.1. Materials and Reagents

3.1.1 Chemicals

Multiwalled carbon nanotubes (MWCNTs) with 98%, N, N-dimethyl formamide (DMF), ethylene glycol, potassium bromate ($KBrO_3$), potassium hexacyanoferrate IV ($K_4(Fe(CN)_6$) (99 %), potassium hexacyanoferrate III ($K_3(Fe(CN)_6$) (99 %), sodium dihydrogen phosphate (NaH_2PO_4) (99.99 %), and disodium hydrogen phosphate (Na_2HPO_4) (99 %) were supplied by Sigma-Aldrich (Darmstadt, Germany). Hydrazine hydrate, 29H, 31H-Phthalocyanine, cobalt acetate tetrahydrate, nickel chloride, sodium borohydride, sulfuric acid, and methanol were obtained from Glassworld Chemicals (Johannesburg, South Africa). The hydrochloric acid (HCl) and sodium hydroxide (NaOH) employed for the pH adjustment were purchased from Merck Chemicals (PTY) LTD (Germiston, South Africa). All reagents were analytical grade. Distilled water was used throughout the experiment.

3.1.2. Equipment

The structural and morphological characterization of the modified electrodes were performed by UV–visible spectrophotometry using UV−Vis spectrometer Carry 300 series by Agilent Technology, Darmstadt, Germany, transmission electron microscopy (TEM) with JEOL2100 instrument fitted with a LaB 6 electron gun from JEOL Ltd, Tokyo, Japan, scanning electron microscopy (SEM) by JEOL JSM-6610 LV, Dearborn, Peabody, MA, USA, Energy diffraction X-ray (EDX) by JEOL JSM-6610 LV, Dearborn, Peabody, MA, USA (EDX), and X-ray diffraction spectrophotometry (XRD) by Bruker Company, Karlsruhe, Germany. All electrochemical and EIS studies were performed on an Autolab Potentiostat PGSTAT 302 (Eco Chemie, Utrecht, The Netherlands) with GPES (version 4.9) software (Utrecht, The Netherlands).

The workstation uses the three-electrode system, which is a glassy carbon electrode (working electrode), platinum electrode (counter electrode), and Ag/AgCl with 3 M KCl (reference electrode). The EIS data were also obtained via Metrohm Autolab (FRA 32) NOVA 2.1.3 software (Utrecht, Netherlands) with a frequency range of 100 kHz–0.1 Hz.

3.2 Methods

3.2.1 Synthesis of Cobalt Nanoparticles

Cobalt nanoparticles CoNPs were synthesized by dissolving 2.0 g of cobalt acetate tetrahydrate in a solution containing 8 mL of ethanol and 2 mL of water and stirred for 15 min. Then, with constant stirring, 5.0 mL of 1.08 M of sodium borohydride solution was added to the mixture in drops (2 drops per second). The greyish black particles obtained were collected with a magnet from the mixture and washed severally with distilled water and lastly with ethanol, and then dried at room temperature for 24 h [241].

3.2.2 Synthesis of Nickel Nanoparticles

The synthesis of nickel nanoparticles (NiNp) was achieved by simultaneous dissolving 0.955 g of nickel chloride and 5.0 mL of hydrazine hydrate in 400.0 mL of ethylene glycol in a closed flask. Then, 4.0 mL of 1 M NaOH solution was added to the reaction mixture and constantly stirred for 1 h at 60°C. The solid black product obtained was completely rinsed with ethanol and dried for 24 h under vacuum at 35°C [242]

3.2.3 Functionalization of MWCNTs

Using the following treatment procedure, -COOH groups were introduced onto raw MWCNTs surfaces. 100 mg of the raw MWCNTs were added to an acidic mixture of 270 mL conc. H_2SO_4 and 90 mL conc. HNO_3 in a round-bottomed flask was subjected to continuous heating for 5 h at 55°C and another 8 h at 80°C. The liquid content of the mixture was decanted off while the solid black particles were washed thoroughly with distilled water till they became neutral. The solid particles obtained were dried at 70°C for 24 h [74].

3.2.4 Fabrication of CoPcMWCNTs and NiPcMWCNTs Nanocomposites

CoPcMWCNTs nanocomposites were prepared by dissolving a mixture of 5.0 mg of 29H, 31H phthalocyanine Pc, and 5.0 mg of CoNp in 1 mL DMF under ultrasonication for 3 h. Afterwards, 2.5 mg of functionalized multiwalled carbon nanotubes fMWCNTs were added to the DMF

mixture containing the Pc and CoNPs and sonicated for an additional 5 h. The cobalt phthalocyanine nanoparticles (CoPc) were then adsorbed onto fMWCNTs by spontaneous adsorption and sonication (as illustrated in Figure 3.1) to obtain CoPcMWCNTs nanocomposites [74]. NiPcMWCNTs nanocomposites were also synthesized using the same procedure but with NiNPs. The ability of Pc to accommodate up to 70 different metal atoms into the rings and to vary the side chain substituents serve as the driving force for the easy combination of Co NPs or Ni NPs with the Pc to form CoPc or NiPc. Additionally, the presence of hydrogen bonds, coordination interactions, and van der Waal forces allow Pc to bind a variety of metals/analytes in an indifferent way [74, 99].

3.3 Preparation of the Analyte

The analyte used for this study was prepared by dissolving 0.167 g $KBrO_3$ in 100 ml of 0.1 M H_2SO_4 (pH 1) to obtain 10 mM BrO_3^-. Every other bromate concentration was prepared by diluting the 10 mM bromate solution.

3.4 Preparation of Bread Samples for Real Sample Analysis

A serial dilution approach was used for preparing the bread samples. 250 mL distilled water was added to 5 g of ground, and powdered bread sample in 250 mL volumetric flask, and the mixture was thoroughly shaken and sonicated for 30 min at room temperature. The mixture was centrifuged (at 3000 RPM), and the liquid fraction was obtained. Prior to this, a preliminary qualitative test was performed directly on the bread samples and obtained liquid fraction. A mixture of 0.6 mL of 12 M hydrochloric acid and 2 mL of 0.01 M promethazine was added to the raw bread samples. The change in colour of the bread samples to pink indicates the presence of potassium bromate. This was also carried out on the obtained liquid fraction. A 0.5 mL of the bread sample solution was transferred into a 100 mL volumetric flask and made up to the 100 mL mark with 0.1 M H_2SO_4 (pH 1). This was followed by a 100-fold dilution of 0.5 mL of this stock solution. Afterwards, 10 mL of the diluted bread sample solutions were transferred into four different 50 mL volumetric flasks. One of the four flasks containing the diluted bread sample solution was spiked with the desired amount of bromate, and the other samples were left unspiked.

3.5 Electrode Modification

The surface of the glassy carbon electrode (GCE) was thoroughly cleaned before the modification by gently polishing over a micro cotton pad containing an aqueous slurry of alumina nanopowder. After that, the GCE was completely rinsed with distilled water and absolute ethanol for 5 min under ultrasonic surface vibration to remove any leftovers of alumina particles on the GCE's surface. Various suspensions of the nanocatalysts were obtained by dissolving 5 mg of each of the prepared fMWCNTs, CoNp, NiNp, Pc, NiPcMWCNTs, and CoPcMWCNTs in 1 mL DMF and subjected to 20 min of ultrasonication. The prepared nanocatalyst suspensions were then used to modify the GCE via a drop-dry approach. Five milliliters of the suspensions of fMWCNTs, CoNp, NiNp, Pc, CoPcMWCNTs, and NiPcMWCNTs were dropped on the surface of the cleaned GCE and left to dry for 5 min at 50 ^{o}C.

3.6 Characterization of Fabricated Nanomaterials

The successful synthesis of the nanomaterials and the nanocomposites was confirmed by scanning electron microscopy, transmission electron microscopy techniques, X-ray diffraction spectrophotometry, Energy Dispersive Analysis Analysis EDX, and UV–visible spectrophotometry.

About 1 mg of each of the nanomaterial and the nanocomposite were dissolved in 5 mL DMF and sonicated for 30 min. Afterwards, the resultant solution was analyzed using the UV−Vis spectrometer Carry 300 series by Agilent Technology, Darmstadt, Germany. Dry samples of the nanomaterials and the nanocomposites were used for the XRD, SEM, TEM, and EDX analysis.

3.7 Electrochemical and Impedance Studies

An EIS experiment was carried out in 5 mM $[Fe(CN)_6]^{4-/3-}$ produced in 0.1 M PBS at a pH 7 using an Autolab Potentiostat PGSTAT 302 at a frequency range of 100 kHz-0.1 Hz and a fixed potential of 0.3V versus Ag/AgCl, saturated with 3M KCl in order to thoroughly investigate the specific capacitance and electron transport properties of the GCE and modified electrodes. A potential of 0.3 V was chosen for this experiment because it had the highest capacitance/current peak. All the impedance data obtained were fitted using the Metrohm Autolab NOVA 2.1.3 program (Utrecht, Netherlands). The bare and the modified electrodes (GCE-Pc, GCE-Ni, GCE-Co, GCE-fMWCNTs, GCE-CoPcMWCNTs, and GCE-NiPcMWCNTs) were used as the working

electrodes. The counter electrode was platinum wire, while the reference electrode used was Ag/AgCl in saturated KCl. All experiments were conducted at 25 ± 1 °C. Moreover, electrochemical impedance spectroscopy (EIS) and cyclic voltammetry (CV) techniques confirmed the successful modification of the working electrodes.

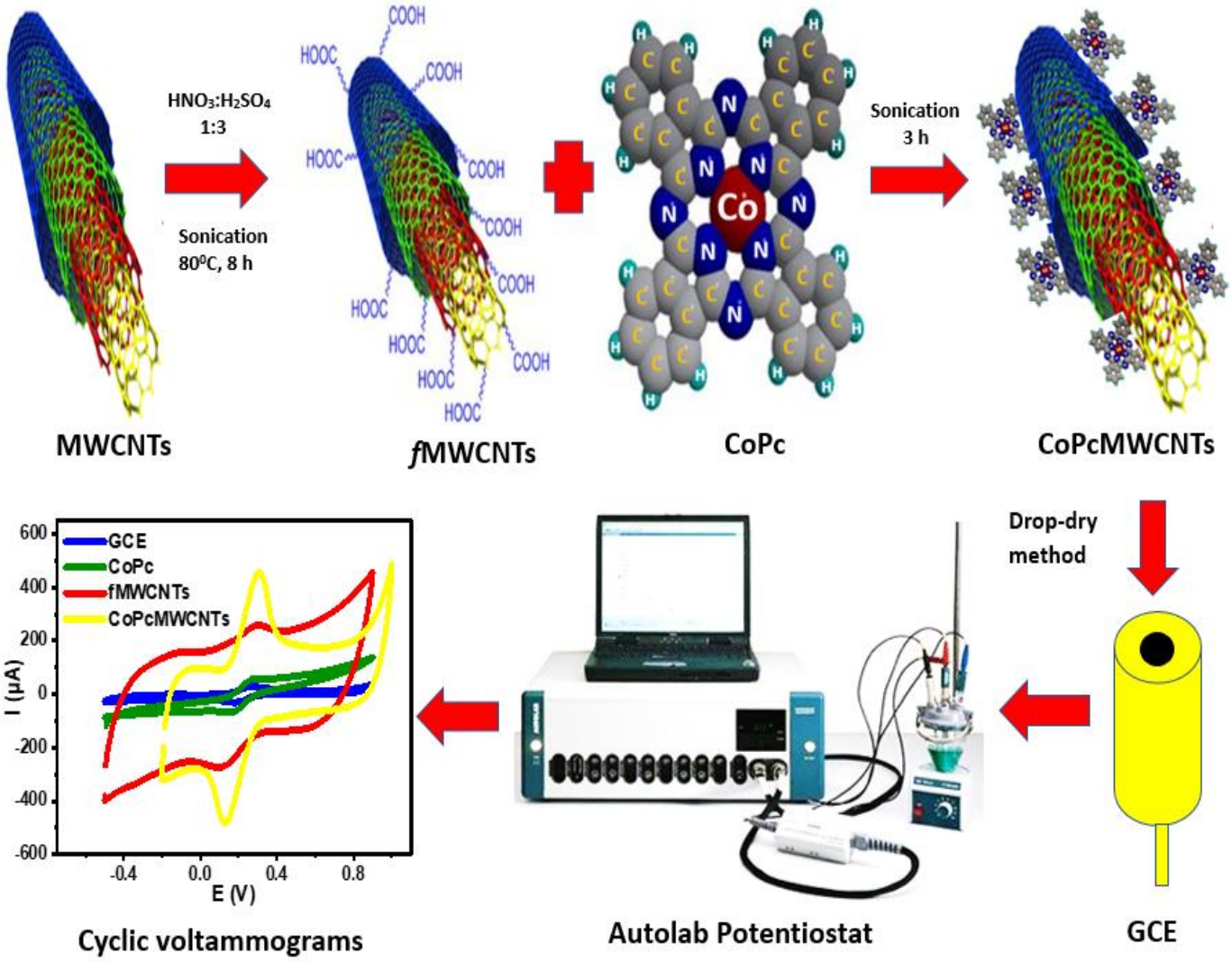

Figure 3.1. Fabrication and modification process of CoPcMWCNTs nanocomposite.

3.8 Concentration Studies

In 0.1 M H_2SO_4 (pH 1), the effect of the concentration of the bromate (24 – 167 µM) on the charge transfer resistance R_{ct} was investigated at the modified electrodes using electrochemical

impedance spectroscopy. The analyte's limit of detection (LoD), the limit of quantitation (LoQ), and the linear dynamic range (LDR) of the nanocomposites modified electrodes were obtained from the calibration curve of the concentrations of the analyte against the R_{ct} values. The LoD and LoQ were estimated using 3.3 σ/m and 10 σ/m, respectively, where m and σ denote the slope and the standard deviation of the intercept of the calibration curve, respectively.

3.9 Interference Studies

The interference experiment of the proposed bromate sensors (GCE-CoPcMWCNTs and GCE-NiPcMWCNTs) was carried out by comparing the EIS response of 0.1 mM bromate before and after adding some possible interferents at a fixed potential (−0.3 V) in the 0.1 M H_2SO_4 solution at a pH of 1. This involves measuring the EIS of 0.1 mM bromate alone, followed by the EIS of the mixture of 10 fold of each interfering molecule (Na^+, K^+, Cl^-, SO_4^{2-}, ClO_3^-, NH_4^+ and CO_3^{2-}) and 0.1 mM bromate. The selectivity of the bromate sensor was taken to be the R_{ct} ratio of the mixtures (1 mM) of each interfering molecule in the presence of 0.1 mM bromate compared to that of 0.1 mM bromate alone.

3.10 Real Sample Analysis

The real sample analysis was performed using the standard addition technique with bread samples containing bromate. The concentration of the analyte obtained from the unspiked real sample (C_o) and that of the samples spiked with a known analyte concentration (C_2) were recorded. The concentration of the analytes added to the unspiked sample was also recorded (C_1). For each sample, the experiments were carried out in triplicate, and the percentage recovery (% recovery) was estimated using Equation 3.1.

$$\% \text{ recovery} = \frac{C_1}{C_2 - C_0}\ x\ 100 \qquad (3.1)$$

3.11 Stability, Scan Rate and Reproducibility Studies

The stability of the fabricated sensor was carried out, firstly by modifying the GCE with CoPcMWCNTs or NiPcMWCNTs nanocomposite. Afterward, the GCE-CoPcMWCNTs or GCE-NiPcMWCNTs were subjected to 20 repeated scans at a scan rate of 50 mVs^{-1} and 75 mVs^{-1}, respectively, in 1 mM $KBrO_3$ prepared in 0.1 M H_2SO_4 (pH 1) using CV.

For the scan rate studies, the GCE-CoPcMWCNTs or GCE-NiPcMWCNTs were subjected to a CV scan at a scan rate of 25 - 300 mVs^{-1} in 1 mM $KBrO_3$ prepared in 0.1 M H_2SO_4 (pH 1).

The reproducibility of the fabricated sensor was investigated in 1 mM $KBrO_3$ prepared in 0.1 M H_2SO_4 (pH 1) using cyclic voltammetry. The bare GCE was modified with CoPcMWCNTs or NiPcMWCNTs nanocomposite three different times and the subjected to a scan rate of 25 mVs^{-1} in 1 mM $KBrO_3$ prepared in 0.1 M H_2SO_4 (pH 1) using CV. The produced cyclic voltammogram for each CV experiment was recorded. The percentage relative standard deviation (% RSD) of the current responses recorded for the three consecutive modifications was then calculated.

3.12 Effect of Electrolytes and pH

Impedance spectroscopy experiment was carried out on GCE-CoPcMWCNTs, or GCE-NiPcMWCNTs in four different electrolytes to ascertain the most suitable supporting electrolyte for bromate detection. The modified electrodes were then subjected to an EIS experiments in four different electrolytes such as 0.1 M $KBrO_3$ prepared in 0.1 M sodium acetate buffer (SAB) (pH 7), 0.1 M $KBrO_3$ prepared in 0.1 M H_2SO_4 (pH 1), 0.1 M $KBrO_3$ prepared in 0.1 M Na_2SO_4 (pH 2), and 0.1 M $KBrO_3$ prepared in 0.1 M PBS (pH 7) to determine the R_{ct} values of the electrodes.

Four different 0.1 M H_2SO_4 containing 1 mM $KBrO_3$ solutions with different pH values (1, 2, 3, & 5) were prepared. The fabricated electrodes were then subjected to CV experiments with each of the electrolyte containing varying pH at the same experimental conditions, to investigate the electrolyte with the highest cathodic peak current and the best reduction peak resolution for bromate detection.

CHAPTER FOUR

Results and Discussion

4.1 Characterization

4.1.1 X-ray Diffraction (XRD)

The crystalline structure of the prepared cobalt (CoNPs) and nickel nanoparticles (NiNPs) were determined. The XRD patterns of CoNPs and NiNPs, as depicted in Figure 4.1(a) shows three similar diffraction peaks each at 2θ = 44.7^o (1 1 1), 52.0^o (2 0 0), 76.3^o (2 2 0), and 44.5^o (1 1 1), 51.9^o (2 0 0), 76.5^o (2 2 0) corresponding to face-centered cubic of pure cobalt and nickel respectively. The peaks are similar to those in literature [24, 242, 243], confirming that the synthesized nanoparticles are purely cobalt and nickel nanoparticles. 18 nm and 12 nm were obtained as average crystallite size (D) for the synthesized CoNPs and NiNPs, respectively, using Scherrer's equation (Eqn. 4.1) below [244].

$$D = \frac{0.89\lambda}{\mathrm{B}\cos\theta} \tag{4.1}$$

where:

λ stands for the wavelength,

B denotes the full width at half-maximum peak, and

θ represents the XRD peak's Bragg angle.

The XRD pattern of the raw MWCNTs and functionalized MWCNTs are shown in Figure 4.1b. The diffraction peak at 2θ of 26.34^o (002) is assigned to rMWCNTs, while 25.98^o (002) and 42.32^o (101) are for fMWCNTs. A well-pronounced diffraction peak observed at 2θ of 25.98^o confirms that the rMWCNTs was successfully functionalized [245, 246]. The pristine Pc displayed a XRD pattern as shown in Figure 4.1c with its characteristic peaks at 6.85 (100), 9.04 (102), 13.68 (202), 15.03 (200), and 18.19 (101). In Figure 4.1d, six peaks were observed for the CoPcMWCNTs nanocomposites. The peaks at 44.47^o, 51.79^{o,} and 76.23^o are attributed to CoNPs, a wide and duplet peak at 26.5^o (002) is assigned to the fMWCNTs, while the peaks at 10.94^o, and 17.40^o are distinctive peaks of phthalocyanines [247]. Similar diffraction peaks were also observed for the NiPcMWCNTs nanocomposites as shown in Figure 4.1e. The peaks at 44.70 ^{o}, 51.97^{o,} and 76.60^o

are attributed to NiNPs, a wide and strong peak at 26.31° (002) is assigned to the fMWCNTs, while the peaks at 6.93°, 9.20°, and 17.40°, are distinctive peaks of phthalocyanines. These peaks are similar to those reported in literature [33, 122]. The appearance of Co/Ni, fMWCNTs and Pc in the nanocomposites spectral (Figure 4.1d & 4.1e), confirmed the successful fabrication of both CoPcMWCNTs and NiPcMWCNTs nanocomposites.

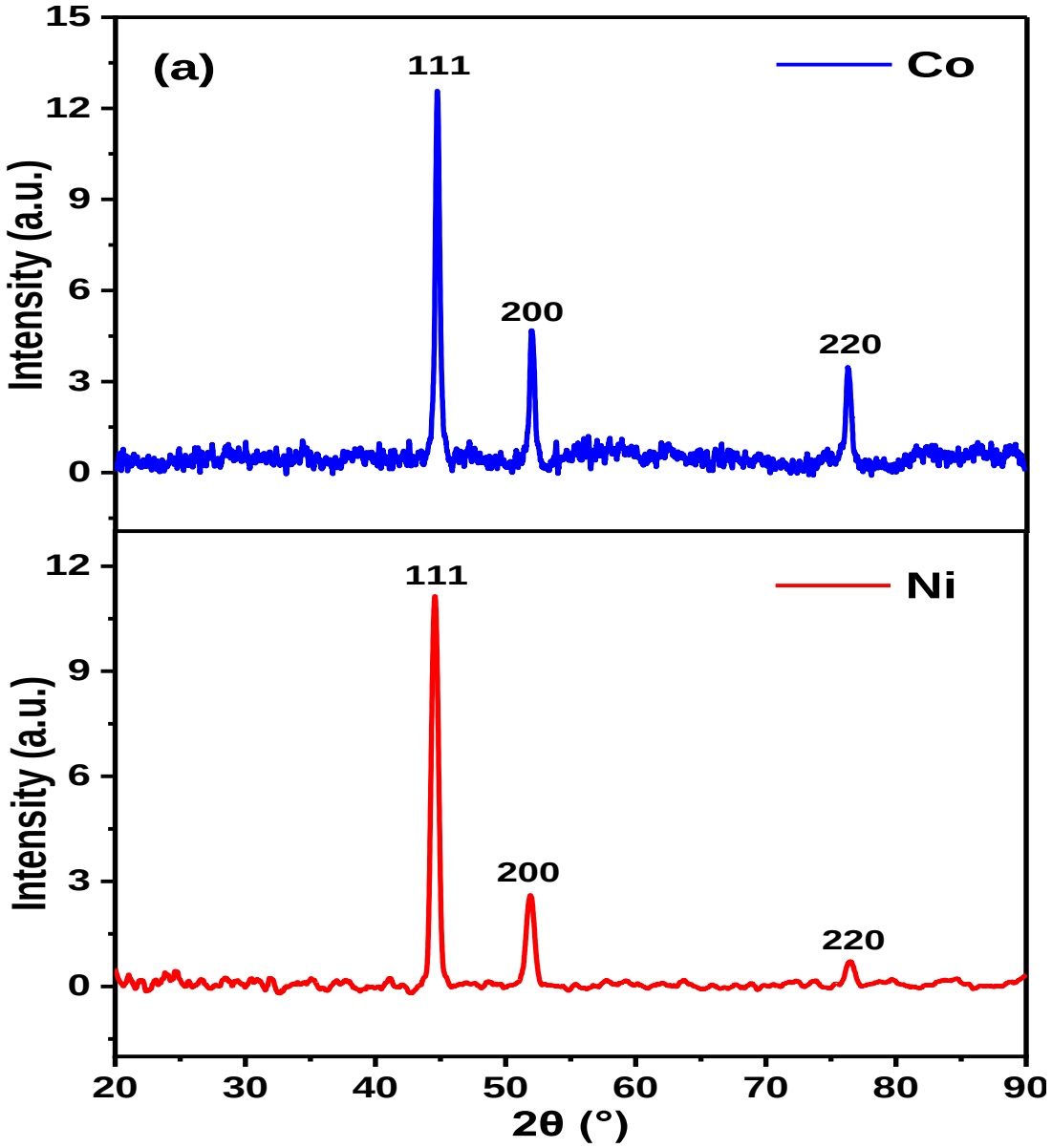

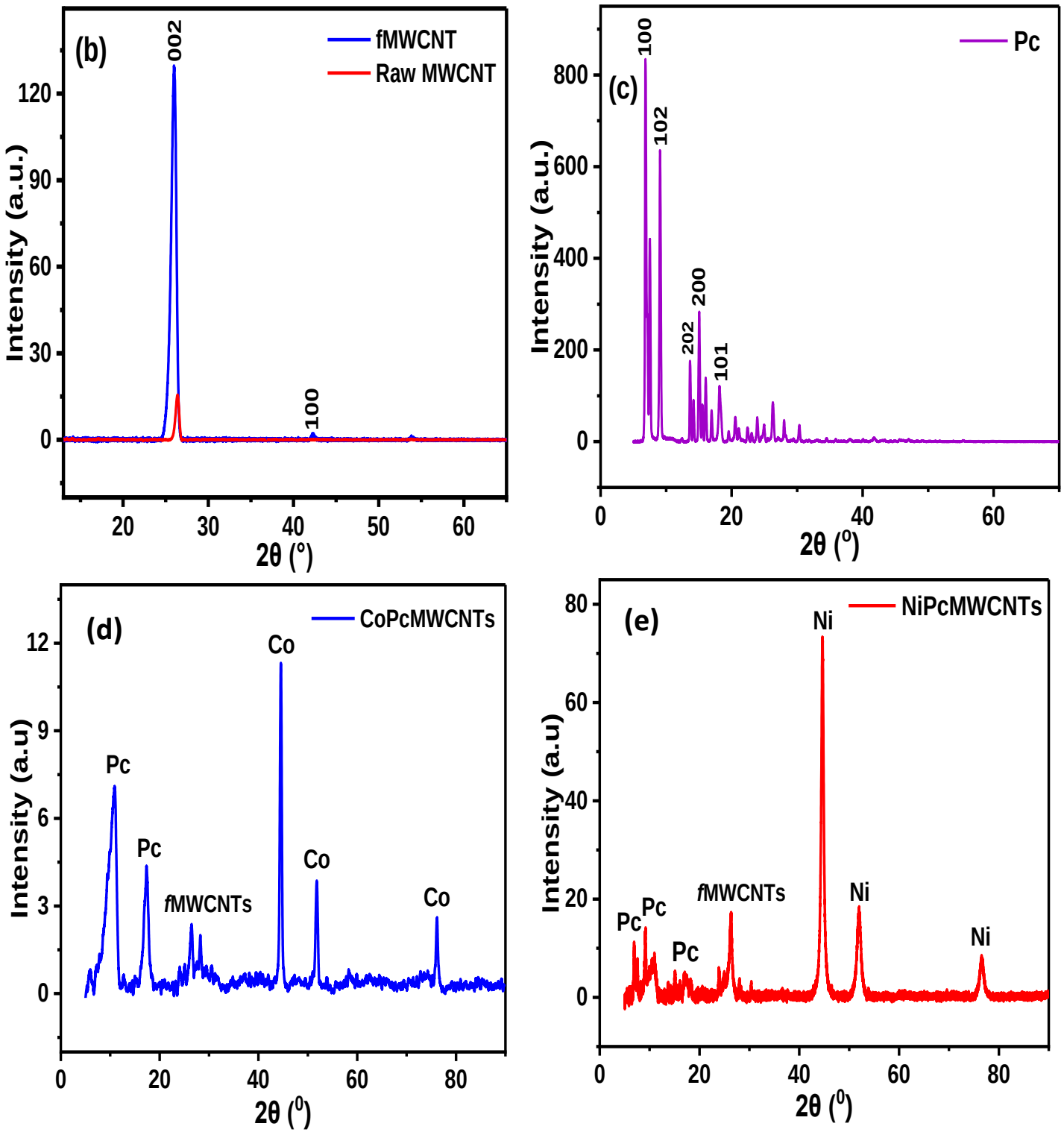

Figure 4.1. XRD spectra of (**a**) CoNPs and NiNPs, (**b**) rMWCNTs and fMWCNTs, (c) Pc, (**d**) CoPcMWCNTs nanocomposites, and (e) NiPcMWCNTs nanocomposites.

4.1.2 Energy Dispersive X-ray (EDX)

The EDX spectra depicted in Figure 4.2 reveal the elemental composition of (a) nickel nanoparticles, (b) cobalt nanoparticles, (c) CoPcMWCNTs nanocomposite, and (d) NiPcMWCNTs nanocomposite. The appearance of carbon, oxygen and sodium in the NiNp and CoNp spectral (Figure 4.2a & b) are infiltrated impurities from the precursors. Likewise, the sulphur and chlorine in the NiPcMWCNTs nanocomposites' spectrum (Figure 4.2d) are from the concentrated H_2SO_4 and HCl used to functionalize the MWCNTs. The presence of carbon and nitrogen (indicating phthalocyanine), carbon and oxygen (indicating *f*MWCNTs), and nickel and cobalt in the nanocomposites' spectral (Figures 4.2c and 4.2d) confirmed that both CoPcMWCNTs and NiPcMWCNTs nanocomposites were successfully fabricated.

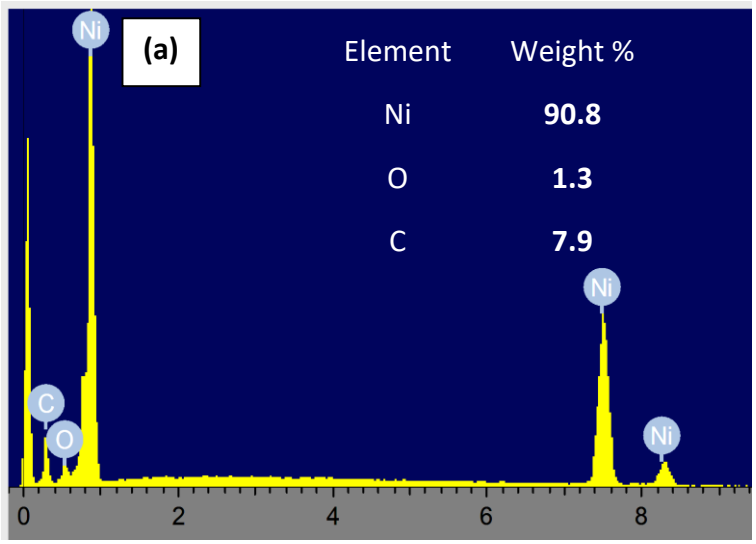

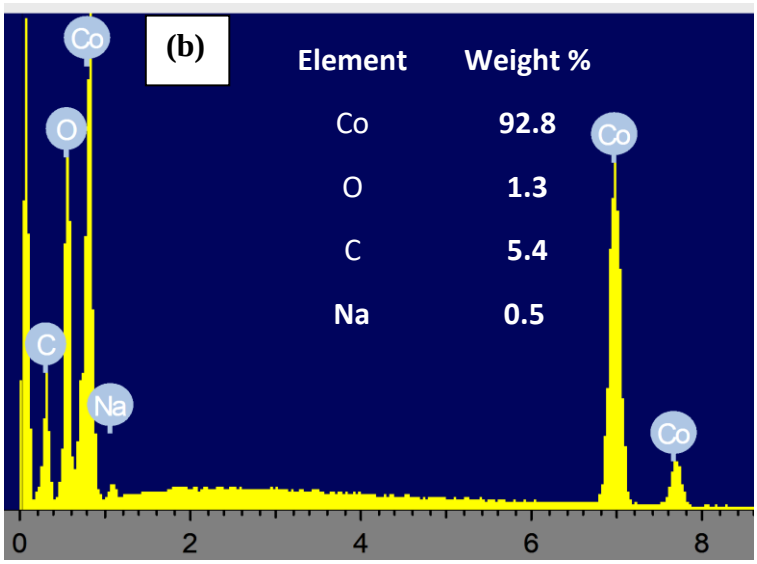

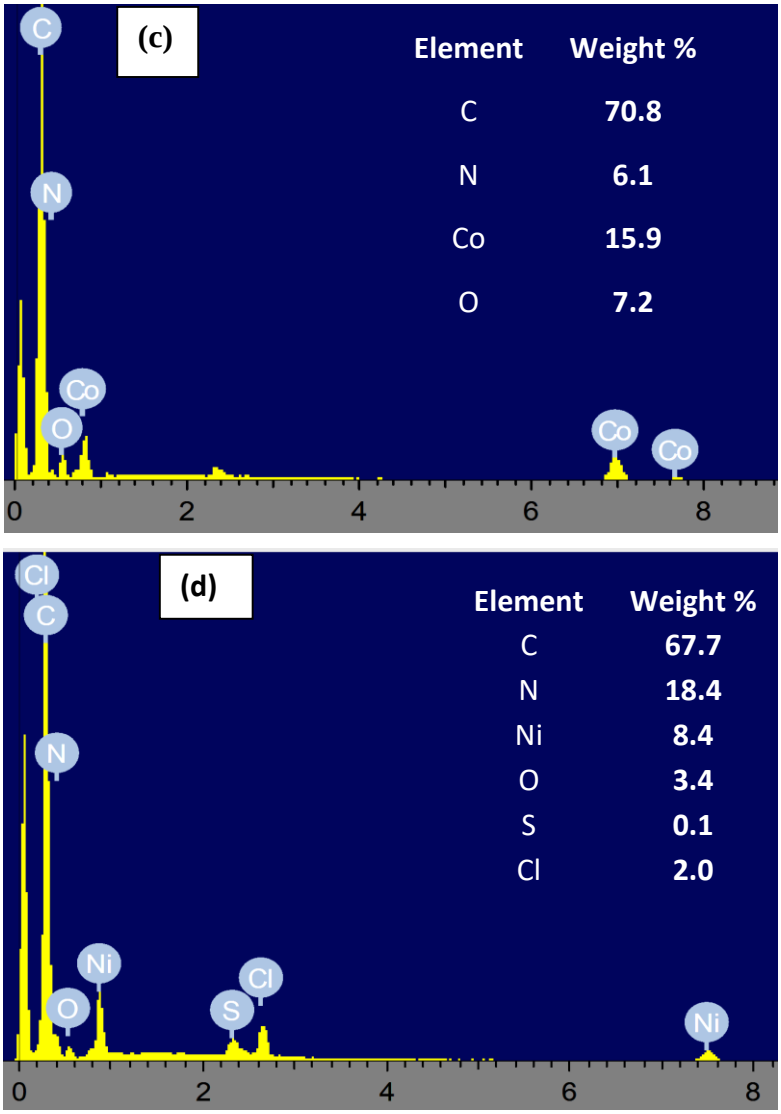

Figure 4.2. EDX spectra of (a) NiNPs, (b) CoNPs (c) CoPcMWCNTs and (d) NiPcMWCNTs nanocomposites.

4.1.3 Ultraviolet-Visible

Figure 4.3 elucidates the UV–vis absorption spectra of (a) CoNPs and NiNPs, (b) rMWCNTs and fMWCNTs, (c) CoPcMWCNTs nanocomposite, and (d) NiPcMWCNTs nanocomposite. Figure 4.3a represents the absorption spectral of CoNPs and NiNPs having absorption peaks at 298 nm and 293 nm respectively. Figure 4.3b shows a clear difference in the absorption peaks of rMWCNTs and fMWCNTs at 289 and 294 nm, indicating that the raw MWCNTs were successfully functionalized. The interaction between the molecular orbitals of the 18 electrons of

the aromatic system and the overlapping orbitals of the central metal atom [248] accounts for the phthalocyanine UV-vis spectrum [118].

The spectrum is generated by electronic transitions either from the highest occupied molecular orbital (HOMO) to the lowest unoccupied molecular orbital (LUMO) or vice visa, i.e., $\pi^* \rightarrow \pi$ or $\pi \rightarrow \pi^*$ transitions. Phthalocyanines are peculiar with two intense absorption bands (B-band and Q-band). The Q-band, which is caused by $\pi \rightarrow \pi^*$ transitions, occurs at 667 nm, while the B-band, which results from $\pi^* \rightarrow \pi$ transitions, occurs in the UV region between 335 and 450 nm. The Q-band splitting occurs at 667 nm in the spectrum due to the D2h symmetry of the compound. The absorption spectra of the CoPcMWCNTs and NiPcMWCNTs nanocomposites, as depicted in Figures 4.3c and 4.3d, exhibit similar B-Bands and Q-bands splitting with all the characteristic peaks for CoNp, NiNp, Pc, and fMWCNTs.

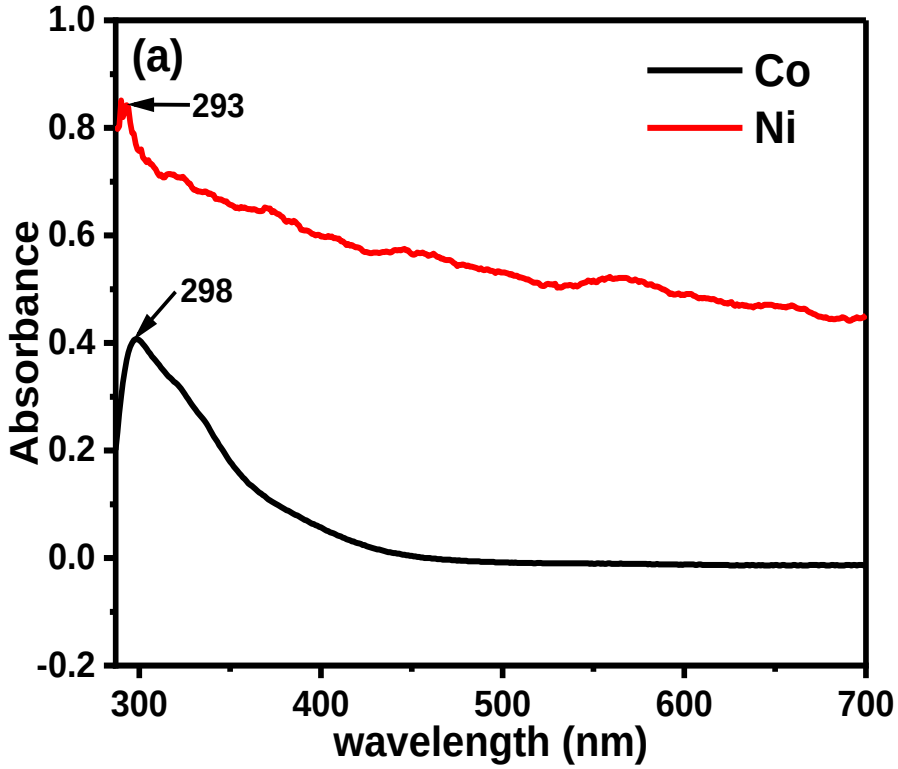

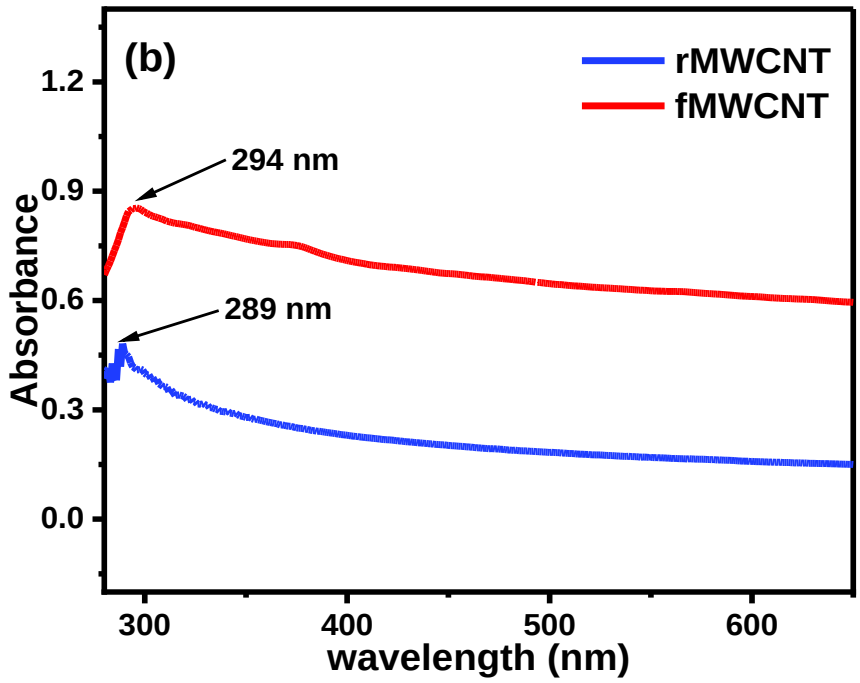
(b)
rMWCNT
fMWCNT
294 nm
289 nm
Absorbance
1.2
0.9
0.6
0.3
0.0
300
400
500
600
wavelength (nm)

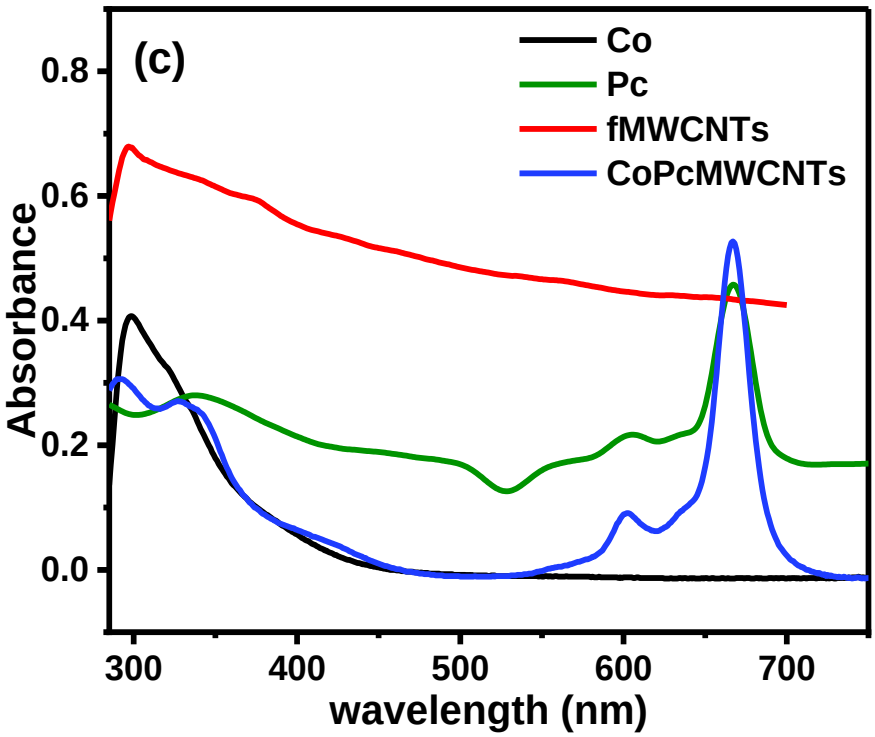
(c)
Co
Pc
fMWCNTs
CoPcMWCNTs
Absorbance
0.8
0.6
0.4
0.2
0.0
300
400
500
600
700
wavelength (nm)

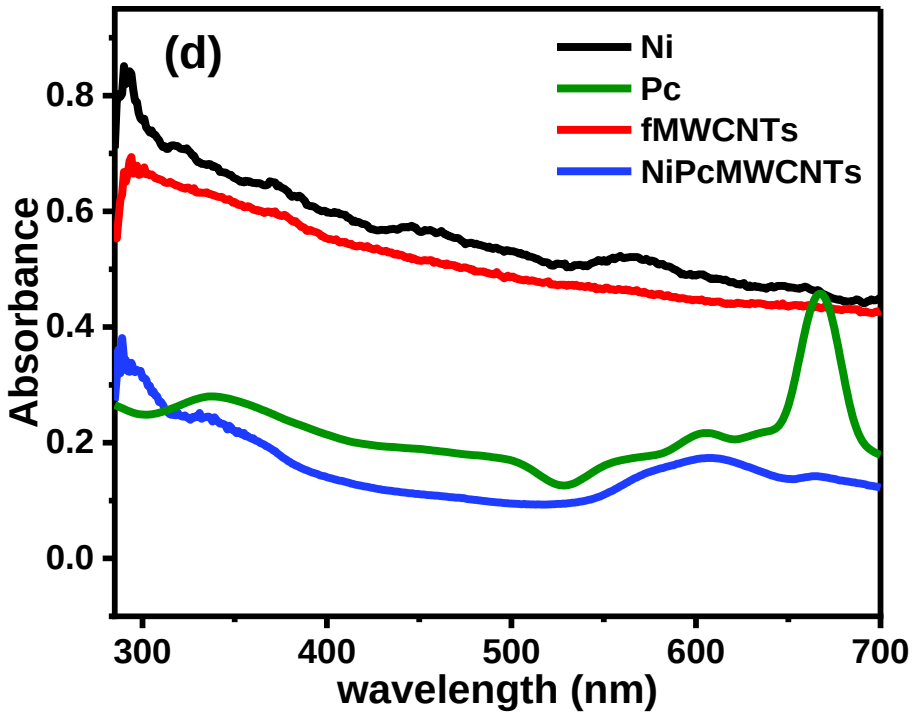

Figure 4.3. UV–vis Spectra for (a) NiNPs & CoNPs (b) rMWCNTs & fMWCNTs, (c) CoNPs, Pc, *f*MWCNTs, and CoPcMWCNTs nanocomposite, and (d) NiNPs, Pc, *f*MWCNTs, and NiPcMWCNTs nanocomposite.

4.1.4 Transmission Electron Microscopy (TEM)

The synthesized nanomaterials' size and shape were determined using TEM. Figure 4.4 displays the TEM images of the NiNPs, CoNPs, Pc, fMWCNTs, CoPcMWCNTs, and NiPcMWCNTs nanocomposite. In Figure 5a, the TEM image of NiNp shows a non-spherical particle shape with smooth but irregular particle morphology, having an average crystallite size of 18 nm, which is closer to the value obtained using Scherrer's equation. The TEM image of the NiPcMWCNTs nanocomposite depicted in Figure 4.4e shows larger aggregates of NiNPs and Pc unevenly dispersed on the fMWCNTs' surfaces. Whereas, in Figure 4.4f, CoNPs and Pc are uniformly attached to the fMWCNTs' surfaces.

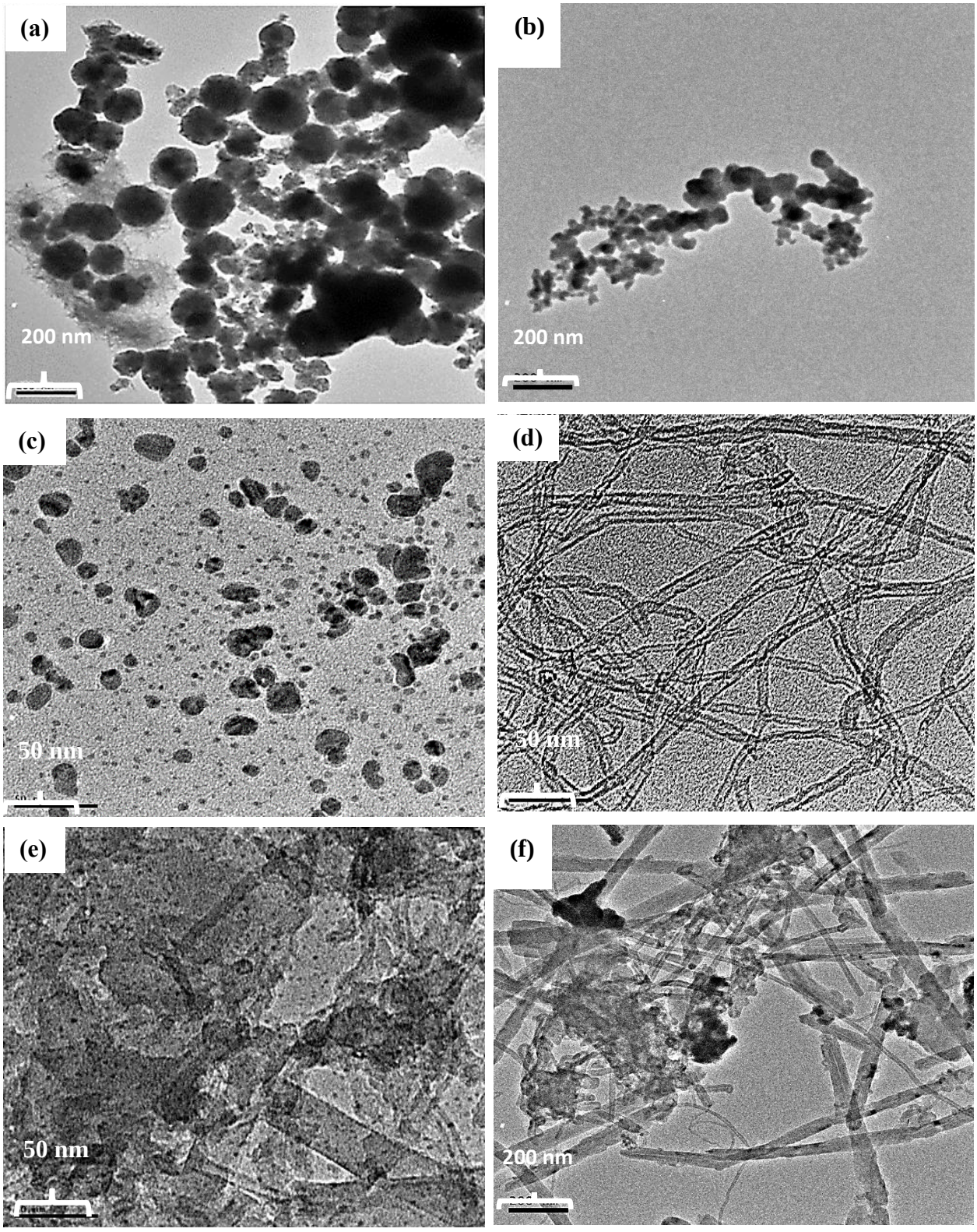

Figure 4.4. TEM images of (a) NiNPs, (b) CoNPs, (c) Pc, (d) fMWCNTs, (e) NiPcMWCNTs nanocomposites, and (f) CoPcMWCNTs nanocomposites.

4.1.5 Scanning Electron Microscopy (SEM)

SEM images of the CoNPs, NiNPs, Pc, fMWCNTs, CoPcMWCNTs, and NiPcMWCNTs nanocomposites are illustrated in Figures 4.5a–f, respectively. The images in Figure 4.5e & f show that the CoNPs, NiNPs, and Pc were fully attached to the surface of the fMWCNTs and therefore, indicating the successful fabrication of CoPcMWCNTs and NiPcMWCNTs nanocomposites.

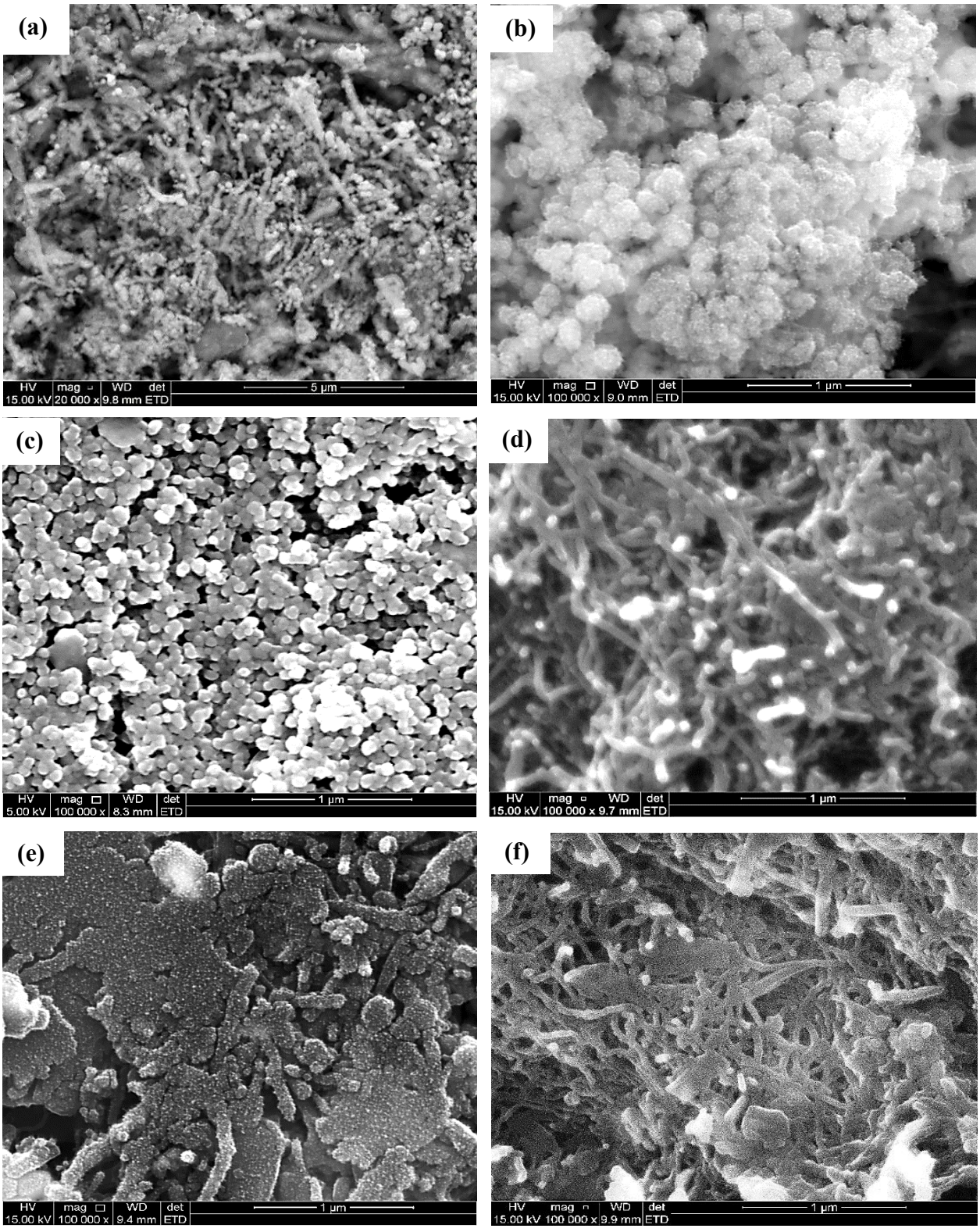

Figure 4.5. SEM images of (a) NiNPs, (b) CoNPs, (b) Pc, (d) fMWCNTs, (e) CoPcMWCNTs and (f) NiPcMWCNTs nanocomposite.

4.2 Electrochemical Characterization of Bare and Modified Electrodes

The electrochemical characterization of bare and modified electrodes was done using the cyclic voltammetry and electrochemical impedance spectroscopy (EIS) technique. A suitable technique for investigating the electron transport properties of electrochemical materials is cyclic voltammetry. Going by the cyclic voltammograms (Figure 4.6), all the electrodes (bare and modified) showed a pair of redox peaks in 5 mM $[Fe(CN)_6]^{4-/3-}$ produced in 0.1 M PBS (pH 7) at a scan rate of 25 mV s^{-1}. As shown in Table 8, 0.39, 0.37, 0.18, 0.13, 0.20, and 0.18 V were obtained for the GCE, GCE-Co, GCE-Ni, GCE-fMWCNTs, GCE-CoPcMWCNTs, and GCE-NiPcMWCNTs, respectively as the electrodes peak separation (E_p) values. These results demonstrate that the reactions at the electrodes are quasi-reversible because they are higher than the predicted 0.059 V for a quick one-electron transfer [249-251]. Table 8 further demonstrates that the I_{pa}/I_{pc} values of all electrodes are approximately one, implying that the reactions at the surface of both the unmodified and modified electrodes were purely reversible. Considering the voltammogram depicted in Figure 4.6, the current response obtained for both modified and unmodified electrodes are in increasing order of GCE-Co (15.7 μA) < GCE (25.0 μA) < GCE-Ni (35.6 μA) < GCE-fMWCNTs (58.0 μA) < GCE-CoPcMWCNTs (259.1 μA) < GCE-NiPcMWCNTs (457.0 μA). The anodic peak current (I_{pa}) response of GCE-NiPcMWCNTs (457.0 μA) is higher than that of GCE-CoPcMWCNTs (259.1 μA), although the two are far greater than those obtained for the GCE and other modified electrodes. GCE-CoPcMWCNTs and GCE-NiPcMWCNTs modified electrodes are 10 and 18 times greater than the bare electrode. This result suggests that the GCE-NiPcMWCNTs electrode has the quickest ability to transport electrons among all electrodes, followed closely by GCE-CoPcMWCNTs. It also demonstrates the successful fabrication of the nanocomposite modified electrodes. The enhanced current response and fast electron transport of the GCE-CoPcMWCNTs and GCE-NiPcMWCNTs-modified electrodes are credited to the synergistic effect of CoNPs/NiNPs, fMWCNTs, and Pc, owing to the Pc and fMWCNTs' larger surface area, and the high electrical conductivity of the cobalt/nickel, and fMWCNTs [118].

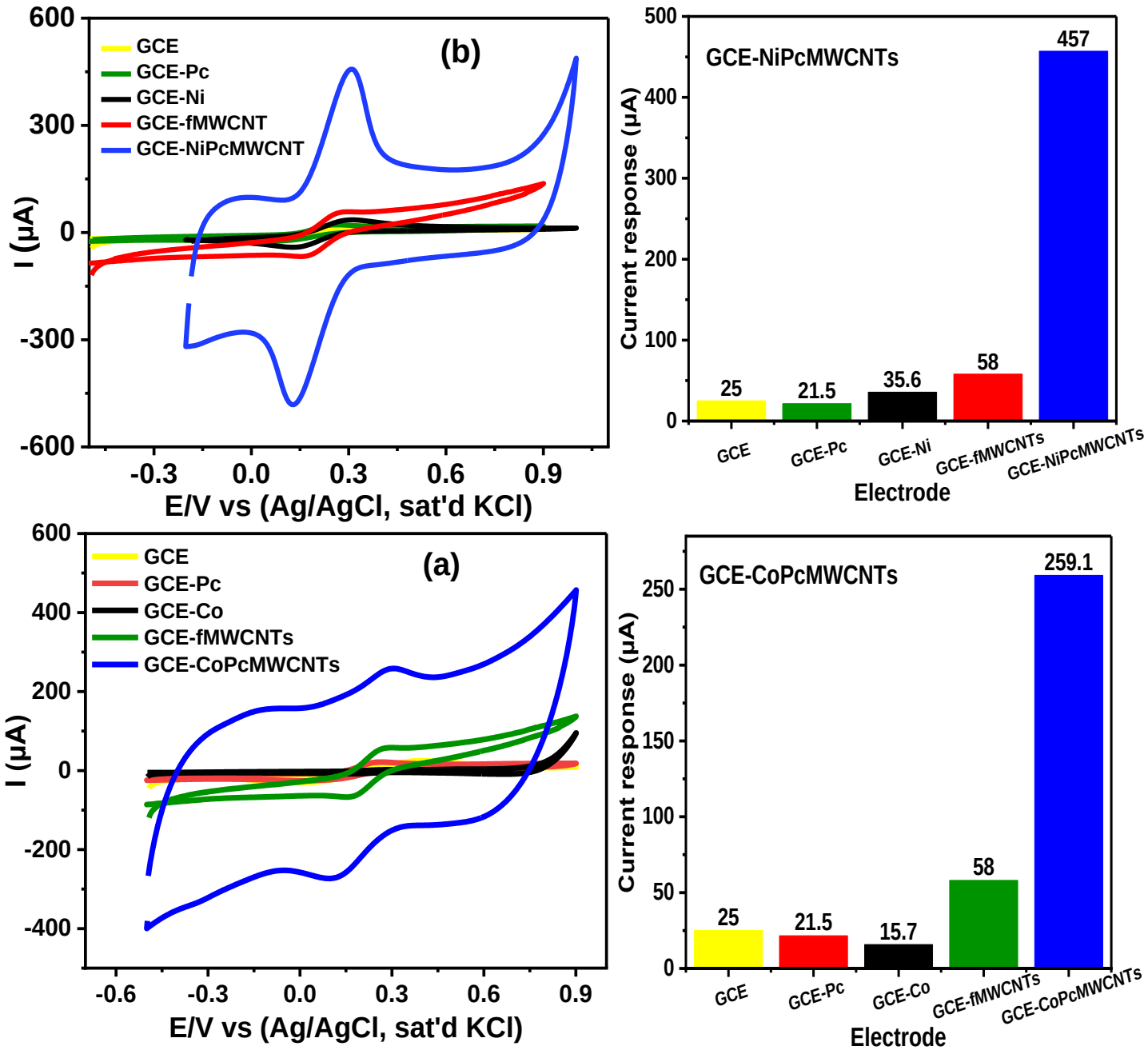

Figure 4.6. Cyclic voltammograms of the GCE and modified electrodes in 5 mM $[Fe(CN)_6]^{4-/3-}$ produced in 0.1 M PBS at a pH 7 (Scan rate:25 mV s^{-1}) with their respective histogram.

The surface area of the bare GCE and modified electrodes was calculated from equation 4.2,

$$I_p = 2.69\ x\ 10^5 n^{3/2} A D o^{1/2} C v^{1/2} \qquad (4.2)$$

where;

I_p represents the peak current (A),

N stands for number of electrons,

V denotes scan rate (V s^{-1}),

D_o stands for diffusion coefficient (cm^2 s^{-1}),

A represents electroactive surface area (cm^2), and

C is the bulk concentration of analyte (mol. cm^{-3}).

Taking 7.6 X 10^{-6} cm^2 s^{-1} as the diffusion coefficient of the redox probe [362], the electroactive surface area obtained were 1.35, 0.85, 1.97, 3.13, 14.0, and 24.7 cm^2 for the GCE, GCE-Co, GCE-Ni, GCE-fMWCNTs, GCE-CoPcMWCNTs, and GCE-NiPcMWCNTs, respectively. The NiPcMWCNTs modified electrode exhibits the highest electroactive surface area and I_{ap}, indicating that the GCE was modified with NiPcMWCNTs to enhance its conductivity and electroactive surface area. As a result of the modified electrode's improved electronic conductivity, electrons are transferred to the redox probe more quickly.

Table 8. Summary of CV results of GCE and modified electrodes in 5 mM $[Fe(CN)_6]^{4-/3-}$ produced in 0.1 M PBS at a pH 7 (Scan rate:25 mV s^{-1}).

Working Electrodes	I_{pa} (μA)	I_{pc} (μA)	I_{pa}/I_{pc}	E_{pa} (V)	E_{pc} (V)	ΔEp (V)	E° (V)	Cp (F/g)
Bare GCE	25.0	−30.0	−0.83	0.40	0.01	0.39	0.20	0.17
GCE-Pc	21.5	−25.9	−0.83	0.26	0.01	0.25	0.13	0.26
GCE-Co	15.7	−22.2	−0.71	0.39	0.02	0.37	0.19	0.30
GCE-Ni	35.6	−41.3	−0.86	0.31	0.13	0.18	0.09	0.31
GCE-fMWCNTs	58.0	−67.1	−0.87	0.29	0.16	0.13	0.07	0.63
GCE-CoPcMWCNTs	259.1	−273.0	−0.95	0.30	0.10	0.20	0.10	7.47
GCE-NiPcMWCNTs	457.0	−482.0	−0.95	0.31	0.13	0.18	0.09	6.80

NiPcMWCNTs and CoPcMWCNTs display higher capacitive currents, indicating that their charge/discharge ability are higher than the other electrodes. From the cyclic voltammograms, the specific capacitances (Cp) of the modified electrodes were estimated using the equation (4.3) below.

$$Cp = \frac{A}{2mk(V_2 - V_1)} \quad (4.3)$$

Where A denotes the area inside the CV curve in A V,

m stands for the mass of active material in g,

k denotes scan rate in mV/s, and

(V2 - V1) denotes the potential window in V/s.

In Table 8, The Cp values obtained for the electrodes were in increasing order of 0.17, 0.30, 0.31, 0.63, 6.80, and 7.47 F g^{-1} for GCE, GCE-Co, GCE-Ni, GCE-fMWCNTs, GCE-NiPcMWCNTs, and GCE-CoPcMWCNTs, respectively. Contrary to the trend observed for the current response, the GCE-CoPcMWCNTs electrode has a much higher specific capacitance value than the GCE-NiPcMWCNTs electrode. Though both GCE-CoPcMWCNTs and GCE-NiPcMWCNTs electrode produced higher specific capacitance values than the other modified electrodes. The enhanced capacitive behavior displayed by the GCE-CoPcMWCNTs over the GCE-NiPcMWCNTs electrode is due to the larger current coverage area of the former. The electrodes' capacitive properties were further investigated using the EIS technique.

4.2.1 Scan Rate Study

The impact of scan rate (25-300 mVs^{-1}) on the electrochemical processes taking place on the surface of GCE-CoPcMWCNTs and GCE-NiPcMWCNTs electrodes were evaluated in a 5 mM $[Fe(CN)_6]^{4-/3-}$ solution prepared in 0.1 M PBS (pH 7) via CV technique. It is clearly shown in Figure 4.7 (a & b), that increase in peak currents are directly proportional to the scan rates. The plot of the peak currents vs the square root of the scan rates in Figure 4.7 (x & y), show a linear trend, leading to the regression equations shown in (Eqn. 4.4, 4.5, 4.6 & 4.7)

For GCE-CoPcMWCNTs

$I_{pa} = 0.0080\ v^{1/2} + 0.0004;$ $(R^2 = 0.9889)$ (4.4)

I_{pc} = -0.0072 $v^{1/2}$ + 0.0004; (R^2 = 0.9881) (4.5)

For GCE-NiPcMWCNTs

I_{pa} = 0.0054 $v^{1/2}$ - 0.0004; (R^2 = 0.9987) (4.6)

I_{pc} = -0.0048 $v^{1/2}$ + 0.0003; (R^2 = 0.9990) (4.7)

The linearity between the square root of the scan rate and peak currents in GCE-CoPcMWCNTs and GCE-NiPcMWCNTs demonstrates a typical diffusion-controlled process.

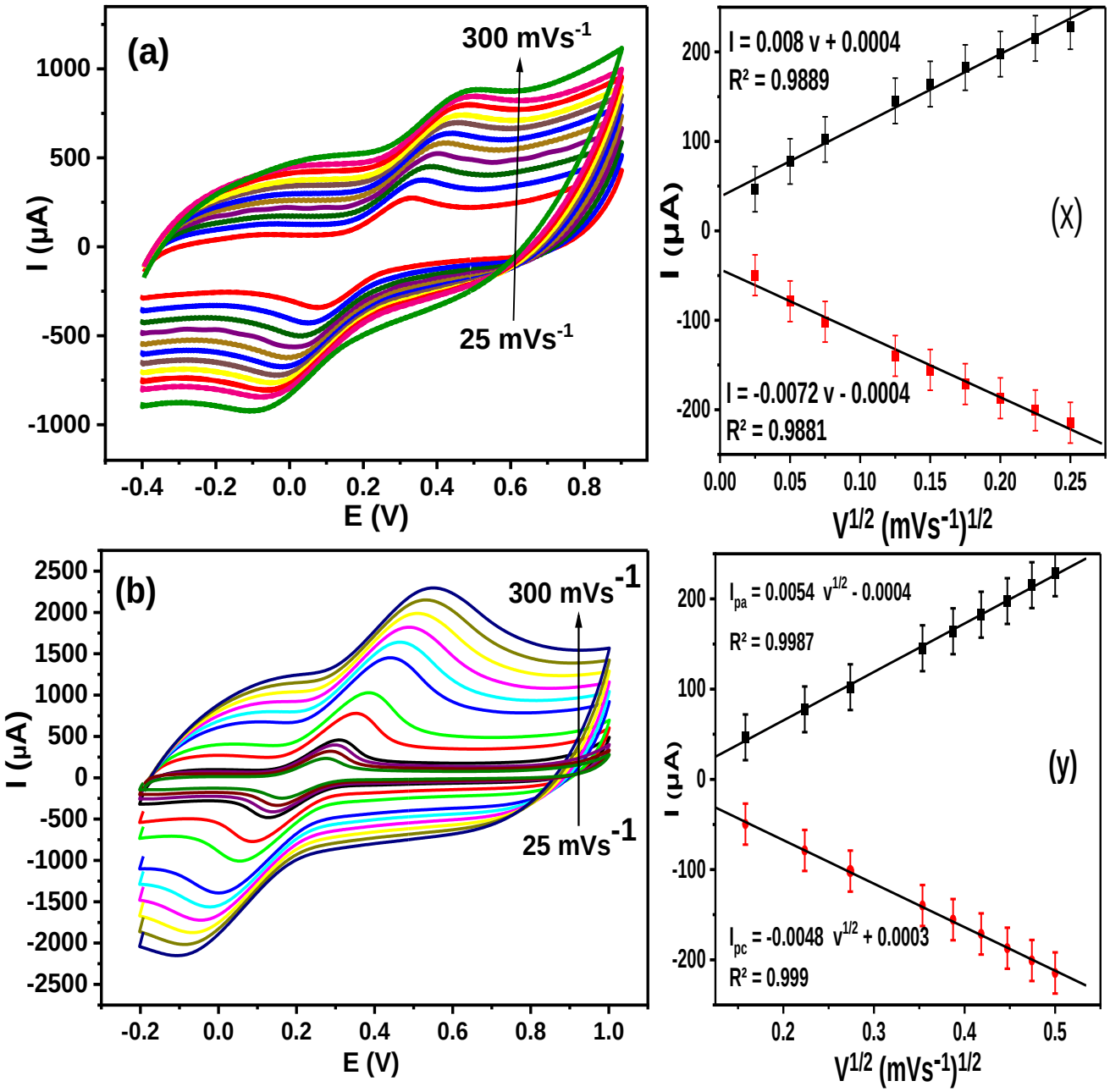

Figure 4.7. (a-b) Cyclic voltammograms of GCE-CoPcMWCNTs and GCE-NiPcMWCNTs (scan rate, 25–300 mVs^{-1}) and (x-y) linear graph of the peak currents versus square root of scan rates in 5 mM $[Fe(CN)_6]^{4-/3-}$ solution in 0.1 M PBS (pH 7).

Figure 4.8(a & b) shows the fitted Nyquist plots of the unmodified GCE and modified electrodes in 5 mM $[Fe(CN)_6]^{4-/3-}$ produced in 0.1 M PBS at a pH 7 while X, Y denoting the circuit diagrams employed to fit the EIS data. In the circuit, C stands for capacitance, CPE represents constant phase element, Rs represents solution resistance, R_{ct} represents charge-transfer resistance, and W stands for Warburg impedance. Table 9 displays a summary of the fitted impedance data along with their chi-square (x^2) values. The low percentage errors (in brackets) and negative chi-square values obtained show the successful fitting of the EIS data.

The R_{ct} values obtained for the electrodes as shown in Table 9, are in decreasing order GCE(8.73) > GCE-Co (2.99), GCE-Ni(1.39) > GCE-Pc (0.89) > GCE-fMWCNTs (0.44) > GCE-NIPc-MWCNTs (0.18) > GCE-CoPcMWCNTs (0.11) KΩ with GCE-CoPcMWCNTs having the lowest R_{ct} value, indicating that it has the quickest electrons transport capability than the other electrodes. The R_{ct} value of GCE-CoPcMWCNTs (0.11) was a bit lower than that of the GCE-NiPcMWCNTs electrode. There is no doubt that the R_{ct} values of GCE-CoPcMWCNTs (0.11) and GCE-NiPcMWCNTs (0.20) electrode are significantly lower than other electrodes. The fast electron transport of the GCE-CoPcMWCNTs and GCE-NiPcMWCNTs is due to the functionalized MWCNTs' high conductivity, which serves as a good electron conductor between CoNPs or NiNPs and Pc and the electrode surface. The reduction in Rct values of the modified electrodes, suggests the successful modification of the bare GCE.

The result obtained here is similar to the current response result in CV. This also led to the high Cp values of the modified electrodes, especially the GCE-NiPcMWCNTs and GCE-CoPcMWCNTs electrode. The n values ranging from 0.72–0.97 for all electrodes may be attributable to the ease with which ions diffuse to and from the electrode/solution contact.

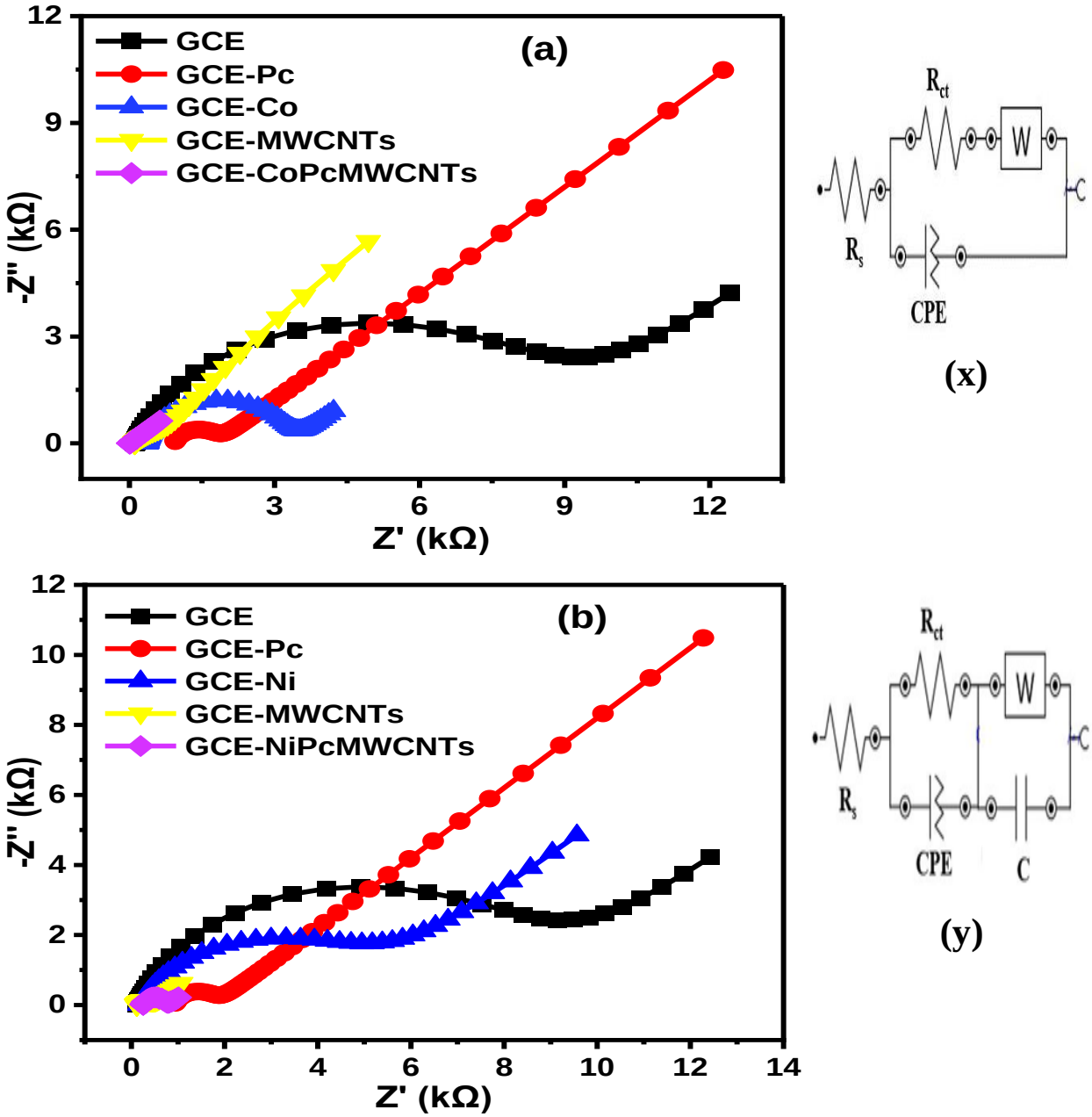

Figure 4.8. (a & b) Nyquist plots of GCE and modified electrodes in 5 mM $[Fe(CN)_6]^{4-/3-}$ produced in 0.1 M PBS at a pH 7 and (x and y) are the circuits used for EIS data fitting.

Table 9. Summary of fitted EIS parameters of bare and modified electrodes.

Impedance Spectroscopy Data (the percentage errors are in parentheses)							
Electrode	R_s (Ω)	R_{ct} (Ω)	CPE (μF)	W (F)	N	X^2	f°
Bare GCE	110 (3.78)	8.73 (5.31)	3.80 (16.7)	226 (1.84)	0.80	0.555	1.68
GCE-Pc	928 (4.42)	0.89 (8.60)	0.16 (79.6)	85.1 (2.44)	0.86 (9.30)	0.357	1.27
GCE-Co	349 (1.59)	2.99 (2.02)	2.07 (10.1)	995 (10.9)	0.86 (1.59)	0.204	2.00
GCE-Ni	301 (2.03)	1.39 (3.43)	6.70 (16.3)	524 (4.46)	0.72 (2.91)	0.215	3.16
GCE- fMWCNTs	85 (2.32)	0.44 (5.99)	2644 (29.9)	667 (3.31)	0.97 (12.9)	0.164	5.18
GCE- CoPcMWCNTs	103 (0.66)	0.11 (7.16)	257 (0.95)	1711 (4.48)	0.81 (0.45)	0.046	9.10
GCE- NiPcMWCNTs	104 (0.94)	0.18 (5.60)	27.2 (4.85)	148 (9.70	0.72 (0.94)	0.507	7.94

The “knee” frequency (f°) of the electrodes was also determined to further investigate the electrodes’ capacitive behaviours. The term "knee" frequency refers to the frequency where capacitive behaviour is most pronounced. It determines the power of a supercapacitor since it serves as the junction of the low-frequency and high-frequency components. This “knee” frequency determines the power density as well as the charge and discharge ability of a supercapacitor. A higher f° leads to a huge power density and a faster charge and discharge capability of a supercapacitor [74-76].

f° values obtained for the electrodes are in increasing order of 1.68, 1.27, 2.00, 3.16, 5.18, 7.94 and 9.10 Hz for the GCE, GCE-Pc, GCE-Co, GCE-Ni, GCE-fMWCNTs, GCE-NiPcMWCNTs, and GCE-CoPcMWCNTs, respectively, with the GCE-CoPcMWCNTs electrode having the highest f° value (9.10 Hz), followed closely by the GCE-NiPcMWCNTs (7.94 Hz). The high f° values exhibited by both GCE-CoPcMWCNTs, and GCE-NiPcMWCNTs are indicative of their higher power density over other electrodes. These values corroborate high electron transport capability and high Cp of the nanocomposite electrodes (GCE-CoPcMWCNTs, and GCE-NiPcMWCNTs) and are therefore very significant. According to a study [252], the majority of commercially available supercapacitors, especially those made for higher power applications, operate at frequencies lower than 1 Hz.

The phase angle value of a material under investigating is another important parameter for assessing the capacitive property of such material. Figure 4.9 illustrates the Bode plots of phase angle (°) vs. log f° and plots of log Z vs. log f° at −1.0 Hz for the nanocomposite electrodes with their corresponding plots of −Z″ vs. 1/ f°. The phase angles of 32°, and 49° were obtained for the GCE-NiPcMWCNTs, and GCE-CoPcMWCNTs, respectively. Both GCE-CoPcMWCNTs and GCE-NiPcMWCNTs electrodes exhibit phase angle values that were less than the expected 90° for an ideal capacitor [225, 253]. Such changes in phase angles and frequencies are clear-cut indication of the structural differences of the electrode surfaces. This serves as a further confirmation that the GCE-CoPcMWCNTs and GCE-NiPcMWCNTs are totally non-ideal capacitor.

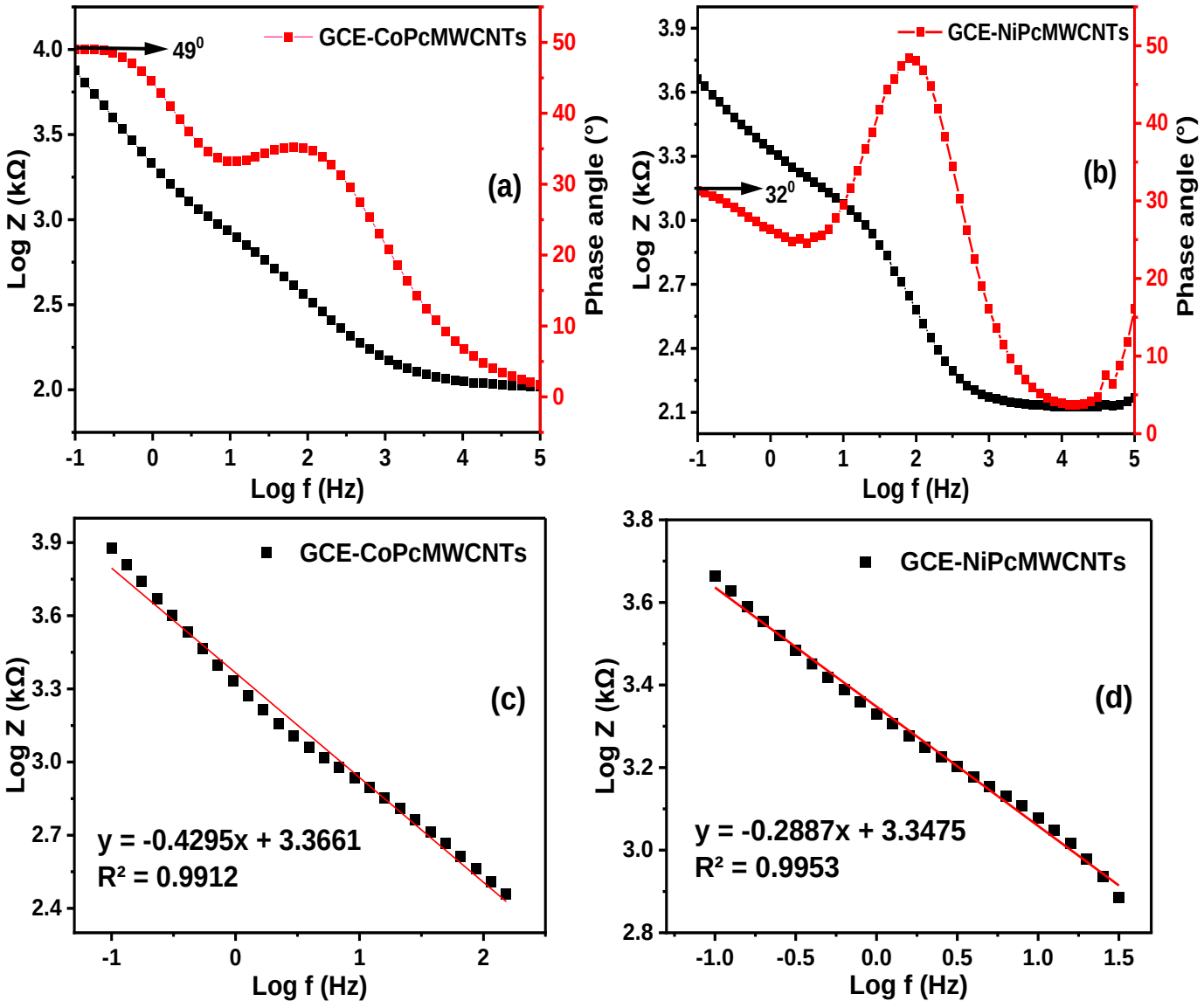

Figure 4.9. Bode plots of phase angle (^{0}) vs. log f° and plots of log Z vs. log f° of (a) GCE-CoPcMWCNTs, and (b) GCE-NiPcMWCNTs in 5 mM $[Fe(CN)_6]^{4-/3-}$ produced in 0.1 M PBS at a pH 7. (c) and (d) are the corresponding linear plots of Log Z vs Log f.

Similarly, the slope values obtained from the plot of log Z vs. log f is also a useful parameter employed for investigating the capacitive behaviours of materials. The slope values of -0.4 and -0.3 were obtained for the GCE-CoPcMWCNTs, and GCE-NiPcMWCNTs, respectively. These values are less than the expected slope of 1.0 for pure capacitive behaviours [74], thus affirming that the GCE-CoPcMWCNTs and GCE-NiPcMWCNTs electrodes investigated are high-specific-capacitance, high-energy-density hybrid supercapacitor that combines the faradaic pseudocapacitive and electric double-layer system.

4.3 Electrochemical Detection of Bromate

4.3.1 Choice/Effects of Electrolyte

Prior to the detection of bromate, impedance spectroscopy experiment was carried out on GCE-CoPcMWCNTs, and GCE-NiPcMWCNTs in four different electrolytes. This study was done to ascertain the most suitable supporting electrolyte for bromate detection. The four electrolytes investigated were 0.1 M $KBrO_3$ prepared in 0.1 M sodium acetate buffer (SAB) (pH 7), 0.1 M $KBrO_3$ prepared in 0.1 M H_2SO_4 (pH 1), 0.1 M $KBrO_3$ prepared in 0.1 M Na_2SO_4 (pH 2), and 0.1 M $KBrO_3$ prepared in 0.1 M PBS (pH 7).

Figure 4.10 and 4.11 depict the Nyquist plots of GCE-CoPcMWCNTs and GCE-NiPcMWCNTs in PBS, H_2SO_4, Na_2SO_4, and SAB supporting electrolytes. The R_{ct} values obtained for the GCE-CoPcMWCNTs in the four supporting electrolytes were 0.01, 0.2, 0.3 and 0.5 kΩ for the H_2SO_4, PBS, SAB, and Na_2SO_4, respectively (as shown in Table 10). A similar trend in R_{ct} values was also observed for the GCE-NiPcMWCNTs in the four supporting electrolytes, having the values of 0.06, 0.36, 1.98, and 9.04 kΩ for H_2SO_4, SAB, PBS, and Na_2SO_4, respectively. The lowest R_{ct} values obtained for both GCE-CoPcMWCNTs and GCE-CoPcMWCNTs was in H_2SO_4 electrolyte while the highest was in Na_2SO_4.

This is an indicative that the H_2SO_4 electrolyte serves as a better medium for rapid transfer of electron compared to the other electrolytes investigated. Hence, one the reasons for the choice of H_2SO_4 as the suitable electrolyte for the detection of bromate in this study.

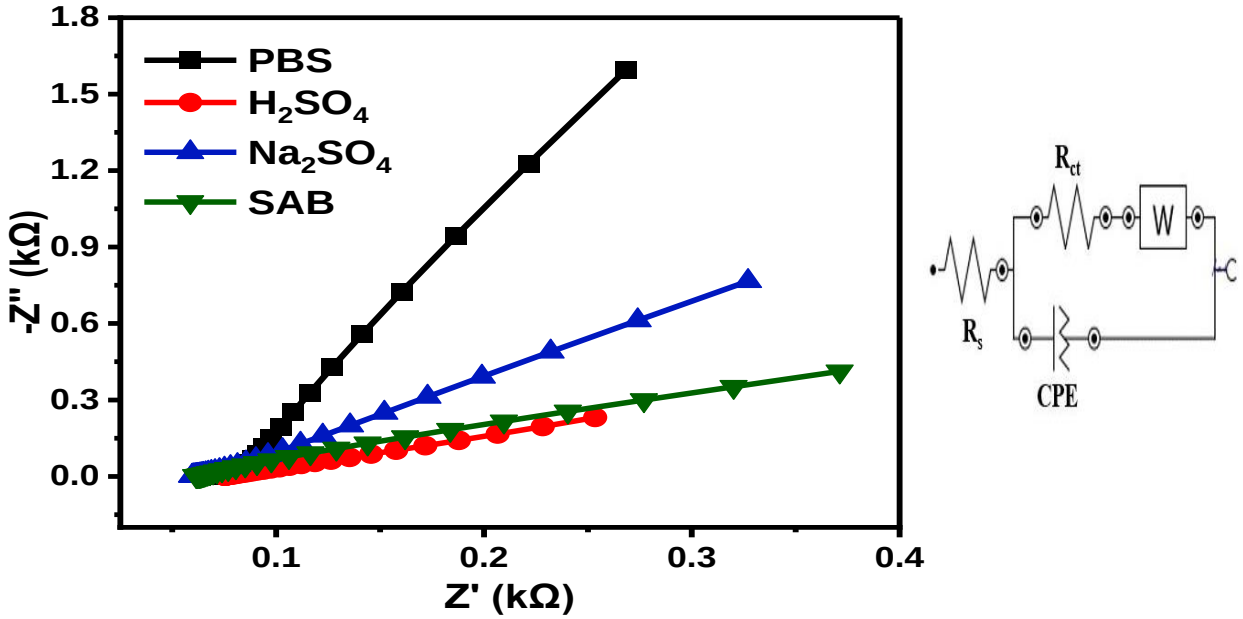

Figure 4.10. Nyquist plots of GCE-CoPcMWCNTs electrode in PBS, H_2SO_4, Na_2SO_4, and SAB electrolytes.

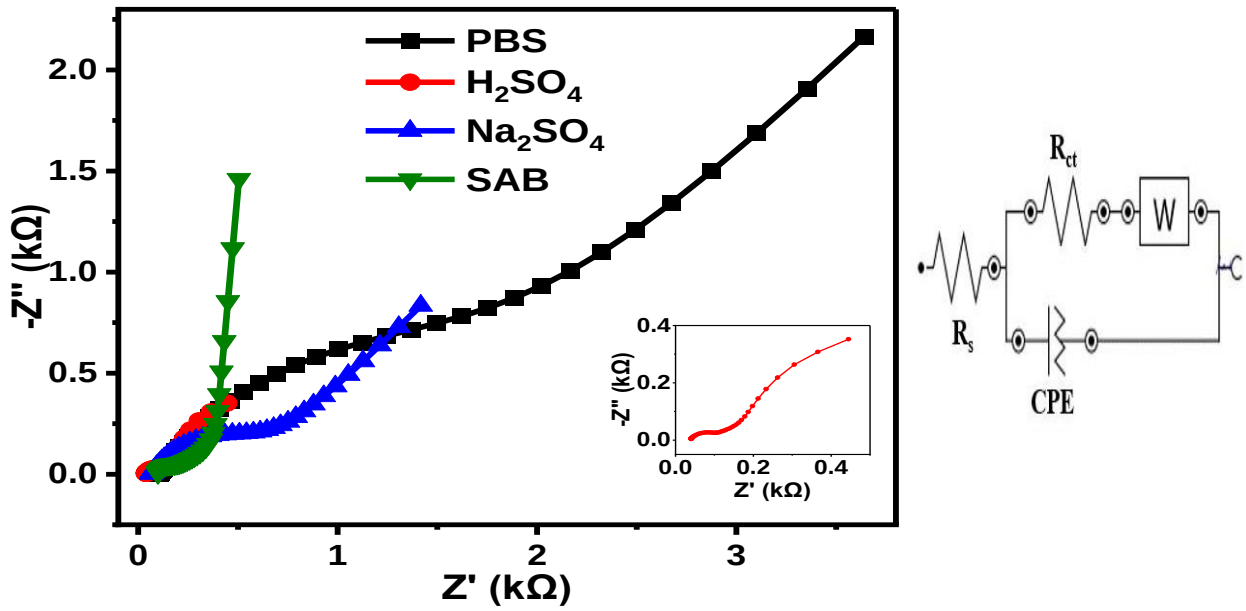

Figure 4.11. Nyquist plots of GCE-CoPcMWCNTs electrode in PBS, H_2SO_4, Na_2SO_4, and SAB electrolytes

Table 10. Comparative result of EIS parameters for GCE-CoPcMWCNTs and GCE-NiPcMWCNTs modified electrodes in all the electrolytes.

Impedance Spectroscopy Parameter							
	Electrolytes	R_s (Ω)	CPE (μF)	R_{ct} (kΩ)	W (μF)	n	X^2
CoPcMWCNTs	H_2SO_4	58.1 (3.51)	500 (5.59)	0.01 (10.3)	517(4.78)	0.82(1.25)	0.428
	Na_2SO_4	57.8 (1.32)	991 (3.09)	0.05 (16.6)	116 (10.4)	0.72 (1.98)	0.431
	PBS	68.5 (1.34)	246 (7.28)	0.02 (5.27)	191 (6.90)	0.79 (4.26)	0.124
	SAB	72.7 (0.19)	248 (2.98)	0.03 (7.81)	191 (0.62)	0.93 (0.87)	0.039
NiPcMWCNTs	H_2SO_4	39.9 (2.95)	42.0 (53.2)	0.06 (9.53)	3130 (3.96)	0.79 (8.22)	0.320
	Na_2SO_4	62.6 (1.96)	17.8 (8.06)	9.04 (21.8)	37.5 (5.88)	0.78 (1.49)	0.186
	PBS	105 (2.20)	43.4 (10.65)	1.98 (7.21)	407 (5.98)	0.63 (2.38)	0.164
	SAB	91 (2.50)	306 (11.5)	0.36 (5.12)	714 (5.70)	0.50 (3.68)	0.192

The fast electron transport ability of the nanocomposite electrodes in H_2SO_4 electrolyte accounted for its choice as the suitable electrolyte for bromate detection.

Both GCE-CoPcMWCNTs and GCE-NiPcMWCNTs exhibited high energy, high power densities and high specific capacitance. The enhanced electron transport capability and capacitive properties of the GCE-CoPcMWCNTs and GCE-NiPcMWCNTs in H_2SO_4 compared to the other electrolytes were credited to relatively fewer H^+ ions in the acid, allowing for easier ion penetration in the acidic electrolyte. The improved capacitive behaviour of GCE-CoPcMWCNTs and GCE-NiPcMWCNTs- modified electrode was also credited to the greater surface area of the fMWCNTs and phthalocyanine and the high electrical conductivity of the Cobalt/nickel and fMWCNTs.

Summarily, the results of the EIS studies of GCE-CoPcMWCNTs and GCE-NiPcMWCNTs in four different electrolytes showed that these two nanocomposite electrodes are suitable electrochemical sensors for detecting bromate, especially in H_2SO_4 electrolyte. A lot of studies on the usage of H_2SO_4 for bromate detection have been reported in literature [12, 202, 254, 255].

4.4 Detection of Bromate at GCE-CoPcMWCNTs

The electrocatalytic reduction of bromate was carried out in the presence of 1 mM $KBrO_3$ prepared in 0.1 M H_2SO_4 (pH 1) at a scan rate of 25 mV s^{-1} using cyclic voltammetry. Figure 4.12 (a) displays the cyclic voltammograms (CV) of the bare GCE, GCE-Pc, GCE-Co, GCE-fMWCNTs, and GCE-CoPcMWCNTs modified electrode. The CV reveals that the GCE-CoPcMWCNTs exhibited the highest cathodic peak current, confirming the anticipated superiority of the GCE-CoPcMWCNTs over the other electrodes that was previously demonstrated with the characterization of all electrodes using the $[Fe(CN)6]^{4-/3-}$ redox probe. With respect to the CVs of the bare and the modified electrodes depicted in Figure 4.12 (a), a well-defined bromate reduction peak was observed for GCE-CoPcMWCNTs compared to the other electrodes. From the Table 11, bromate reduction current (I_{pc}) and potential (E_{pc}) recorded were -23.19 μA (-0.2332 V), -36.70 μA (-0.3124 V), -306.59 μA (-0.2208 V), and -979.95 μA (-0.0297 V) for GCE, GCE-Pc, GCE-fMWCNTs, and GCE-CoPcMWCNTs, respectively. Electrocatalytic reduction process was observed in the voltammograms for all the electrodes except GCE-Co that displayed an oxidation process with an anodic peak and potential of 328.72 μA (-0.2855 V). The CoPcMWCNTs had better electrocatalytic response towards the bromate reduction compared to other electrodes. This

enhanced current response is attributed to the electronic conductivity of nanocomposites (Pc, Co, and fMWCNTs), their biocompatibility with the bromate and their high surface area. However, a well pronounced bromate reduction peak was observed at GCE-CoPcMWCNTs resulting from rapid transfer of electron during bromate reduction.

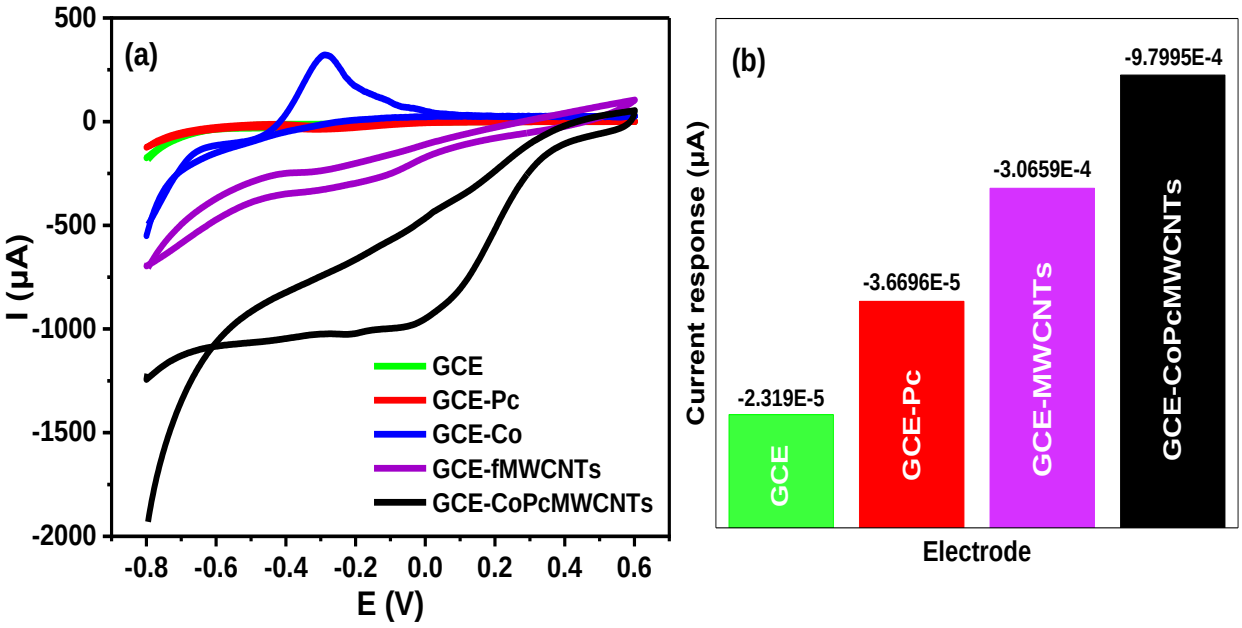

Figure 4.12. (a) Cyclic voltammogram and (b) histogram of the GCE and the modified electrodes in 1 mM $KBrO_3$ prepared in 0.1 M H_2SO_4 (pH 1).

Table 11. Summary of CV results of GCE and modified electrodes in 1 mM $KBrO_3$ prepared in 0.1 M H_2SO_4 (pH 1) at a scan rate of 25 mV s^{-1}.

Working Electrode	**I_{pc} (µA)**	**E_{pc} (V)**	**I_{pa} (µA)**	**E_{pa} (V)**
Bare GCE	-23.19	-0.2332		
GCE-Pc	-36.70	-0.3124		
GCE-Co			328.72	-0.2855
GCE-fMWCNTs	-306.59	-0.2208		
GCE-CoPcMWCNTs	-979.95	-0.0297		

4.4.1 Effect of Varying Scan Rate

Cyclic voltammetry was used to examine the impact of scan rate variation at GCE-CoPcMWCNTs in 0.1 mM H_2SO_4 solution containing 1 mM bromate concentration. With an increase in scan rate between 25 and 300 mVs^{-1}, reduction (cathodic) peak current gradually increased, and the peak potentials shifted to a more positive state, confirming a diffusion-controlled process (Figure 4.13a). A linear relationship exists between cathodic peak currents I_{pc} and the square root of the scan rate $v^{1/2}$ giving linear regression (Equation 4.8). This suggests that the GCE-CoPcMWCNTs reduction process is likewise a diffusion-controlled process [256]. Again, with an increase in the scan rate, the cathodic peak potentials move significantly to the positive side. The linear relationship between the peak potentials and the square root of the scan rates is shown in Figure 4.13 (c) and the linear equation is represented with equation 4.9.

I_{pc} = -6.04E-05 $v^{1/2}$ - 0.0007 (R^2 = 0.9950) (4.8)

E_{pc} = -0.02443 $v^{1/2}$ - 0.08111 (R^2 = 0.9979) (4.9)

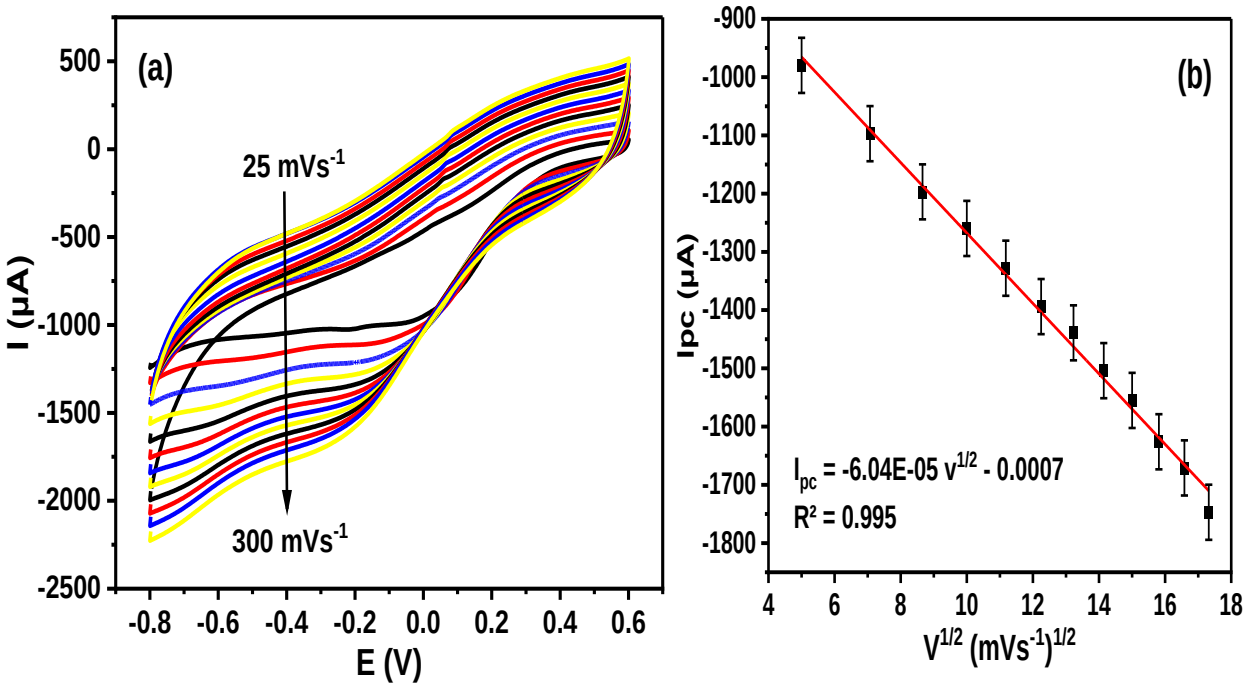

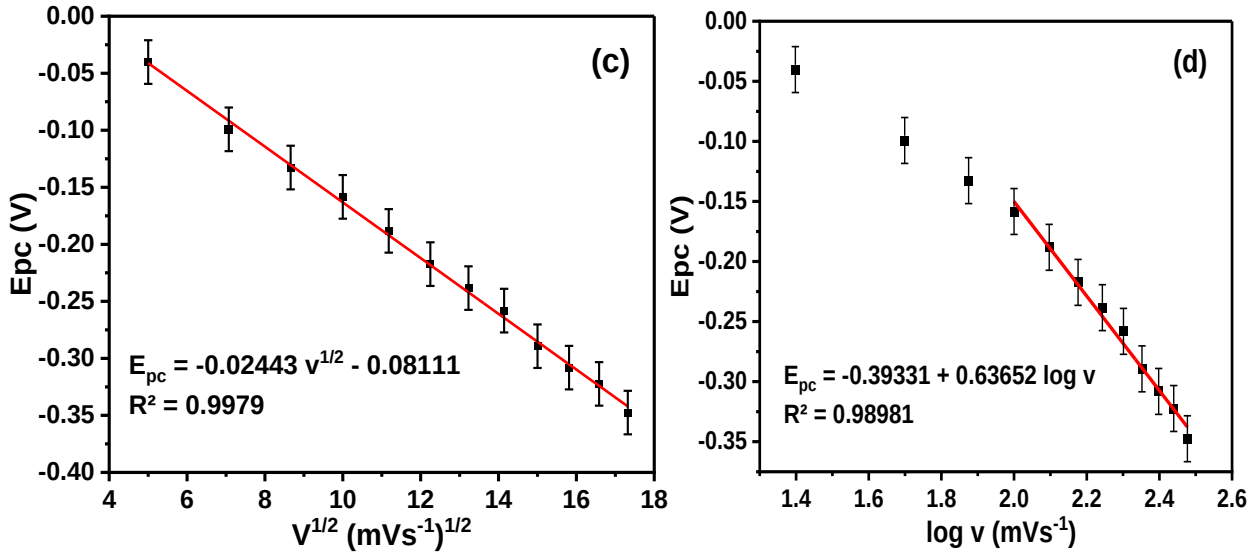

Figure 4.13. (a) Cyclic voltammogram obtained for GCE-CoPcMWCNTs (25–300 mVs^{-1}; inner to outer) in 1 mM $KBrO_3$ prepared in 0.1 M H_2SO_4 (pH 1), (b) linear plot of cathodic peak current I_{pc} against square root of scan rate, and (c) linear plot of cathodic potential E_{pc} vs square root of scan rate, and (d) linear plot of cathodic potential E_{pc} vs logarithm of scan rate.

Figure 4.13(d) depicts the plot of cathodic potential E_{pc} vs logarithm of scan rate. A linear relationship also exists between the cathodic peaks potential (E_{pc}) and the logarithm of the scan rate (Equation 4.10) mostly above 200 mVs^{-1}. Using Laviron equation, given that the slope of the graph of E_{pc} versus log v is b1 (Equation 4.11), the number of electrons transferred (n) and the electron transfer coefficient (α) can then be calculated.

$$E_{cp} = -0.39331 + 0.63652 \log v \qquad (R^2 = 0.98981) \qquad (4.10)$$

$$b1 = \frac{RT}{\propto nF} \qquad (4.11)$$

$$E_p = \frac{b}{2}\log v + K \qquad (4.12)$$

where n, R, T and F retain their usual meaning. The Tafel slope b is calculated as 238 mV dec^{-1} from equation 4.12. A Tafel slope obtain within the range of 60-120 mV suggests a one-electron process at the rate-determining step, while a Tafel plot greater than 120 mV dec^{-1} suggests an adsorptive process at the electrode surface [257]. The strong binding force between the electrode modifier and the analyte has been attributed as the cause of this kind of adsorption [258]. The Tafel slope for bromate reduction (238 mV dec^{-1}) is higher than 120 mV dec^{-1} indicating the occurrence

of an adsorptive process at GCE-CoPcMWCNTs electrode [257]. A proposed mechanism for the reduction of bromate to bromide is illustrated in scheme 2.

$Co^{II}Pc \longrightarrow Co^{III}Pc + e^{-}$

$6Co^{III}Pc + BrO3^{-} + 6H^{+} \longrightarrow 6Co^{II}Pc + Br^{-} + 3H_2O$

Scheme 2. Mechanism for the reduction of bromate

4.4.2 Effects of pH

The reduction rate of BrO_3^{-} to Br^{-} is strongly depended on solution pH, a low pH tends to accelerates the reduction rate [259]. The effect of the pH of the electrolyte on the electrochemical performance of GCE-CoPcMWCNTs towards bromate reduction was studied in 0.1 M H_2SO_4 containing 1 mM $KBrO_3$ solution at a varying pH values (1, 2, 3 & 5) using cyclic cyclic voltammetry. The main objective of this investigation was to achieve the highest sensitivity and best reduction peak resolution for bromate detection. With an increasing pH of the electrolyte, a negative and positive shift in the cathodic peak potentials was observed, suggesting that the electrocatalytic reduction of bromate involves electron transfer at the modified nanocomposite electrodes [259]. The highest cathodic peak current of bromate was achieved at the pH of 1 and subsequently reducing with increasing pH. For this reason, pH of 1 was used throughout the experiment. Interestingly, the electroanalysis of bromate at a pH of 1 has been widely reported [260, 261]

4.4.3. Concentration Studies

4.4.3.1 EIS bromate Detection at GCE-CoPcMWCNTs

Since the fabricated GCE-CoPcMWCNTs have demonstrated a favourable electrochemical response towards bromate BrO_3^{-}, it has been used for the determination of bromate. Electrochemical impedance spectroscopy technique was used to improve the sensitivity of the developed sensors for BrO_3^{-} detection. Figure 4.14 (a) show the Nyquist plot of GCE-CoPcMWCNTs in the presence of 48-167 µM bromate. The charge-transfer resistance R_{ct} decreased with the increase in the BrO_3^{-} concentration. Figure 4.14 (b) depicts the linear relationship between the R_{ct} response and BrO_3^{-} concentration. The relationship between the BrO_3^{-} charge-transfer resistance and concentration was found to be linear over a concentration range of 4.8×10^{-5} – 1.7×10^{-4} µM for GCE-CoPcMWCNTs. The limit of detection LOD and limit of

quantification LoQ for BrO_3^- with respect to the nanocomposite electrode was calculated using equation (4.13) and equation (4.14)

$$LoD = \frac{3.3\delta}{\mathrm{m}} \tag{4.13}$$

$$LoQ = \frac{10\delta}{\mathrm{m}} \tag{4.14}$$

Where:

δ is the relative standard deviation of the intercept, and

m is the slope of the intercept.

The LoD and LoQ obtained for the GCE-CoPcMWCNTs are 11.54 µM and 34.96 µM, respectively. The limit of detection obtained for GCE-CoPcMWCNTs is compared to those reported for other electrodes in literature (Table 15).

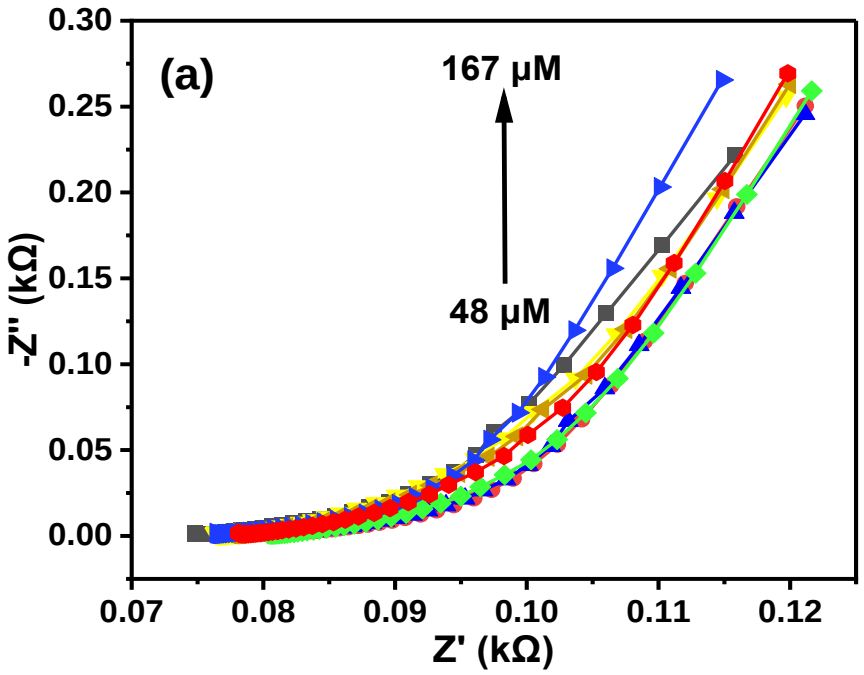

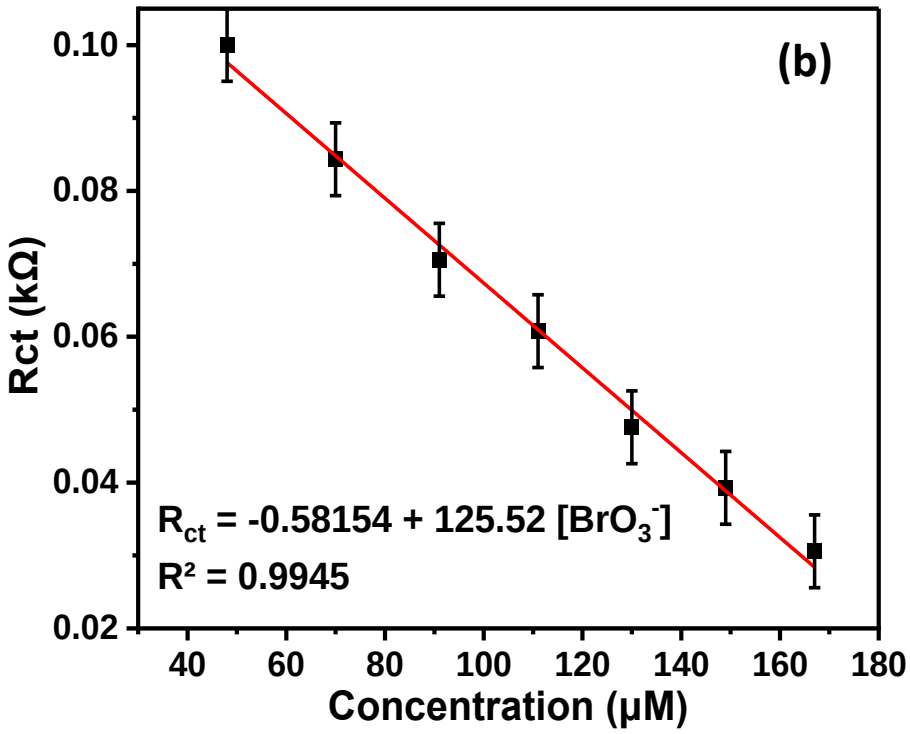

Figure 4.14. Nyquist plot of (a) GCE-CoPcMWCNTs over BrO_3^- concentration range of 48-167 μM at pH 1. (b) Plot of R_{ct} versus concentration obtained from (a).

4.4.3.1 SWV Bromate Detection at GCE-CoPcMWCNTs

The electrocatalytic reduction of bromate BrO_3^- at GCE-CoPcMWCNTs was also investigated using square wave voltammetry SWV. Figure 4.15 (a) depicts the CV of GCE-CoPcMWCNTs in the presence of 24-149 μM bromate. The peak current decreased with the increase in the BrO_3^- concentration. Figure 4.15 (b) shows the linear relationship between the current response and BrO_3^- concentration. The relationship between the BrO_3^- concentration and the current was found linear over a concentration range of 24 to 149 μM for GCE-CoPcMWCNTs. The LoD and LoQ obtained with the developed sensor were found to be 8.75 and 39.52 μM, respectively. Obviously, the LoD and LoQ obtained by SWV is better when compared with the EIS results. The sensor also offers a very high sensitivity (893.92 μA μM^{-1}).

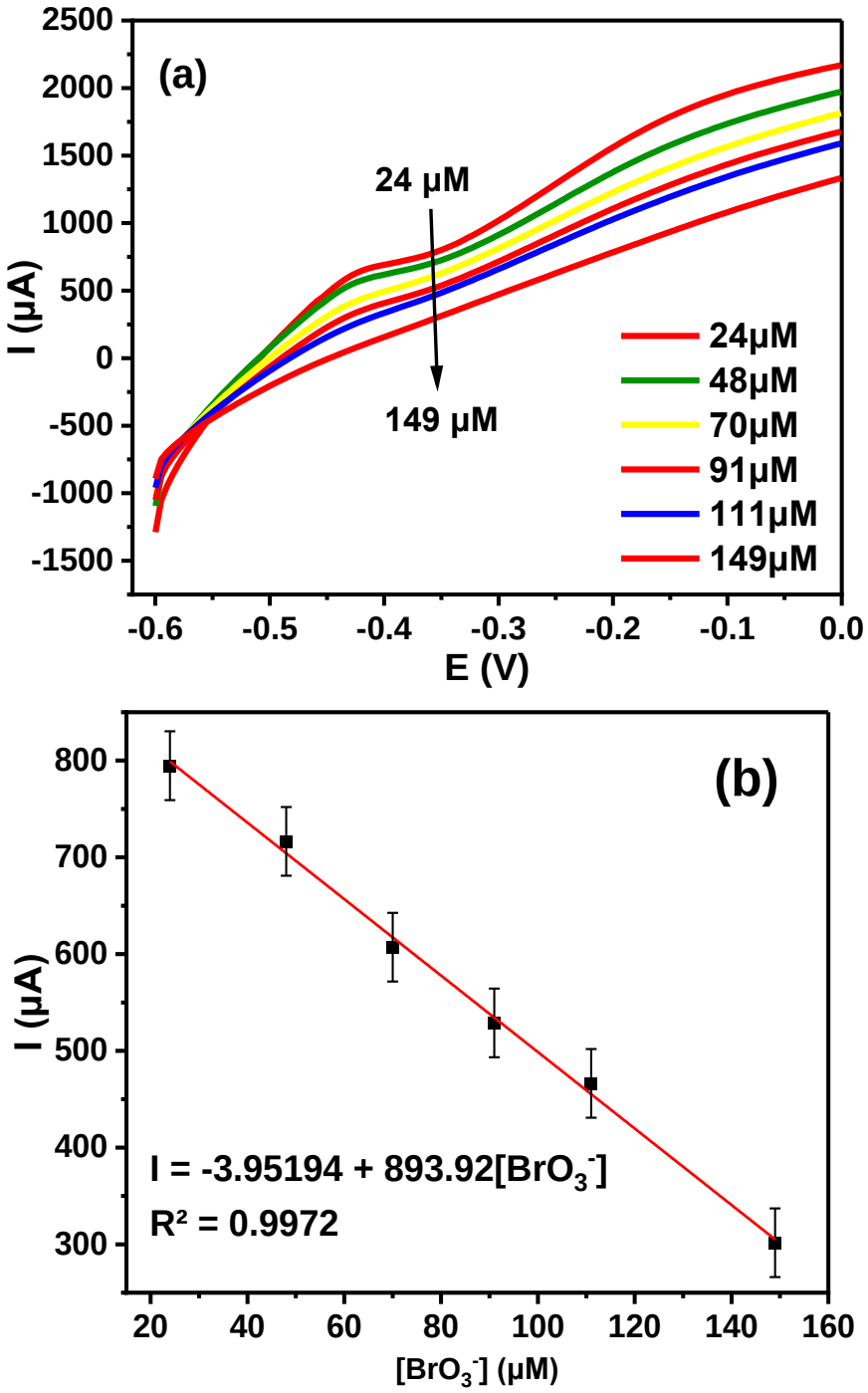

Figure 4.15. (a) Square wave voltammograms of GCE-CoPcMWCNTs over BrO_3^- concentration range of 24-149 µM at pH 1. (b) Plot of current versus concentration obtained from (a).

4.4.4 Interference studies

One of the qualities of a good sensor is its capability to distinguish between the common ions that coexist with the target analytes in real samples. As a result, the performance of the fabricated sensor is examined in relation to several potential interfering species. The interferential experiment of the proposed bromate sensor based on the GCE-CoPcMWCNTs is carried out by comparing the EIS response of 0.1 mM bromate before and after adding some possible interferents at a fixed potential (−0.3 V) into the 0.1 M H_2SO_4 solution at a pH of 1. The selectivity of the GCE-CoPcMWCNTs towards bromate detection was investigated through EIS technique. The Nyquist plot demonstrated that an increase in the concentration of the analyte while keeping the interfering ions concentration constant were recorded over the desired potential range. The requirement for the selectivity of the bromate sensor is taken to be the R_{ct} ratio of the mixtures (1 mM) of each interfering molecule in the presence of 0.1 mM bromate compared to that of 0.1 mM bromate alone. As illustrated from Table 12, the addition of 10-fold excesses of these species (Na^+, K^+, Cl^-, SO_4^{2-}, ClO_3^-, NH_4^+ and CO_3^{2-}) do not interfere with the R_{ct} value of the bromate; except for IO_3^{2-} and Mg^{2+} that show little degree of interference. There was about 2.2% and 3.2% drop in R_{ct} value of the proposed sensor upon the addition of IO_3^{2-} and Mg^{2+}. The IO_3^{2-} reacts and under oxidation in the H_2SO_4 solution, which is largely responsible for its interference. The interference caused by Mg^{2+} is possibly due to the precipitates formed by the interfering ion (Mg^{2+}) in the electrolyte solution.

Table 12. Effect of possible interfering ions on the GCE-CoPcMWCNTs electrode.

Interfering species	Initial R_{ct} (Ω)	Final R_{ct} (Ω)	% drop of Rct
Na^+	467.21	467.21	Nil
CO_3^{2-}	467.21	467.20	0.002
K^+	467.21	467.21	Nil
Cl^-	467.21	467.19	0.004
SO_4^{2-}	467.21	467.20	0.002
ClO_3^-	467.21	467.21	Nil
Mg^{2+}	467.21	456.82	2.2
IO_3^{2-}	467.21	482.25	3.2

4.4.5 Real Sample Analysis

Prior to the real sample analysis of bromate in bread samples, a preliminary qualitative test was performed directly on a portion of each bread sample with 1 mL of 0.01 M promethazine and 0.3 mL of 0.1 M hydrochloric acid. The change in colour of each bread sample to pink indicates the presence of potassium bromate. This preliminary qualitative test is important to determine the bromate presence in each bread sample. Three different bread samples were used for this analysis.

The real sample analysis of bromate in the bread sample was investigated with the constructed sensor (GCE-CoPcMWCNTs) using the standard addition method. About 5 g of dried bread samples were ground, powdered using mortar and pestle, and dissolved in distilled water to form a homogeneous paste by continuously shaking the mixture for 60 min at room temperature. The resultant paste was sufficiently diluted and left for 24 h. This solution was filtered and centrifuged at 3000 rpm to obtain a clear supernatant. The supernatant was spiked with a known bromate concentration (20, 30 and 50 μM) and the bromate content of each spiked bread sample was analyze using the square wave voltammetry technique. The preliminary test result shows that none of the three bread samples test positive.

Table 13 summarizes the mean percentage recovery of bromate from the bread samples after a triplicate determination. The mean percentage recovery obtained with the GCE-CoPcMWCNTs sensor were 103.1, 102.9 and 103.5 %, with the percentage relative standard deviation (% RSD) of 1.36, 3.62, and 2.80 % for sample X, Y, and Z sample, respectively. From Table 13, it is clearly established that the GCE-CoPcMWCNTs exhibited a good percentage recovery. The bromate % recovery offered by this sensor competes favorably with similar fabricated bromate sensors in various real samples [262]. This result also established the reliability of the GCE-CoPcMWCNTs as suitable sensors for bromate detection in bread and flour / baked products.

Table 13. Real sample analysis of bromate in bread samples.

Electrode	Bread Sample	Amount added (µM)	Amount found (µM)	% recovery	% RSD
GCE-CoPcMWCNTs	X	20	20.85	104.3	1.36
		30	31.20	104.0	
		50	50.50	101.0	
	Y	20	21.48	107.4	3.62
		30	29.20	97.3	
		50	52.15	104.0	
	Z	20	20.60	103.0	2.80
		30	32.38	107.9	
		50	49.86	99.7	

4.4.6 Stability and Reproducibility of GCE-CoPcMWCNTs

The stability of GCE-CoPcMWCNTs was investigated via CV with 20 repeated scans (50 mVs^{-1}) in 1 mM $KBrO_3$ prepared in 0.1 M H_2SO_4 (pH 1). The GCE-CoPcMWCNTs experienced a very little current drop of 6.5 %, indicating that the GCE-CoPcMWCNTs electrode is highly stable (Figure 4.16). This electrode offered a very high stability (93.5 %) compared with other fabricated bromate sensors [193].

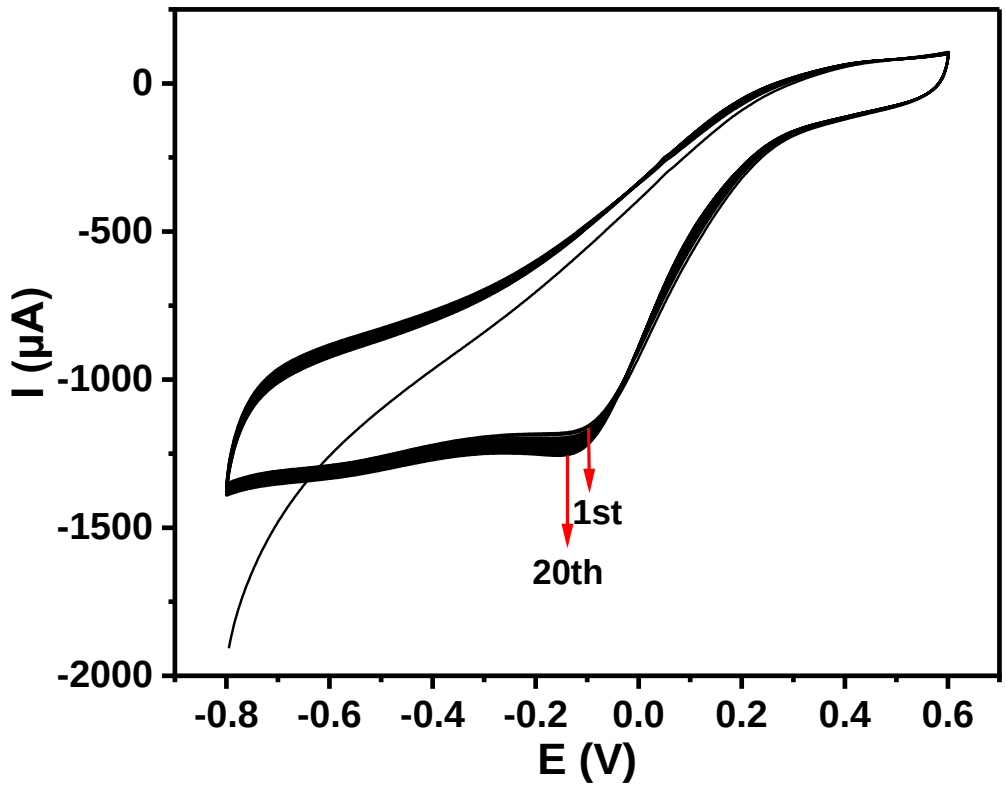

Figure 4.16. Cyclic voltammograms of 20 scans (50 mVs^{-1}) of GCE-CoPcMWCNTs in 1 mM $KBrO_3$ prepared in 0.1 M H_2SO_4 (pH 1).

The reproducibility of the fabricated electrode was investigated in 1 mM $KBrO_3$ prepared in 0.1 M H_2SO_4 (pH 1) using cyclic voltammetry. The bare electrode was modified with CoPcMWCNTs nanocomposite three different times before the electroanalysis of the bromate and the produced cyclic voltammogram was recorded. Figure 4.17 depicts the GCE-CoPcMWCNTs cyclic voltammograms. The cathodic current responses recorded for the GCE-CoPcMWCNTs after the three consecutive modifications gave the percentage relative standard deviation (% RSD) of 3.9%. The GCE-CoPcMWCNTs gave a low % RSD, suggesting that the GCE-CoPcMWCNTs displayed a more reproducible result. The fabricated sensor offers a high reproducibility compared to various bromate sensors in literature.

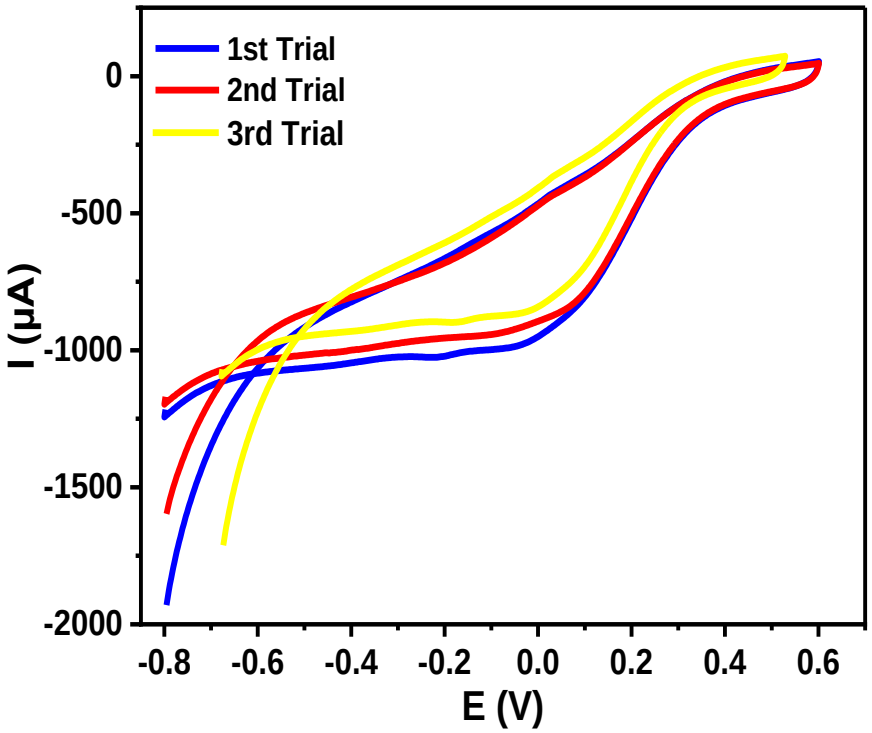

Figure 4.17. Cyclic voltammograms of GCE-CoPcMWCNTs in 1 mM $KBrO_3$ prepared in 0.1 M H_2SO_4 (pH 1, scan rate: 25 mV s^{-1}) for three different electrode modification trials.

4.5 Detection of Bromate at GCE-NiPcMWCNTs

The electrocatalytic reduction of bromate was performed in the presence of in 0.1 M H_2SO_4 (pH 1) containing 1 mM $KBrO_3$ (scan rate: 25 mV s^{-1}) using cyclic voltammetry. The cyclic voltammograms (CV) of the bare GCE, GCE-Pc, GCE-Ni, GCE-fMWCNTs, and GCE-NiPcMWCNTs is displayed in Figure 4.18 (a). The GCE-NiPcMWCNTs displayed the highest cathodic peak current, just like in GCE-CoPcMWCNTs. This confirms the expected superiority of the GCE-NiPcMWCNTs over the other electrodes that was previously established with the characterization of all electrodes using the $[Fe(CN)6]^{4-/3-}$. The GCE-NiPcMWCNTs showed a well-defined bromate reduction peak at cathodic current and potentials better than other electrodes. Going by Table 14, the bromate reduction current (I_{pc}) and potential (E_{pc}) obtained for the GCE, GCE-Pc, GCE-Ni, GCE-fMWCNTs, and GCE-NiPcMWCNTs are -23.19 µA (-0.2332 V), -36.70 µA (-0.3124 V), -11.78 µA (-0.2978 V), -306.59 µA (-0.2208 V), and -1299.10 µA (-0.0430 V), respectively. Aside the reduction (cathodic) peak exhibited by all the electrodes, GCE-NiPcMWCNTs also exhibited an anodic peak as shown in Figure 4.18 but disappeared with

increased scan rate. A better electrocatalytic response towards bromate reduction was achieved by the GCE-NiPcMWCNTs electrode compared to other electrodes. The electronic conductivity of nanocomposites (Pc, Ni, and fMWCNTs), their biocompatibility with the bromate, and their large surface area are responsible for this improved current response. However, a clearly visible bromate reduction peak was seen at GCE-NiPcMWCNTs as a result of an electron transfer that happened quickly during the bromate reduction process.

Table 14. Summary of CV Results of GCE and Modified Electrodes in 1 mM $KBrO_3$ prepared in 0.1 M H_2SO_4 (pH 1) at a scan rate of 25 mV s^{-1}.

Working Electrode	**I_{pc} (µA)**	**E_{pc} (V)**	**I_{pa} (µA)**	**E_{pa} (V)**
Bare GCE	-23.19	-0.2332		
GCE-Pc	-36.70	-0.3124		
GCE-Ni	-11.78	-0.2978		
GCE-fMWCNTs	-306.59	-0.2208		
GCE-NiPcMWCNTs	-1299.10	-0.0430	203.20	0.1795

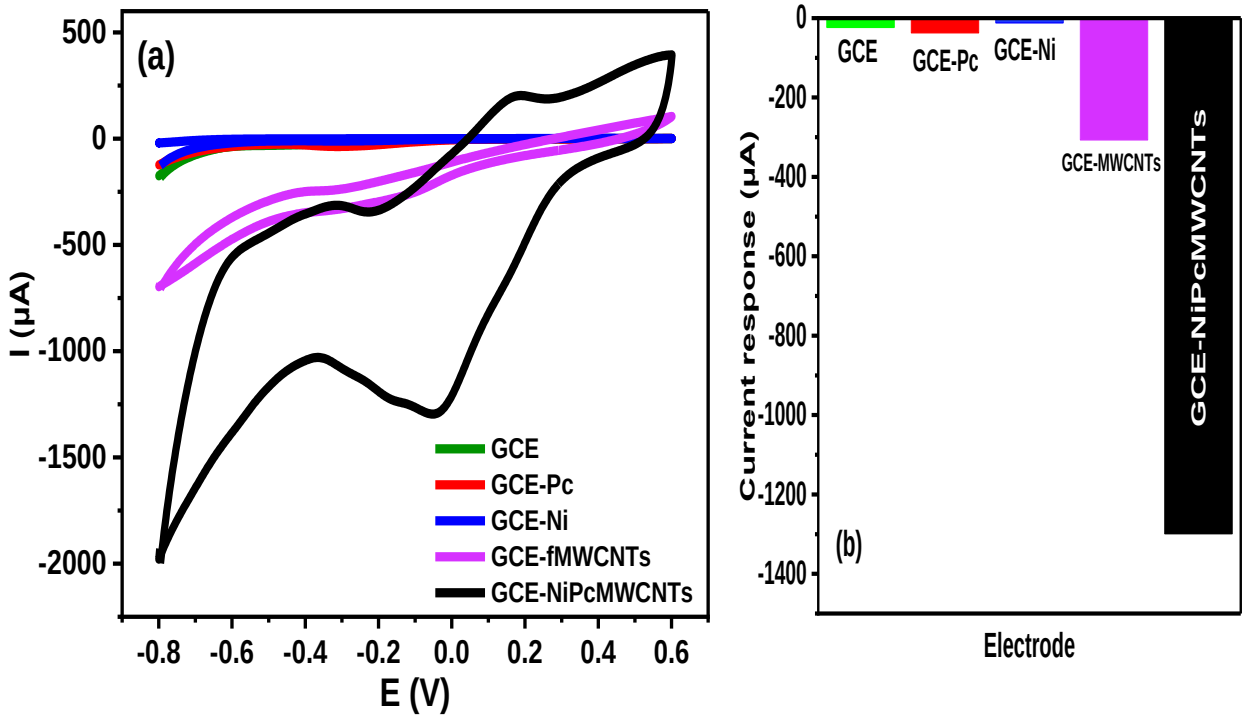

Figure 4.18. (a) Cyclic voltammogram and (b) histogram of the GCE and the modified electrodes in 1 mM $KBrO_3$ prepared in 0.1 M H_2SO_4 (pH 1).

4.5.1. Effect of Varying Scan Rate

Cyclic voltammetry was used to examine the impact of scan rate variation at GCE-NiPcMWCNTs in 0.1 mM H_2SO_4 solution containing 1 mM bromate. With an increase in scan rate between 25 and 300 mVs^{-1}, reduction (cathodic) peak current gradually increased, and the peak potentials shifted to a more positive state, confirming a diffusion-controlled process Figure 4.19a. A linear relationship exists between cathodic peak currents I_{ep} and the square root of the scan rate $v^{1/2}$ giving linear regression Equation 4.12. This suggests that the GCE-NiPcMWCNTs reduction process is likewise a diffusion-controlled process [256]. Again, with an increase in the scan rate, the cathodic peak potentials move significantly to the positive side. The linear relationship between the peak potentials and the square root of the scan rates is shown in Figure 4.19a and the linear equation is represented with equations (4.13)

$$I_{pc} = -1.283E\text{-}04 \quad v^{1/2} - 6.7592E\text{-}4 \qquad (R^2 = 0.9899) \qquad (4.12)$$

$$E_{pc} = -0.27133 + 0.32003 \log v \qquad (R^2 = 0.99849) \qquad (4.13)$$

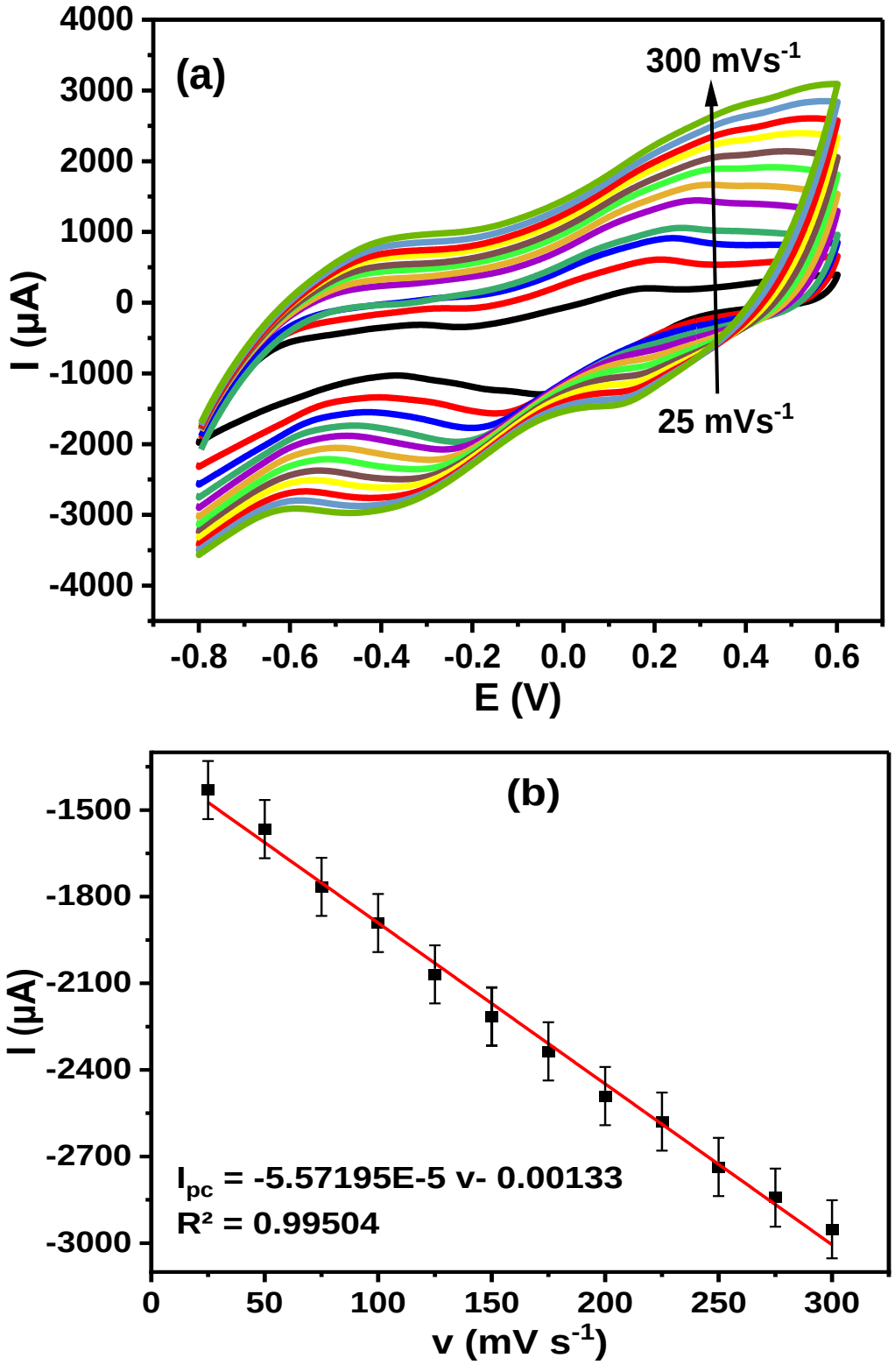
(a)
300 mVs-1
25 mVs-1
I (µA)
E (V)
4000
3000
2000
1000
0
-1000
-2000
-3000
-4000
-0.8
-0.6
-0.4
-0.2
0.0
0.2
0.4
0.6
(b)
Ipc = -5.57195E-5 v- 0.00133
R² = 0.99504
I (µA)
v (mV s-1)
-1500
-1800
-2100
-2400
-2700
-3000
0
50
100
150
200
250
300

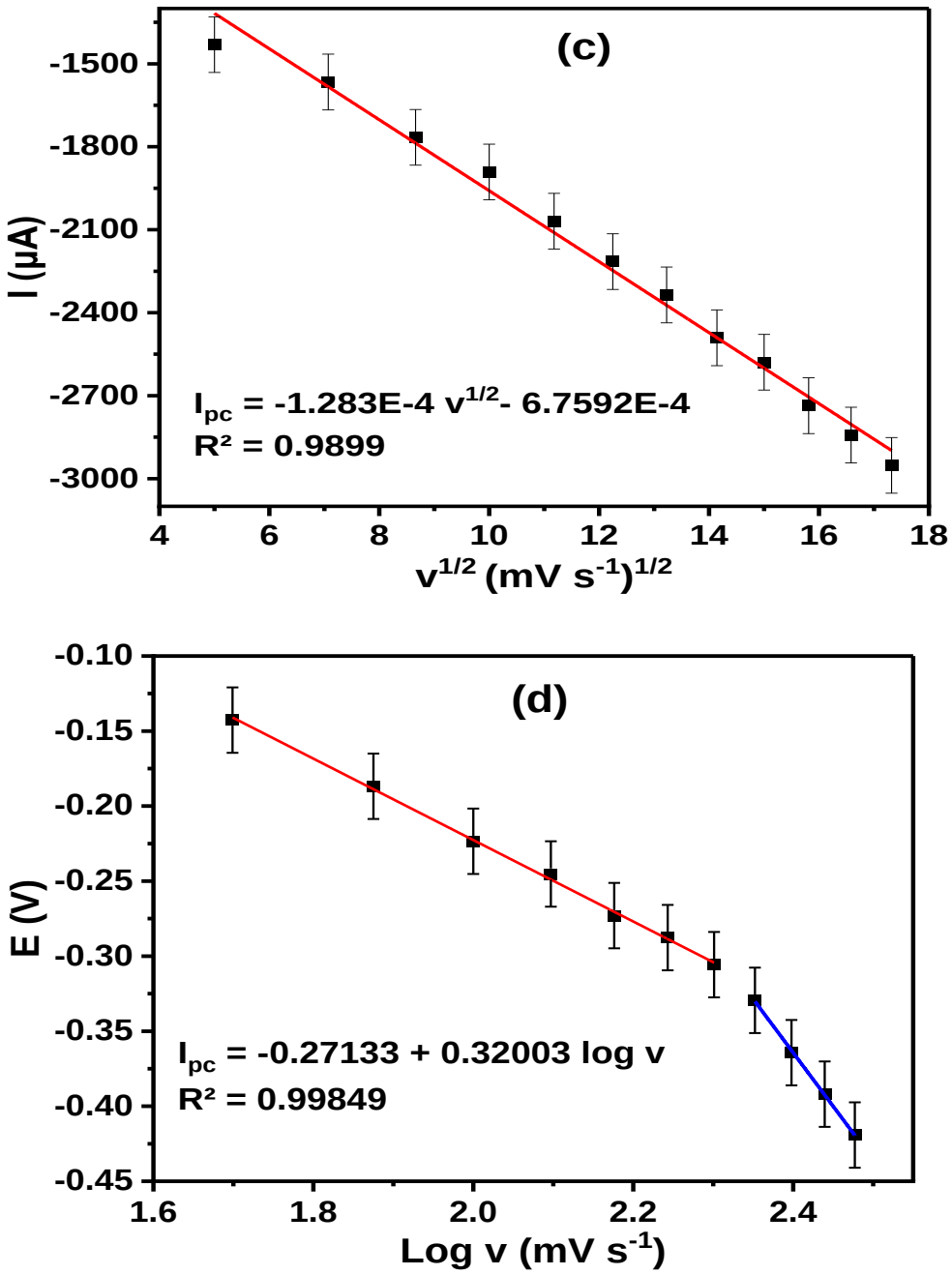

Figure 4.19. (a) Cyclic voltammogram obtained for GCE-CoPcMWCNTs (25–300 mVs^{-1}; inner to outer) in 1 mM $KBrO_3$ prepared in 0.1 M H_2SO_4 (pH 1), (b) linear plot of cathodic peak current I_{pc} against square root of scan rate, (c) linear plot of cathodic potential E_{pc} vs square root of scan rate, and (d) linear plot of cathodic potential E_{pc} vs logarithm root of scan rate.

Figure 4.19(d) illustrates the plot of cathodic potential E_{pc} vs logarithm of scan rate. A linear relationship also exists between the cathodic peaks potential (E_{pc}) and the logarithm of the scan rate (Equation 4.15) between 50 - 175 mVs^{-1}. Using Laviron equation, given that the slope of the graph of E_{pc} versus log v is b1 (Equation 4.16), the number of electrons transferred (n) and the electron transfer coefficient (α) can then be calculated.

$$E_{cp} = -0.39331 + 0.63652 \log v \qquad (R^2 = 0.98981) \qquad (4.15)$$

$$b1 = \frac{RT}{\propto nF} \qquad (4.16)$$

$$E_p = \frac{b}{2}\log v + K \qquad (4.17)$$

Where n, R, T and F retain their usual meaning. The Tafel slope b is calculated as 225 mV dec^{-1} from Equation 4.17. A Tafel slope obtain within the range of 60-120 mV suggests a one-electron process at the rate-determining step, while a Tafel plot greater than 120 mV dec^{-1} suggests an adsorptive process at the electrode surface [375]. The strong binding force between the electrode modifier and the analyte has been attributed as the cause of this kind of adsorption [375, 376]. The Tafel slope for bromate reduction (225 mV dec^{-1}) is higher than 120 mV dec^{-1} indicating the occurrence of an adsorptive process at GCE-CoPcMWCNTs electrode [375]. The proposed mechanism for bromate reduction is given in Scheme 3.

$$Ni^{II}Pc \longrightarrow Ni^{III}Pc + e^-$$

$$6Ni^{III}Pc + BrO_3^- + 6H^+ \longrightarrow 6Ni^{II}Pc + Br^- + 3H_2O$$

Scheme 3. Mechanism of bromate reduction at NiPcMWCNTs

4.5.2 Effects of pH

The effect of the pH of the electrolyte solution pH on the electrochemical performance of GCE-NiPcMWCNTs towards bromate reduction was studied in 0.1 M H_2SO_4 solution at a varying pH values (1, 2, 3, & 5) using cyclic cyclic voltammetry. The main objective of this investigation was to achieve the highest sensitivity and best reduction peak resolution for bromate detection. With an increasing pH of the electrolyte, a negative and positive shift in the cathodic peak potentials was observed, suggesting that the electrocatalytic reduction of bromate involves proton transfer at

the modified nanocomposite electrodes. The highest cathodic peak current of bromate was achieved at the pH of 1 and subsequently reducing with increasing pH. For this reason, pH of 1 was used throughout the experiment. Interestingly, the electroanalysis of bromate at a pH of 1 has been widely reported [190, 194].

4.5.3 Concentration Studies

4.5.3.1 EIS Bromate Detection at GCE-NiPcMWCNTs

Since the fabricated GCE-NiPcMWCNTs has demonstrated a favourable electrochemical response towards bromate BrO_3^-, it has been used for determination of bromate. Electrochemical impedance spectroscopy technique has been used to improve the sensitivity of the developed sensors for BrO_3^- detection. Figure 4.20(a) show the Nyquist plot of GCE-NiPcMWCNTs in the presence of 48-200 µM BrO_3^-. As expected, the charge-transfer resistance R_{ct} decreased with the increase in the BrO_3^- concentration. Figure 4.20(b) depicts the linear relationship between the R_{ct} response and BrO_3^- concentration. The relationship between the BrO_3^- charge-transfer resistance and concentration was found linear over a concentration range of $4.8 \times 10^{-5} - 2.0 \times 10^{-4}$ µM for GCE-NiPcMWCNTs. The limit of detection LoD and limit of quantification LoQ for BrO_3^- with respect to the GCE-NiPcMWCNTs electrode were calculated using equation (4.13) and equation (4.14), respectively. All the parameters maintain their usual meaning.

$$LoD = \frac{3.3\delta}{\mathrm{m}} \tag{4.13}$$

$$LoQ = \frac{10\delta}{\mathrm{m}} \tag{4.14}$$

The LoD obtained for the GCE-NiPcMWCNTs is 21.81 µM. The GCE-CoPcMWCNTs offered a better LoD than the GCE-NiPcMWCNTs. The limit of detection obtained for both GCE-CoPcMWCNTs and GCE-NiPcMWCNTs electrodes are compared to those reported for other electrodes in literature (Table 15). Additionally, the LoQ obtained for GCE-NiPcMWCNTs was calculated as 66.10 µM.

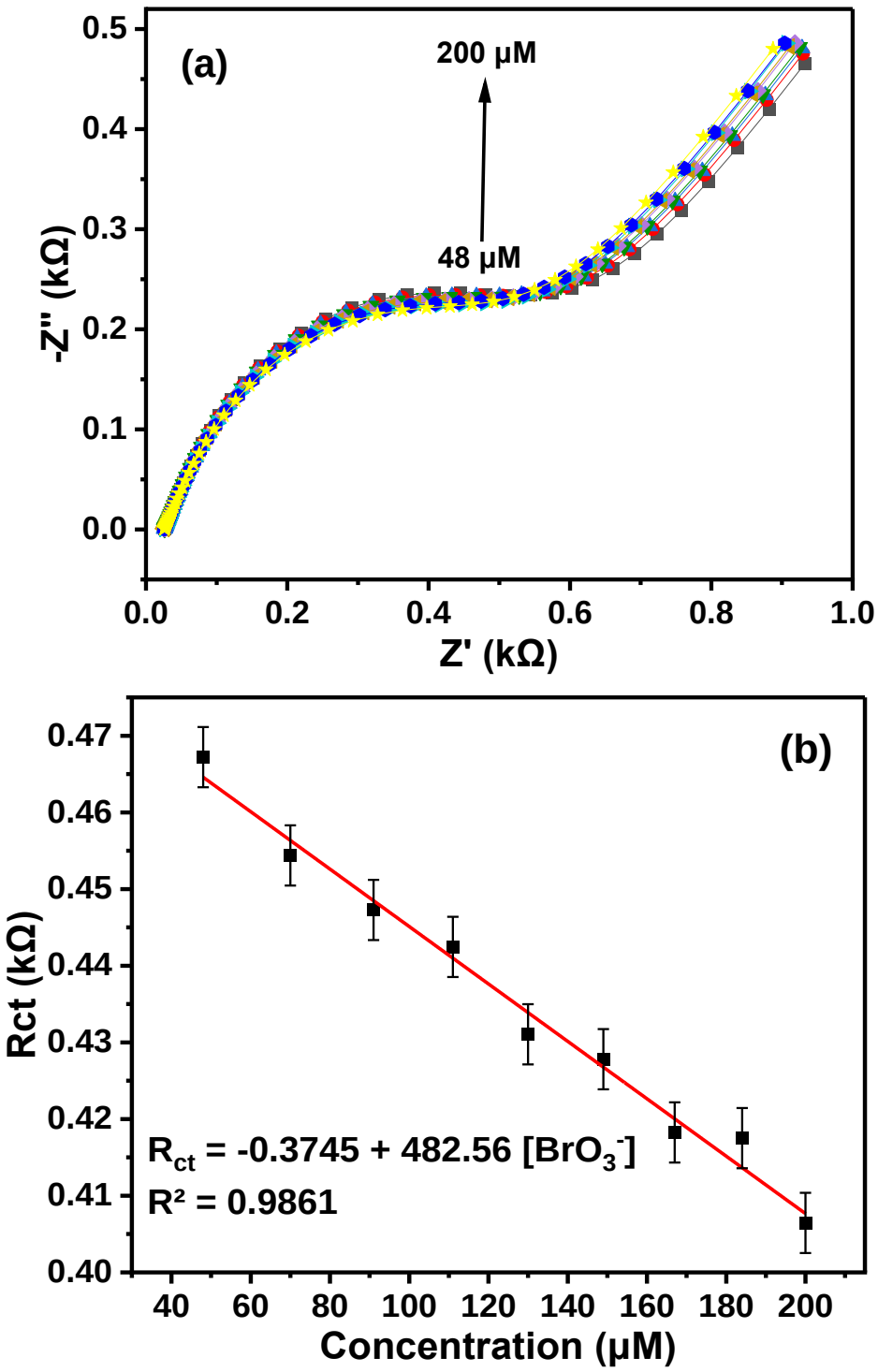

Figure 4.20. (a) Nyquist plot of GCE-NiPcMWCNTs over BrO_3^- concentration range of 48-200 µM at pH 1. (b) Plot of R_{ct} versus concentration obtained from (a).

4.5.3.1 SWV Bromate Detection at GCE-NiPcMWCNTs

Using square wave voltammetry SWV, the electrocatalytic reduction of bromate BrO_3^- at GCE-NiPcMWCNTs was also studied. The CV of GCE-NiPcMWCNTs in the presence of 24 - 111 µM bromate is shown in Figure 4.21(a). Here, the peak current increased with the increase in the BrO_3^- concentration. The linear relationship between the current response and BrO_3^- concentration is depicted in Figure 4.21(b). At the developed sensor, a linear relationship exists between the BrO_3^- concentration and the current over a LDR of 24 to 111 µM. The developed sensor's LoD and LoQ were discovered to be 3.09 and 9.36 µM, respectively. When compared to the results from the EIS, it is clear that the LoD and LoQ achieved using SWV are superior. Additionally, the sensor has an extremely high sensitivity (1290 µA μM^{-1}).

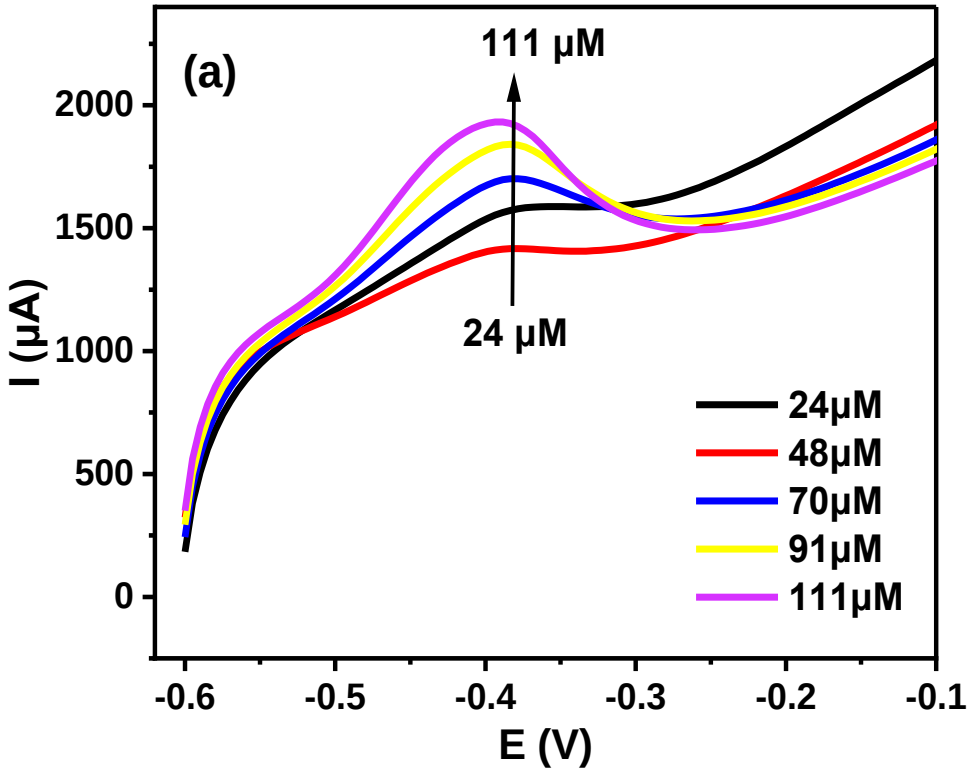

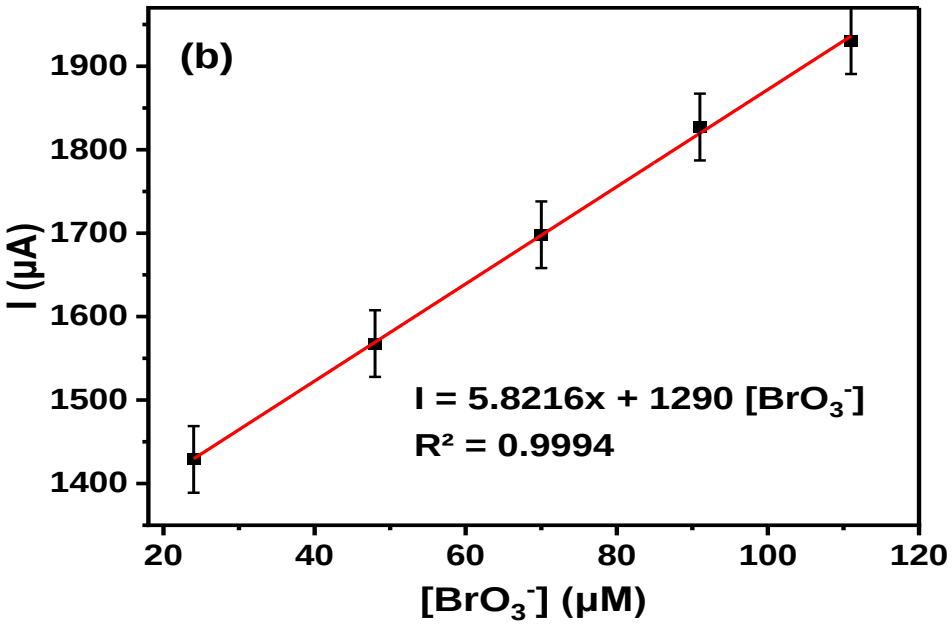

Figure 4.21. (a) Square wave voltammograms of GCE-NiPcMWCNTs over BrO_3^- concentration range of 24-117 μM at pH 1. (b) Plot of current versus concentration obtained from (a).

Table 15. Comparison of the proposed sensors with previous bromate sensors.

Electrode	**Technique**	**LoD** (μM)	**LDR** (μM)	**Sensitivity (μA μM^{-1})**	**Ref**
NENU-3 film	AP	12	50-7.3 X 10^4		[263]
Nafion/Hb/FeS-MoS_2-C/CILE	CV	17	50-2.5 X 10^4		[264]
PTh-D/nafion/AuE	ECL	1	1-1x10^5		[173]
$CoW_{11}Co$/PVP/TiO_2/GCE	CV	5	20-4.4 X10^3		[179]
GCE-CoPcMWCNTs	EIS	11.54	48–167	125.50	This
	SWV	8.75	24-149	893.92	work
GCE-NiPcMWCNTs	EIS	21.81	48-200	482.56	This
	SWV	3.09	24-111	1290.0	work

NENU-3 film - electroactive metal–organic framework film; Nafion/Hb/FeS-MoS_2-C/CILE - Petal-shaped FeS@MoS_2-C nanocomposite uniformly dispersed nanocomposite, hemoglobin (Hb) and Nafion mixture prepared carbon ionic liquid electrode (CILE); PTh-D/nafion/AuE - poly[3-(1,1′-dimethyl-4-piperidinemethylene)thiophene-2,5-diylchloride] (PTh-D); $CoW_{11}Co$/PVP/TiO_2/GCE – tetrabutyammonium cobalt (III) 12- tungsten poly (4-vinylpyridine)(PVP) in a TiO_2 sol–gel matrix

4.5.4 Interference Studies

One of the qualities of a good sensor is its capability to distinguish between the common ions that coexist with the target analytes in real samples. As a result, the performance of the fabricated sensor was examined in relation to several potential interfering species. The interferential experiment of the proposed bromate sensor based on the GCE-NiPcMWCNTs is carried out by comparing the EIS response of 0.1 mM bromate before and after adding some possible interferents at a fixed potential (−0.3 V) into the 0.1 M H_2SO_4 solution at a pH of 1. The selectivity of the GCE-NiPcMWCNTs towards bromate detection was investigated through EIS technique. The Nyquist plot demonstrated an increase in the concentration of the analyte while keeping the interfering ions concentration constant were recorded over the desired potential range. The requirement for the selectivity of the bromate sensor is taken to be the Rct ratio of the mixtures (1 mM) of each interfering molecule in the presence of 0.1 mM bromate compared to that of 0.1 mM bromate alone., As it can be seen from Table 16, the addition of 10-fold excesses of these species (Na^+, K^+, Cl^-, SO_4^{2-}, ClO_3^-, NH_4^+ and CO_3^{2-}) do not interfere with the R_{ct} value of the bromate; except for IO_3^{2-} and Mg^{2+} that show little degree of interference. There was about 2.2% and 3.2% drop in Rct value of the proposed sensor upon the addition of IO_3^{2-} and Mg^{2+}. The IO_3^{2-} reacts and under oxidation in the H_2SO_4 solution, which is largely responsible for its interference. The interference caused by Mg^{2+} is possibly due to the precipitates formed by the interfering ion (Mg^{2+}) in the electrolyte solution.

Table 16. Effect of possible interfering ions on the GCE-NiPcMWCNTs.

Interfering species	**Initial R_{ct} (Ω)**	**Final R_{ct} (Ω)**	**% drop of Rct**
Na^+	452.76	452.70	0.01
CO_3^{2-}	452.76	452.76	Nil
K^+	452.76	452.76	Nil
Cl^-	452.76	452.76	Nil
SO_4^{2-}	452.76	452.62	0.03
ClO_3^-	452.76	452.76	Nil
Mg^{2+}	452.76	470.25	3.9
IO_3^{2-}	452.76	446.36	1.4

4.5.5 Real Sample Analysis

The bread sample preparation and the real sample analysis procedures follow the same methods with the one earlier described for GCE-CoPcMWCNTs. A negative result was obtained from the preliminary test of the three bread samples i.e none of the three bread samples contain bromate when subjected to the preliminary test. Table 17 summarizes the mean percentage recovery of bromate from the bread samples after a triplicate determination. The mean percentage recovery obtained for the GCE-NiPcMWCNTs sensor were 103.3%, 100.9%, and 102.8% with the percentage relative standard deviation (% RSD) of 1.58%, 3.60%, and 2.24% for sample X, Y, and Z, respectively.

Going by the results in the Table 17, the GCE-NiPcMWCNTs exhibited a good percentage recovery. In comparison with the GCE-CoPcMWCNTs, the two sensors offered relatively the same % RSD. The bromate % recovery offered by the two sensors competes favorably with similar fabricated bromate sensors in various real samples [265, 266]. This result also established the reliability of the GCE-NiPcMWCNTs as suitable sensor for bromate detection in food products.

Table 17. Bromate analysis in bread samples for GCE-NiPcMWCNTs.

Electrode	Bread Sample	Amount added (µM)	Amount found (µM)	% recovery	% RSD
GCE-NiPcMWCNTs	X	20.00	20.48	102.4	1.58
		30.00	31.75	105.8	
		50.00	50.92	101.8	
	Y	20.00	21.25	106.3	3.60
		30.00	29.67	98.9	
		50.00	48.72	97.4	
	X	20.00	19.88	99.4	2.24
		30.00	31.49	105.0	
		50.00	52.00	104.0	

4.5.6 Stability and Reproducibility of GCE-NiPcMWCNTs

The stability of GCE-NiPcMWCNTs was investigated via CV with 20 repeated scans (75 mVs^{-1}) in 0.1 M H_2SO_4 (pH 1) containing 1 mM $KBrO_3$. As depicted in Figure 4.22, there was only 4.5% current drop, indicating that the GCE-NiPcMWCNTs is very stable. Comparing both electrodes, GCE-NiPcMWCNTs offers a better stability. The electrode offered a very high stability (95.5%) compared with other fabricated bromate sensors [267, 268].

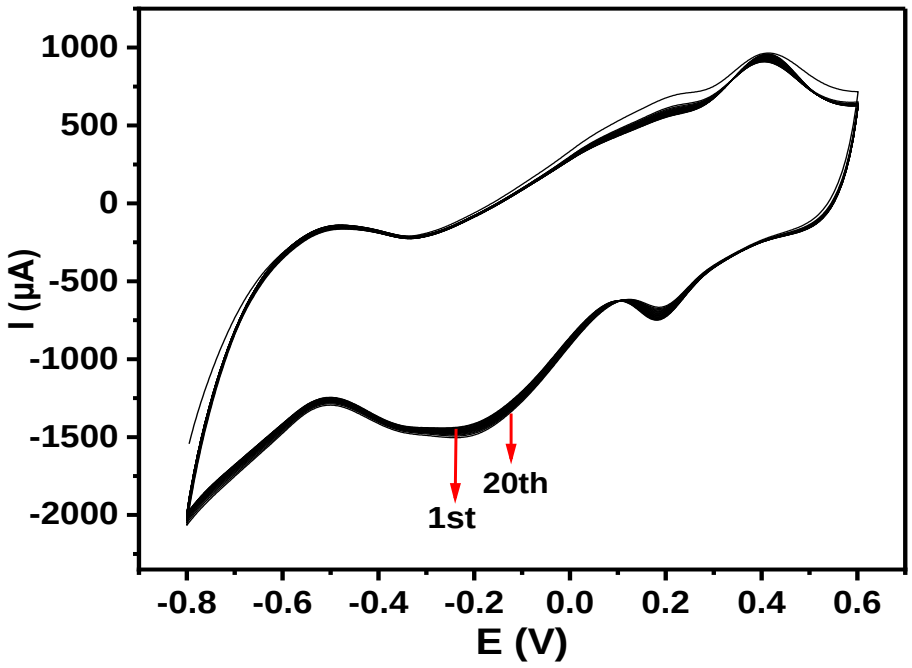

Figure 4.22. Cyclic voltammograms of 20 scans of GCE-NiPcMWCNTs in 1 mM $KBrO_3$ prepared in 0.1 M H_2SO_4 (pH 1).

The reproducibility of the fabricated electrode was investigated via cyclic voltammetry in 1 mM $KBrO_3$ prepared in 0.1 M H_2SO_4 (pH 1). The bare electrode was modified with NiPcMWCNTs nanocomposite three different times before the electroanalysis of the bromate and the produced cyclic voltammogram was recorded. Figure 4.23 depicts the GCE-NiPcMWCNTs cyclic voltammograms. The cathodic current responses recorded for the GCE-NiPcMWCNTs after the three consecutive modifications gave the percentage relative standard deviation (% RSD) of 3.5 %. The GCE-NiPcMWCNTs gave a low % RSD, suggesting that the GCE-NiPcMWCNTs displayed a more reproducible result. The fabricated sensor offers a high reproducibility compared to various bromate sensors in literature [179, 269].

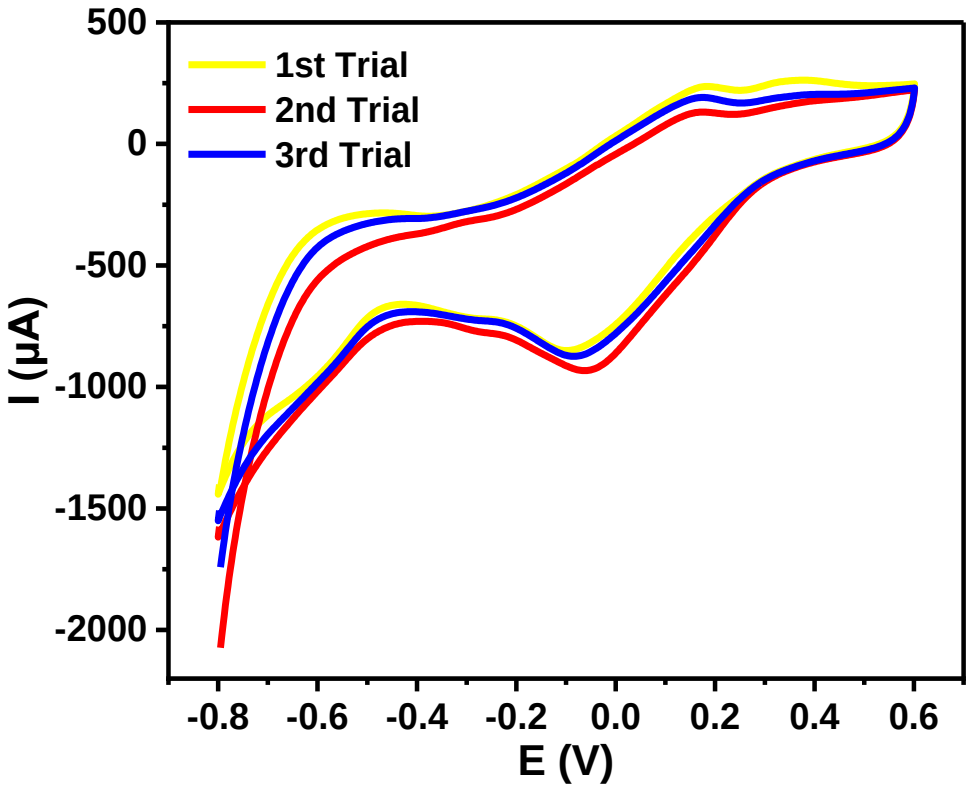

Figure 4.23. Cyclic voltammograms of GCE-NiPcMWCNTs in 1 mM $KBrO_3$ prepared in 0.1 M H_2SO_4 (pH 1, scan rate: 25 mV s^{-1}) for three different electrode modification trials.

CHAPTER FIVE

Conclusion and Recommendations

5.1 Conclusion

The study explored the electrochemical impedance spectroscopy measurement of bromate in food using cobalt phthalocyanine multiwalled carbon nanotubes (GCE-CoPcMWCNTs) and nickel phthalocyanine multiwalled carbon nanotubes modified glassy carbon electrodes (GCE-NiPcMWCNTs). The two nanocomposites (GCE-CoPcMWCNTs and GCE-NiPcMWCNTs) were prepared from the synthesized cobalt/ nickel nanoparticles, phthalocyanine and the functionalized MWCNTs. The successful fabrication of these sensors was confirmed by XRD, UV/vis spectroscopy, EDX, TEM and SEM. The CV and EIS studies revealed that the two nanocomposite sensors, demonstrated fast electron transport and better bromate response when compared with the other fabricated sensors (GCE, GCE-Pc, GCE-Co, GCE-Ni and GCE-fMWCNTs). The study also showed that the nanocomposite electrodes exhibited rapid electron transfer ability, higher power density and super-capacitive behavior in H_2SO_4 electrolyte than in the other investigated electrolytes (Na_2SO_4, PBS and SAB).

The electrochemical detection of bromate at GCE-CoPcMWCNTs and GCE-NiPcMWCNTs was achieved using EIS and SWV technique. In EIS, GCE-CoPcMWCNTs gave a lower detection limit than GCE-NiPcMWCNTs while in terms of linear dynamic range (LDR) and sensitivity, the GCE-NiPcMWCNTs is better. Whereas, with square wave voltammetry (SWV), the GCE-CoPcMWCNTs exhibit a lower LoD, a wider LDR and a higher sensitivity. The two sensors have demonstrated that they can only detect bromine at a micromolar level. The mechanism of bromate at the interface of the modified electrode surfaces of GCE-CoPcMWCNTs and GCE-NiPcMWCNTs was found to be diffusion controlled.

The developed sensors exhibited a very high stability - GCE-CoPcMWCNTs (93.5 %) and GCE-NiPcMWCNTs (95.5%) and a good reproducibility with % RSD of 3.9% for GCE-CoPcMWCNTs and 3.5% for GCE-NiPcMWCNTs. The two sensors demonstrated similar stability and reproducibility. The proposed sensors were effectively used for bromate determination in bread samples with a good recovery. Thus, they are suitable and reliable sensors for bromate detection in real sample (food).

5.2 Recommendations

Based on the results of the findings, while using GCE-CoPcMWCNTs and GCE-NiPcMWCNTs for bromate detection, the following recommendations should be considered for future bromate detection.

1. The proposed chemical method of preparation has shown to be effective. To mitigate the effect of aggregation and hydrophobicity of CoPc and NiPc nanoparticles, electrodeposition method of nanocomposite synthesis is recommended.
2. A broader scope of the developed sensors application for environmental pollutant control and pharmaceutical applications should be explored.
3. The use of other nanocatalysts should be considered for future study.
4. To develop more precise and sensitive sensor devices, the use of the printed electrodes, gold, and platinum in sensor fabrication should be harnessed.
5. The low charge transfer resistance, specific capacitance and power density of the nanocatalysts investigated in the study could be explore form application in battery and solar cell.

Appendix

OUTPUT: The listed publications are my published articles, emanated from my work.

1. Balogun, S. A., & Fayemi, O. E. (2022). Recent Advances in the Use of CoPc-MWCNTs Nanocomposites as Electrochemical Sensing Materials. *Biosensors*, *12*(10), 850.

2. Balogun, S. A., & Fayemi, O. E. (2022). Effects of Electrolytes on the Electrochemical Impedance Properties of NiPcMWCNTs-Modified Glassy Carbon Electrode. *Nanomaterials*, *12*(11), 1876.

3. Balogun, S. A., & Fayemi, O. E. (2021). Electrochemical Sensors for Determination of Bromate in Water and Food Samples. *Biosensors*, *11*(6), 172.

Articles under-review

4. Electrochemical impedance spectroscopy detection of bromate at CoPcMWCNTs modified glassy carbon electrode.

5. Electrochemical impedance spectroscopy detection of bromate at NiPcMWCNTs modified glassy carbon electrode.

6. Synthesis, characterization and anti-microbial study of cobalt and nickel nanoparticles.

Reference

1. Akinola, B. K., Olawuyi, T. S., and Ogunmokunwa, A. E., *The Protective Effects of Telfairia Occidentalis on Potassium Bromate Induced Hepatotoxicity in Adult Wistar Rats.* African Journal of Biological Sciences, 2020. **2**(3): p. 51-61.
2. Crofton, K., *Bromate: concern for developmental neurotoxicity?* Toxicology, 2006. **221**(2-3): p. 212-216.
3. Fawell, J. and Walker M., *Approaches to determining regulatory values for carcinogens with particular reference to bromate.* Toxicology, 2006. **221**(2-3): p. 149-153.
4. Balamurugan, A. and Chen, S.M., *Silicomolybdate-Doped PEDOT Modified electrode: electrocatalytic reduction of bromate and oxidation of ascorbic acid.* Electroanalysis: An International Journal Devoted to Fundamental and Practical Aspects of Electroanalysis, 2007. **19**(15): p. 1616-1622.
5. Organization, W.H. and WHO., *Guidelines for drinking-water quality*. Vol. 1. 2004: World Health Organization.
6. Shanmugavel, V., Santhi, K. K., Kurup, A. H., Kalakandan, S., Anandharaj, A., and Rawson, A., *Potassium bromate: Effects on bread components, health, environment and method of analysis: A review.* Food Chemistry, 2020. **311**: p. 125964.
7. Rahali, Y., Benmoussa, A., Ansar, M., Benziane, H., Lamsaouri, J., Idrissi, M. O. B., and Taoufik, J., *A simple and rapid method for spectrophotometric determination of bromate in bread.* Electronic Journal of Environmental, Agricultural & Food Chemistry, 2011. **10**(1).
8. Snyder, S.A., Vanderford, B.J., and Rexing, D.J., *Trace analysis of bromate, chlorate, iodate, and perchlorate in natural and bottled waters.* Environmental Science & Technology, 2005. **39**(12): p. 4586-4593.
9. Zakaria, P., Bloomfield, C., Shellie, R. A., Haddad, P. R., and Dicinoski, G. W., *Determination of bromate in sea water using multi-dimensional matrix-elimination ion chromatography.* Journal of Chromatography A, 2011. **1218**(50): p. 9080-9085.
10. Kim, H. J., and Shin, H. S., *Ultra trace determination of bromate in mineral water and table salt by liquid chromatography–tandem mass spectrometry.* Talanta, 2012. **99**: p. 677-682.

11. Menendez-Miranda, M., Fernandez-Argüelles, M. T., Costa-Fernandez, J. M., Pereiro, R., and Sanz-Medel, A., *Room temperature phosphorimetric determination of bromate in flour based on energy transfer.* Talanta, 2013. **116**: p. 231-236.
12. Majidi, M. R., Ghaderi, S., Asadpour-Zeynali, K., and Dastangoo, H., *Electrochemical determination of bromate in different types of flour and bread by a sensitive amperometric sensor based on palladium nanoparticles/graphene oxide nanosheets.* Food Analytical Methods, 2015. **8**(8): p. 2011-2019.
13. Stetter, J.R., Penrose, W.R., and Yao, S., *Sensors, chemical sensors, electrochemical sensors, and ECS.* Journal of The Electrochemical Society, 2003. **150**(2): p. S11. 127.
14. Gründler, P. and J. Janata, *Chemical sensors: an introduction for scientists and engineers.* Physics Today, 2008. **61**(3): p. 56.
15. Balogun, S.A. and Fayemi, O.E., *Recent Advances in the Use of CoPc-MWCNTs Nanocomposites as Electrochemical Sensing Materials.* Biosensors, 2022. **12**(10): p. 850.
16. Hannah, W. and Thompson, P.B., *Nanotechnology, risk and the environment: a review.* Journal of Environmental Monitoring, 2008. **10**(3): p. 291-300.
17. McNeil, S.E., *Nanotechnology for the biologist.* Journal of Leukocyte Biology, 2005. **78**(3): p. 585-594.
18. Khan, M., Khan, A. U., Rafatullah, M., Alam, M., Bogdanchikova, N., and Garibo, D., *Search for effective approaches to fight microorganisms causing high losses in agriculture: Application of P. lilacinum metabolites and mycosynthesised silver nanoparticles.* Biomolecules, 2022. **12**(2): p. 174.
19. Lakshmi, S. J., Bai, R. R. S., Sharanagouda, H., and Nidoni, U. K., *A review study of zinc oxide nanoparticles synthesis from plant extracts.* Green Chemistry Technology Letter, 2017. **3**(2): p. 26-37.
20. Saif, S., Tahir, A., and Chen, Y., *Green synthesis of iron nanoparticles and their environmental applications and implications.* Nanomaterials, 2016. **6**(11): p. 209.
21. Karimi-Maleh, H., Ayati, A., Ghanbari, S., Orooji, Y., Tanhaei, B., Karimi, F., Alizadeh, M., Rouhi, J., Fu, L. and Sillanpää, M., *Recent advances in removal techniques of Cr (VI) toxic ion from aqueous solution: A comprehensive review.* Journal of molecular liquids, 2021. **329**: p. 115062.

22. Luo, X., Morrin, A., Killard, A.J. and Smyth, M.R., *Application of nanoparticles in electrochemical sensors and biosensors.* Electroanalysis: An International Journal Devoted to Fundamental and Practical Aspects of Electroanalysis, 2006. **18**(4): p. 319-326.
23. El-Ansary, A. and Faddah, L.M., *Nanoparticles as biochemical sensors.* Nanotechnology, science and applications, 2010. **3**: p. 65.
24. Eluri, R. and Paul, B., *Synthesis of nickel nanoparticles by hydrazine reduction: mechanistic study and continuous flow synthesis.* Journal of Nanoparticle Research, 2012. **14**(4): p. 1-14.
25. Imran Din, M. and Rani, A., *Recent advances in the synthesis and stabilization of nickel and nickel oxide nanoparticles: a green adeptness.* International Journal of Analytical Chemistry, 2016. **2016**.
26. Chen, D.H. and Hsieh, C.H., *Synthesis of nickel nanoparticles in aqueous cationic surfactant solutions.* Journal of Materials Chemistry, 2002. **12**(8): p. 2412-2415.
27. Salavati-Niasari, M., Fereshteh, Z., and Davar, F., *Synthesis of cobalt nanoparticles from [bis (2-hydroxyacetophenato) cobalt (II)] by thermal decomposition.* Polyhedron, 2009. **28**(6): p. 1065-1068.
28. Mourdikoudis, S., Pallares, R.M., and Thanh, N.T., *Characterization techniques for nanoparticles: comparison and complementarity upon studying nanoparticle properties.* Nanoscale, 2018. **10**(27): p. 12871-12934. 128.
29. Titus, D., Samuel, E.J.J., and Roopan, S.M., *Nanoparticle characterization techniques*, in *Green synthesis, characterization and applications of nanoparticles*. 2019, Elsevier. p. 303-319.
30. Song, K., *Interphase characterization in rubber nanocomposites*, in *Progress in Rubber Nanocomposites*. 2017, Elsevier. p. 115-152.
31. Wang, F.X., Liu, Y.D. and Pan, G.B., *Vapor growth and photoconductivity of single-crystal nickel-phthalocyanine nanorods.* Materials Letters, 2011. **65**(5): p. 933-936.
32. Qiu, S., Li, Y., Xu, H., Liang, Q., Zhou, M., Rong, J., Li, Z. and Xu, S., *Efficient catalytic oxidation of benzyl alcohol by tetrasubstituted cobalt phthalocyanine-MWCNTs composites.* Solid State Sciences, 2022. **129**: p. 106905.

33. Wang, L., Pan, D., Zhou, M., Liang, Q. and Li, Z., *Effect of phthalocyanines supported carbon nanotube for the catalytic oxidation of benzyl alcohol.* Solid State Sciences, 2021. **113**: p. 106546.
34. Wang, H. and Chu, P.K., *Surface characterization of biomaterials*, in *Characterization of biomaterials*. 2013, Elsevier. p. 105-174.`
35. Pentassuglia, S., Agostino, V. and Tommasi, T., *EAB—electroactive biofilm: a biotechnological resource.* 2018.
36. Gaikwad, S.U., Patil, R.R., Moharil, S.V. and Kulkarni, M.S., *Structural characterization techniques of materials*. in *AIP Conference Proceedings*. 2019. AIP Publishing LLC.
37. Ali, A., Chiang, Y.W., and Santos, R.M., *X-ray Diffraction Techniques for Mineral Characterization: A Review for Engineers of the Fundamentals, Applications, and Research Directions.* Minerals, 2022. **12(**2): p. 205.
38. Fayemi, O.E., *Electrochemical properties of nanoporous based materials doped with metal oxide nanoparticles for potential application as sensors*. 2015, North-West University (South Africa).
39. Uwaya, G., *Electrochemical detection of choline at green mediated nanocomposites modified electrode*. 2021, North-West University (South Africa).
40. Wu, C.K., Yin, M., O'Brien, S. and Koberstein, J.T., *Quantitative analysis of copper oxide nanoparticle composition and structure by X-ray photoelectron spectroscopy.* Chemistry of Materials, 2006. **18(**25): p. 6054-6058.
41. Zamani Kouhpanji, M.R. and Stadler, B.J., *A guideline for effectively synthesizing and characterizing magnetic nanoparticles for advancing nanobiotechnology: A review.* Sensors, 2020. **20**(9): p. 2554.
42. Akhtar, K., Khan, S.A., Khan, S.B. and Asiri, A.M., *Scanning electron microscopy: Principle and applications in nanomaterials characterization*, in *Handbook of materials characterization*. 2018, Springer. p. 113-145.
43. Von der Kammer, F., Ferguson, P.L., Holden, P.A., Masion, A., Rogers, K.R., Klaine, S.J., Koelmans, A.A., Horne, N. and Unrine, J.M., *Analysis of engineered nanomaterials in complex matrices (environment and biota): general considerations and conceptual case studies.* Environmental Toxicology and Chemistry, 2012. **31**(1): p. 32-49. 129.

44. Fultz, B. and Howe, J.M., *Transmission electron microscopy and diffractometry of materials*. 2012: Springer Science & Business Media.
45. Dias, L.G., Meirinho, S.G., Veloso, A.C., Rodrigues, L.R. and Peres, A.M., *Electronic tongues and aptasensors,* in *Bioinspired Materials for Medical Applications*. 2017, Elsevier. p. 371-402.
46. Thomas, D., Rasheed, Z., Jagan, J.S. and Kumar, K.G., *Study of kinetic parameters and development of a voltammetric sensor for the determination of butylated hydroxyanisole (BHA) in oil samples.* Journal of Food Science and Technology, 2015. **52**(10): p. 6719-6726.
47. Thomas, F.G. and Henze, G., *Introduction to voltammetric analysis: theory and practice*. 2000: Csiro Publishing.
48. Zhuang, X., Wang, H., He, T. and Chen, L., *Enhanced voltammetric determination of dopamine using a glassy carbon electrode modified with ionic liquid-functionalized graphene and carbon dots.* Microchimica Acta, 2016. **183**(12): p. 3177-3182.
49. Boehler, C., Stieglitz, T. and Asplund, M., *Nanostructured platinum grass enables superior impedance reduction for neural microelectrodes.* Biomaterials, 2015. **67**: p. 346-353.
50. Rahman, M.M., Hussein, M.A., Alamry, K.A., Al-Shehry, F.M. and Asiri, A.M., *Polyaniline/graphene/carbon nanotubes nanocomposites for sensing environmentally hazardous 4-aminophenol.* Nano-Structures & Nano-Objects, 2018. **15**: p. 63-74.
51. Liao, Y.T., Yao, H., Lingley, A., Parviz, B. and Otis, B.P., *A 3-$\mu\hbox {W} $ CMOS Glucose Sensor for Wireless Contact-Lens Tear Glucose Monitoring.* IEEE Journal of Solid-State Circuits, 2011. **47**(1): p. 335-344.
52. Stetter, J.R. and Li, J., *Amperometric gas sensors a review.* Chemical reviews, 2008. **108**(2): p. 352-366.
53. Elgrishi, N., Rountree, K.J., McCarthy, B.D., Rountree, E.S., Eisenhart, T.T. and Dempsey, J.L., *A practical beginner's guide to cyclic voltammetry.* Journal of Chemical Education, 2018. **95**(2): p. 197-206.
54. Faulkner, L.R., *Understanding electrochemistry: Some distinctive concepts*. 1983, ACS Publications.

55. Baca, G. and Dennis, A.L., *Electrochemistry in a nutshell A general chemistry experiment.* Journal of Chemical Education, 1978. **55**(12): p. 804.
56. Ameur, Z.O. and Husein, M.M., *Electrochemical behavior of potassium ferricyanide in aqueous and (w/o) microemulsion systems in the presence of dispersed nickel nanoparticles.* Separation Science and Technology, 2013. **48**(5): p. 681-689.
57. Mak, W.F., Wee, G., Aravindan, V., Gupta, N., Mhaisalkar, S.G. and Madhavi, S., *High-energy density asymmetric supercapacitor based on electrospun vanadium pentoxide and polyaniline nanofibers in aqueous electrolyte.* Journal of the Electrochemical Society, 2012. **159**(9): p. A1481. 130.
58. Scholz, F., *Electroanalytical methods*. Vol. 1. 2010: Springer.
59. Brett, C.M., *Electroanalytical techniques for the future: the challenges of miniaturization and of real-time measurements.* Electroanalysis: An International Journal Devoted to Fundamental and Practical Aspects of Electroanalysis, 1999. **11**(14): p. 1013-1016.
60. Sandifer, J.R., *Electroanalytical techniques.* Kirk-Othmer Encyclopedia of Chemical Technology, 2000.
61. Balogun, S.A. and Fayemi, O.E., *Electrochemical sensors for determination of bromate in water and food samples—review.* Biosensors, 2021. **11**(6).
62. Kounaves, S.P., *Voltammetric techniques.* Handbook of Instrumental Techniques for Analytical Chemistry, 1997: p. 709-726.
63. Zhang, J., Wu, J., Zhang, H. and Zhang, J., *PEM fuel cell testing and diagnosis*. 2013: Newnes.
64. Rusling, J.F. and Suib, S.L., *Characterizing materials with cyclic voltammetry.* Advanced Materials, 1994. **6**(12): p. 922-930.
65. Mabbott, G.A., *An introduction to cyclic voltammetry.* Journal of Chemical Education, 1983. **60**(9): p. 697.
66. Simões, F.R. and Xavier, M.G., *Electrochemical sensors.* Nanoscience and its Applications, 2017: p. 155-178.
67. Mirceski, V., Gulaboski, R., Lovric, M., Bogeski, I., Kappl, R. and Hoth, M., *Square-wave voltammetry: a review on the recent progress.* Electroanalysis, 2013. **25**(11): p. 2411-2422.
68. Krause, M.S. and Ramaley, L., *Analytical application of square wave voltammetry.* Analytical Chemistry, 1969. **41**(11): p. 1365-1369.

69. Ribeiro, D. and Abrantes, J., *Application of electrochemical impedance spectroscopy (EIS) to monitor the corrosion of reinforced concrete: A new approach.* Construction and Building Materials, 2016. **111**: p. 98-104.
70. Tiginyanu, I., Topala, P., and Ursaki, V., *Nanostructures and thin films for multifunctional applications*. Vol. 42. 2016: Springer.
71. Reece, C., *An introduction to electrochemical impedance spectroscopy.* Jefferson Lab, 2005.
72. Azzarello, E., Masi, E., and Mancuso, S., *Electrochemical impedance spectroscopy*, in *Plant Electrophysiology*. 2012, Springer. p. 205-223.
73. Cesiulis, H., Tsyntsaru, N., Ramanavicius, A. and Ragoisha, G., *The study of thin films by electrochemical impedance spectroscopy*, in *Nanostructures and thin films for multifunctional applications*. 2016, Springer. p. 3-42.
74. Balogun, S.A. and Fayemi, O.E., *Effects of Electrolytes on the Electrochemical Impedance Properties of NiPcMWCNTs-Modified Glassy Carbon Electrode.* Nanomaterials, 2022. **12**(11): p. 1876.
75. Du, C. and Pan, N., *Supercapacitors using carbon nanotubes films by electrophoretic deposition.* Journal of Power Sources, 2006. **160**(2): p. 1487-1494. 131.
76. Huang, C.W., Wu, Y.T., Hu, C.C. and Li, Y.Y., *Textural and electrochemical characterization of porous carbon nanofibers as electrodes for supercapacitors.* Journal of Power Sources, 2007. **172**(1): p. 460-467.
77. Merkoçi, A., Pumera, M., Llopis, X., Pérez, B., Del Valle, M. and Alegret, S., *New materials for electrochemical sensing VI: carbon nanotubes.* TrAC Trends in Analytical Chemistry, 2005. **24**(9): p. 826-838.
78. Ma, L., Dong, X., Chen, M., Zhu, L., Wang, C., Yang, F. and Dong, Y., *Fabrication and water treatment application of carbon nanotubes (CNTs)-based composite membranes: a review.* Membranes, 2017. **7**(1): p. 16.
79. Jia, X. and Wei, F., *Advances in production and applications of carbon nanotubes.* Single-Walled Carbon Nanotubes, 2019: p. 299-333.
80. Wang, Y., Tang, L., Li, Y., Li, Q. and Bai, B., *Preparation of modified multi-walled carbon nanotubes as a reinforcement for epoxy shape-memory polymer composites.* Polymers for Advanced Technologies, 2021. **32**(1): p. 67-75.

81. Lai, M., Jiang, L., Wang, X., Zhou, H., Huang, Z. and Zhou, H., *Effects of multi-walled carbon nanotube/graphene oxide-based sizing on interfacial and tribological properties of continuous carbon fiber/poly(ether ether ketone) composites.* Materials Chemistry and Physics, 2022. **276**.
82. Li, Q., Wang, Z., Liang, Q., Zhou, M., Xu, S., Li, Z. and Sun, D., *Tetra-substituted cobalt (II) phthalocyanine/multi-walled carbon nanotubes as new efficient catalyst for the selective oxidation of styrene using tert-butyl hydroperoxide.* Fullerenes, Nanotubes and Carbon Nanostructures, 2020. **28**(10): p. 799-807.
83. Reddy, K.K., Satyanarayana, M., Goud, K.Y., Gobi, K.V. and Kim, H., *Carbon nanotube ensembled hybrid nanocomposite electrode for direct electrochemical detection of epinephrine in pharmaceutical tablets and urine.* Materials Science and Engineering: C, 2017. **79**: p. 93-99.
84. Khaghani, R., Esrafili, A., Zeynalzadeh, D. and Asl, F.B., *Synthesis of magnetic multiwalled carbon nano tubes and investigation of isotherm and kinetic models for cleanup of carbaryl pesticide.* Global Nest Journal, 2020. **22**(3): p. 281-288.
85. Matute, R.A., Toro-Labbé, A., Oyarzún, M.P., Ramirez, S., Ortega, D.E., Oyarce, K., Silva, N. and Zagal, J.H., *Mapping experimental and theoretical reactivity descriptors of fe macrocyclic complexes deposited on graphite or on multi walled carbon nanotubes for the oxidation of thiols: Thioglycolic acid oxidation.* Electrochimica Acta, 2021. **391**: p. 138905.
86. Baghayeri, M., Amiri, A., Fayazi, M., Nodehi, M. and Esmaeelnia, A., *Electrochemical detection of bisphenol a on a MWCNTs/CuFe2O4 nanocomposite modified glassy carbon electrode.* Materials Chemistry and Physics, 2021. **261**: p. 124247.
87. Savk, A., Özdil, B., Demirkan, B., Nas, M.S., Calimli, M.H., Alma, M.H., Asiri, A.M. and Şen, F., *Multiwalled carbon nanotube-based nanosensor for ultrasensitive detection of uric acid, dopamine, and ascorbic acid.* 2019. *Materials Science and Engineering: C, 99,* pp.248-254. 132.
88. Wu, B., Yeasmin, S., Liu, Y. and Cheng, L.J., *Ferrocene Functionalized Gold Nanoparticles on Carbon Nanotube Electrodes for Portable Dopamine Sensor*. in *ECS Meeting Abstracts*. 2021. IOP Publishing.

89. Gurusamy, T., Rajaram, R., Murugan, R. and Ramanujam, K., *A web of poly (bisbenzimidazolatocopper (ii)) around multiwalled carbon nanotubes for the electrochemical detection of hydrogen peroxide.* New Journal of Chemistry, 2022. **46**(3): p. 1222-1231.
90. Reddy, K. V., Yuvaraja, D., Manriquez, J. M., Lokesh, K. S., and Amshumali, M. K., *Novel Schiff base iron (ii) phthalocyanine with composite MWCNTs on modified GCE: electrochemical sensor development for paracetamol.* Reaction Chemistry & Engineering, 2022. ***7***(12), 2550-2561.
91. Tahernejad-Javazmi, F., Shabani-Nooshabadi, M., and Karimi-Maleh, H., *Analysis of glutathione in the presence of acetaminophen and tyrosine via an amplified electrode with MgO/SWCNTs as a sensor in the hemolyzed erythrocyte.* Talanta, 2018. **176**: p. 208-213.
92. Musarraf Hussain, M., Asiri, A.M., Uddin, J., Marwani, H.M. and Rahman, M.M., *Development of a L-cysteine Sensor Based on Thallium Oxide Coupled Multi-walled Carbon Nanotube Nanocomposites with Electrochemical Approach.* Chemistry–An Asian Journal, 2022. **17**(3): p. e202101117.
93. Shao, W., Mai, J., and Wei, Z., *Nonenzymatic Lactic Acid Detection Using Cobalt Polyphthalocyanine/Carboxylated Multiwalled Carbon Nanotube Nanocomposites Modified Sensor.* Chemosensors, 2022. **10**(2): p. 83.
94. Kweon, H., Hosking, A., Mushfiq, M. and Alam, M.M., *Selective and trace level detection of hydrazine using functionalized single-walled carbon nanotube-based microelectronic devices.* ACS Applied Electronic Materials, 2021. **3**(2): p. 711-719.
95. Ghanam, A., Haddour, N., Mohammadi, H., Amine, A., Sabac, A. and Buret, F., *Nanoporous Cauliflower-like Pd-Loaded Functionalized Carbon Nanotubes as an Enzyme-Free Electrocatalyst for Glucose Sensing at Neutral pH: Mechanism Study.* Sensors, 2022. **22**(7): p. 2706.
96. Yao, Y., Yin, C., Xu, S., Jiang, M., Zhu, L., Zou, R. and Sun, W., *Preparation of Horseradish Peroxidase Modified Gold Nanoparticle/Coiled Carbon Nanotube Nanocomposite and its application for bromate and nitrite determination.* Int. J. Electrochem. Sci, 2022. **17**(220546): p. 2.
97. Kaya, E.N., Tuncel, S., Basova, T.V., Banimuslem, H., Hassan, A., Gürek, A.G., Ahsen, V. and Durmuş, M., *Effect of pyrene substitution on the formation and sensor properties*

of phthalocyanine-single walled carbon nanotube hybrids. Sensors and Actuators B: Chemical, 2014. **199**: p. 277-283.

98. Das, G., Sain, B. and Kumar, S., *Synthesis, characterization and catalytic activity of cobalt phthalocyanine dichloride in sweetening of heavier petroleum fractions.* Catalysis today, 2012. **198**(1): p. 228-232.
99. Reddy, K.V., *Sensitive and reliable electrochemical detection of nitrite and H2O2 embellish-CoPc coupled with appliance of composite MWCNTs.* Analytica Chimica Acta, 2020. **1108**: p. 98-107. 133.
100. Yadav, K.K., Ahmad, S., Narang, U., Bhattacharya, S. and Chauhan, S.M.S., *Xanthenedione Substituted Metallophthalocyanines as an Efficient and Recyclable Catalyst for One–pot Three Component Synthesis of 3-Substituted Indoles.* ChemistrySelect, 2016. **1**(13): p. 3635-3639.
101. Saka, E.T., Uzun, S., and Çağlar, Y., *Synthesis, structural characterization, catalytic activity on aerobic oxidation of novel Co (II) and Fe (II) phthalocyanines and computational studies of 4-[2-(2, 3-dichlorophenoxy) ethoxy] phthalonitrile.* Journal of Organometallic Chemistry, 2016. **810**: p. 25-32.
102. Nandan, D., Zoppellaro, G., Medřík, I., Aparicio, C., Kumar, P., Petr, M., Tomanec, O., Gawande, M.B., Varma, R.S. and Zbořil, R., *Cobalt-entrenched N-, O-, and S-tridoped carbons as efficient multifunctional sustainable catalysts for base-free selective oxidative esterification of alcohols.* Green Chemistry, 2018. **20**(15): p. 3542-3556.
103. Saka, E.T. and Çağlar, Y., *New Co (II) and Cu (II) phthalocyanine catalysts reinforced by long alkyl chains for the degradation of organic pollutants.* Catalysis Letters, 2017. **147**(6): p. 1471-1477.
104. Eyele-Mezui, S., Vialat, P., Higy, C., Bourzami, R., Leuvrey, C., Parizel, N., Turek, P., Rabu, P., Rogez, G. and Mousty, C., *Electrocatalytic properties of metal phthalocyanine tetrasulfonate intercalated in metal layered simple hydroxides (Metal: Co, Cu, and Zn).* The Journal of Physical Chemistry C, 2015. **119**(23): p. 13335-13342.
105. de Barros, M.R., Winiarski, J.P., de Matos Morawski, F., Marim, R.G., Chaves, E.S., Blacha-Grzechnik, A. and Jost, C.L., *A high-performance electrochemical sensor based on a mesoporous silica/titania material and cobalt (II) phthalocyanine for sensitive pentachlorophenol determination.* Microchimica Acta, 2022. **189**(8): p. 1-14.

106. Li, H., Pan, Y., Wang, Z., Yu, Y., Xiong, J., Du, H., Lai, J., Wang, L. and Feng, S., *Coordination engineering of cobalt phthalocyanine by functionalized carbon nanotube for efficient and highly stable carbon dioxide reduction at high current density.* Nano Research, 2022. **15**(4): p. 3056-3064.

107. Han, N., Wang, Y., Ma, L., Wen, J., Li, J., Zheng, H., Nie, K., Wang, X., Zhao, F., Li, Y. and Fan, J., *Supported cobalt polyphthalocyanine for high-performance electrocatalytic CO2 reduction.* Chem, 2017. **3**(4): p. 652-664.

108. Mei, B., Liu, C., Li, J., Gu, S., Du, X., Lu, S., Song, F., Xu, W. and Jiang, Z., *Operando HERFD-XANES and surface sensitive Δμ analyses identify the structural evolution of copper (II) phthalocyanine for electroreduction of CO2.* Journal of Energy Chemistry, 2022. **64**: p. 1-7.

109. Jiang, Z., Wang, Y., Zhang, X., Zheng, H., Wang, X. and Liang, Y., *Revealing the hidden performance of metal phthalocyanines for CO2 reduction electrocatalysis by hybridization with carbon nanotubes.* Nano Research, 2019. **12**(9): p. 2330-2334.

110. Zhu, M., Chen, J., Huang, L., Ye, R., Xu, J. and Han, Y.F., *Covalently grafting cobalt porphyrin onto carbon nanotubes for efficient CO2 electroreduction.* Angewandte Chemie International Edition, 2019. **58**(20): p. 6595-6599. 134.

111. Chen, K., Liu, K., An, P., Li, H., Lin, Y., Hu, J., Jia, C., Fu, J., Li, H., Liu, H. and Lin, Z., *Iron phthalocyanine with coordination induced electronic localization to boost oxygen reduction reaction.* Nature communications, 2020. **11**(1): p. 1-8.

112. Wang, J., Huang, X., Xi, S., Xu, H. and Wang, X., *Axial modification of cobalt complexes on heterogeneous surface with enhanced electron transfer for carbon dioxide reduction.* Angewandte Chemie International Edition, 2020. **59**(43): p. 19162-19167.

113. Gu, S., Marianov, A.N., Zhu, Y. and Jiang, Y., *Cobalt porphyrin immobilized on the TiO2 nanotube electrode for CO2 electroreduction in aqueous solution.* Journal of Energy Chemistry, 2021. **55**: p. 219-227.

114. Shi, Y.M., Zhang, X., Mei, L., Han, D.E., Hu, K., Chao, L.Q. and Li, X.M., *Sensitive acetaminophen electrochemical sensor with amplified signal strategy via non-covalent functionalization of soluble tetrahydroxyphthalocyanine and graphene.* Microchemical Journal, 2021. **160**: p. 105609.

115. Shen, C., Li, Y., Gong, M., Zhou, C., An, Q., Xu, X. and Mai, L., *Ultrathin Cobalt Phthalocyanine@ Graphene Oxide Layer-Modified Separator for Stable Lithium–Sulfur Batteries.* ACS Applied Materials & Interfaces, 2021. **13**(50): p. 60046-60053.
116. Nemakal, M. and Sannegowda, L., *Hybrid composites based on phthalocyanine and carbonaceous materials for sensing applications: a review.* Int J Biosen Bioelectron, 2021. **7**(3): p. 84-89.
117. Ozoemena, K.I., Nyokong, T., Nkosi, D., Chambrier, I. and Cook, M.J., *Insights into the surface and redox properties of single-walled carbon nanotube—cobalt (II) tetra-aminophthalocyanine self-assembled on gold electrode.* Electrochimica acta, 2007. **52**(12): p. 4132-4143.
118. Mphuthi, N.G., Adekunle, A.S., Fayemi, O.E., Olasunkanmi, L.O. and Ebenso, E.E., *Phthalocyanine doped metal oxide nanoparticles on multiwalled carbon nanotubes platform for the detection of dopamine.* Scientific reports, 2017. **7**(1): p. 1-23.
119. Kantize, K., Booysen, I.N. and Mambanda, A., *Electrochemical sensing of acetaminophen using nanocomposites comprised of cobalt phthalocyanines and multiwalled carbon nanotubes.* Journal of Electroanalytical Chemistry, 2019. **850**: p. 113391.
120. Winiarski, J.P., de Barros, M.R., Wecker, G.S., Nagurniak, G.R., Parreira, R.L.T., Affeldt, R.F., Peralta, R.A. and Jost, C.L., *A novel hybrid organic–inorganic silsesquioxane and cobalt (ii) tetrasulphophthalocyanine material as an efficient electrochemical sensor for the simultaneous determination of the anti-hypertensive nifedipine and its metabolite.* Journal of Materials Chemistry C, 2020. **8**(20): p. 6839-6850.
121. Guaraldo, T.T., Goulart, L.A., Moraes, F.C. and Lanza, M.R., *Carbon black nanospheres modified with Cu (II)-phthalocyanine for electrochemical determination of Trimethoprim antibiotic.* Applied Surface Science, 2019. **470**: p. 555-564.
122. Gorduk, O., Gencten, M., Gorduk, S., Sahin, M. and Sahin, Y., *Electrochemical fabrication and supercapacitor performances of metallo phthalocyanine/functionalized-multiwalled carbon nanotube/polyaniline modified hybrid electrode materials.* Journal of Energy Storage, 2021. **33**: p. 102049. 135.
123. Kutluay, A. and Aslanoglu, M., *An electrochemical sensor prepared by sonochemical one-pot synthesis of multi-walled carbon nanotube-supported cobalt nanoparticles for the*

simultaneous determination of paracetamol and dopamine. Analytica chimica acta, 2014. **839**: p. 59-66.

124. Zuo, X., Zhang, H., and Li, N., *An electrochemical biosensor for determination of ascorbic acid by cobalt (II) phthalocyanine–multi-walled carbon nanotubes modified glassy carbon electrode.* Sensors and Actuators B: Chemical, 2012. **161**(1): p. 1074-1079.
125. Jilani, B.S., Pari, M., Reddy, K.V. and Lokesh, K.S., et al., *Simultaneous and sensitive detection of ascorbic acid in presence of dopamine using MWCNTs-decorated cobalt (II) phthalocyanine modified GCE.* Microchemical Journal, 2019. **147**: p. 755-763.
126. Reddy, K.V., *Novel garnished cobalt (II) phthalocyanine with MWCNTs on modified GCE: sensitive and reliable electrochemical investigation of paracetamol and dopamine.* New Journal of Chemistry, 2020. **44**(39): p. 16831-16844.
127. Cruz Moraes, F., Cabral, M.F., Machado, S.A. and Mascaro, L.H., *Electrocatalytic behavior of glassy carbon electrodes modified with multiwalled carbon nanotubes and cobalt phthalocyanine for selective analysis of dopamine in presence of ascorbic acid.* Electroanalysis: An International Journal Devoted to Fundamental and Practical Aspects of Electroanalysis, 2008. **20**(8): p. 851-857.
128. Wang, H.H., Li, N., Li, K., Bu, Y., Dai, W.L. and Zuo, X.. *Multiwalled Carbon Nanotubes Covered with Cobalt (II) Phthalocyanine by In Situ Synthesis and its Electrochemical Sensing Performance towards DA and UA*. in *Materials Science Forum*. 2015. Trans Tech Publications Ltd.
129. Reddy, K.V., *Decorated CoPc with appliance of MWCNTs on GCE: sensitive and reliable electrochemical investigation of heavy metals.* Microchemical Journal, 2021. **160**: p. 105610.
130. Lu, S., Hummel, M., Kang, S. and Gu, Z., *Selective voltammetric determination of nitrite using cobalt phthalocyanine modified on multiwalled carbon nanotubes.* Journal of The Electrochemical Society, 2020. **167**(4): p. 046515.
131. Reddy, K.V., *The electrochemical investigation of carboxamide-PEG 2-biotin-CoPc using composite MWCNTs on modified GCE: the sensitive detections for glucose and hydrogen peroxide.* New Journal of Chemistry, 2020. **44**(8): p. 3330-3340.

132. Moraes, F.C., Mascaro, L.H., Machado, S.A. and Brett, C.M., *Direct electrochemical determination of carbaryl using a multi-walled carbon nanotube/cobalt phthalocyanine modified electrode.* Talanta, 2009. **79**(5): p. 1406-1411.
133. Aragão, J.S., Ribeiro, F.W., Portela, R.R., Santos, V.N., Sousa, C.P., Becker, H., Correia, A.N. and de Lima-Neto, P., *Electrochemical determination diethylstilbestrol by a multi-walled carbon nanotube/cobalt phthalocyanine film electrode.* Sensors and Actuators B: Chemical, 2017. **239**: p. 933-942.
134. de Holanda, L.F., Ribeiro, F.W.P., Sousa, C.P., da Silva Casciano, P.N., de Lima-Neto, P. and Correia, A.N., *Multi-walled carbon nanotubes–cobalt phthalocyanine modified electrode for electroanalytical determination of acetaminophen.* Journal of Electroanalytical Chemistry, 2016. **772**: p. 9-16. 136.
135. Moraes, F.C., Golinelli, D.L., Mascaro, L.H. and Machado, S.A., *Determination of epinephrine in urine using multi-walled carbon nanotube modified with cobalt phthalocyanine in a paraffin composite electrode.* Sensors and Actuators B: Chemical, 2010. **148**(2): p. 492-497.
136. Agboola, B.O., Vilakazi, S.L., and Ozoemena, K.I., *Electrochemistry at cobalt (II) tetrasulfophthalocyanine-multi-walled carbon nanotubes modified glassy carbon electrode: a sensing platform for efficient suppression of ascorbic acid in the presence of epinephrine.* Journal of Solid State Electrochemistry, 2009. **13**(9): p. 1367-1379.
137. Yang, Z.H., Zhuo, Y., Yuan, R. and Chai, Y.Q., *Electrochemical activity and electrocatalytic property of cobalt phthalocyanine nanoparticles-based immunosensor for sensitive detection of procalcitonin.* Sensors and Actuators B: Chemical, 2016. **227**: p. 212-219.
138. Kantize, K., Booysen, I.N., and Mambanda, A., *Electrocatalytic Determination of Nevirapine Using a Platinum Electrode Modified with a Polymeric CoPc-Nafion-carbon nanotube Composite.* Int. J. Electrochem. Sci, 2022. **17**(22067): p. 2.
139. Pari, M. and Reddy, K.R.V., *Electrochemical Investigation of Uric Acid using MWCNTs-Decorated Novel Substituted Cobalt (II) Phthalocyanine Modified GCE.* Anal. Bioanal. Electrochem, 2019. **11**: p. 1383-1397.

140. de Fátima Giarola, J. and César Pereira, A., *Development and application of a sensor based on carbonaceous materials and cobalt phthalocyanine composite for electrochemical determination of uric acid.* Electroanalysis, 2016. **28**(6): p. 1348-1355.

141. Porras Gutierrez, A., Rangel Argote, M., Griveau, S., Zagal, J.H., Gutierrez Granados, S., Alatorre Ordas, A. and Bedioui, F., *Catalytic activity of electrode materials based on polypyrrole, multi-wall carbon nanotubes and cobalt phthalocyanine for the electrooxidation of glutathione and L-cysteine.* Journal of the Chilean Chemical Society, 2012. **57**(3): p. 1244-1247.

142. Rangel Argote, M., Sanchez Guillen, E., Gutierrez Porras, A.G., Serrano Torres, O., Richard, C., Zagal, J.H., Bedioui, F., Gutierrez Granados, S. and Griveau, S., *Preparation and characterization of electrodes modified with pyrrole surfactant, multiwalled carbon nanotubes and metallophthalocyanines for the electrochemical detection of thiols.* Electroanalysis, 2014. **26**(3): p. 507-512.

143. Sun, X., Li, F., Shen, G., Huang, J. and Wang, X., *Aptasensor based on the synergistic contributions of chitosan–gold nanoparticles, graphene–gold nanoparticles and multi-walled carbon nanotubes-cobalt phthalocyanine nanocomposites for kanamycin detection.* Analyst, 2014. **139**(1): p. 299-308.

144. Mounesh, Sharan Kumar, T.M., Praveen Kumar, N.Y. and Venugopal Reddy, K.R., *Poly (L-lactide)-carboxamide-CoPc with composite MWCNTs on glassy carbon electrode sensitive detection of hydrazine and L-cysteine.* Analytical Chemistry Letters, 2020. **10**(5): p. 620-635.

145. Porto, L.S., da Silva, D.N., Silva, M.C. and Pereira, A.C., *Electrochemical Sensor Based on Multi-walled Carbon Nanotubes and Cobalt Phthalocyanine Composite for Pyridoxine Determination.* Electroanalysis, 2019. **31**(5): p. 820-828. 137.

146. Mounesh, K. Venugopal Reddy, and Fasiulla, *Novel tetracinnamide cobalt (II) phthalocyanine immobilized on MWCNTs for amperometic sensing of glucose.* Analytical Chemistry Letters, 2020. **10**(2): p. 137-151.

147. Devasenathipathy, R., Karuppiah, C., Chen, S.M., Palanisamy, S., Lou, B.S., Ali, M.A. and Al-Hemaid, F.M., *A sensitive and selective enzyme-free amperometric glucose biosensor using a composite from multi-walled carbon nanotubes and cobalt phthalocyanine.* RSC advances, 2015. **5**(34): p. 26762-26768.

148. Wang, Z., Sun, Z., Li, Q., Zhou, M., Liang, Q., Li, Z. and Sun, D., *Selective oxidation of styrene to benzaldehyde by cobalt phthalocyanine-multi-walled carbon nanotube composites.* Solid State Sciences, 2020. **101**: p. 106122.

149. Ju, L., Li, Z., Xu, S. and Li, Q., *Synthesis and catalytic activity of different substituted metal phthalocyanine-MWCNTs hybrid materials for selective oxidation of styrene.* Fullerenes, Nanotubes and Carbon Nanostructures, 2017. **25**(5): p. 335-341.

150. Xu, Z., Li, H., Cao, G., Zhang, Q., Li, K. and Zhao, X., *Electrochemical performance of carbon nanotube-supported cobalt phthalocyanine and its nitrogen-rich derivatives for oxygen reduction.* Journal of Molecular Catalysis A: Chemical, 2011. **335**(1-2): p. 89-96.

151. Kruusenberg, I., Matisen, L., and Tammeveski, K., *Oxygen electroreduction on multi-walled carbon nanotube supported metal phthalocyanines and porphyrins in acid media.* Int. J. Electrochem. Sci, 2013. **8**: p. 1057-1066.

152. Kruusenberg, I., Matisen, L., and Tammeveski, K., *Oxygen electroreduction on multi-walled carbon nanotube supported metal phthalocyanines and porphyrins in alkaline media.* Journal of Nanoscience and Nanotechnology, 2013. **13**(1): p. 621-627.

153. Giddaerappa, Manjunatha, N., Shantharaja, Hojamberdiev, M. and Sannegowda, L.K., *Tetraphenolphthalein Cobalt (II) Phthalocyanine Polymer Modified with Multiwalled Carbon Nanotubes as an Efficient Catalyst for the Oxygen Reduction Reaction.* ACS omega, 2022. **7**(16): p. 14291-14304.

154. Praats, R., Käärik, M., Kikas, A., Kisand, V., Aruväli, J., Paiste, P., Merisalu, M., Sarapuu, A., Leis, J., Sammelselg, V. and Douglin, J.C., *Electroreduction of oxygen on cobalt phthalocyanine-modified carbide-derived carbon/carbon nanotube composite catalysts.* Journal of Solid State Electrochemistry, 2021. **25**(1): p. 57-71.

155. Sun, C., Hou, Y., Lüdi, N., Hu, H., de Jesús Gálvez-Vázquez, M., Liechti, M., Kong, Y., Liu, M., Erni, R., Rudnev, A.V. and Broekmann, P., *Improving the lifetime of hybrid CoPc@ MWCNT catalysts for selective electrochemical CO2-to-CO conversion.* Journal of Catalysis, 2022. **407**: p. 198-205.

156. Mirzaeian, M., Rashidi, A.M., Zare, M., Ghabezi, R. and Lotfi, R., *Mercaptan removal from natural gas using carbon nanotube supported cobalt phthalocyanine nanocatalyst.* Journal of Natural Gas Science and Engineering, 2014. **18**: p. 439-445.

157. Mohammad, E.J., Kareem, M.M., and Atiyah, A.J., *Photocatalytic oxidation of butan-2-ol over multi walled carbon nanotubes/cobalt phthalocynanine composites.* Bulletin of the Chemical Society of Ethiopia, 2022. **36**(1): p. 197-207. 138.

158. Bhowmick, G.D., Kibena-Põldsepp, E., Matisen, L., Merisalu, M., Kook, M., Käärik, M., Leis, J., Sammelselg, V., Ghangrekar, M.M. and Tammeveski, K., *Multi-walled carbon nanotube and carbide-derived carbon supported metal phthalocyanines as cathode catalysts for microbial fuel cell applications.* Sustainable Energy & Fuels, 2019. **3**(12): p. 3525-3537.

159. Elouarzaki, K., Haddad, R., Holzinger, M., Le Goff, A., Thery, J. and Cosnier, S., *MWCNT-supported phthalocyanine cobalt as air-breathing cathodic catalyst in glucose/O2 fuel cells.* Journal of Power sources, 2014. **255**: p. 24-28.

160. Boutin, E., Wang, M., Lin, J.C., Mesnage, M., Mendoza, D., Lassalle-Kaiser, B., Hahn, C., Jaramillo, T.F. and Robert, M., *Aqueous electrochemical reduction of carbon dioxide and carbon monoxide into methanol with cobalt phthalocyanine.* Angewandte Chemie International Edition, 2019. **58**(45): p. 16172-16176.

161. Taşaltın, N., Zirek, Y., Şan, M., Taşaltın, C., Karakuş, S. and Kilislioğlu, A., *Flexible GO-CoPc and GO-NiPc nanocomposite electrodes for hybrid supercapacitors.* Physica E: Low-dimensional Systems and Nanostructures, 2020. **116**: p. 113766.

162. Yue, Z., Ou, C., Ding, N., Tao, L., Zhao, J. and Chen, J., *Advances in metal phthalocyanine based carbon composites for electrocatalytic CO2 reduction.* ChemCatChem, 2020. **12**(24): p. 6103-6130.

163. Li, Q., Sun, Z., Zhou, M., Liang, Q., Li, Z. and Xu, S., *Synthesis of asymmetric zinc phthalocyanine supported on multi-walled carbon nanotubes and its improvement of catalytic activity on styrene oxidation.* Journal of Materials Science: Materials in Electronics, 2019. **30**(6): p. 6277-6286.

164. Karuppiah, C., Devasenathipathy, R., Chen, S.M., Arulraj, D., Palanisamy, S., Mani, V. and Vasantha, V.S., *Fabrication of nickel tetrasulfonated phthalocyanine functionalized multiwalled carbon nanotubes on activated glassy carbon electrode for the detection of dopamine.* Electroanalysis, 2015. **27**(2): p. 485-493.

165. Kang, T.F., Shen, G.L. and Yu, R.Q., *Voltammetric behaviour of dopamine at nickel phthalocyanine polymer modified electrodes and analytical applications.* Analytica chimica acta, 1997. **354**(1-3): p. 343-349.

166. Siswana, M.P., *Electrocatalytic detection of pesticides with electrodes modified with nanoparticles of phthalocyanines and multiwalled carbon nanotubes*. 2013, Rhodes University.

167. de Oliveira, M.S., de Oliveira Farias, E.A., de Sousa, A.M.S., Dionísio, N.A., Teixeira, P.R.S., Teixeira, A.S.D.N.M., da Silva, D.A. and Eiras, C., *Composite films based on copper nanoparticles and nickel phthalocyanine as electrochemical sensors for serotonin detection.* Surfaces and Interfaces, 2021. **25**: p. 101245.

168. Wu, Y.Y., Li, C., Dou, Z.Y., Cui, L.L., Liu, D.J. and He, X.Q., *A novel nitrite sensor fabricated through anchoring nickel-tetrahydroxy-phthalocyanine and polyethylene oxide film onto glassy carbon electrode by a two-step covalent modification approach.* Journal of Solid State Electrochemistry, 2014. **18**(9): p. 2625-2635.

169. Wen, Z.H. and Kang, T.F., *Determination of nitrite using sensors based on nickel phthalocyanine polymer modified electrodes.* Talanta, 2004. **62**(2): p. 351-355. 139.

170. Erady, V., Mascarenhas, R.J., Satpati, A.K., Bhakta, A.K., Mekhalif, Z. and Delhalle, J., *Sensitive voltammetric determination of Morin in Psidium guajava leaf extract at Nickel (II) phthalocyanine modified carbon paste electrode.* Surfaces and Interfaces, 2020. **19**: p. 100517.

171. O'Donoghue, C.S., Shumba, M. and Nyokong, T., *Electrode modification through click chemistry using Ni and Co alkyne phthalocyanines for electrocatalytic detection of hydrazine.* Electroanalysis, 2017. **29**(7): p. 1731-1740.

172. Beitollahi, H., Safaei, M., and Tajik, S., *Different electrochemical sensors for determination of dopamine as neurotransmitter in mixed and clinical samples: A review.* Analytical and Bioanalytical Chemistry Research, 2019. **6**(1): p. 81-96.

173. Li, X., Li, J., Wang, H., Li, R., Ma, H., Du, B. and Wei, Q., *An electrochemiluminescence sensor for bromate assay based on a new cationic polythiophene derivative.* Analytica Chimica Acta, 2014. **852**: p. 69-73.

174. Salimi, A., MamKhezri, H., Hallaj, R. and Zandi, S., *Modification of glassy carbon electrode with multi-walled carbon nanotubes and iron (III)-porphyrin film: Application to chlorate, bromate and iodate detection.* Electrochimica Acta, 2007. **52**(20): p. 6097-6105.

175. Lee, Y.G., Lee, H.J. and Jang, A., *Amperometric bromate-sensitive sensor via layer-by-layer assembling of metalloporphyrin and polyelectrolytes on carbon nanotubes modified surfaces.* Sensors and Actuators B: Chemical, 2017. **244**: p. 157-166.

176. Wang, N., He, S., and Zhu, Y., *Low-level bromate analysis by ion chromatography on a polymethacrylate-based monolithic column followed by a post-column reaction.* European Food Research and Technology, 2012. **235**(4): p. 685-692.

177. Ali, B., Laffir, F., Kailas, L., Armstrong, G., Kailas, L., O'Connell, R. and McCormac, T., *Electrochemical Characterisation of NiII-Crown-Type Polyoxometalate-Doped Polypyrrole Films for the Catalytic Reduction of Bromate in Water.* European Journal of Inorganic Chemistry, 2019. **2019**(3-4): p. 394-401.

178. Dong, S., Cheng, L., and Zhang, X., *Electrochemical studies of a lanthanide heteropoly tungstate/molybdate complex in polypyrrole film electrode and its electrocatalytic reduction of bromate.* Electrochimica Acta, 1998. **43**(5-6): p. 563-568.

179. Li, Y., Bu, W., Wu, L. and Sun, C., *A new amperometric sensor for the determination of bromate, iodate and hydrogen peroxide based on titania sol–gel matrix for immobilization of cobalt substituted Keggin-type cobalttungstate anion by vapor deposition method.* Sensors and Actuators B: Chemical, 2005. **107**(2): p. 921-928.

180. Casella, I.G. and Contursi, M., *Electrochemical and spectroscopic characterization of a tungsten electrode as a sensitive amperometric sensor of small inorganic ions.* Electrochimica acta, 2005. **50**(20): p. 4146-4154.

181. Zou, X., Shen, Y., Peng, Z., Zhang, L., Bi, L., Wang, Y. and Dong, S., *Preparation of a phosphopolyoxomolybdate P2Mo18O626− doped polypyrrole modified electrode and its catalytic properties.* Journal of Electroanalytical Chemistry, 2004. **566**(1): p. 63-71. 140.

182. Pan, D., Chen, J., Tao, W., Nie, L. and Yao, S., *Phosphopolyoxomolybdate absorbed on lipid membranes/carbon nanotube electrode.* Journal of Electroanalytical Chemistry, 2005. **579**(1): p. 77-82.

183. Fay, N., Dempsey, E., and McCormac, T., *Assembly, electrochemical characterisation and electrocatalytic ability of multilayer films based on [Fe (bpy) 3] 2+, and the Dawson heteropolyanion,[P2W18O62] 6−.* Journal of Electroanalytical Chemistry, 2005. **574**(2): p. 359-366.

184. Rasheed, P.A., Pandey, R.P., Rasool, K. and Mahmoud, K.A., *Ultra-sensitive electrocatalytic detection of bromate in drinking water based on Nafion/Ti3C2Tx (MXene) modified glassy carbon electrode.* Sensors and Actuators B: Chemical, 2018. **265**: p. 652-659.

185. YueHong, P., et al., *Determination of bromate in drinking water by capillary electrophoresis coupled with chemically modified electrode electrochemical detection.* Scientia Sinica Chimica, 2012. **42**(2): p. 157-163.

186. Sheen, S., Jos, T., Rajith, L. and Kumar, K.G., *Manganese porphyrin sensor for the determination of bromate.* Journal of food science and technology, 2016. **53**(3): p. 1561-1566.

187. De La Torre, G., Vázquez, P., Agullo-Lopez, F. and Torres, T., *Role of structural factors in the nonlinear optical properties of phthalocyanines and related compounds.* Chemical Reviews, 2004. **104**(9): p. 3723-3750.

188. Campidelli, S., Ballesteros, B., Filoramo, A., Díaz, D.D., de la Torre, G., Torres, T., Rahman, G.A., Ehli, C., Kiessling, D., Werner, F. and Sgobba, V., *Facile decoration of functionalized single-wall carbon nanotubes with phthalocyanines via "click chemistry".* Journal of the American Chemical Society, 2008. **130**(34): p. 11503-11509.

189. Zhu, L., Yang, R., Zhai, J. and Tian, C., *Bienzymatic glucose biosensor based on co-immobilization of peroxidase and glucose oxidase on a carbon nanotubes electrode.* Biosensors and Bioelectronics, 2007. **23**(4): p. 528-535.

190. Li, Z., Chen, J., Pan, D., Tao, W., Nie, L. and Yao, S., *A sensitive amperometric bromate sensor based on multi-walled carbon nanotubes/phosphomolybdic acid composite film.* Electrochimica Acta, 2006. **51**(20): p. 4255-4261.

191. Salimi, A., Kavosi, B., Babaei, A. and Hallaj, R., *Electrosorption of Os (III)-complex at single-wall carbon nanotubes immobilized on a glassy carbon electrode: Application to nanomolar detection of bromate, periodate and iodate.* analytica chimica acta, 2008. **618**(1): p. 43-53.

192. Vilian, A.E., Chen, S.M., Kwak, C.H., Hwang, S.K., Huh, Y.S. and Han, Y.K., *Immobilization of hemoglobin on functionalized multi-walled carbon nanotubes-poly-l-histidine-zinc oxide nanocomposites toward the detection of bromate and H2O2.* Sensors and Actuators B: Chemical, 2016. **224**: p. 607-617.

193. Salimi, A., Korani, A., Hallaj, R., Khoshnavazi, R. and Hadadzadeh, H., *Immobilization of [Cu (bpy) 2] Br2 complex onto a glassy carbon electrode modified with α-SiMo12O404− and single walled carbon nanotubes: Application to nanomolar detection of hydrogen peroxide and bromate.* Analytica chimica acta, 2009. **635**(1): p. 63-70. 141.

194. Zhou, D.D., Ding, L., Cui, H., An, H., Zhai, J.P. and Li, Q., *Fabrication of high dispersion Pd/MWNTs nanocomposite and its electrocatalytic performance for bromate determination.* Chemical engineering journal, 2012. **200**: p. 32-38.

195. Li, Y., Chen, S.M., Thangamuthu, R., Ajmal Ali, M. and Al-Hemaid, F.M., *Preparation, Characterization, and Bioelectrocatalytic Properties of Hemoglobin Incorporated Multiwalled Carbon Nanotubes-Poly-L-lysine Composite Film Modified Electrodes Towards Bromate.* Electroanalysis, 2014. **26**(5): p. 996-1003.

196. Shao, Y., Wang, J., Wu, H., Liu, J., Aksay, I.A. and Lin, Y., *Graphene based electrochemical sensors and biosensors: a review.* Electroanalysis: An International Journal Devoted to Fundamental and Practical Aspects of Electroanalysis, 2010. **22**(10): p. 1027-1036.

197. Baby, T.T., Aravind, S.J., Arockiadoss, T., Rakhi, R.B. and Ramaprabhu, S., *Metal decorated graphene nanosheets as immobilization matrix for amperometric glucose biosensor.* Sensors and Actuators B: Chemical, 2010. **145**(1): p. 71-77.

198. Liu, H., Gao, J., Xue, M., Zhu, N., Zhang, M. and Cao, T., *Processing of graphene for electrochemical application: noncovalently functionalize graphene sheets with water-soluble electroactive methylene green.* Langmuir, 2009. **25**(20): p. 12006-12010.

199. Tang, L., Wang, Y., Li, Y., Feng, H., Lu, J. and Li, J., *Preparation, structure, and electrochemical properties of reduced graphene sheet films.* Advanced Functional Materials, 2009. **19**(17): p. 2782-2789.

200. Xu, J., Wang, Y., and Hu, S., *Nanocomposites of graphene and graphene oxides: synthesis, molecular functionalization and application in electrochemical sensors and biosensors. A review.* Microchimica Acta, 2017. **184**(1): p. 1-44.

201. Palanisamy, S., Wang, Y.T., Chen, S.M., Thirumalraj, B. and Lou, B.S., *Direct electrochemistry of immobilized hemoglobin and sensing of bromate at a glassy carbon electrode modified with graphene and β-cyclodextrin.* Microchimica Acta, 2016. **183**(6): p. 1953-1961.
202. Ding, L., Liu, Y., Guo, S.X., Zhai, J., Bond, A.M. and Zhang, J., *Phosphomolybdate@ poly (diallyldimethylammonium chloride)-reduced graphene oxide modified electrode for highly efficient electrocatalytic reduction of bromate.* Journal of Electroanalytical Chemistry, 2014. **727**: p. 69-77.
203. Zhang, Y., Li, J., and Liu, H., *Synergistic Removal of Bromate and Ibuprofen by Graphene Oxide and TiO2 Heterostructure Doped with F: Performance and Mechanism.* Journal of Nanomaterials, 2020. **2020**.
204. Kıran, T.R., Atar, N., and Yola, M.L., *A methyl parathion recognition method based on carbon nitride incorporated hexagonal boron nitride nanosheets composite including molecularly imprinted polymer.* Journal of The Electrochemical Society, 2019. **166**(12): p. H495.
205. Tian, K., Zhang, Y., Zhang, S. and Dong, Y., *Electrogenerated Chemiluminescence of ZnO/MoS2 Nanocomposite and Its Application for Cysteine Detection.* Journal of The Electrochemical Society, 2019. **166**(12): p. H527.
206. Lu, L., Hu, X., Zhu, Z., Li, D., Tian, S. and Chen, Z., *Electrochemical sensors and biosensors modified with binary nanocomposite for food safety.* Journal of The Electrochemical Society, 2019. **167**(3): p. 037512.
207. Wang, J., *Nanoparticle-based electrochemical DNA detection.* Analytica Chimica Acta, 2003. **500**(1-2): p. 247-257.
208. Ourari, A., Ketfi, B., Malha, S.I.R. and Amine, A., *Electrocatalytic reduction of nitrite and bromate and their highly sensitive determination on carbon paste electrode modified with new copper Schiff base complex.* Journal of Electroanalytical Chemistry, 2017. **797**: p. 31-36.
209. Zhuang, R., Jian, F., and Wang, K., *An electrochemical sensing platform based on a new Cd (II)-containing ionic liquid for the determination of trichloroacetic acid and bromate.* Ionics, 2010. **16**(7): p. 661-666.

210. Manivel, A., Sivakumar, R., Anandan, S. and Ashokkumar, M., *Ultrasound-assisted synthesis of hybrid phosphomolybdate–polybenzidine containing silver nanoparticles for electrocatalytic detection of chlorate, bromate and iodate ions in aqueous solutions.* Electrocatalysis, 2012. **3**(1): p. 22-29.
211. Akinremi, C.A., Oyelude, V.B., Adewuyi, S., Amolegbe, S.A. and Arowolo, T., *Reduction of bromate in water using zerovalent cobalt 2, 6-pyridine dicarboxylic acid crosslinked chitosan nanocomposite.* Journal of Macromolecular Science, Part A, 2013. **50**(4): p. 435-440.
212. Sun, C., Deng, N., An, H., Cui, H. and Zhai, J., *Electrocatalytic reduction of bromate based on Pd nanoparticles uniformly anchored on polyaniline/SBA-15.* Chemosphere, 2015. **141**: p. 243-249.
213. Cheng, C.Y., Thiagarajan, S. and Chen, S.M., *Electrochemical fabrication of AuRh nanoparticles and their electroanalytical applications.* Int. J. Electrochem. Sci, 2011. **6**: p. 1331-1341.
214. Chen, P.Y., Yang, H.H., Huang, C.C., Chen, Y.H. and Shih, Y., *Involvement of Cu (II) in the electrocatalytic reduction of bromate on a disposable nano-copper oxide modified screen-printed carbon electrode: hair waving products as an example.* Electrochimica Acta, 2015. **161**: p. 100-107.
215. Tamiji, T. and Nezamzadeh-Ejhieh, A., *Sensitive voltammetric determination of bromate by using ion-exchange property of a Sn (II)-clinoptilolite-modified carbon paste electrode.* Journal of Solid State Electrochemistry, 2019. **23**(1): p. 143-157.
216. Baker, S.N. and Baker, G.A., *Luminescent carbon nanodots: emergent nanolights.* Angewandte Chemie International Edition, 2010. **49**(38): p. 6726-6744.
217. Tuerhong, M., Yang, X., and Xue-Bo, Y., *Review on carbon dots and their applications.* Chinese Journal of Analytical Chemistry, 2017. **45**(1): p. 139-150.
218. Molaei, M.J., *Principles, mechanisms, and application of carbon quantum dots in sensors: a review.* Analytical Methods, 2020. **12**(10): p. 1266-1287. 143.
219. Liu, R., Li, H., Kong, W., Liu, J., Liu, Y., Tong, C., Zhang, X. and Kang, Z., *Ultra-sensitive and selective Hg2+ detection based on fluorescent carbon dots.* Materials Research Bulletin, 2013. **48**(7): p. 2529-2534.

220. Zu, F., Yan, F., Bai, Z., Xu, J., Wang, Y., Huang, Y. and Zhou, X., *The quenching of the fluorescence of carbon dots: a review on mechanisms and applications.* Microchimica Acta, 2017. **184**(7): p. 1899-1914.

221. Xiang, G., Fan, H., Zhang, H., He, L., Jiang, X. and Zhao, W., *Carbon dot doped silica nanoparticles as fluorescent probe for determination of bromate in drinking water samples.* Canadian Journal of Chemistry, 2018. **96**(1): p. 24-29.

222. Li, P., Sun, X.Y., Shen, J.S. and Liu, B., *A novel photoluminescence sensing system sensitive for and selective to bromate anions based on carbon dots.* RSC advances, 2016. **6**(66): p. 61891-61896.

223. Li, L., Lai, X., Xu, X., Li, J., Yuan, P., Feng, J., Wei, L. and Cheng, X., *Determination of bromate via the chemiluminescence generated in the sulfite and carbon quantum dot system.* Microchimica Acta, 2018. **185**(2): p. 1-7.

224. Luo, X.L., Xu, J.J., Zhang, Q., Yang, G.J. and Chen, H.Y., *Electrochemically deposited chitosan hydrogel for horseradish peroxidase immobilization through gold nanoparticles self-assembly.* Biosensors and Bioelectronics, 2005. **21**(1): p. 190-196.

225. Qiu, S., Gao, S., Liu, Q., Lin, Z., Qiu, B. and Chen, G., *Electrochemical impedance spectroscopy sensor for ascorbic acid based on copper (I) catalyzed click chemistry.* Biosensors and Bioelectronics, 2011. **26**(11): p. 4326-4330.

226. Zouaoui, F., Bourouina-Bacha, S., Bourouina, M., Alcacer, A., Bausells, J., Jaffrezic-Renault, N., Zine, N. and Errachid, A., *Electrochemical impedance spectroscopy microsensor based on molecularly imprinted chitosan film grafted on a 4-aminophenylacetic acid (CMA) modified gold electrode, for the sensitive detection of glyphosate.* Frontiers in chemistry, 2021: p. 263.

227. Boumya, W., Laghrib, F., Lahrich, S., Farahi, A., Achak, M., Bakasse, M. and El Mhammedi, M.A., *Electrochemical impedance spectroscopy measurements for determination of derivatized aldehydes in several matrices.* Heliyon, 2017. **3**(10): p. e00392.

228. Palanna, M., Mohammed, I., Aralekallu, S., Nemakal, M. and Sannegowda, L.K., *Simultaneous detection of paracetamol and 4-aminophenol at nanomolar levels using biocompatible cysteine-substituted phthalocyanine.* New Journal of Chemistry, 2020. **44**(4): p. 1294-1306.

229. Santos, L.M. and Baldwin, R.P., *Liquid chromatography/electrochemical detection of carbohydrates at a cobalt phthalocyanine containing chemically modified electrode.* Analytical Chemistry, 1987. **59**(14): p. 1766-1770.
230. Meenakshi, S., Pandian, K., Jayakumari, L.S. and Inbasekaran, S., *Enhanced amperometric detection of metronidazole in drug formulations and urine samples based on chitosan protected tetrasulfonated copper phthalocyanine thin-film modified glassy carbon electrode.* Materials Science and Engineering: C, 2016. **59**: p. 136-144.
231. Mafatle, T. and Nyokong, T., *Use of cobalt (II) phthalocyanine to improve the sensitivity and stability of glassy carbon electrodes for the detection of cresols, chlorophenols and phenol.* Analytica Chimica Acta, 1997. **354**(1-3): p. 307-314.
232. Xu, H., Xiao, J., Liu, B., Griveau, S. and Bedioui, F., *Enhanced electrochemical sensing of thiols based on cobalt phthalocyanine immobilized on nitrogen-doped graphene.* Biosensors and Bioelectronics, 2015. **66**: p. 438-444.
233. Nantaphol, S., Jesadabundit, W., Chailapakul, O. and Siangproh, W., *A new electrochemical paper platform for detection of 8-hydroxyquinoline in cosmetics using a cobalt phthalocyanine-modified screen-printed carbon electrode.* Journal of Electroanalytical Chemistry, 2019. **832**: p. 480-485.
234. Lei, P., Zhou, Y., Zhu, R., Liu, Y., Dong, C. and Shuang, S., *Facile synthesis of iron phthalocyanine functionalized N, B–doped reduced graphene oxide nanocomposites and sensitive electrochemical detection for glutathione.* Sensors and Actuators B: Chemical, 2019. **297**: p. 126756.
235. Basova, T., Gürek, A.G., Ahsen, V. and Ray, A., *Electrochromic lutetium phthalocyanine films for in situ detection of NADH.* Optical Materials, 2013. **35**(3): p. 634-637.
236. Wang, H., Bu, Y., Dai, W., Li, K., Wang, H. and Zuo, X., *Well-dispersed cobalt phthalocyanine nanorods on graphene for the electrochemical detection of hydrogen peroxide and glucose sensing.* Sensors and Actuators B: Chemical, 2015. **216**: p. 298-306.
237. Li, X., Jiang, Y., Xie, G., Tai, H., Sun, P. and Zhang, B., *Copper phthalocyanine thin film transistors for hydrogen sulfide detection.* Sensors and Actuators B: Chemical, 2013. **176**: p. 1191-1196.

238. Ozoemena, K.I. and Nyokong, T., *Electrocatalytic oxidation and detection of hydrazine at gold electrode modified with iron phthalocyanine complex linked to mercaptopyridine self-assembled monolayer.* Talanta, 2005. **67**(1): p. 162-168.
239. Kumar, A., Brunet, J., Varenne, C., Ndiaye, A., Pauly, A., Penza, M. and Alvisi, M., *Tetra-tert-butyl copper phthalocyanine-based QCM sensor for toluene detection in air at room temperature.* Sensors and actuators B: Chemical, 2015. **210**: p. 398-407.
240. Azzouzi, S., Ali, M.B., Abbas, M.N., Bausells, J., Zine, N. and Errachid, A., *Novel iron (III) phthalocyanine derivative functionalized semiconductor based transducers for the detection of citrate.* Organic Electronics, 2016. **34**: p. 200-207.
241. Cruz, J.C., Nascimento, M.A., Amaral, H.A., Lima, D.S., Teixeira, A.P.C. and Lopes, R.P., *Synthesis and characterization of cobalt nanoparticles for application in the removal of textile dye.* Journal of environmental management, 2019. **242**: p. 220-228.
242. Wu, X., Xing, W., Zhang, L., Zhuo, S., Zhou, J., Wang, G. and Qiao, S., *Nickel nanoparticles prepared by hydrazine hydrate reduction and their application in supercapacitor.* Powder technology, 2012. **224**: p. 162-167.
243. Wu, Z.G., Munoz, M., and Montero, O., *The synthesis of nickel nanoparticles by hydrazine reduction.* Advanced Powder Technology, 2010. **21**(2): p. 165-168.
244. Klug, H.P. and Alexander, L.E., *X-ray diffraction procedures: for polycrystalline and amorphous materials*. 1974. 145.
245. Li, H., Xu, Z., Li, K., Hou, X., Cao, G., Zhang, Q. and Cao, Z., *Modification of multi-walled carbon nanotubes with cobalt phthalocyanine: effects of the templates on the assemblies.* Journal of Materials Chemistry, 2011. **21**(4): p. 1181-1186.
246. Cao, L., Chen, H.Z., Li, H.Y., Zhou, H.B., Sun, J.Z., Zhang, X.B. and Wang, M., *Fabrication of rare-earth biphthalocyanine encapsulated by carbon nanotubes using a capillary filling method.* Chemistry of materials, 2003. **15**(17): p. 3247-3249.
247. Kareem, M.M., Kadem, B.Y., Mohammad, E.J. and Atiyah, A.J., *Synthesis, Characterization and Gas Sensor Application of New Composite Based on MWCNTs: CoPc: Metal Oxide.* Baghdad Sci. J, 2021. **18**: p. 384.
248. Chidembo, A.T., *Nickel (II) phthalocyanine-multi-walled carbon nanotube hybrids as supercapacitors*. 2010, University of Pretoria.

249. Yamada, H., Yoshii, K., Asahi, M., Chiku, M. and Kitazumi, Y., *Cyclic Voltammetry Part 1: Fundamentals.* Electrochemistry, 2022. **90**(10): p. 102005-102005.

250. Waelder, J. and Maldonado, S., *Beyond the Laviron Method: A New Mathematical Treatment for Analyzing the Faradaic Current in Reversible, Quasi-Reversible, and Irreversible Cyclic Voltammetry of Adsorbed Redox Species.* Analytical Chemistry, 2021. **93**(37): p. 12672-12681.

251. Zangeneh Kamali, K., Alagarsamy, P., Huang, N.M., Ong, B.H. and Lim, H.N., *Hematite nanoparticles-modified electrode based electrochemical sensing platform for dopamine.* The Scientific World Journal, 2014. **2014**.

252. Adekunle, A.S., Ozoemena, K.I., and Agboola, B.O., *MWCNTs/metal (Ni, Co, Fe) oxide nanocomposite as potential material for supercapacitors application in acidic and neutral media.* Journal of Solid State Electrochemistry, 2013. **17**(5): p. 1311-1320.

253. Bhengo, T., Moyo, M., Shumba, M. and Okonkwo, O.J., *Simultaneous oxidative determination of antibacterial drugs in aqueous solutions using an electrode modified with MWCNTs decorated with Fe 3 O 4 nanoparticles.* New Journal of Chemistry, 2018. **42**(7): p. 5014-5023.

254. Zhang, Y., Zhang, Y., Li, L., Chen, J., Li, P. and Huang, W., *One-step in situ growth of high-density POMOFs films on carbon cloth for the electrochemical detection of bromate.* Journal of Electroanalytical Chemistry, 2020. **861**: p. 113939.

255. Hassan, S.S., Liu, Y., Solangi, A.R., Bond, A.M. and Zhang, J., *Phosphomolybdate-doped-poly (3, 4-ethylenedioxythiophene) coated gold nanoparticles: Synthesis, characterization and electrocatalytic reduction of bromate.* Analytica Chimica Acta, 2013. **803**: p. 41-46.

256. Wierzbicka, E. and Sulka, G.D., *Nanoporous spongelike Au–Ag films for electrochemical epinephrine sensing.* Journal of Electroanalytical Chemistry, 2016. **762**: p. 43-50.

257. Ndebele, N., Sen, P., and Nyokong, T., *Electrochemical detection of dopamine using phthalocyanine-nitrogen-doped graphene quantum dot conjugates.* Journal of Electroanalytical Chemistry, 2021. **886**: p. 115111.

258. Fang, Y.H. and Liu, Z.P., *Tafel kinetics of electrocatalytic reactions: from experiment to first-principles.* ACS Catalysis, 2014. **4**(12): p. 4364-4376. 146.

259. Kishimoto, N. and Matsuda, N., *Bromate ion removal by electrochemical reduction using an activated carbon felt electrode.* Environmental science & technology, 2009. **43**(6): p. 2054-2059.

260. Papagianni, G.G., Stergiou, D.V., Armatas, G.S., Kanatzidis, M.G. and Prodromidis, M.I., *Synthesis, characterization and performance of polyaniline–polyoxometalates (XM12, X= P, Si and M= Mo, W) composites as electrocatalysts of bromates.* Sensors and Actuators B: Chemical, 2012. **173**: p. 346-353.

261. Wang, X., Lin, J., Li, H., Wang, C. and Wang, X., *Carbazole-based bis-imidazole ligand-involved synthesis of inorganic–organic hybrid polyoxometalates as electrochemical sensors for detecting bromate and efficient catalysts for selective oxidation of thioether.* RSC advances, 2022. **12**(8): p. 4437-4445.

262. Wang, J., Wang, S., Zhang, Z. and Wang, C., *Preparation of Cu/GO/Ti electrode by electrodeposition and its enhanced electrochemical reduction for aqueous nitrate.* Journal of environmental management, 2020. **276**: p. 111357.

263. Shi, E., Zou, X., Liu, J., Lin, H., Zhang, F., Shi, S., Liu, F., Zhu, G. and Qu, F., *Electrochemical fabrication of copper-containing metal–organic framework films as amperometric detectors for bromate determination.* Dalton Transactions, 2016. **45**(18): p. 7728-7736.

264. Zhang, S., Cheng, H., Wang, B., Shi, F., Yan, L., Zeng, L., Li, L., He, S. and Sun, W., *An electrochemical biosensor based on hemoglobin and FeS@ MoS2-C nanocomposite for nitrite, hydrogen peroxide and bromate detection.* Int. J. Electrochem. Sci, 2022. **17**(221023): p. 2.

265. Zhang, W., Xiahou, C., Ji, X., Zhang, Y., Zhang, H., Song, S. and Niu, X., *Utilization of molybdenum disulfide-graphene aerogel composite for hemoglobin-based electrochemical sensor for highly sensitive detection of bromate.* International Journal of Electrochemical. Science, 2022. **17**(220946): p. 2.

266. Kirowa-Eisner, E., Schwarz, M., Rosenblum, M. and Gileadi, E., *Negative apparent electrochemical enthalpy of activation: the reduction of bromate at the dropping mercury electrode in alkaline solutions.* Journal of the Electrochemical Society, 1994. **141**(5): p. 1183.

267. Mao, R., Zhao, X., Lan, H., Liu, H. and Qu, J., *Graphene-modified Pd/C cathode and Pd/GAC particles for enhanced electrocatalytic removal of bromate in a continuous three-dimensional electrochemical reactor.* Water Research, 2015. **77**: p. 1-12.

268. Zhong, Y., Yang, Q., Li, X., Yao, F., Xie, L., Zhao, J., Chen, F., Xie, T. and Zeng, G., *Electrochemically induced pitting corrosion of Ti anode: Application to the indirect reduction of bromate.* Chemical Engineering Journal, 2016. **289**: p. 114-122.

269. Mao, R., Zhao, X., Lan, H., Liu, H. and Qu, J., *Efficient electrochemical reduction of bromate by a Pd/rGO/CFP electrode with low applied potentials.* Applied Catalysis B: Environmental, 2014. **160**: p. 179-187.